Technical Report

TR-05-17

Probabilistic analysis and material characterisation of canister insert for spent nuclear fuel

Summary report

Claes-Göran Andersson
Svensk Kärnbränslehantering AB

Mats Andersson, Bo Erixon
ÅF Industriteknik

Lars-Erik Björkegren
Swedish Foundry Association

Peter Dillström
DNV Technology Sweden

Philip Minnebo, Karl-Fredrik Nilsson
European Commission, DG-JRC, Institute for Energy

Fred Nilsson
Royal Institute of Technology, KTH – Solid Mechanics

November 2005

Svensk Kärnbränslehantering AB
Swedish Nuclear Fuel
and Waste Management Co
Box 5864
SE-102 40 Stockholm Sweden
Tel 08-459 84 00
+46 8 459 84 00
Fax 08-661 57 19
+46 8 661 57 19

Probabilistic analysis and material characterisation of canister insert for spent nuclear fuel

Summary report

Claes-Göran Andersson
Svensk Kärnbränslehantering AB

Mats Andersson, Bo Erixon
ÅF Industriteknik

Lars-Erik Björkegren
Swedish Foundry Association

Peter Dillström
DNV Technology Sweden

Philip Minnebo, Karl-Fredrik Nilsson
European Commission, DG-JRC, Institute for Energy

Fred Nilsson
Royal Institute of Technology, KTH – Solid Mechanics

November 2005

Summary

The KBS-3 canister for geological disposal of spent nuclear fuel in Sweden consists of a ductile cast iron insert and a copper shielding. The canister should inhibit release of radionuclides for at least 100,000 years. The copper protects the canister from corrosion whereas the ductile cast iron insert provides the mechanical strength. In the repository the hydrostatic pressure from the groundwater and the swelling pressure from the surrounding bentonite, which in total results in a maximum pressure of 14 MPa, will load the canisters in compression. During the extreme time scales, ice ages are expected with a maximum ice thickness of 3,000 m resulting in an additional pressure of 30 MPa. The maximum design pressure for the KBS-3 canisters has therefore been set to be 44 MPa.

A relatively large number of canisters have been manufactured as part of SKB's development programme. To verify the strength of the canisters at this stage of development SKB initiated a project in cooperation with the European commissions Joint Research Centre (JRC), Institute of Energy in Petten in the Netherlands, together with a number of other partners. Three inserts manufactured by different Swedish foundries were used in the project. A large statistical test programme was developed to determine statistical distributions of various material parameters and defect distributions. These data together with the results from stress and strain finite element analysis were subsequently used in probabilistic analysis to determine the probability for plastic collapse caused by high pressure or fracture by crack growth in regions with tensile stresses.

The main conclusions from the probabilistic analysis are:

1. At the design pressure of 44 MPa, the probability of failure is insignificant ($\sim 2\times10^{-9}$). This is the case even though several conservative assumptions have been made.
2. The stresses in the insert caused by the outer pressure are mainly compressive. The regions with tensile stresses are spatially very limited provided that the requirements for the eccentricity and corner radius of the cassette are met.
3. The probability of fracture by crack growth in regions with tensile stresses dominates at external pressures under 44 MPa. Local plastic collapse dominates at higher pressure.
4. The analysis of plastic collapse only considers the first local collapse event. A total collapse of the insert will occur at a much higher pressure.
5. The tensile tests of the material in the three inserts gave a considerable spread mainly in the elongation values. Low elongation could be attributed to the presence of slag inclusions and areas with low nodularity (roundness) of the graphite and in some case areas with high pearlite content. As the production methods improve, the failure probability will be further reduced.

Contents

1 Introduction 7

2 Material testing 9
2.1 Statistical test programme 9
2.2 Test results 10
2.2.1 Tensile tests 10
2.2.2 Microstructure 11
2.2.3 Compression tests 14
2.2.4 Fracture mechanics tests 16

3 Analysis 19
3.1 Semi-analytic determination of defect distributions 19
3.2 Stress and strain FE-analysis of the canister 22

4 Probabilistic analysis of canister 25

5 Discussion 27

6 Conclusions 29

References 31

Appendix A 33

Appendix B 45

Appendix C 57

Appendix D 73

Appendix E 77

Appendix F 81

1 Introduction

For the licensing procedures of repositories for spent nuclear fuel safety analyses are performed. Among other items it is required to obtain an estimate of the probability of mechanical failure of canisters even by considering the effects of a possible ice age. At the end of 2002 a project was initiated to obtain such an estimate. Different activities such as material testing, stress and strain calculations, full-scale testing as well as probabilistic analyses have been conducted by different organisations. The work has been initiated and coordinated by SKB in cooperation with European Commission, DG-JRC, Institute for Energy in Petten in the Netherlands. In the present report the different activities and conclusions are summarised. The primary reports from the organizations involved are appended to this report or given in the reference list.

The KBS-3 canister for geological disposal of spent fuel in Sweden consists of a ductile cast iron insert and a copper shielding, Figure 1-1. The copper protects the canister from corrosion whereas the ductile cast iron insert provides the mechanical strength. The canister should inhibit release of radionuclides for at least 100,000 years. In the repository the canisters will be loaded in compression by the hydrostatic pressure and the swelling pressure from the surrounding bentonite, giving a total pressure of 14 MPa. During the extreme time scales, several ice ages are expected with a maximum ice-sheet of 3 km resulting in an additional pressure of 30 MPa. The maximum design pressure for the KBS-3 canisters has therefore been assumed to be 44 MPa.

Figure 1-1. *Canister for final depository of spent nuclear fuel.*

A relatively large number of canisters have been manufactured as part of SKB's development programme. The canister material is the ductile iron grade EN-GJS-400-15U, in accordance with EN 1563. An issue that caused some concern was that the tensile properties (in particular the ductility) of the inserts fell below the initial requirements and that there was a large variation between individual inserts. Therefore the question was raised whether the relatively poor tensile properties could lead to unacceptable failure probabilities for the canisters during their design life. A secondary objective was to provide a basis for acceptance criteria for defects and material properties. In order to achieve these objectives as well as acquiring manufacturing experience, three inserts (herein referred to as I24, I25 and I26) were manufactured in accordance with the preliminary requirements by three Swedish different foundries.

2 Material testing

2.1 Statistical test programme

Specimens for the material characterisation tests were taken in accordance with a statistical test plan to derive distributions for the material properties to be used in the analysis of the canister. Specimens from the homogeneous bottom as well as from the top of the insert with essentially the same cutting plan for all three inserts. The details of the cutting plan are given in /A/and /B/. The different types of specimens were:

a) Three-point-bend specimens for fracture toughness determination. The fracture properties were needed for determining defect distributions and for the probabilistic tensile fracture analysis of canisters.

b) Specimens for tensile testing. The assumption at the start of the project was that casting defects caused the low values for the elongation. The tensile test data together with the fracture properties could therefore by used to determine defect distributions as outlined below.

c) Specimens for compression testing. The compression data were needed as input to the plastic collapse analysis.

Figure 2-1 shows a drawing of how different specimens are taken from the upper part containing the fuel channels.

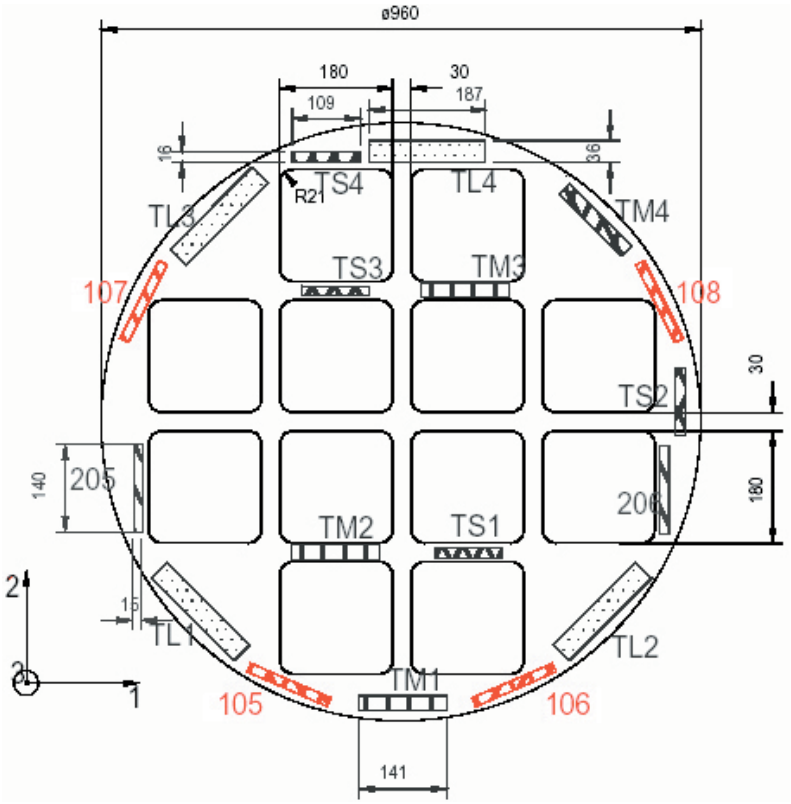

Figure 2-1. *Example of sampling drawing addressing canister insert top segment.*

2.2 Test results

2.2.1 Tensile tests

JRC-IE and the Swedish Foundry Association (Gjuteriföreningen, GF) performed tensile tests using about 50 specimens from each of the three inserts according to EN 1563. Yield stress, tensile strength and elongation at fracture were determined. All tests for insert I26 and most of the tests for inserts I24 and I25 were performed with specimens with 14 mm diameter. The results from JRC and GF were very consistent with respect to the mean and standard deviation of yield stress, tensile strength and elongation at fracture (Tables 2-1 and 2-2) and also to systematic variation between different inserts and locations of specimen. A summary of test results and a statistical analysis of these data are given in /3/. The variation in elongation at fracture between the three inserts and between top (transverse and longitudinal direction) and bottom are also plotted in Figure 2-2. The large variations are remarkable especially for the elongation and in particular that a) insert I25 has a significantly higher failure strain and different distribution than specimens from inserts I24 and I26 and b) that the specimens from the bottom slab have a higher failure strain. This is particularly obvious for insert I24 where the specimens from top and bottom appear as separate populations. The minimum, maximum, mean, median values and standard deviations for the failure strain are given in Table 2-2 for the three inserts.

The minimum requirements for these properties stipulated by EN Grade GJS-400-15U are as follows:

$R_{p0.2}$ = 240 MPa, R_m = 370 MPa; A_5 = 11%.

It is obvious that the ductility requirement was in many cases not met: It should be remarked that these low tensile strength values could be correlated to the lowest elongation figures measured. Regarding the yield strength it must be noted, however, that the minimum value was always met.

The tensile curves measured by JRC were more or less identical until fracture occurs. This observation suggested that the fracture process was controlled by the nature and size of the defect(s) present in the specimen tested.

Table 2-1. Mean value and standard deviation of yield stress, tensile strength and fracture strain for JRC and GF test series.

Organisation	Yield stress (MPa)		Ultimate tensile strength (MPa)		Elongation at fracture (%)	
JRC	310	± 6.2	397	± 26	7.2	± 4.2
GF	316	± 5.8	400	± 27	6.9	± 5.3

Table 2-2. Elongation at fracture and for the three tested inserts.

	Elongation at fracture A (%)				
Canister	Min	Max	Median	Mean	St dev
I24	1.4	24.7	6.0	11.0	8.8
I25	4.7	19.7	11.0	11.2	3.0
I26	2.3	19.9	5.6	7.3	4.7

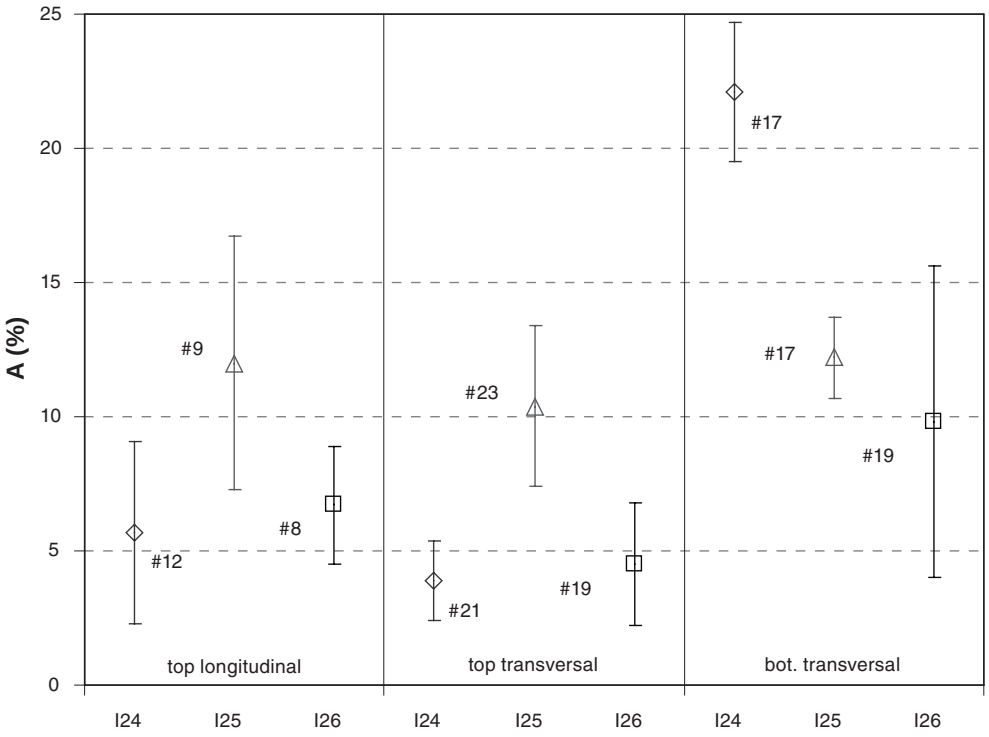

Figure 2-2. *Elongation at fracture, mean values and error bars (= ± standard deviation) plotted for I) canister insert (I24, I25, I26), ii/ sampling region (top, bottom) and ii/ specimen orientation (longitudinal, transversal). The hatches indicated the number of specimens for each data set.*

2.2.2 Microstructure

The microstructure of the inserts was investigated by Gjuteriföreningen /C/ after testing at a location about 10 mm from the fracture surface of the tensile test samples. The nodularity (roundness of the graphite particles), nodule counts and amount of pearlite are summarised in Table 2-3a–c. Here σ denotes the standard deviation.

Table 2-3a. Microstructural properties of insert I 24.

Property	Specification	Top	Bottom	Comments
Nodularity (%) 1)	Min 80			
Average		90	90	Good
1σ		± 0	± 0	Good
Min		90	90	Good
Max		90	90	–
Nodule density 2)	Min 100			
Average		93	156	Good
1σ		± 87	± 112	–
Min		35	90	T = low
Max		255	415	OK
Pearlite (%)				
Average		1,4	1	Good
Min		0	0	Good
Max		2	1	Good

1) Graphite form V and VI according to EN ISO 945.

2) Number of nodules/mm^2.

Table 2-3b. Microstructural properties of insert I25.

Property	Specification	Top	Bottom	Comments
Nodularity (%) 1)	Min 80			
Average		75	68	Too low
1σ		± 7	± 7	–
Min		70	60	Too low
Max		90	80	–
Nodule density 2)	Min 100			
Average		132	43	T = Good
1σ		± 103	± 12	–
Min		40	30	Low
Max		315	60	Large variation
Pearlite (%)				
Average		1	1	Good
Min		0	0	Good
Max		3	5	Good

1) Graphite form V and VI according to EN ISO 945.

2) Number of nodules/mm^2.

Table 2-3c. Microstructural properties of insert I26.

Property	Specification	Top	Bottom	Comments
Nodularity (%) 1)	Min 80			
Average	–	75	75	Too low
1σ	–	± 11	± 5	
Min value	–	60	70	Too low
Max value	–	90	85	–
Nodule count 2)	Max 100			
Average	–	181	124	Good
1σ	–	± 126	± 37	
Min value	–	60	40	Somewhat low
Max value	–	410	170	
Pearlite (%)	–			
Average	–	9.5	8.6	Somewhat high
1σ	–	4.2	4.5	
Min. value	–	5	5	Too high
Max value	–	15	20	Too high

1) Graphite form V and VI according to EN ISO 945.

2) Number of nodules/mm^2.

It is well known that for cast iron, ductility generally increases with nodularity and that it decreases with pearlite content of the cast iron e.g. /1/. It is reasonable to assume that the large scatter in failure strain and in particular the low failure strain values are due to casting defects. To verify such an assumption all specimens tested at JRC were radiographed prior to testing. For insert I26 radiography revealed that defects could be sized and at least qualitatively related to low ductility values whereas for I24 and I25 almost no defects could be quantified. Fractographic and metallographic studies were performed on broken specimens

to check for defects. This was done by first performing a detailed and unbiased analysis for a number of specimens to screen for defects or microstructural imperfections that might cause low failure strain.

From this investigation the slag defects with oxidized areas and areas with clustered graphite were singled for more systematic study as the most likely ones affecting failure strain; the slag defects are expected to behave similarly to cracks whereas the high-density graphite areas carry less load. Typical examples fracture surfaces with these defects are illustrated in Figure 2-3a) and b) respectively whereas Figure 2-3c) shows a homogenous graphite structure typical for specimens that failed at high strains. Another important reason for selecting these defect types was that they could be sized in a quantitative analysis. The slag defects were sized by two methods; D_{max}, which was taken as the length of the largest slag defect and D_{eff}, which was the diameter of a penny-shaped defect with the same area as the sum of all the slag defects on the fracture surface. The dense graphite area was sized

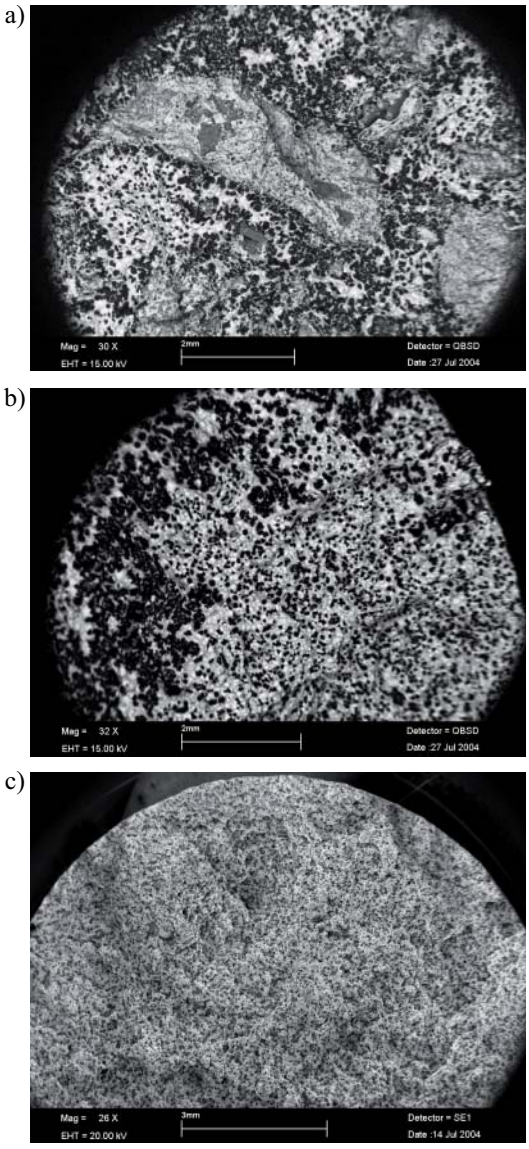

Figure 2-3. *Typical examples of observed fracture surfaces from three specimens. a) Macroscopic slag defect (oxidation) I24 TM4, A = 3.9%, b) Non-homogenous graphite distribution, I24 TL2, A = 6.9, c) Defect free and homogenous graphite I24 BTM3, A = 21.9%.*

in terms of its estimated fraction of the total fracture surface. The measured elongation at fracture is plotted in Figure 2-4 versus the estimated defect sizes D_{max} and D_{eff} for the 75 specimens investigated by fractography. There is a clear trend that the failure strain decreases with increasing defect size. As expected there is quite a bit of scatter but that is hardly surprising given the difference in elongation at fracture between inserts shown in Table 2-2 difference in defect shape, the sizing and most importantly the fact that all defect types mentioned above may affect the failure strain. The failure strain was also plotted against the clustered graphite area fraction, the pearlite content and nodularity, but there was no clear correlation. However, clear trends were obvious when data with large slag defects were filtered out as shown for the nodularity in Figure 2-5 below. This clearly indicates that all these defect types and microstructural contribute to the variation in elongation but with slag defects as the dominant one.

2.2.3 Compression tests

The compression test data exhibited very small variations, which was expected since such data are not controlled by defects. The compressive stress-strain curve exhibited more hardening than tension as shown in Figure 2-6.

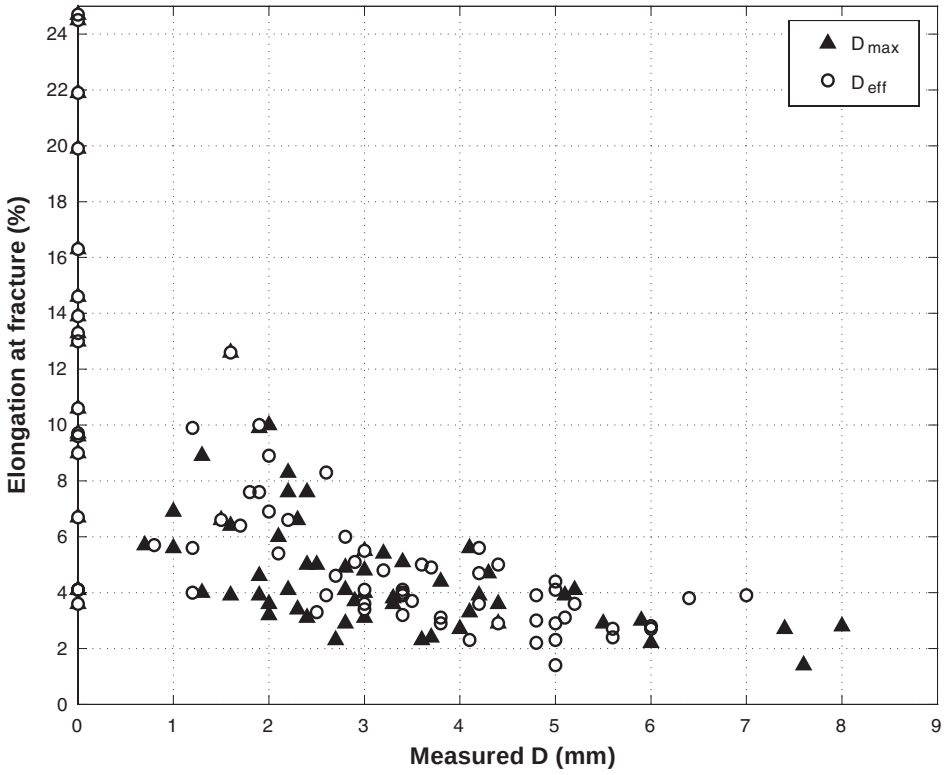

Figure 2-4. *The measured failure strain versus measured size of slag defects using D_{max} and D_{eff}.*

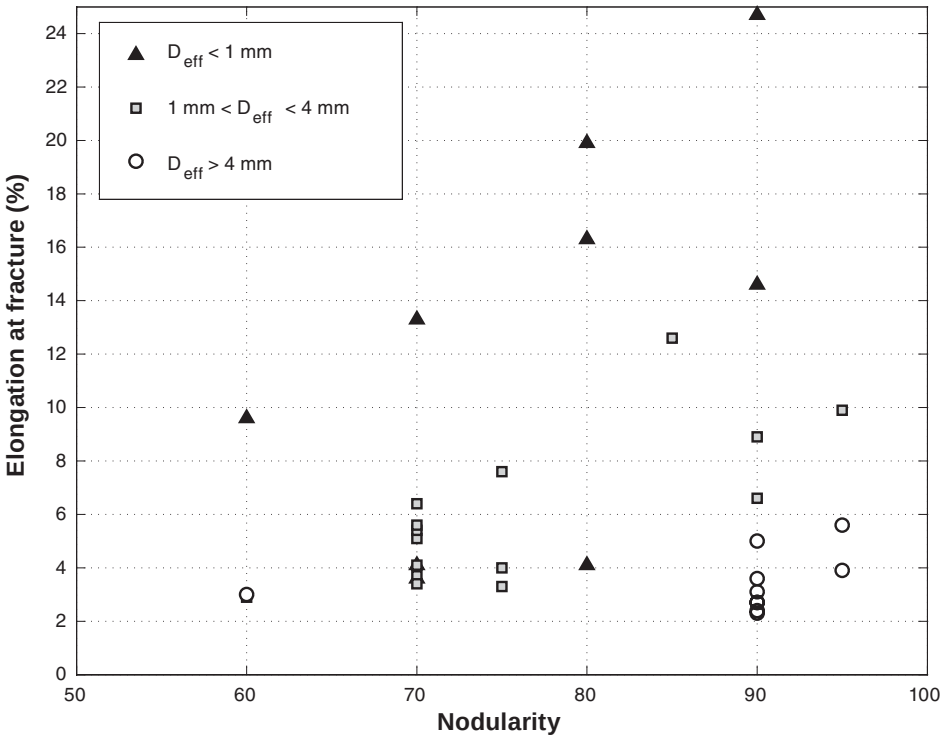

Figure 2-5. *Measured elongation at fracture versus nodularity for different slag defect sizes.*

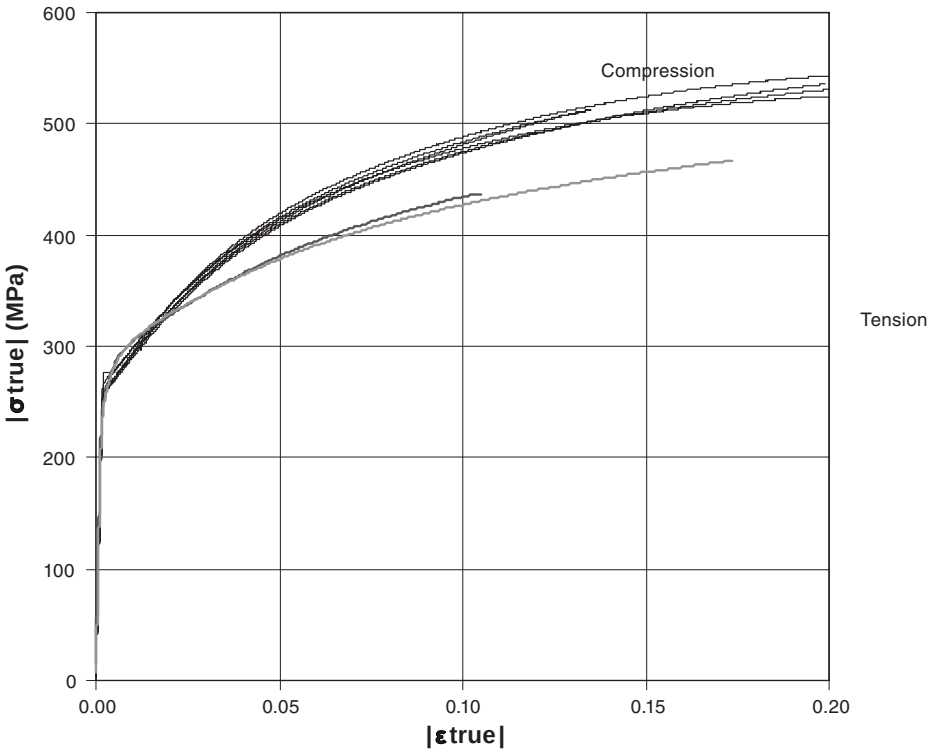

Figure 2-6. *Compressive true stress – true strain curves measured for I24 and I25 together with two selected tensile true stress – true strain plots (same sampling orientation).*

2.2.4 Fracture mechanics tests

The Royal Institute of Technology (KTH) and JRC performed fracture mechanics tests on three-point bend specimens using the ASTM E 1820 standard. The tests were performed mainly at room temperature and to a more limited extent at 0°C, 50°C and 100°C according to Table 2-4, where also the results are summarised. The KTH testing of insert I26 is reported in /D/, while the results for inserts I24 and I25 are reported in /E/. The JRC results are reported in reference /7/.

In all cases the fracture mechanics tests exhibited ductile behaviour with rising $J - \Delta a$ curves as is exemplified in Figure 2-7. Very clearly in these cases the actual initiation value recorded depends on the particular way of evaluation. The ASTM code prescribes an evaluation for an estimated crack growth of 0.2 mm.

It can be noted that there is a non-negligible and consistent difference in fracture toughness between the two test temperatures, which might indicate that there is a change in fracture mechanism. Examination of the fracture surfaces did not show conclusively, however, a difference in mechanisms. There is also a difference between the inserts with insert I25 exhibiting the highest fracture toughness according to the testing performed at KTH. This is different from the JRC test results where the averages from the different inserts showed smaller differences. At present no explanation for difference in results from KTH and JRC, respectively, can be offered.

There was no significant difference between the bottom and upper slab or between specimens taken from the transverse or longitudinal directions. Thus it was concluded that the difference in elongation values was mainly due to differences in inclusions content.

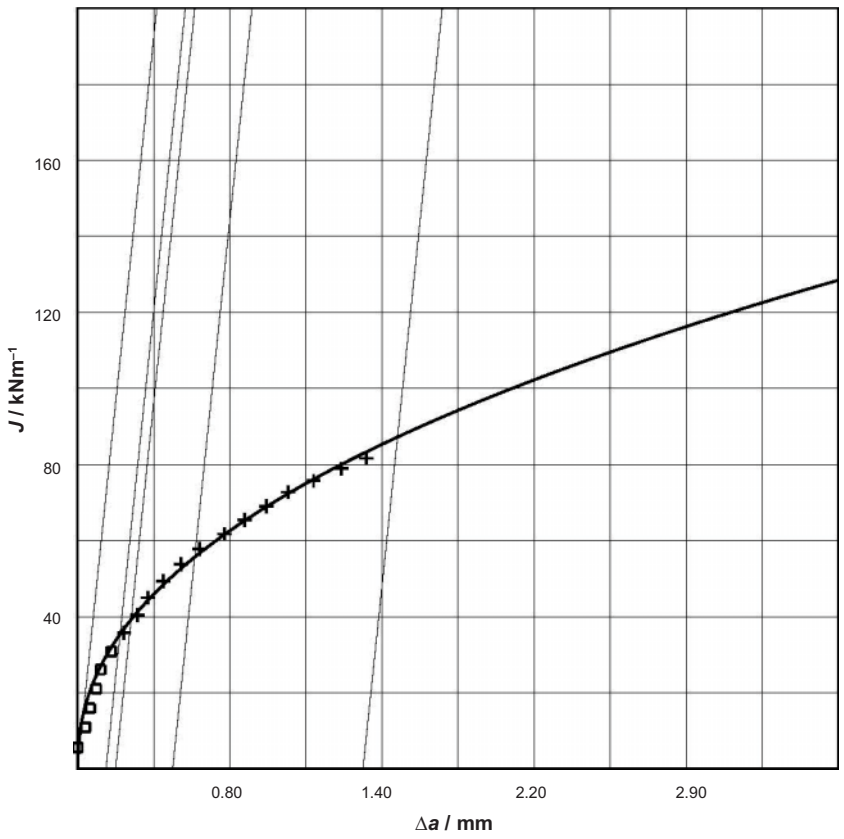

Figure 2-7. *Example of a $J - \Delta a$ curve from one of fracture mechanics experiments at room temperature, J_{Ic} = 39 kN/m.*

Table 2-4. Fracture toughness values J_{Ic}.

Insert number	T = 0°C JRC $J_{Ic}/\mathrm{kNm^{-1}}$	T = 0°C KTH $J_{Ic}/\mathrm{kNm^{-1}}$	T = 23°C JRC $J_{Ic}/\mathrm{kNm^{-1}}$	T = 23°C KTH $J_{Ic}/\mathrm{kNm^{-1}}$	T = 50°C KTH $J_{Ic}/\mathrm{kNm^{-1}}$	T = 100°C KTH $J_{Ic}/\mathrm{kNm^{-1}}$
I24	m = 44	m = 29	m = 42	m = 47	–	–
	s = 4	s = 5	s = 9	s = 10		
I25	m = 39	m = 39	m = 39	m = 59	–	–
	s = 8	s = 8	s = 9	s = 10		
I26	m = 37	m = 21	m = 32	m = 33	m = 25	m = 30
	s = 4	s = 5	s =	s = 4	s = 11	s = 9

3 Analysis

3.1 Semi-analytic determination of defect distributions

The object of this analysis (which is comprehensively described in detail in /4/) was to indirectly determine the defect distribution through the observed elongation behaviour through the following assumptions:

A) The distribution of the failure strain, $f_{\varepsilon}(\varepsilon_0)$ is controlled by:

i) A penny-shaped crack-like defects such as thosse used in the FE-analysis described below and its size distribution, $f_D(D)$, in a given reference volume.

ii) The distribution of the material's fracture toughness, $f_{J_C}(J)$.

B) The crack tip loading, J, is a function of the applied strain, ε_0, and defect distribution $f_D(D)$. It is a stochastic variable because of the defect distribution. There is no interaction between cracks.

C) The crack tip loading and the fracture toughness are independent stochastic variables.

D) The defect size is characterized by an exponential distribution. This is a common assumption for defects and has been supported by many inspections.

An elastic-plastic finite element fracture analysis using the commercial FE-code ABAQUS was first performed to model the reduction in failure strain with defect size. The tensile specimen was modelled as an axisymmetric body with a single penny-shaped crack. Loading was via displacement control. The defect was considered to be flat, i.e. crack-like and located transverse to the loading direction. This is expected to reasonably, but conservatively, represent the slag defects identified on the fracture surfaces. A Ramberg-Osgood deformation plasticity model was adopted to describe the material constitutive behaviour in the analysis. The parameters in the Ramberg-Osgood model were fitted using the room temperature tensile data given in /6, 3/. J-integral values were then calculated versus load for different crack lengths. From these results a fracture strain versus defect size could be inferred for a prescribed fracture toughness.

The computed and experimental relation between elongation at fracture and defect size are shown in Figure 3-1. Two computed curves are given for I26 and I24 respectively. The upper one is with crack growth resistance and the lower one without. The agreement with experiments is rather good. For large defects the computed elongation is below the measured data due to the inherent conservatism in the defect assumption, whereas for very small defects the experimental elongation is below the computed values because the other features become important.

This agreement indicates that observed failure strain values below approximately 6%, are caused by the crack-like defects as seen on the fracture surfaces. The difference in failure strain between the three inserts, and between the top and bottom slabs, can be partly explained by the difference in fracture toughness and the number and size of defects. The data points with small defects (< 2 mm) and low ductility are due to high pearlite content /4/. The scatter in elongation at fracture for a given defect size seen in Figure 3-1 is mainly attributed to various shapes of the defects.

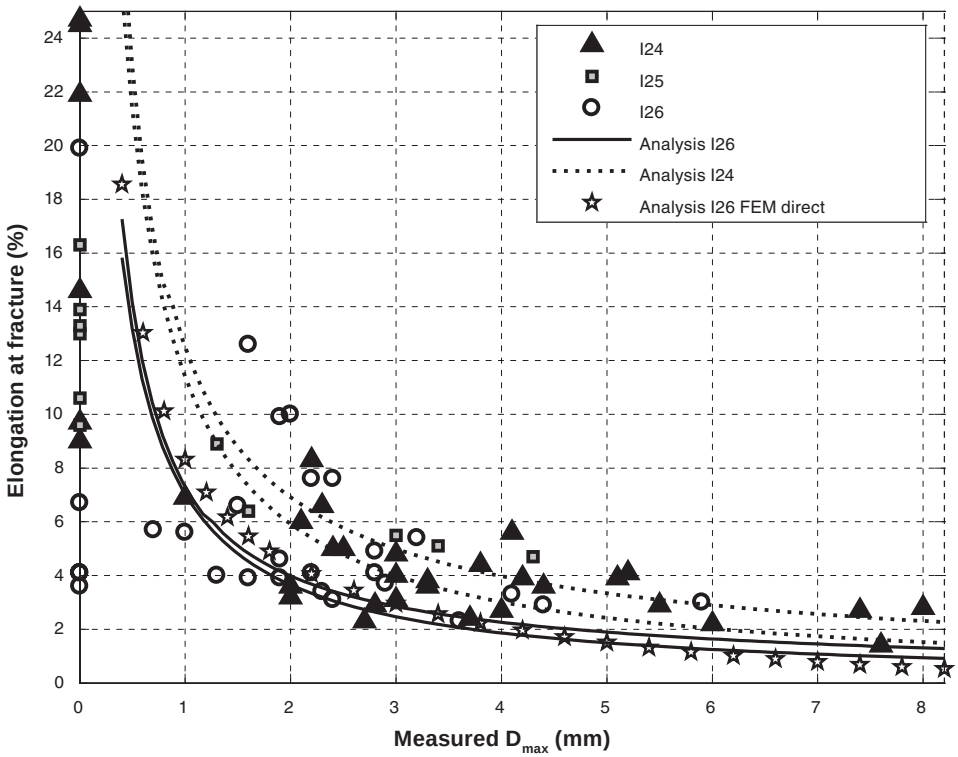

Figure 3-1. *Computed critical strain for I26 and I24 using mean fracture toughness with and without crack growth resistance together with measured elongation at fracture versus measured defect size for insert I24, I25 and I26.*

As mentioned above the size of the largest slag defect is believed to be the main reason for low values and scatter in elongation at fracture. An estimate of the size distribution of a leading slag defect can then be done from the assumptions A)–D). The probability for failure, p_f, can be described by the integral

$$p_f = \int_0^\infty F_{J_C}(x) f_J(x) dx, \tag{1}$$

where $F_{Jc}(x)$ denotes the distribution function for the fracture toughness.

To evaluate the reliability integral the density function $f_J(x)$ must be determined. The stochastic feature of the crack tip loading J results from the distribution of the defect size, $f_D(D)$ and can determined by the transformation,

$$f_J(J) = f_D(D) \cdot \left| \frac{dD}{dJ} \right|. \tag{2}$$

The defect size is assumed to have an exponential distribution, i.e.,

$$f_D(D) = ve^{-vD}, \tag{3}$$

where the mean rate of occurrence, v, (mean defect size is $1/v$) for a specific insert was determined by prescribing measured and computed elongation at fracture to be equal.

The computed critical strain depends much more on the scatter in defect size than the variation in fracture toughness for a particular insert. As a first approximation the fracture toughness can be regarded as a non-random constant. A slightly more general approach was to assign a triangular distribution for the fracture toughness. The above procedure was used to analyse the tensile tests from the three inserts I24, I25 and I26. To assess the

sensitivity to modeling aspects five different cases were analysed for insert I26. Model $I26_N^{32}$ and $I26_N^{60}$ assume no variation in the fracture toughness but use the mean value (32 kN/m) and a value typical after 2 mm of stable tearing (60 kN/m). The method $I26_N^T$ differs from $I26_N^{32}$ in that it uses the triangular fracture toughness distribution. In Model $I26_1^{32}$ it is postulated that there is only one defect in the specimen, whereas for the models with subscript N, the number of defects per specimen was determined as part of the problem (N = 3). The model $NLI26_N^{32}$ is based on nonlinear J-relation inferred from finite element results whereas the other cases uses a linear relation.

The computed probability density functions, f_ε (ε_0), and cumulative density functions, F_ε (ε_0), are depicted in Figure 3-2 versus the applied strain together with the corresponding test data for I26. There is virtually no difference between the triangular and zero-scatter fracture toughness distributions. The model with number of defects free gives a much better overall agreement with the experimental distribution.

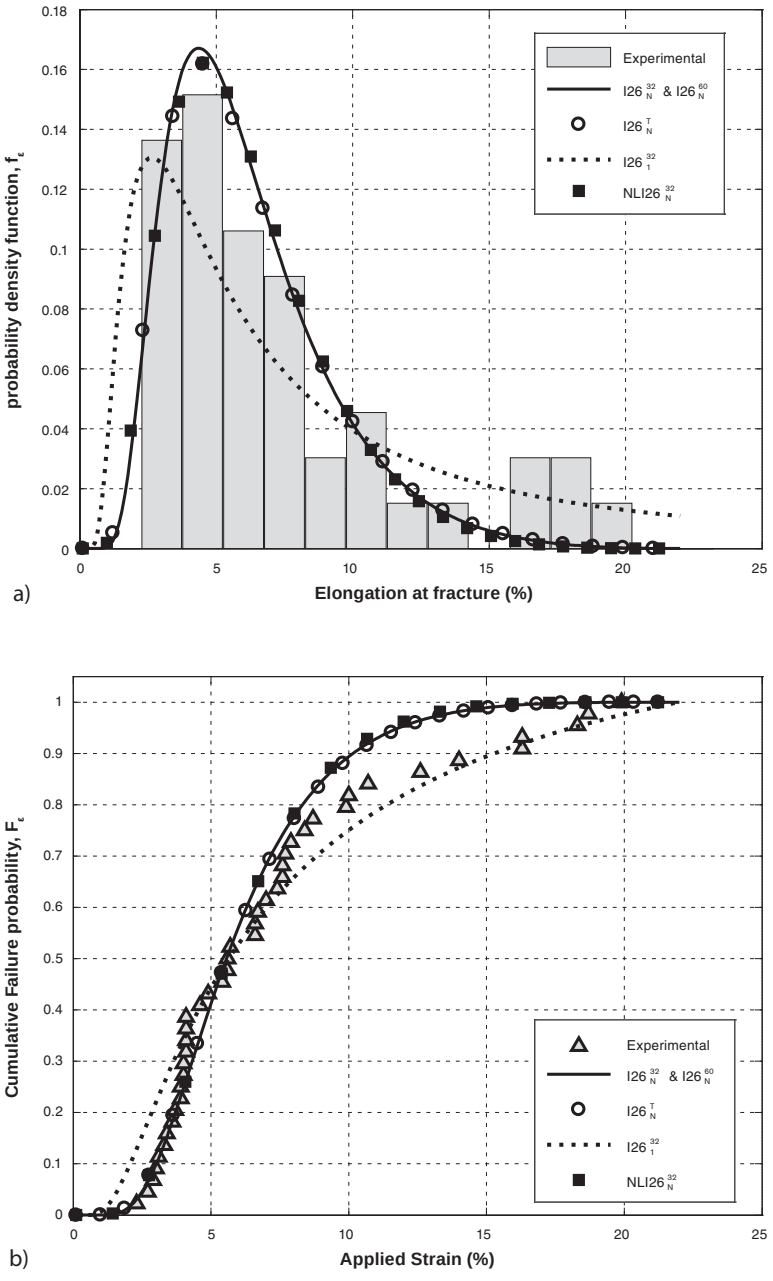

Figure 3-2. *Experimental and computed a) probability density function and b) cumulative failure probability for insert I26.*

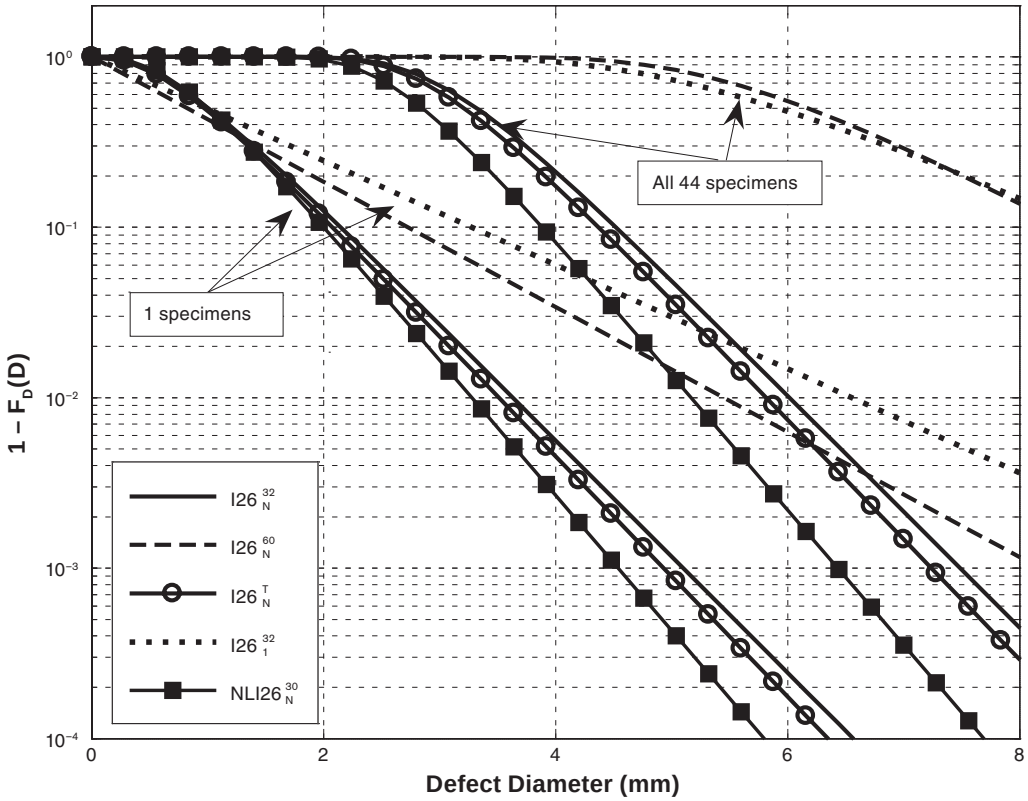

Figure 3-3. *Computed distribution of defect size for insert I26 for the five I26 models.*

The probability that the modelled defect is larger than a specific defect size D is given by $1–F_D(D)$, where F_D (D) is the cumulative defect distribution. This is shown in Figure 3-3 for the I26 models for single specimen and all 44 tested specimens. Note that the five models give different values of the mean defect size.

Corresponding results for the inserts I24 and I25 are reported in /4/. The agreement between computed and measured data for distribution of elongation at fracture and its dependence on the defect size is remarkably good given the various idealizations. There is, however, clearly scope for improving the model further by also accounting for other microstructural features and to account for defect shape and crack growth resistance. Computed mean defect distribution corresponding to "one defect per specimen" was used as input to the probabilistic analysis below.

3.2 Stress and strain FE-analysis of the canister

A large number of Finite Element (FE) analyses (reported in /E/) with aid of the programme ANSYS were performed in order to provide input to the subsequent probabilistic analysis. Since the amount of computational work was very large, the bulk of the analyses were performed on two-dimensional models. In order to verify the relevance of these a comparison with full three-dimensional analysis was conducted. The results of this comparison showed that the two-dimensional computations gave satisfactory accurate results.

From the base model variation of the following properties of the model were made.

a) Influence of internal channel corner radius.

b) Influence of eccentricity of steel cassette. This influence was simulated by changing the outer radius of the canister.

c) Influence of change of the material properties i.e. yield strength and ultimate tensile strength.

The total parameter matrix is summarised in Table 3-1.

In all cases the stress state of the insert was mainly compressive, but there was also a region with tensile stresses at the fuel channel facing the outside of the insert. The size of the region with tensile stresses increased with the applied pressure and also increased as the corner radius became smaller. The total maximum strain could differ by several orders of magnitude at the maximum design load depending on the assumed geometry and yield stress. In Figures 3-4 and 3-5 the maximum strain and stress, respectively, are shown as function the pressure for different corner radii and in Figures 3-6 and 3-7 for different eccentricities.

These results led to the requirement that the corner radius must be between 15–25 mm and that the eccentricity must at most be ± 5 mm**.**

Apart from the small regions around corners discussed above, all stresses were compressive and thus not of any direct interest for considerations of tensile fracture. The critical condition under compression was in the probabilistic analysis assumed to be the attainment of a critical equivalent strain. The computations of the strain levels were performed according to the parameter set in Table 3-1.

Table 3-1. Values of varied parameters.

Parameter	Variable	Index	Number	1	2	3	4	5	Unit
Outer radius	r_1	1	4	474.5	469.5	464.5	459.5		mm
Corner radius	r_2	2	3	15	20	25			mm
Yield stress	$R_{p0.2}$	3	5	200	250	270	290	350	MPa
Ultimate tensile strength	R_m	4	5	400	450	475	500	550	MPa
Total number of combinations (analyses)			300						

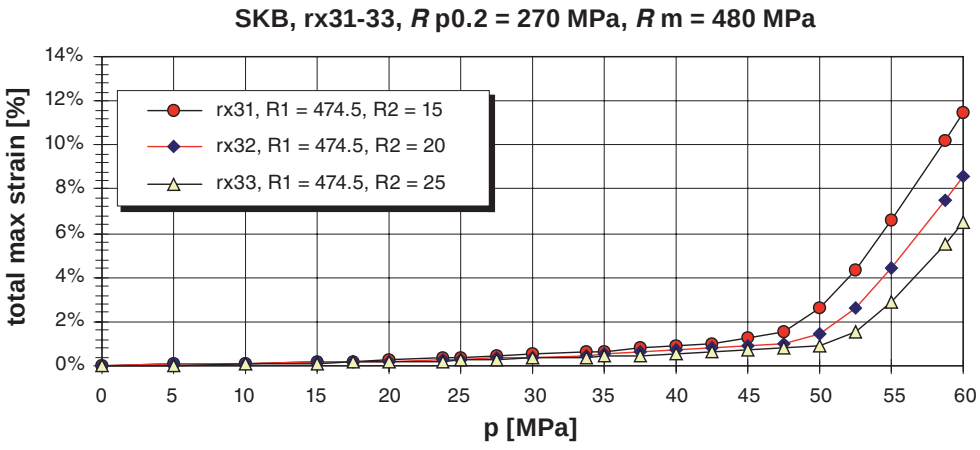

Figure 3-4. *Maximum strain as a function of pressure for different values of the corner radius.*

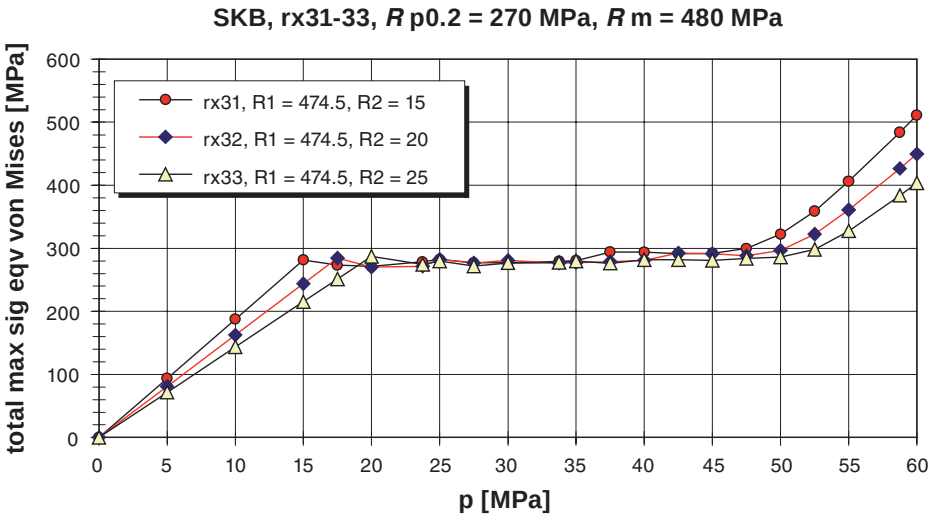

Figure 3-5. *Maximum effective stress as a function of pressure for different values of the corner radius.*

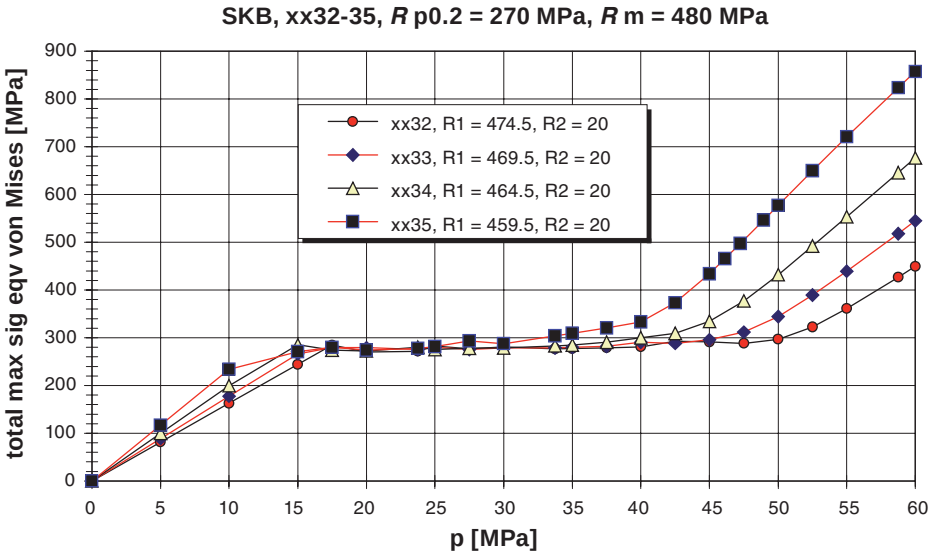

Figure 3-6. *Maximum effective stress as a function of pressure for different values of the eccentricity.*

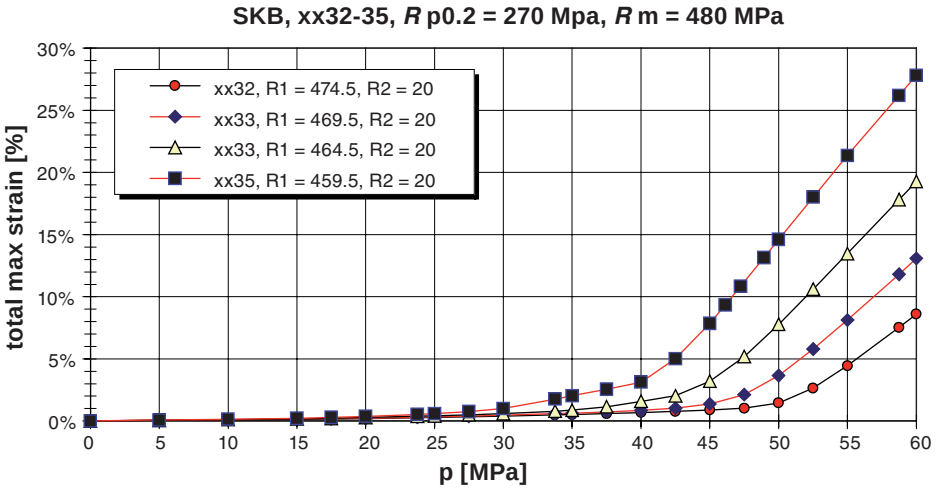

Figure 3-7. *Maximum strain as functions of pressure for different values of the eccentricity.*

4 Probabilistic analysis of canister

Based on the different sets of data obtained from the above-discussed activities, probabilistic analyses were performed using both the FORM and the Monte Carlo methods. These analyses are described in detail in /6/. The material data in Table 4-1 were used throughout the entire investigation. These data were taken from the investigations /C/, /3/ and /4/.

A crucial property for the fracture mechanics analysis is the defect distribution. The exponential distribution derived in /4/ was used for this purpose. It is important to realise what these data represent. The theoretical development in /4/ assumes that this defect size distribution represents the largest defect in a tensile specimen (diameter 14 mm). Thus the probability of occurrence of a defect in a specimen is unity. The probabilistic analysis in /6/ considers the failure probability due a single crack situated at the apex of a corner. This leads to that the so calculated failure probability is that of a slice of the cassette containing the corner and of a thickness roughly corresponding the tensile specimen diameter d. Along the entire length of the cassette L, $n = L/d$ such slices can be considered. Assuming statistical independence the combined failure probability of one corner (there are eight) will be

$$p_{\mathrm{f}}^{\mathrm{tot}} = 1 - (1 - p_{\mathrm{f}})^{n} \approx np_{\mathrm{f}}, \tag{4}$$

the latter since $p_{\mathrm{f}} << 1$. Using $d = 14$ mm will also be a conservative assumption since the crack size distribution will contain cracks that can not be contained in a 14 mm cylinder. In the analysis an exponential distribution was chosen for the crack depth. An aspect ratio (crack length/crack depth) of six and an expected value of the crack depth equal to 1.9 mm were chosen for the basic set of analyses.

There is another extreme assumption as compared to the assumption of statistical independency inherent in (4). This is to assume that all the material properties are constant in the cassette and only the crack size is variable. The results of for instance /5/ indicate that such an assumption in general leads to somewhat smaller estimates of the failure probability than assuming independency.

The failure probability calculations were performed for the different combinations of input data shown in Table 4-1. The results are shown in Table 4-2. Again the importance of limiting possible eccentricity is demonstrated by the values of the failure probabilities.

The combined probability of initiation of crack growth is therefore estimated to be $P_{initiation}^{combined} = 1.98\times10^{-9}$ (for the baseline case using $p = 44$ MPa, $r_{\mathrm{corner}} = 20$ mm, $\delta_{cassette} = 0$ mm).

The corresponding probabilities for plastic collapse are given in Table 4-3. It is clearly seen that at design pressure and lower, the probabilities for tensile fracture dominate over the collapse probability.

Table 4-1. Material properties used in probabilistic analyses.

Property	Type of distribution	Expected value	Standard deviation
K_{Ic}	Normal	83.5 MPa$\sqrt{m}$	11.8 MPa$\sqrt{m}$
σ_Y, in compression. Also assumed in tension.	Normal	270 MPa	6 MPa
σ_{UTS}, compression	Normal	478 MPa	6 MPa
$\varepsilon_{failure}$	Deterministic	10%	–

Table 4-2. The combined probability of initiation of crack growth when p = 40–50 MPa. Results using r_{corner} = 15–25 mm, $\delta_{cassette}$ = 0–15 mm and μ_a = 1.9 mm.

p/MPa	r_{corner}/mm	$\delta_{cassette}$ = 0 mm	$\delta_{cassette}$ = 5 mm	$\delta_{cassette}$ = 10 mm	$\delta_{cassette}$ = 15 mm
	15	2.22×10^{-9}	–	–	–
40	20	2.01×10^{-9}	2.05×10^{-9}	1.24×10^{-8}	4.81×10^{-5}
	25	2.05×10^{-9}	–	–	–
	15	2.72×10^{-9}	–	–	–
44	20	1.98×10^{-9}	2.04×10^{-9}	6.17×10^{-7}	1.78×10^{-3}
	25	2.16×10^{-9}	–	–	–
	15	2.88×10^{-9}	–	–	–
45	20	1.99×10^{-9}	2.04×10^{-9}	1.67×10^{-6}	4.42×10^{-3}
	25	2.19×10^{-9}	–	–	–
	15	1.49×10^{-8}	–	–	–
50	20	3.11×10^{-9}	2.16×10^{-8}	3.11×10^{-3}	2.00×10^{-3}
	25	2.03×10^{-9}	–	–	–

Note: Empty cells represent combinations that were not part of the sensitivity study.

Table 4-3. Probability of plastic collapse when p = 40–50 MPa. Results for r_{corner} = 15–25 mm and $\delta_{cassette}$ = 0–15 mm.

p/MPa	r_{corner}/mm	$\delta_{cassette}$ = 0 mm	$\delta_{cassette}$ = 5 mm	$\delta_{cassette}$ = 10 mm	$\delta_{cassette}$ = 15 mm
	15	1.13×10^{-20}	–	–	–
40	20	1.96×10^{-44}	3.78×10^{-20}	2.28×10^{-9}	0.142
	25	$< 1.10\times10^{-50}$	–	–	–
	15	1.56×10^{-7}			
44	20	1.40×10^{-21}	7.53×10^{-10}	0.264	1.00
	25	2.39×10^{-41}			
	15	2.30×10^{-5}	–	–	–
45	20	3.47×10^{-17}	6.85×10^{-8}	0.751	1.00
	25	7.37×10^{-35}	–	–	–
	15	0.877	–	–	–
50	20	1.09×10^{-4}	1.00	1.00	1.00
	25	2.28×10^{-14}	–	–	–

Note: Empty cells represent combinations that were not part of the sensitivity study.

5 Discussion

The resulting failure probabilities are so low that their significance can be debated. However, if the resulting failure probability would have been so high as to be within interpretable ranges, these would have shown up in the computations performed.

When performing probabilistic assessments, then preferably the data assumed should be as accurate as possible i.e. all uncertainty should be covered by the assumed distributions. Unfortunately this is almost never possible to achieve and therefore deterministic conservative assumptions are mostly introduced. In the present study a number of such conservative assumptions were used.

- The R6 method for calculating J is a conservative approach.
- No credit has been taken for possible risk reducing effects of non-destructive testing.
- The load bearing capacity of the steel cassette and the copper cylinder has been neglected.
- The results of the present report are based on manufacturing of trial canisters. As the production methods improve, the failure probability will be further reduced.

6 Conclusions

- The regions with tensile stresses are very spatially limited provided that the requirements for eccentricity and corner radius are met. In spite of this the probabilities of tensile fracture dominates at the design pressure and lower.
- The low elongation values for some of the samples could conclusively be attributed mainly to the presence of slag inclusions and also to low nodularity and to high pearlitic content. A simple probabilistic model for the elongation distribution could be successfully connected to the observed inclusion distribution.
- The fracture mechanics tests exhibited a ductile character. Some questions remain regarding the interpretation of the fracture toughness results. This is, however, of no concern for overall failure probability.

References

/1/ **Goodrich G M, 1997.** Cast iron Microstructure Anomalies and Their Causes, Cast Iron Quality Control Committee 5J Report, AFS Transactions, 97–30, 1997, pp 669–683.

/2/ **Moretto, 2004.** Fractography of tensile specimens from canister insert I26, JRC Internal Report TN.P.0310.02.

/3/ **Minnebo P, 2004.** "Statistical analysis of Engineering tensile properties of nuclear waste canister insert material, EUR21487EN, Joint Research Centre of the European Commission.

/4/ **Nilsson K-F, Blagoeva D, Moretto P, 2005.** An experimental and numerical analysis to correlate variation in ductility to defects and microstructure in ductile cast iron components, article to appear in Engineering Fracture Mechanics.

/5/ **Nilsson F, 1977.** A model for fracture mechanical estimation of the failure probability of reactor pressure vessels, Proceedings Third International Conference on Pressure Vessel Technology, Part II, The American Society for Mechanical Engineers, New York, 1977, 593–601.

/6/ **Dillström P, 2005.** Probabilistic analysis of canister inserts for spent nuclear fuel, SKB TR-05-19, Svensk Kärnbränslehantering AB.

/7/ **Minnebo P, 2005.** Fracture Properties of Ductiel Cast Iron used for Thick-Walled Components, Euro Report EUR21841EN, Joint Research Institute of the European Commission.

Appendices

/A/ **Carlsson S, 2003.** Test plan, ÅF-IS Report B729, Rev. 01, June 2003.

/B/ **Carlsson S, 2003.** Test plan for inserts I24 and I25, ÅF-IS Report B757-1, Oct 2003.

/C/ **Björkegren L-E, 2003.** Mechanical properties of the cylinder for nuclear fuel storage, Report19072LEB/et, The Swedish Foundry Association, 2003.

/D/ **Öberg H, 2003.** Fracture toughness testing of nodular cast iron, Report SKB0304rep, Department of Solid Mechanics, KTH, October 2003.

/E/ **Öberg H, 2004.** Fracture toughness testing of nodular cast iron, I24 and I25. Report SKB0401rep, Department of Solid Mechanics, KTH, April 2004.

/F/ **Erixon B, 2004.** Solid mechanics analyses for probalistic analysis of canister structural strength, ÅF-S Report B794, 2004.

Appendix A

Author
Susanna Carlsson
Phone +46-8-6571563
Fax 08-657 37 01
susanna.carlsson@af.se

Date
2003-06-12

Our ref
ssc

ÅF-IS REPORT B729, REV 01

Test plan

Commission nr: 203253

Content **Page**

SUMMARY 3

1 BASIC CONDITIONS 3

2 REFERENCE TESTING, 3PB-SPECIMENS 3

3 TENSILE TESTS 9

4 COMPRESSION TESTS 10

REPORT HISTORY

Report title: Test plan
Commission nr: 203253

Date	Activity	Iss	Chk	App
2003-06-26	Rev 01, geometries of tensile test specimens changed	SSC		

SUMMARY

Within the project uniaxial tensile and compression tests as well as fracture tests will be performed. All testing will be planned, but a detailed planning is first done for insert I26. The detailed test plan for the remaining tests will be based on the outcome from the first test series.

1 BASIC CONDITIONS

The inserts, labelled I24, I25 and I26 respectively, will be manufactured during the spring 2003. The specimen will be taken from at least two slabs of each insert, one from the bottom and one from the top. The bottom slab is homogeneous with a thickness of at least 80 mm, whereas the top slab has a thickness of at least 230 mm and contains holes. Gjuteriföreningen receives half a slab, with thickness about 40 mm, from top and bottom slab respectively to manufacture specimens. Specimens to be tested by KTH and JRC will be manufactured from the remaining parts.

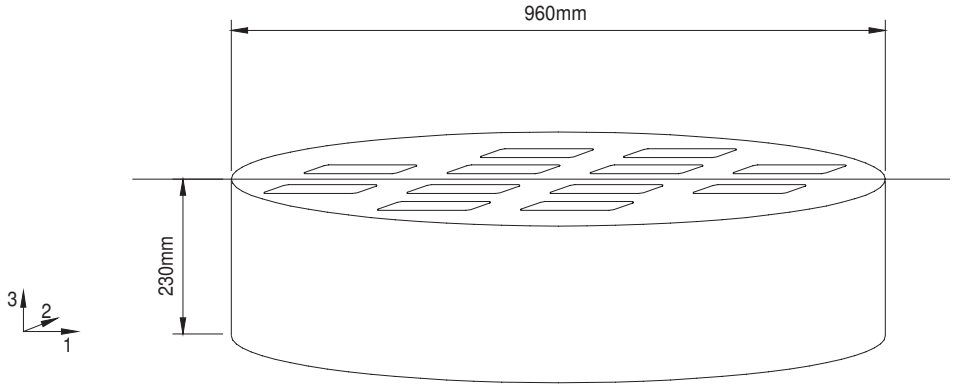

Figure 1. Top slab from insert

2 REFERENCE TESTING, 3PB-SPECIMENS

A reference curve to be used as a basis for the fracture tests will be derived in the temperature interval 0°C to 100°C. This reference curve will be used to select an optimal test temperature for the fracture tests. Specimens for the reference tests will be taken from insert I26. Three-point bend (3PB) is proposed as specimen geometry because it is easier to control the cooling with this geometry compared to CT-specimens.

For non-linear testing the ligament as well as specimen width must satisfy the following size criterion:

$$t, a \geq M \frac{J_{\mathrm{IC}}}{R_{\mathrm{p0.2}}}.$$

Assessment of previous tests resulted in a minimum value for $R_{\mathrm{p0.2}} = 240$ MPa and for $E = 160000$ MPa. Testing of corresponding cast material indicates that

$K_{IC} = 50\ \text{MPa}\sqrt{\text{m}}$. For cleavage M is set to 200 ($M = 200$), which results $t, a \geq 0.013$ m. Specimen with dimension $140 \times 30 \times 15$ will be used, see Figure 2.

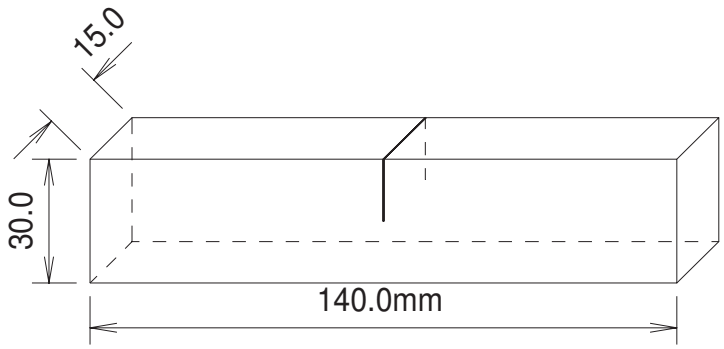

Figure 2. Schematic drawing of three-point bend specimen

The specimen will be oriented such that the 30 mm-direction coincides with the axial direction of the insert. In total 24 in-plane specimens will be taken from the top slab as indicated in Figure 3 to Figure 5.

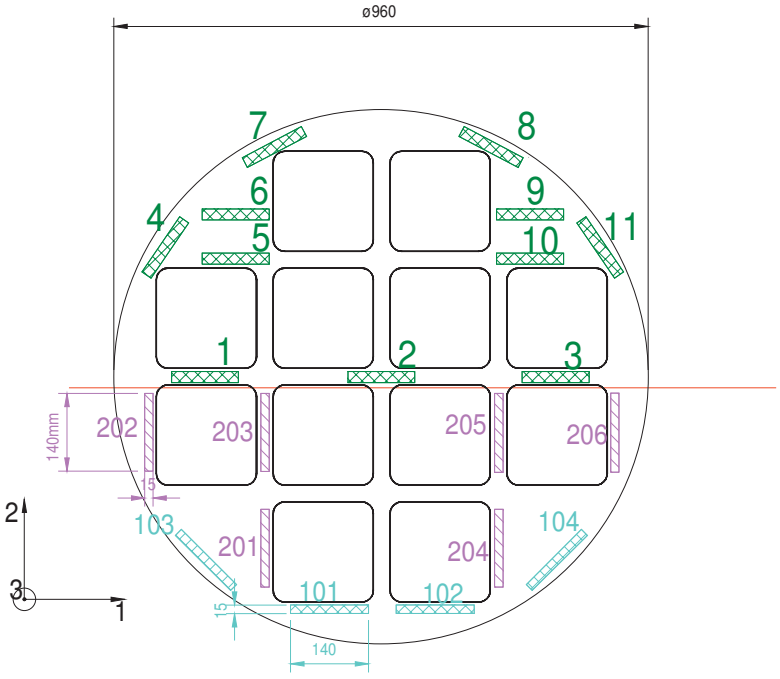

Figure 3. Schematic drawing of in-plane 3PB- specimen with numbering from top layer (Layer 1). The half of the slab above the red line will be sent to Gjuteriföreningen.

In order to have a sufficient number of specimens, specimens will be taken from several layers, see Figure 4. The cutting clearance is estimated to be about 7 mm.

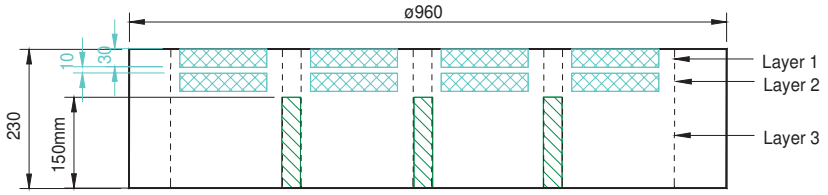

Figure 4. Schematic drawing of axial cross-section.

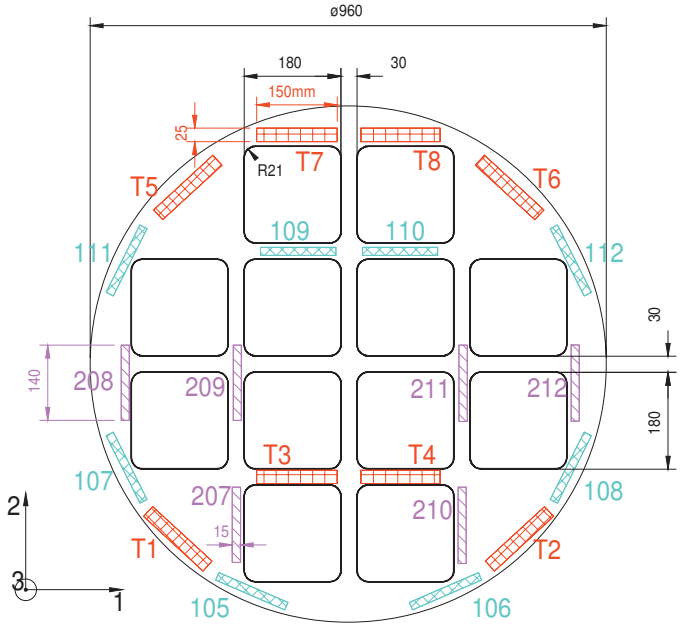

Figure 5. Schematic drawing of layer 2 with specimen numbering. T# indicates in-plane tensile specimens.

In addition eight axial specimens (i.e. parallel to the axial direction of the insert) will be taken out to investigate whether the material properties have a direction dependency. The location of these specimens is indicated in Figure 6 together with the in-plane specimens.

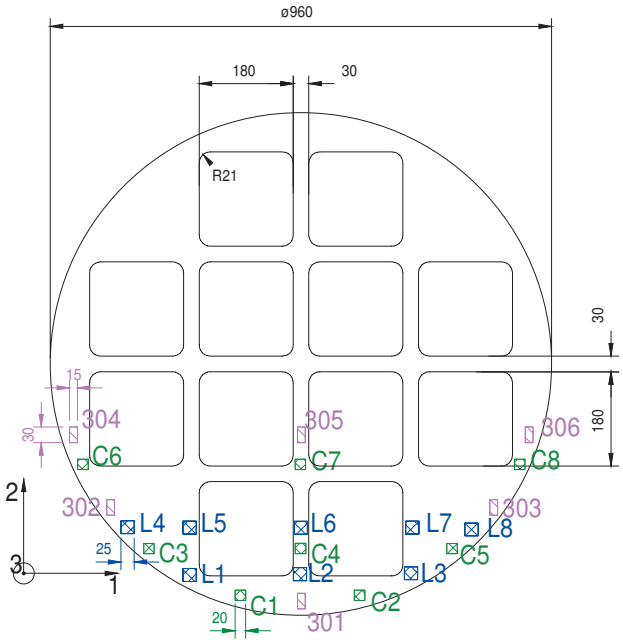

Figure 6. Schematic illustration of the axial 3PB- specimens as well as tensile and compression specimen with numbering, (layer 3). The Prefix L stands for axial tensile specimens and C for compression specimens.

From the bottom slab of insert I26, 24 specimens will be taken as seen Figure 7. 3PB-in-plane specimens will be taken from locations similar to those in the top slab and with corresponding numbering. The thickness of the bottom plate is not sufficient to accommodate axial specimens but the number of specimens is considered sufficient.

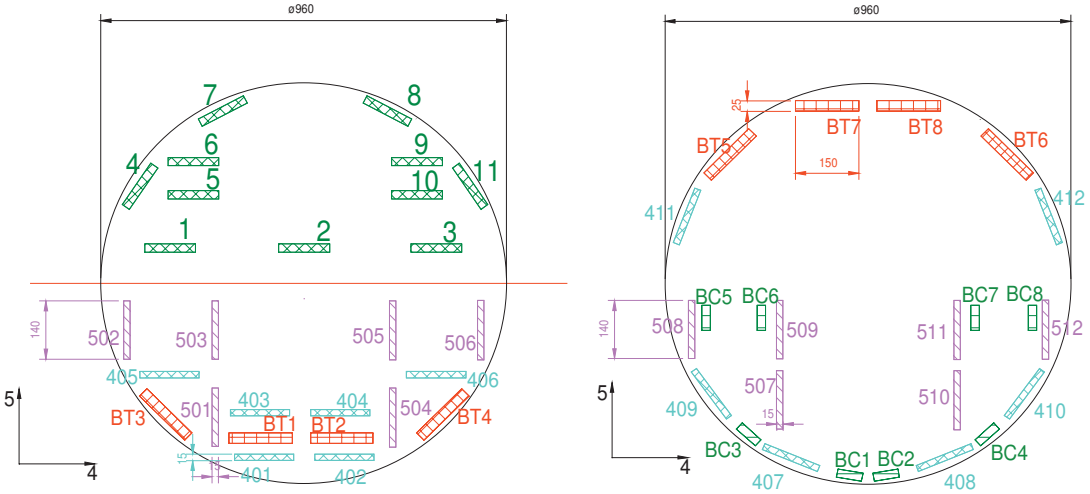

Figure 7. Location and numbering of specimen in layer 1 and 2 of bottom slab, (cf. Figure 8).

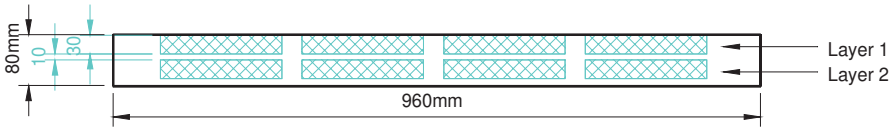

Figure 8. Schematic drawing of axial distribution of specimen in bottom slab.

Sixteen 3PB specimens will be used for the reference tests, where 10 tested are at 0°C and 3+3 at the two other temperatures. From the remaining 3PB specimens KTH will conduct tests at the selected temperature; JRC will perform some complementary tests and some are kept as reserve specimens. The final distribution of the specimens will be determined after assessment of the reference test series. The number of specimens taken out from the inserts I24 and I25 will be reduced if the I26 test series indicate a very limited scatter and/or no dependence of material direction. The order in which the 3PB tests will be conducted as shown in Table 1 to Table 3 has been determined from a random procedure. The reference test series is given in Table 1, whereas the remaining Tables are only indicative until the assessment of the reference tests has been performed

Table 1. Randomly determined order for 3PB-tests, reference test series

Provordn. Nr	Provstav	Temperatur [°C]
1	I26_512	0
2	I26_203	0
3	I26_402	0
4	I26_305	0
5	I26_506	0
6	I26_411	0
7	I26_303	0
8	I26_103	0
9	I26_502	0
10	I26_301	0
11	I26_403	50
12	I26_412	50
13	I26_509	50
14	I26_409	100
15	I26_108	100
16	I26_209	100

Table 2. Randomly determined test order for 3PB tests (not reference test series)

Provordn. Nr	Provstav	Temperatur [°C]
17	I26_511	reserv
18	I26_508	reserv
19	I26_210	reserv
20	I26_507	reserv
21	I26_105	reserv
22	I26_207	reserv
23	I26_501	reserv
24	I26_101	reserv
25	I26_106	provtemperatur
26	I26_202	provtemperatur
27	I26_111	provtemperatur
28	I26_401	provtemperatur
29	I26_204	provtemperatur
30	I26_112	provtemperatur
31	I26_102	provtemperatur
32	I26_410	provtemperatur
33	I26_302	provtemperatur
34	I26_510	provtemperatur
35	I26_304	provtemperatur
36	I26_211	provtemperatur
37	I26_505	provtemperatur
38	I26_307	provtemperatur
39	I26_201	provtemperatur
40	I26_404	provtemperatur
41	I26_504	JRC
42	I26_104	JRC
43	I26_405	JRC
44	I26_208	JRC
45	I26_503	JRC
46	I26_306	JRC
47	I26_408	JRC
48	I26_212	JRC
49	I26_206	JRC
50	I26_109	JRC
51	I26_110	JRC
52	I26_406	JRC
53	I26_205	JRC
54	I26_308	JRC
55	I26_107	JRC
56	I26_407	JRC

3 TENSILE TESTS

Two slightly different tensile specimens will be used. The specimen shown in Figure 9 will be used by Svenska Gjuteriföreningen AB, and the specimen shown in Figure 10 will be used by JRC.

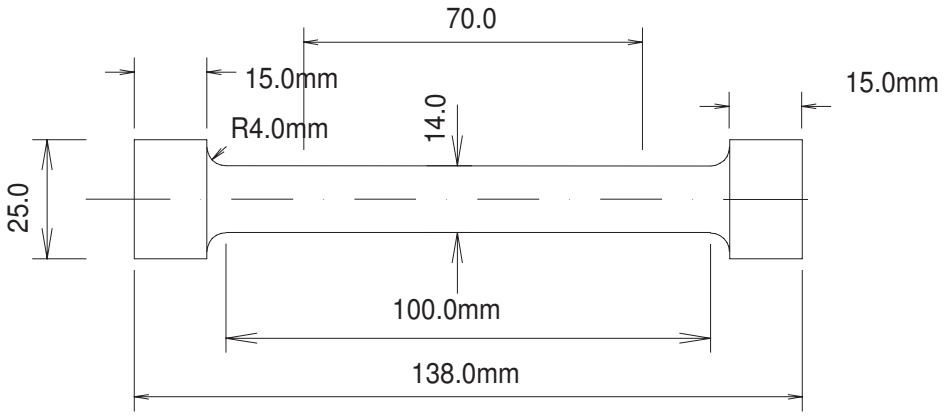

Figure 9. Tensile specimen to be used by Gjuteriföreningen.

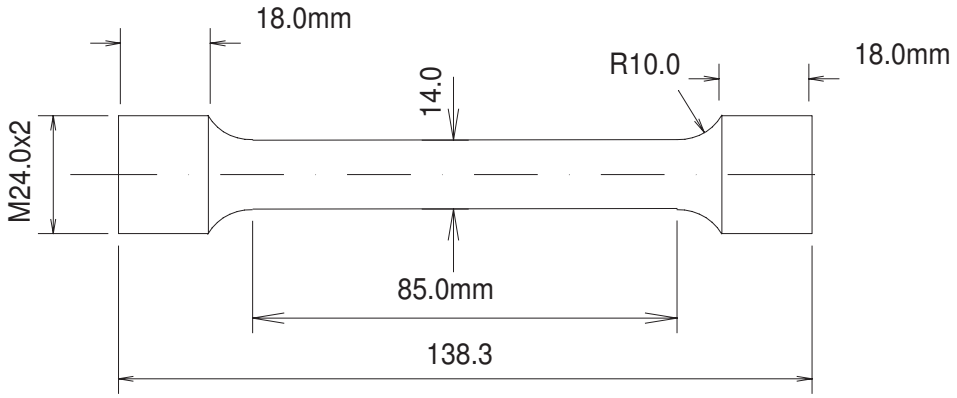

Figure 10. Tensile specimen to be used by JRC.

The specimens will be taken from the slabs as indicated in Figure 5 and Figure 6. Sixteen tensile specimens will be taken from each top slab, with eight in the axial direction and eight in the in-plane direction. The labelling of the eight in-plane tensile specimens from the bottom plate is the same as in the top slab but with a prefix B. Because the specimen length exceeds the thickness of the bottom, specimens in the axial direction will only be taken from the top slab.

Table 3. Randomly determined test order for tensile tests

Provordn. Nr	Provstav
1	I26 T1
2	I26 L8
3	I26 T7
4	I26 BT7
5	I26 BT6
6	I26 L5
7	I26 L1
8	I26 BT8
9	I26 BT4
10	I26 L6
11	I26 BT3
12	I26 L7
13	I26 T5
14	I26 T2
15	I26 T4
16	I26 L2
17	I26 BT2
18	I26 T3
19	I26 BT5
20	I26 L4
21	I26 T6
22	I26 BT1
23	I26 L3
24	I26 T8

In addition to the specimens in Table 3, Gjuteriföreningen will receive 22 specimens.

4 COMPRESSION TESTS

Compression specimens as defined in ASTM E9 will be used with dimensions given in Figure 11.

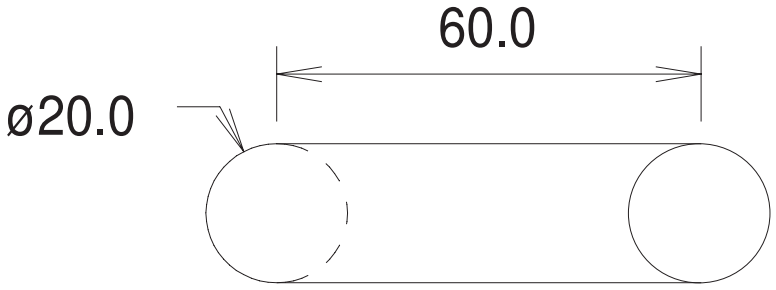

Figure 11. Specimen geometry for compression test.

These specimens (with prefix C) will be taken from the insert from the top and bottom slab as shown in Figure 6 and Figure 7 respectively. Because of the limited thickness of the bottom slab, the compression specimens will here be taken from an in-plane direction instead.

Table 4. Randomly determined test order for compression tests

Provordn. Nr	Provstav
1	I26 C5
2	I26 BC7
3	I26 BC6
4	I26 C8
5	I26 C6
6	I26 BC8
7	I26 BC5
8	I26 BC1
9	I26 BC4
10	I26 BC2
11	I26 C4
12	I26 C1
13	I26 C3
14	I26 C7
15	I26 BC3
16	I26 C2

Author
Susanna Carlsson
Phone +46-8-6571563
Fax 08-657 37 01
susanna.carlsson@af.se

Date
2003-10-22

Our ref
ssc

ÅF-IS REPORT B757, REV 01

Test plan for insert *I24* and *I25*

Commission nr: 203253

Content **Page**

SUMMARY 3

1 BASIC CONDITIONS 3

2 3PB-SPECIMENS 4

3 TENSILE TESTS 7

4 COMPRESSION TESTS 10

5 REFERENCES 11

REPORT HISTORY

Report title: Test plan for insert I24 and I25
Commission nr: 203253

Date	Activity	Iss	Chk
2003-10-03	Report finished	SSC	AND
2003-10-07	Formulation changed	SSC	
2003-10-22	Rev 01, adding compression specimens	SSC	

SUMMARY

Within the project, uniaxial tensile and compression tests as well as fracture tests will be performed. Testing has been perfomed for insert I26, and the detailed test plans for insert I24 and I25 are presented in this report.

1 BASIC CONDITIONS

Specimens will be taken from two slabs of each insert, one from the bottom and one from the top as illustrated in Figure 1. The bottom slab is homogeneous with a thickness of at least 90 mm, whereas the top slab has a thickness of at least 300 mm and contains holes. Gjuteriföreningen has received half a slab, with a thickness of about 40 mm, from top and bottom slab respectively. Specimens to be tested by KTH and JRC will be manufactured from the remaining parts.

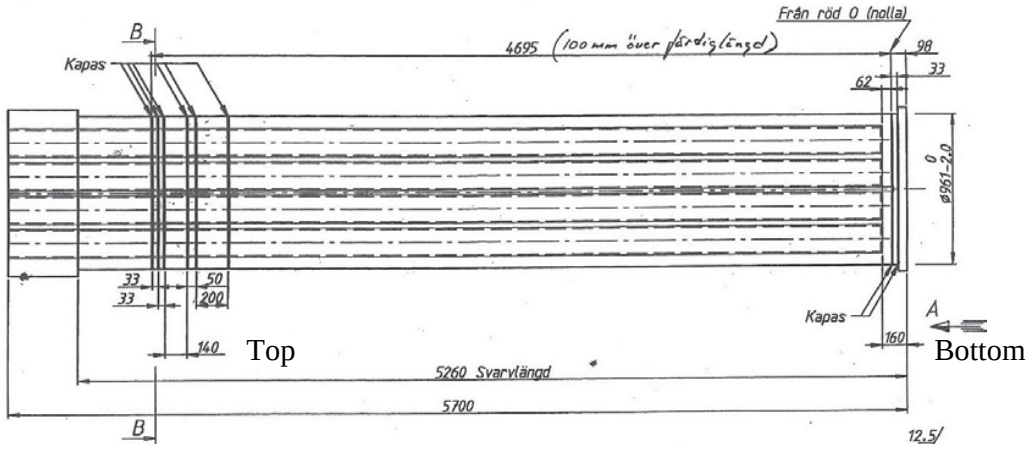

Figure 1. Sketch of canister insert with definition of top and bottom part.

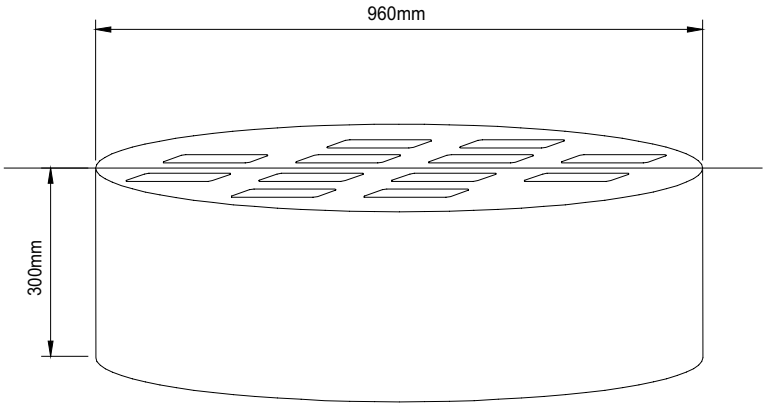

Figure 2. Top slab from insert

2 3PB-SPECIMENS

From the evaluation of test resuls from insert I26, it is decided that the following tests will be performed at 0°C temperature as well as at room temperature. Three-point bend (3PB) specimens with dimension 140· 30· 15 will be used, cf. [1]. The specimen dimensions are illustrated in Figure 3.

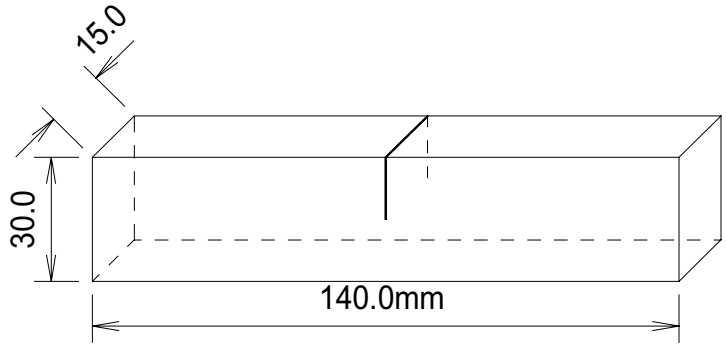

Figure 3. Schematic drawing of three-point bend specimen

In order to have a sufficient number of specimens, specimens will be taken from three layers, see Figure 4. The cutting clearance is estimated to be about 7 mm, but some extra clearence is added.

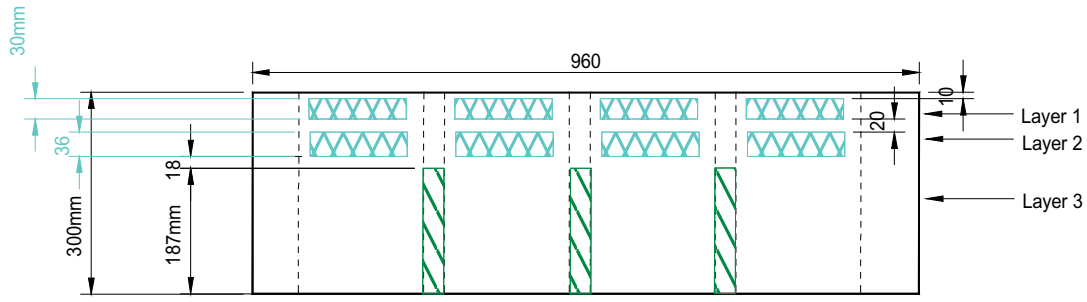

Figure 4. Schematic drawing of axial cross-section.

In total 14 in-plane 3PB-specimens will be taken from the top slab as indicated in Figure 5 and Figure 6. The in-plane specimens will be oriented such that the 30 mm-direction coincides with the axial direction of the insert. In addition, five axial specimens (i.e. parallel to the axial direction of the insert) will be taken out. The location of these specimens (301-305) is indicated in Figure 7.

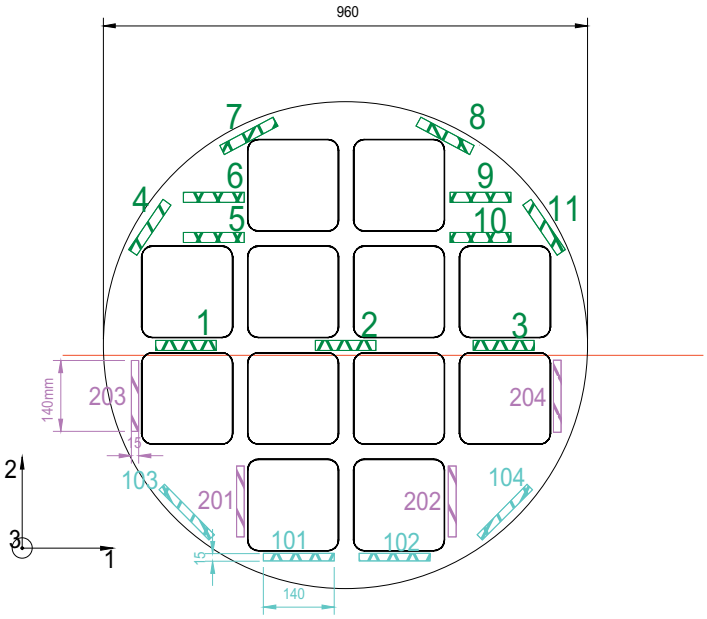

Figure 5. Schematic drawing of in-plane 3PB- specimen with numbering from top layer (Layer 1). The half of the slab above the red line belongs to Gjuteriföreningen.

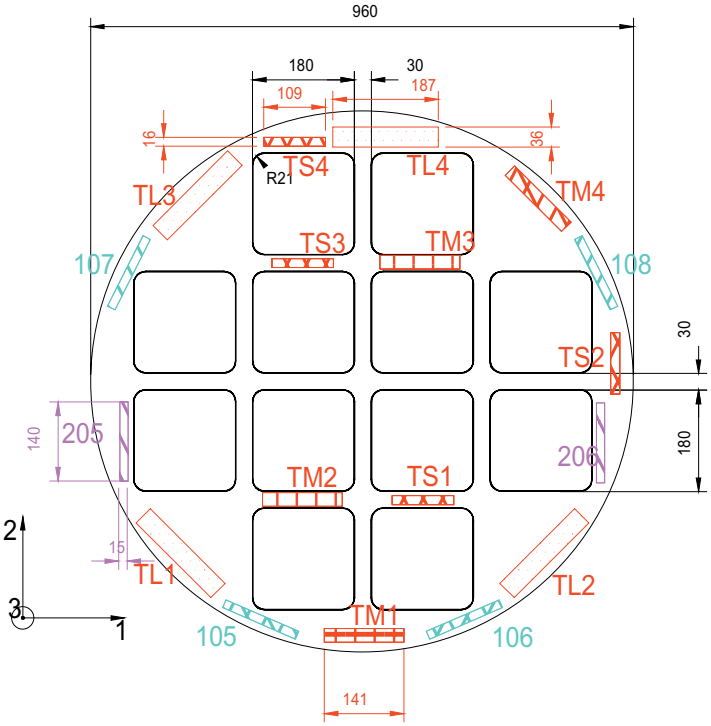

Figure 6. Schematic drawing of layer 2 with specimen numbering. T# indicates in-plane tensile specimens.

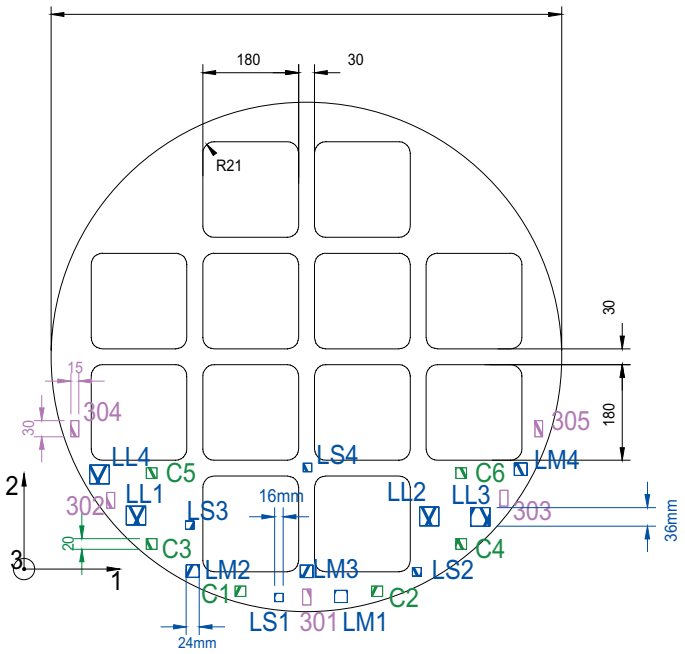

Figure 7. Schematic illustration of the axial 3PB- specimens as well as tensile and compression specimen with numbering, (layer 3). The Prefix L stands for axial tensile specimens and C for compression specimens.

From the bottom slab, 16 3PB-specimens will be taken as seen Figure 8. The specimens will be taken from locations similar to those in the top slab and with corresponding numbering. No axial specimens will be taken from the bottom plate.

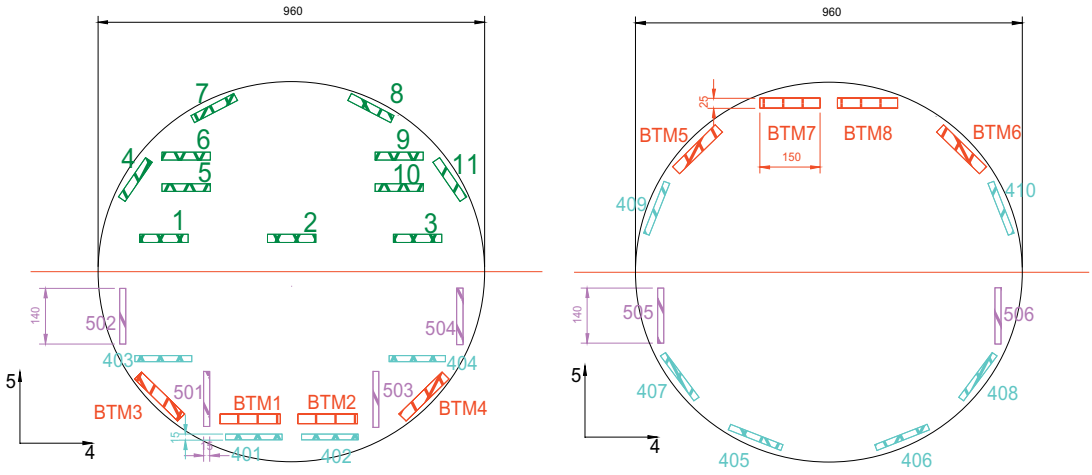

Figure 8. Location and numbering of specimen in layer 1 and 2 of bottom slab, (cf. Figure 9).

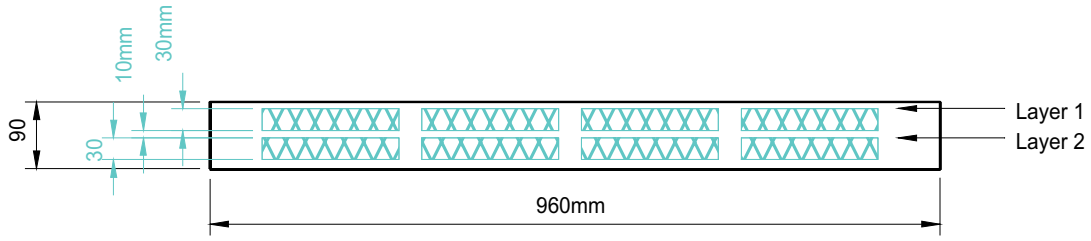

Figure 9. Schematic drawing of axial distribution of specimen in bottom slab.

Both KTH and JRC will test 16 3PB specimens, where eight will be tested at 0°C and eight at room temperature. The number of specimens taken out from the inserts, I24 and I25, are reduced compared with the I26 test series. The order in which the 3PB tests will be conducted is shown in Table 1, and has been determined from a random procedure.

Table 1. Randomly determined order for 3PB-tests

Test order	Test spec.	Temp. [°C]	test institute
1	I24_205	0	KTH
2	I24_503	0	KTH
3	I24_303	0	KTH
4	I24_105	0	KTH
5	I24_404	0	KTH
6	I24_502	0	KTH
7	I24_101	0	KTH
8	I24_405	0	KTH
9	I24_204	room temp.	KTH
10	I24_501	room temp.	KTH
11	I24_302	room temp.	KTH
12	I24_408	room temp.	KTH
13	I24_206	room temp.	KTH
14	I24_108	room temp.	KTH
15	I24_103	room temp.	KTH
16	I24_104	room temp.	KTH
17	I24_406	0	JRC
18	I24_107	0	JRC
19	I24_305	0	JRC
20	I24_102	0	JRC
21	I24_407	0	JRC
22	I24_203	0	JRC
23	I24_505	0	JRC
24	I24_504	0	JRC
25	I24_401	room temp.	JRC
26	I24_301	room temp.	JRC
27	I24_506	room temp.	JRC
28	I24_410	room temp.	JRC
29	I24_402	room temp.	JRC
30	I24_409	room temp.	JRC
31	I24_403	room temp.	JRC
32	I24_202	room temp.	JRC
33	I24_106	reserve	
34	I24_201	reserve	
35		reserve	

Test order	Test spec.	Temp. [°C]	test institute
1	I25_407	0	KTH
2	I25_202	0	KTH
3	I25_410	0	KTH
4	I25_401	0	KTH
5	I25_204	0	KTH
6	I25_406	0	KTH
7	I25_305	0	KTH
8	I25_301	0	KTH
9	I25_405	room temp.	KTH
10	I25_403	room temp.	KTH
11	I25_409	room temp.	KTH
12	I25_504	room temp.	KTH
13	I25_304	room temp.	KTH
14	I25_502	room temp.	KTH
15	I25_104	room temp.	KTH
16	I25_505	room temp.	KTH
17	I25_107	0	JRC
18	I25_106	0	JRC
19	I25_501	0	JRC
20	I25_408	0	JRC
21	I25_103	0	JRC
22	I25_101	0	JRC
23	I25_503	0	JRC
24	I25_105	0	JRC
25	I25_201	room temp.	JRC
26	I25_404	room temp.	JRC
27	I25_108	room temp.	JRC
28	I25_302	room temp.	JRC
29	I25_102	room temp.	JRC
30	I25_506	room temp.	JRC
31	I25_402	room temp.	JRC
32	I25_205	room temp.	JRC
33	I25_303	reserve	
34	I25_203	reserve	
35	I25_206	reserve	

3 TENSILE TESTS

Two slightly different tensile specimens will be used. The specimen shown in Figure 10 will be used by Svenska Gjuteriföreningen AB, and the specimen shown in Figure

12 will be used by JRC. Additionally, JRC will investigate size effects by testing specimens of different cross section areas, using the specimen geometries defined in Figure 11 and Figure 13.

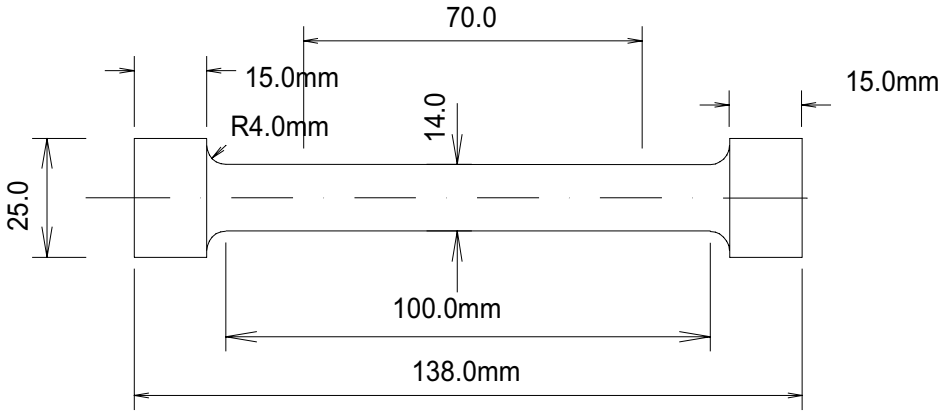

Figure 10. Tensile specimen to be used by Gjuteriföreningen.

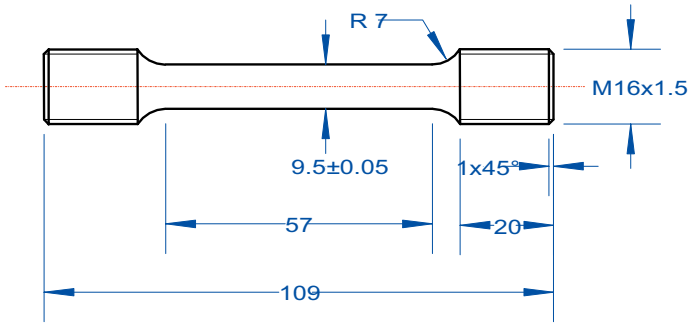

Figure 11. Small tensile test specimen, denoted TS# or LS# in the sketches.

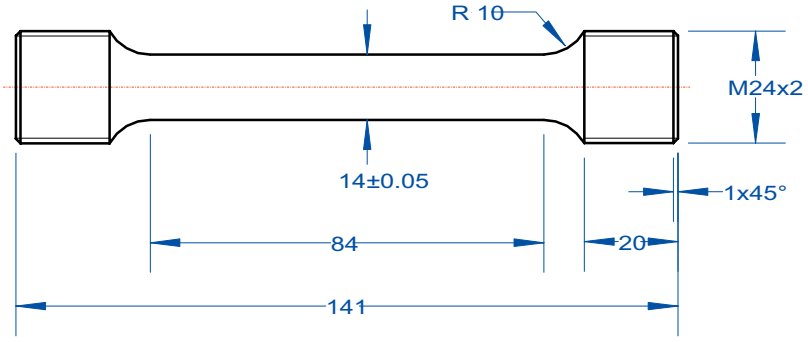

Figure 12. Medium sized tensile test specimen, denoted TM# or LM# in the sketches.

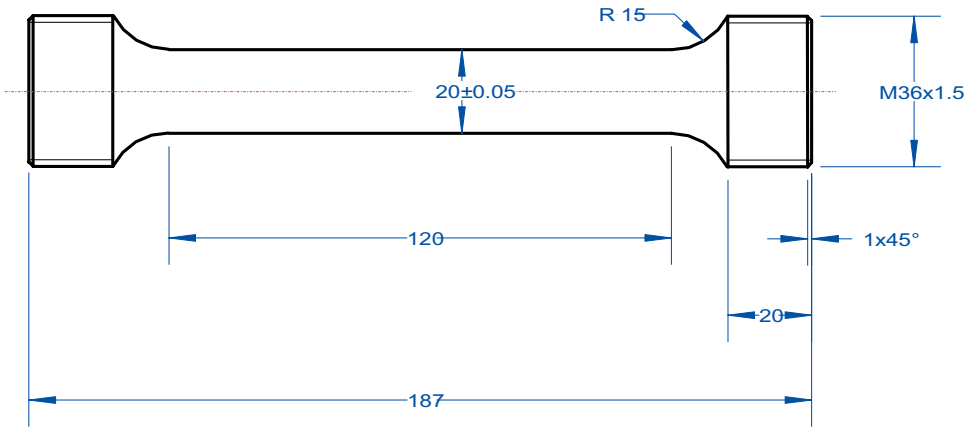

Figure 13. Large tensile test specimen, denoted TL# or LL# in the sketches.

The specimens will be taken from the slabs as indicated in Figure 6 and Figure 7. Eight large, eight medium, and eight small tensile specimens will be taken from the top slab, with four of each size in the axial direction and four of each in the in-plane direction. From the bottom slab, eight medium sized specimens are taken from the axial direction. As the specimen length exceeds the thickness of the bottom, no longitudinal specimens can be achieved. The labelling of the specimens from the bottom plate is similar to the top slab but with a prefix B. The test order for the tensile tests is presented in Table 2.

Table 2. Randomly determined test order for tensile tests

Test order	Test spec. I24	Test spec.I25	Temperature [°C]
1	I24_BTM8	I25_LM2	room temperature
2	I24_TM3	I25_BTM8	room temperature
3	I24_LM4	I25_LM3	room temperature
4	I24_LM3	I25_TM4	room temperature
5	I24_BTM6	I25_BTM7	room temperature
6	I24_BTM3	I25_BTM1	room temperature
7	I24_LM2	I25_TM2	room temperature
8	I24_TM1	I25_BTM2	room temperature
9	I24_BTM5	I25_BTM6	room temperature
10	I24_LM1	I25_TM1	room temperature
11	I24_BTM1	I25_BTM3	room temperature
12	I24_BTM4	I25_TM3	room temperature
13	I24_BTM7	I25_BTM5	0
14	I24_BTM2	I25_LM4	0
15	I24_TM2	I25_BTM4	0
16	I24_TM4	I25_LM1	0
1	I24_TL4	I25_TS1	room temperature
2	I24_TL3	I25_LS2	room temperature
3	I24_LL2	I25_LS3	room temperature
4	I24_TL2	I25_LL3	room temperature
5	I24_LS3	I25_LS4	room temperature
6	I24_LL1	I25_TS4	room temperature
7	I24_TL1	I25_LS1	room temperature
8	I24_LS1	I25_LL4	room temperature
9	I24_LS4	I25_TS2	room temperature
10	I24_TS3	I25_TL3	room temperature
11	I24_TS1	I25_TL2	room temperature
12	I24_LL3	I25_LL1	room temperature
13	I24_TS4	I25_TS3	room temperature
14	I24_TS2	I25_TL4	room temperature
15	I24_LS2	I25_TL1	room temperature
16	I24_LL4	I25_LL2	room temperature

4 COMPRESSION TESTS

As the results of the compression tests from insert I26 showed little scatter, only a few tests will be performed for inserts I24 and I25. Compression specimen as defined in ASTM E9 will be used, with dimensions given in Figure 14. These specimens (with prefix C) will only be taken from layer 3 of the top slab of the inserts, as shown in Figure 7.

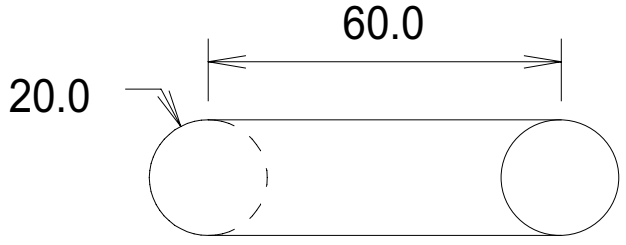

Figure 14. Specimen geometry for compression test.

Table 3. Randomly determined test order for compression tests

Test order	Test spec.	Temperature [°C]
1	I24_C6	room temperature
2	I24_C1	room temperature
3	I24_C3	room temperature
4	I24_C2	room temperature
5	I24_C5	room temperature
6	I24_C4	room temperature
1	I25_C3	room temperature
2	I25_C1	room temperature
3	I25_C6	room temperature
4	I25_C2	room temperature
5	I25_C4	room temperature
6	I25_C5	room temperature

5 REFERENCES

[1] S. Carlsson. Test plan. *ÅF-IS report B729 rev 01,* 2003.

Appendix C

SWEDISH FOUNDRY ASSOCIATION	REPORT	1 (15)
Lars-Erik Björkegren LEB/et	2003-12-10	19072

Mechanical properties of the cylinder for nuclear fuel storage

1 Background and test material

Cylinders have been cast at three different foundries (designated numbers I24, I25, and I26). Each foundry selected the casting method, melt handling, etc., that they considered suitable based on earlier trials.

Samples were taken perpendicular to the cylinder's axis for examination of mechanical properties and microstructure. Two slices were cut from each cylinder. The top slice is marked "T" and the lower slice is marked "U".

Eleven test samples were taken from each slice as shown in Appendix 1. The samples were photographed and tested for tensile strength, hardness, and microstructure. Machining of the samples and testing was done by the Swedish Foundry Association. The results are documented in three reports:

- Materials properties of nodular cast iron insert I24, Examination number 19250-2, 2003-08-25,

- Materials properties of nodular cast iron insert I25, Examination number 19250-3, 2003-08-26,

- Materials properties of nodular cast iron insert I26, Examination number 19250-1, 2003-08-26.

2 Mechanical properties

The results from the measurements that were carried out are summarized in Appendices 2 through 6. SKB has established a requirement of a minimum value of 370 MPa for Rm, a minimum of 240 MPa for RP0.2, and a minimum value of 11% for A5. No foundry has filled SKB's current requirements.

Only I24 (for the bottom part) has acceptable values for ultimate strength, yield strength, and elongation at fracture. The top part has failed mostly with respect to ultimate strength and elongation at fracture. This was caused by defects in the form of slag inclusions and flotation graphite. The yield strength is a little too low, but can be increased by adjusting the chemical composition. See Appendices 2 and 3 for more details.

I25 has good RP0.2 values with very little variation despite a graphite structure that is not fully acceptable. On the other hand, the ultimate strength is not entirely satisfactory, nor is the elongation at fracture. These two properties seem to be more affected by the graphite shape. See Appendices 2 and 4.

It is clear that I26 has high values for Rm, RP0.2, and HBW. The reason that I26 has high values for these properties is because especially the Si, Mn and Ni contents are high. On the other hand, the toughness is low, which is caused by the poor shape (roundness) of the graphite and the high pearlite content (because of high Mn content). See Appendices 2 and 5.

In Appendix 6 the connection between tensile strength and elongation at fracture can be evaluated. Ultimate strength increases when elongation at fracture increases, while yield strength is relatively independent of this. Yield strength is thus independent of defects in the graphite, but not of slag inclusions. A calculation of the difference between ultimate strength and yield strength combined with a comparison of elongation at fracture, table 1, is a good measure of the influence of defects. A high value for the difference and for the elongation at fracture shows that the number of defects is small and the microstructure is good. As seen, the bottom slice of I24 has clearly the best results.

Table 1 *Difference between ultimate strength and yield strength compared with elongation at fracture for top (T) and bottom (U) slices. One value is given in parentheses because of many defects in the material.*

Insert	$R_m - R_{p0,2}$ (MPa)		A (%)	
	T	U	T	U
I 24	(22)	119	3,5	22,2
I 25	102	98	10,3	11,8
I 26	77	92	2,7	9,0

3 Chemical composition

The chemical analyses were carried out by the respective companies and gave the following results:

Table 2 *Chemical composition based on the respective company's own results.*

Element	Insert No		
	I24	I25	I26
C	3.66	3.78	3.56
Si	2.31	2.08	2.39
Mn	0.15	0.21	0.52
P	0.026	0.006	0.03
S	0.009	0.008	0.010
Mg	0.050	0.035	0.063
Cr	0.03	Not reported	Not reported
Ni	0.27	0.50	0.73
Mo	0.01	Not reported	Not reported
Cu	0.11	Not reported	Not reported

The most important difference is for Si, Ni, and Mn, which for foundry I26 are highest. This difference would give, according to the literature and our own research, about 58 MPa higher yield strength than for I25, table 3. A comparison of I24 and I25 gives the results shown in table 4 below. The measured differences agree well with the calculated.

Mn and Cu also raise the properties of ferrite, but too high a content these causes pearlite to form in the base material. The Mn content in I26 is high and a high content of pearlite is found in its samples. An increased pearlite content lowers the material's toughness, but increases the yield strength and ultimate strength.

Table 3 *Analysis comparison between I26 and I25 with I25 as the basis and the effect that the difference in analysis would give on yield strength.*

Element	Analysis difference. %	$R_{p0.2}$ % [1)]	Increase in $R_{p0.2}$ (MPa)
Si	0.31	110	34
Mn	0.31	?	?
P	0.024	449	11
Ni	0.23	50 – 60	12 - 14
		Total	57 - 59

[1)] Data from the literature and our own research given as the change in $R_{P0.2}$ by % in element analysis.

Table 4 *Comparison between measured and calculated yield strength. ΔR_P means the difference in value with I25 as the basis. The theoretical value is calculated according to Table 3. One value was set in parentheses because of many defects in the material.*

Insert	Average $R_{P0,2}$ (MPa)		Analysis %					Teoreti-cal $\Delta R_{P0,2}$ (MPa) I 25 = basis	Measured results $\Delta R_{P0,2}$ (MPa) I 25 = Bas	
	T	U	Si	Mn	P	Ni	Cu		T	U
I 24	(257.3)	288.5	2.31	0.15	0.026	0.27	?	+21	(-10)	26
I 25	267.4	262.7	2.08	0.21	0.006	0.50	?	0	0	0
I 26	316.2	315.9	2.39	0.52	0.03	0.73	0.11	+58	49	53

4 Structure and defects

Microstructure samples were taken about 10 mm from the tensile test fracture. The structure results are summarized in Appendices 3-5.

I24 (Appendix 3) I24 has the best graphite shape (90% nodularity). The extensive inclusion of slag strings and flotation graphite (which also locally gives poorer nodularity) has greatly weakened the strength properties in the top slice (T).

In all the samples (both from T and U samples) except for U7 and U11 there is about 10% degenerated graphite. This has, however, no influence on the mechanical properties according to what one can see from the values obtained from the U samples.

An interesting observation is that U7 and U11 show considerably higher nodule count than the other samples. A closer examination shows that in just these positions the steel reinforcements that anchor the tube are found. These have increased the speed of solidification and given a finer structure.

I25 (Appendix 4) The nodularity is between 60 - 90%. In samples U1 and U3, there is degenerated graphite with a "chunky" appearance. For the rest of the samples the graphite particles are more of Form III graphite (according to ISO 945). The reason for the poor graphite shape is the low Mg content.

I26 (Appendix 5) The nodularity varies (apart from samples T1 and T3 that have better nodule development and nodule count) between 60 - 85% of Form V and VI shape. The remainder (about 15 to 40%) is degenerated graphite, probably chunky graphite. In six of the examined cross sections (both T and U samples) local regions with totally degenerated - chunky - graphite were found.

5 Summary

No foundry has totally fulfilled SKB's requirements.

Only insert I24 (for the lower part, U) has achieved acceptable values for ultimate strength, yield strength, and elongation at fracture. The top part (T) has failed mainly with concern to ultimate strength and elongation at fracture. This was caused by defects in the form of strings of slag inclusions and flotation graphite. The yield strength is somewhat low, but can be raised by adjusting the chemical composition.

Foundry I26 has reached high levels for Rm, RP0.2, and HBW, which is due to the high content of especially Si, Mn and Ni. On the other hand, the toughness is low because of the poor shape (nodularity) of the graphite. The Mn content is also high and has caused a relatively high content of pearlite, which lowers the material's toughness.

Lars-Erik Björkegren 2003-12-10 19072
LEB/aj

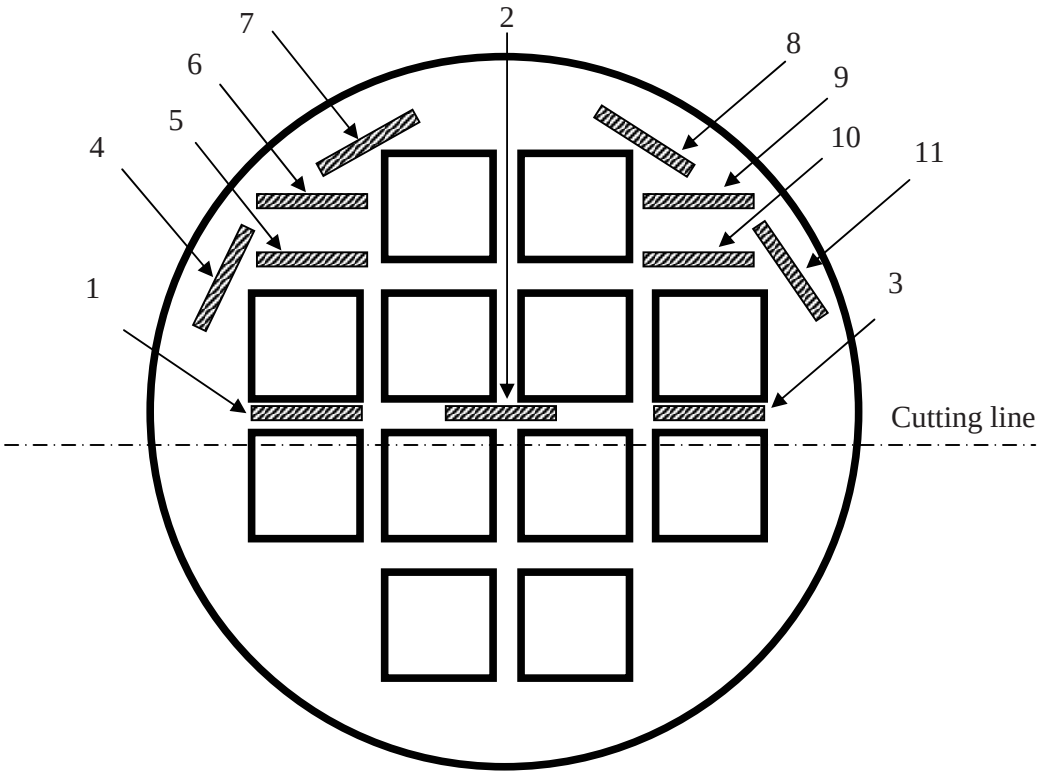

Cross section of the cylinder that shows the distribution of samples (filled rectangles) perpendicular to the symmetry axis. The unfilled squares are steel pipes that only are found in the top slice.

Lars-Erik Björkegren 2003-12-10 19072
LEB/aj

FOUNDRY I 24

	Specification	T	U	Comments
$R_{P0.2}$ (MPa) Mean Std. Dev.	Min. 240	 257 ±18.1	 289 ±2.8	 U – Good T – Not acceptable
R_m (MPa) Mean Std. Dev.	Min. 370	 299 ±36.3	 408 ±7.1	 U – Good T – Too low, large spread
A_5 (%) Mean Std. Dev.	Min. 11	 3.5 ±1.6	 22.2 ±3.2	 U- Very good T – Too low
HBW Mean Std. Dev.		 136 ±4.1	 144 ±3.0	

	Specification	T	U	Comments
Nodularity (%)1) Mean Std. Dev. Min. Max.	Min. 80	 90 ±0 90 90	 90 ±0 90 90	 Good Good Good
Nodule count 2) Mean Std. Dev. Min. Max.	Min. 100	 93 ±87 35 255	 156 ±112 90 415	 Good T - low OK
Pearlite (%) Mean Min. Max.		 1.4 0 2	 1 0 1	 Good Good Good

1) Graphite Form V and VI according to EN ISO 945
2) Number of nodules/mm^2

Lars-Erik Björkegren 2003-12-10 19072
LEB/aj

FOUNDRY I 25

	Specification	T	U	Comments
$R_{P0.2}$ (MPa)	Min. 240			
Mean		267	263	Good
Std. Dev.		±2.0	±2.0	Good
R_m (MPa)	Min. 370			
Mean		370	360	Too low
Std. Dev.		±9.0	±4.2	OK
A_5 (%)	Min. 11			
Mean		10.3	11.8	Not entirely acceptable
Std. Dev.		±3.4	±1.4	Good
HBW				
Mean		139	133	
Std. Dev.		±3	±1	

	Specification	T	U	Comments
Nodularity (%)1)	Min. 80			
Mean		75	68	Too low
Std. Dev.		±7	±7	
Min.		70	60	Too low
Max.		90	80	
Nodule count 2)	Min. 100			
Mean		132	43	T – Good
Std. Dev.		±103	±12	
Min.		40	30	Low
Max.		315	60	Large variation
Pearlite (%)				
Mean		1	1	Good
Min.		0	0	Good
Max.		3	5	Good

1) Graphite Form V and VI according to EN ISO 945
2) Number of nodules/mm^2

Lars-Erik Björkegren 2003-12-10 19072
LEB/aj

FOUNDRY I 26

	Specification	T	U	Comments
$R_{P0.2}$ (MPa)	Min. 240			
Mean		316	316	Good
Std. Dev.		±7.4	±4.1	OK
R_m (MPa)	Min. 370			
Mean		393	408	Good
Std. Dev.		±26.5	±25.9	Large variation
A_5 (%)	Min. 11			
Mean		4.8	9.0	Too low
Std. Dev.		±2.7	±6.5	
HBW				
Mean		157	155	
Std. Dev.		±2.0	±0.8	

	Specification	T	U	Comments
Nodularity (%)1)	Min. 80			
Mean		75	75	Too low
Std. Dev.		±11	±5	
Min.		60	70	Too low
Max.		90	85	
Nodule count 2)	Min. 100			
Mean		181	124	Good
Std. Dev.		±126	±37	
Min.		60	40	Somewhat low
Max.		410	170	
Pearlite (%)				
Mean		9.5	8.6	Somewhat high
Std. Dev.		±4.2	±4.5	
Min.		5	5	Too high
Max.		15	20	Too high

1) Graphite Form V and VI according to EN ISO 945
2) Number of nodules/mm^2

Lars-Erik Björkegren 2003-12-10 19072
LEB/aj

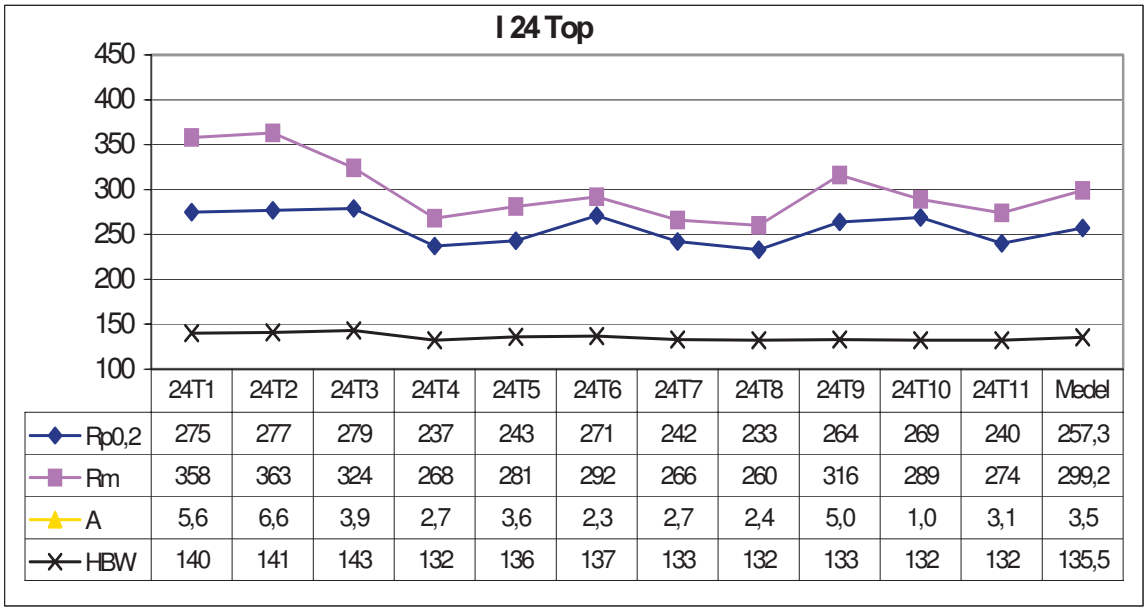

	24T1	24T2	24T3	24T4	24T5	24T6	24T7	24T8	24T9	24T10	24T11	Medel
Rp0,2	275	277	279	237	243	271	242	233	264	269	240	257,3
Rm	358	363	324	268	281	292	266	260	316	289	274	299,2
A	5,6	6,6	3,9	2,7	3,6	2,3	2,7	2,4	5,0	1,0	3,1	3,5
HBW	140	141	143	132	136	137	133	132	133	132	132	135,5

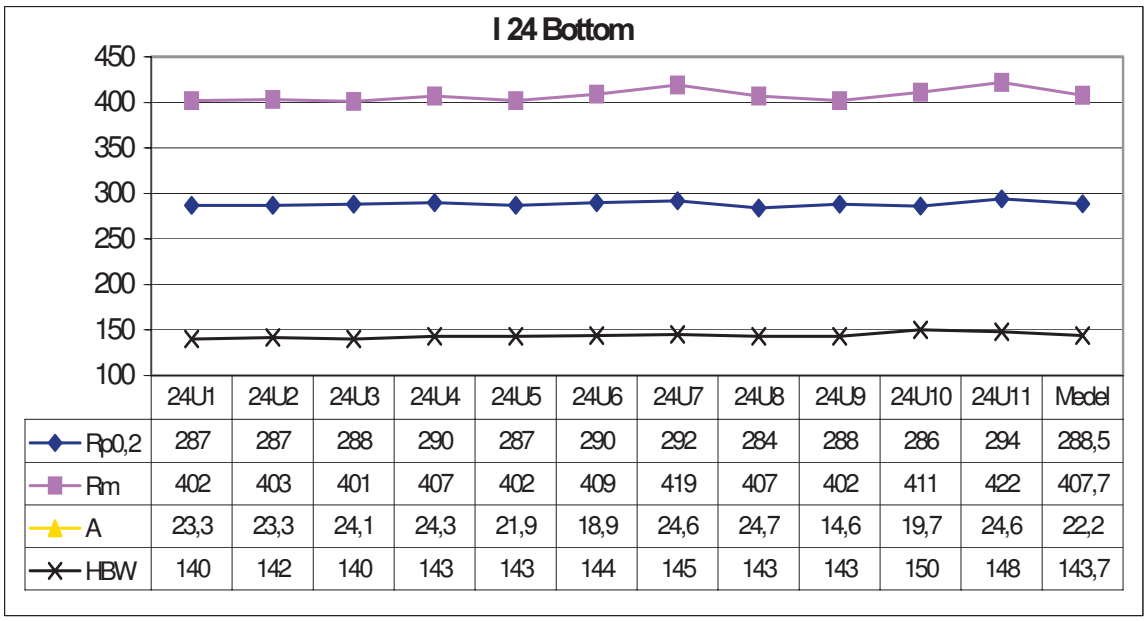

	24U1	24U2	24U3	24U4	24U5	24U6	24U7	24U8	24U9	24U10	24U11	Medel
Rp0,2	287	287	288	290	287	290	292	284	288	286	294	288,5
Rm	402	403	401	407	402	409	419	407	402	411	422	407,7
A	23,3	23,3	24,1	24,3	21,9	18,9	24,6	24,7	14,6	19,7	24,6	22,2
HBW	140	142	140	143	143	144	145	143	143	150	148	143,7

Lars-Erik Björkegren 2003-12-10 19072
LEB/aj

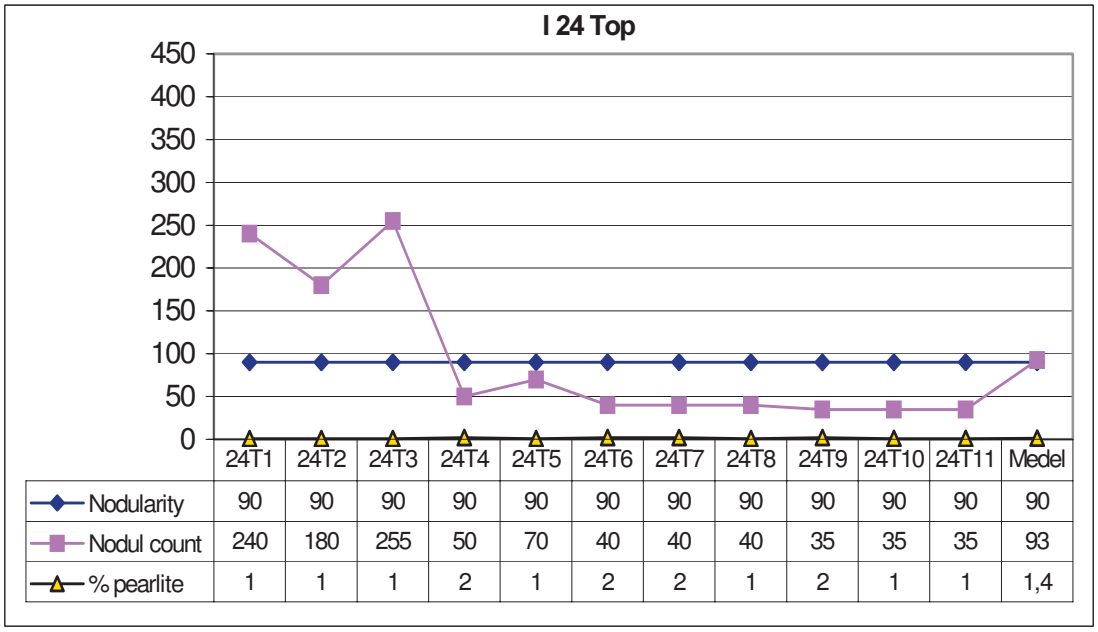

	24T1	24T2	24T3	24T4	24T5	24T6	24T7	24T8	24T9	24T10	24T11	Medel
Nodularity	90	90	90	90	90	90	90	90	90	90	90	90
Nodul count	240	180	255	50	70	40	40	40	35	35	35	93
% pearlite	1	1	1	2	1	2	2	1	2	1	1	1,4

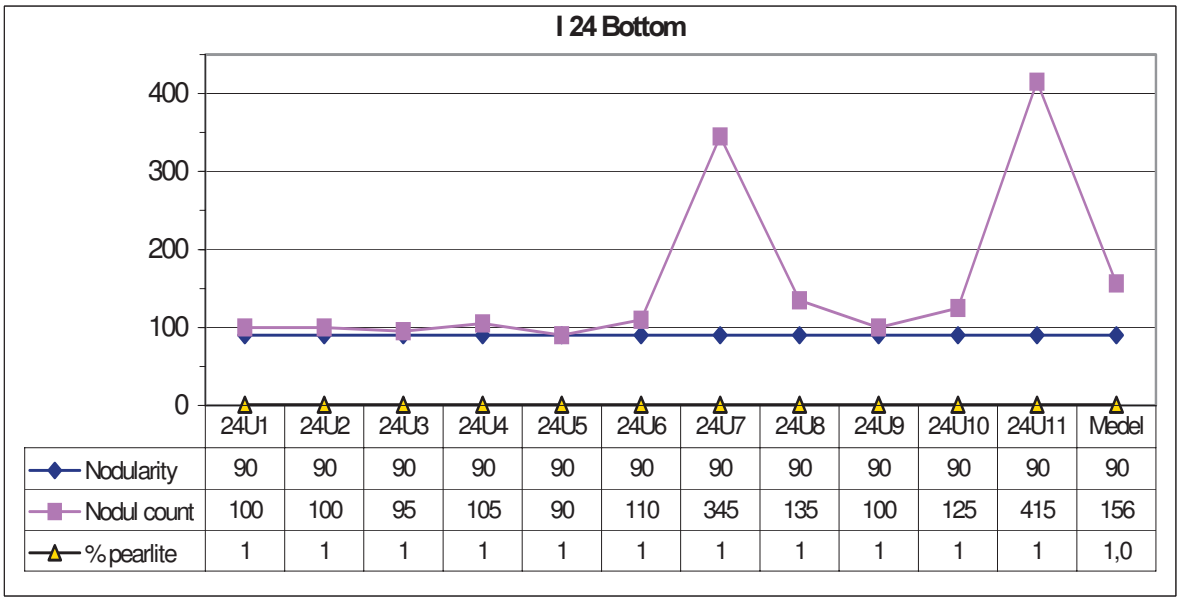

	24U1	24U2	24U3	24U4	24U5	24U6	24U7	24U8	24U9	24U10	24U11	Medel
Nodularity	90	90	90	90	90	90	90	90	90	90	90	90
Nodul count	100	100	95	105	90	110	345	135	100	125	415	156
% pearlite	1	1	1	1	1	1	1	1	1	1	1	1,0

Lars-Erik Björkegren 2003-12-10 19072
LEB/aj

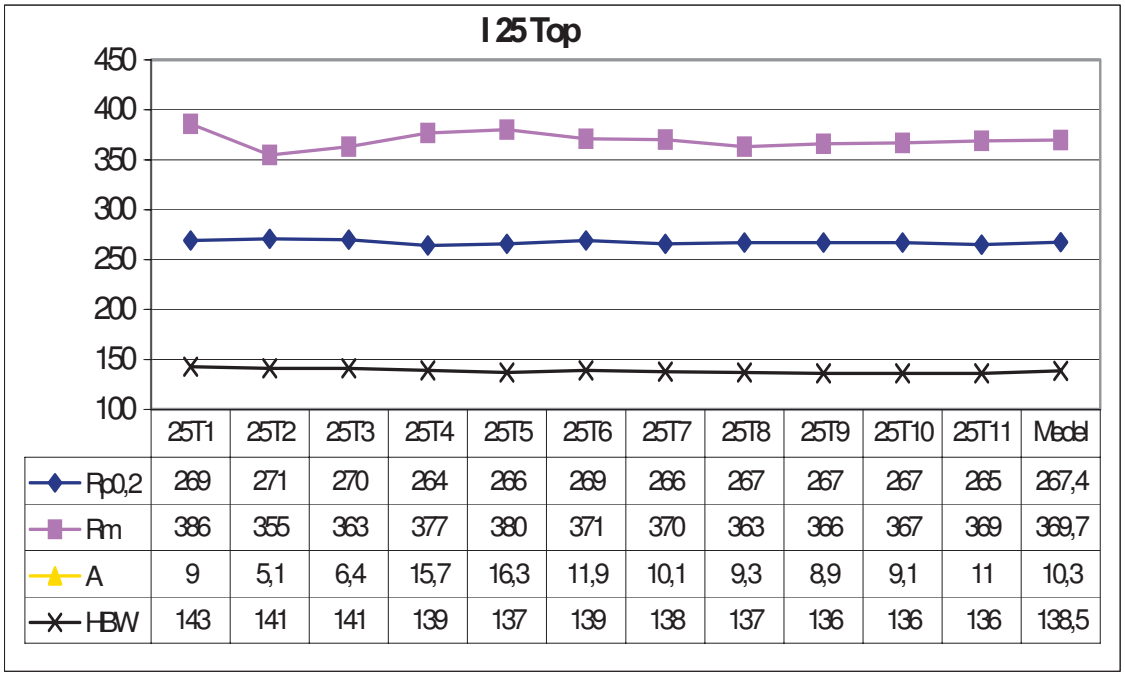

	25T1	25T2	25T3	25T4	25T5	25T6	25T7	25T8	25T9	25T10	25T11	Medel
Rp0,2	269	271	270	264	266	269	266	267	267	267	265	267,4
Rm	386	355	363	377	380	371	370	363	366	367	369	369,7
A	9	5,1	6,4	15,7	16,3	11,9	10,1	9,3	8,9	9,1	11	10,3
HBW	143	141	141	139	137	139	138	137	136	136	136	138,5

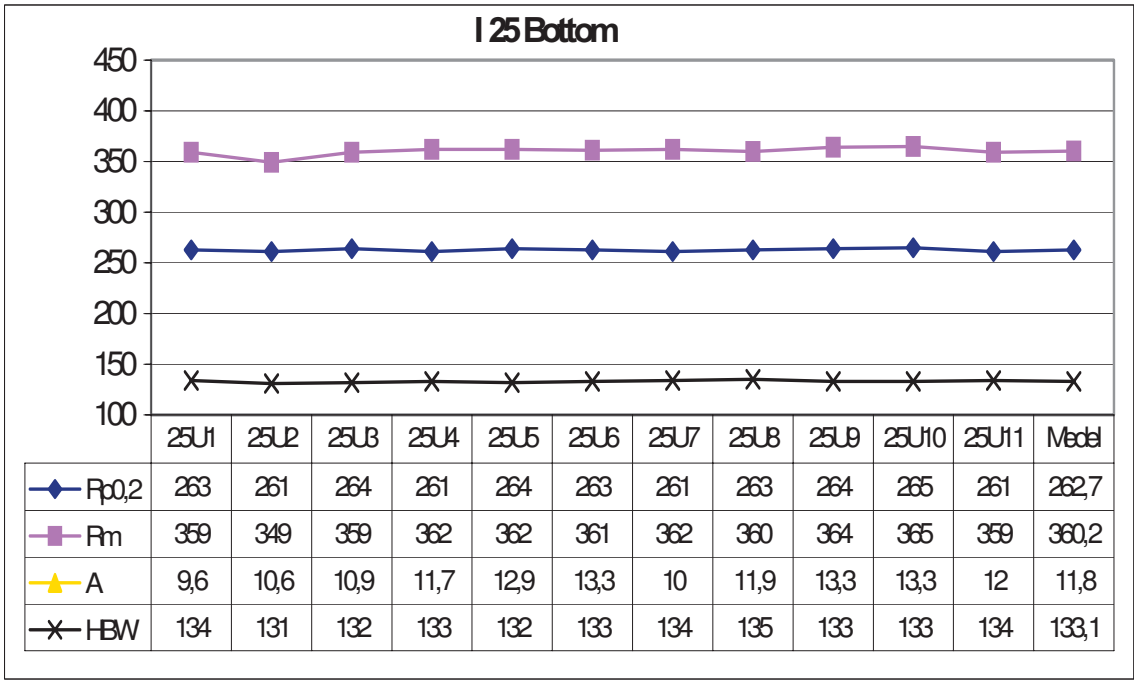

	25U1	25U2	25U3	25U4	25U5	25U6	25U7	25U8	25U9	25U10	25U11	Medel
Rp0,2	263	261	264	261	264	263	261	263	264	265	261	262,7
Rm	359	349	359	362	362	361	362	360	364	365	359	360,2
A	9,6	10,6	10,9	11,7	12,9	13,3	10	11,9	13,3	13,3	12	11,8
HBW	134	131	132	133	132	133	134	135	133	133	134	133,1

Lars-Erik Björkegren 2003-12-10 19072
LEB/aj

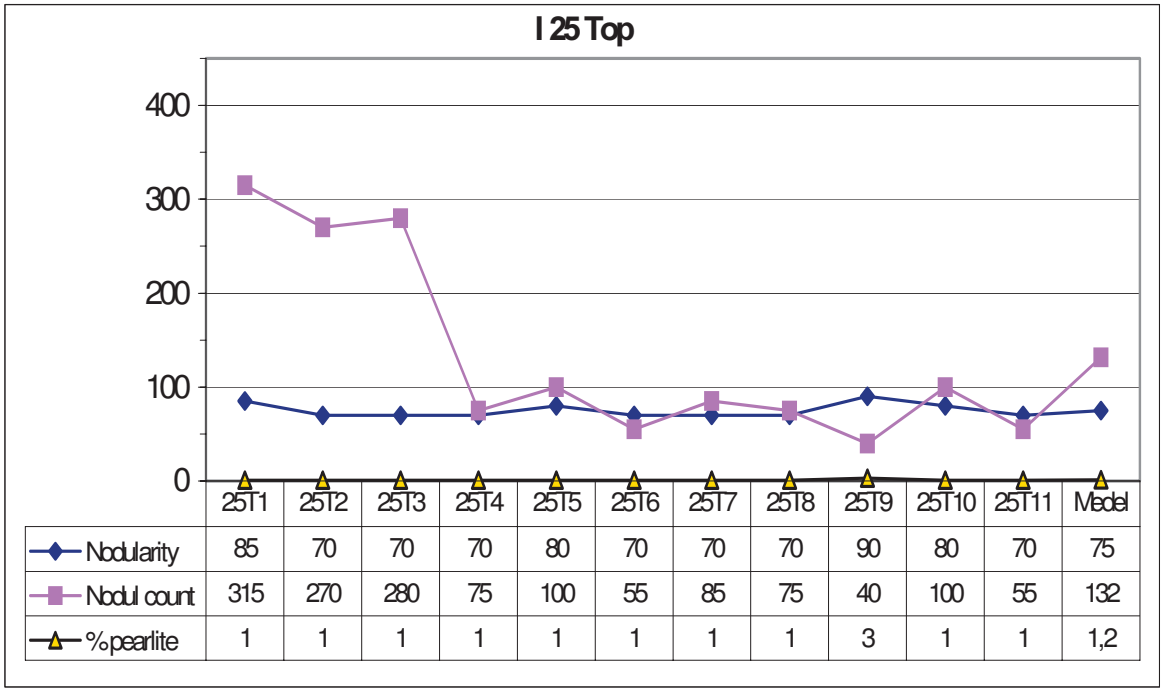

	25T1	25T2	25T3	25T4	25T5	25T6	25T7	25T8	25T9	25T10	25T11	Medel
Nodularity	85	70	70	70	80	70	70	70	90	80	70	75
Nodul count	315	270	280	75	100	55	85	75	40	100	55	132
%pearlite	1	1	1	1	1	1	1	1	3	1	1	1,2

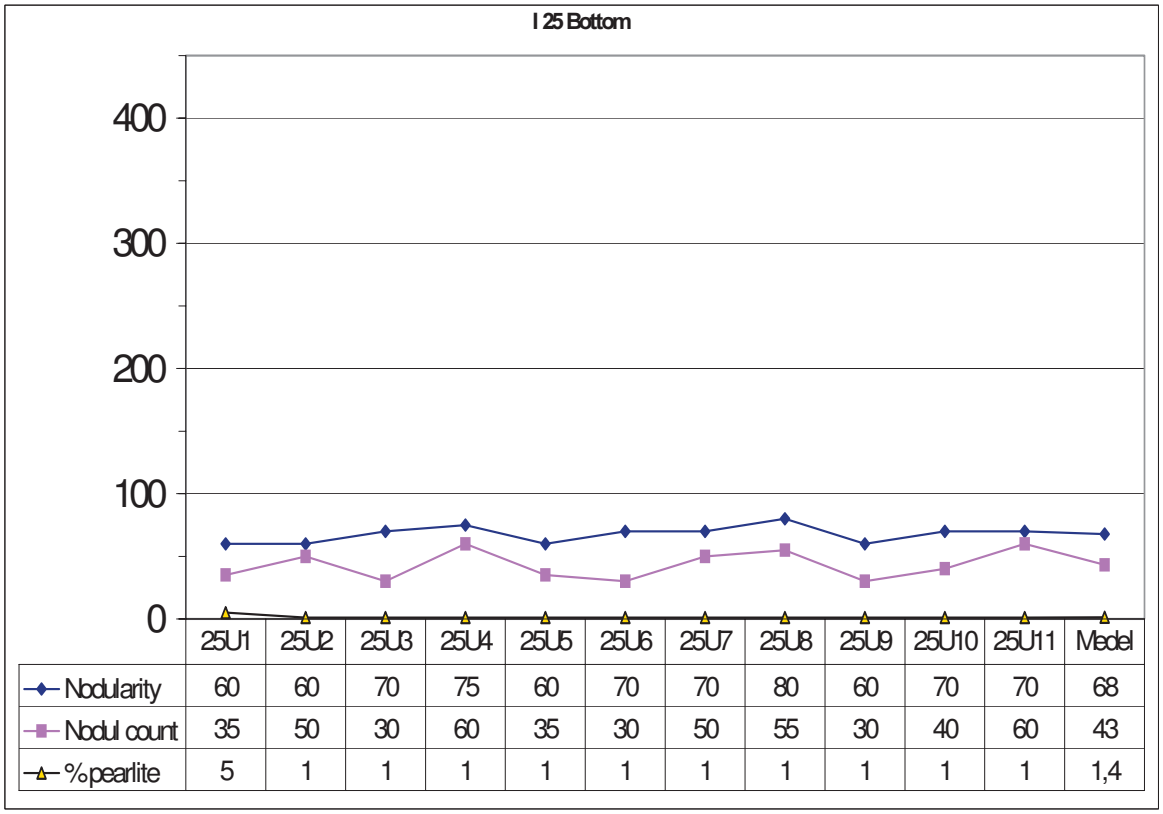

	25U1	25U2	25U3	25U4	25U5	25U6	25U7	25U8	25U9	25U10	25U11	Medel
Nodularity	60	60	70	75	60	70	70	80	60	70	70	68
Nodul count	35	50	30	60	35	30	50	55	30	40	60	43
%pearlite	5	1	1	1	1	1	1	1	1	1	1	1,4

Lars-Erik Björkegren 2003-12-10 19072
LEB/aj

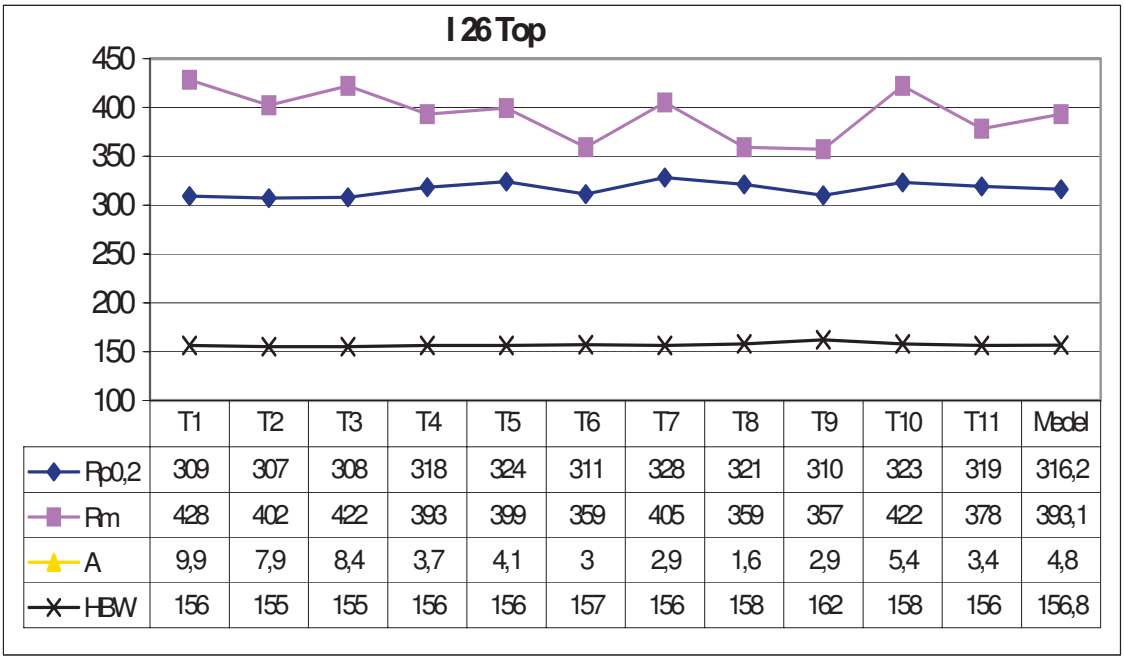

	T1	T2	T3	T4	T5	T6	T7	T8	T9	T10	T11	Medel
Rp0,2	309	307	308	318	324	311	328	321	310	323	319	316,2
Rm	428	402	422	393	399	359	405	359	357	422	378	393,1
A	9,9	7,9	8,4	3,7	4,1	3	2,9	1,6	2,9	5,4	3,4	4,8
HBW	156	155	155	156	156	157	156	158	162	158	156	156,8

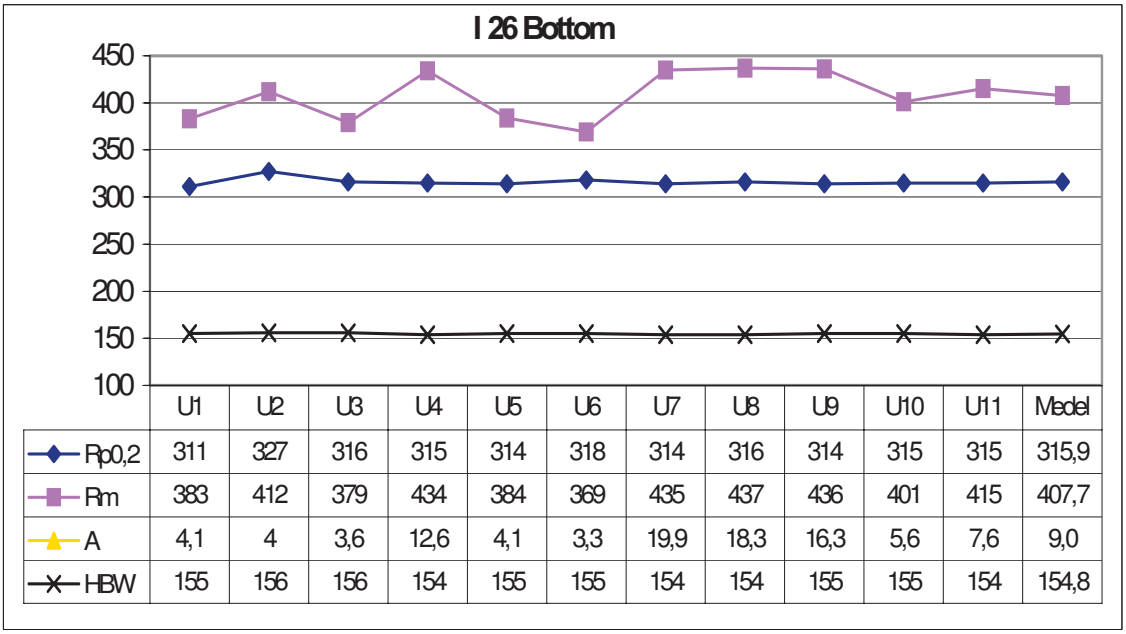

	U1	U2	U3	U4	U5	U6	U7	U8	U9	U10	U11	Medel
Rp0,2	311	327	316	315	314	318	314	316	314	315	315	315,9
Rm	383	412	379	434	384	369	435	437	436	401	415	407,7
A	4,1	4	3,6	12,6	4,1	3,3	19,9	18,3	16,3	5,6	7,6	9,0
HBW	155	156	156	154	155	155	154	154	155	155	154	154,8

Lars-Erik Björkegren 2003-12-10 19072
LEB/aj

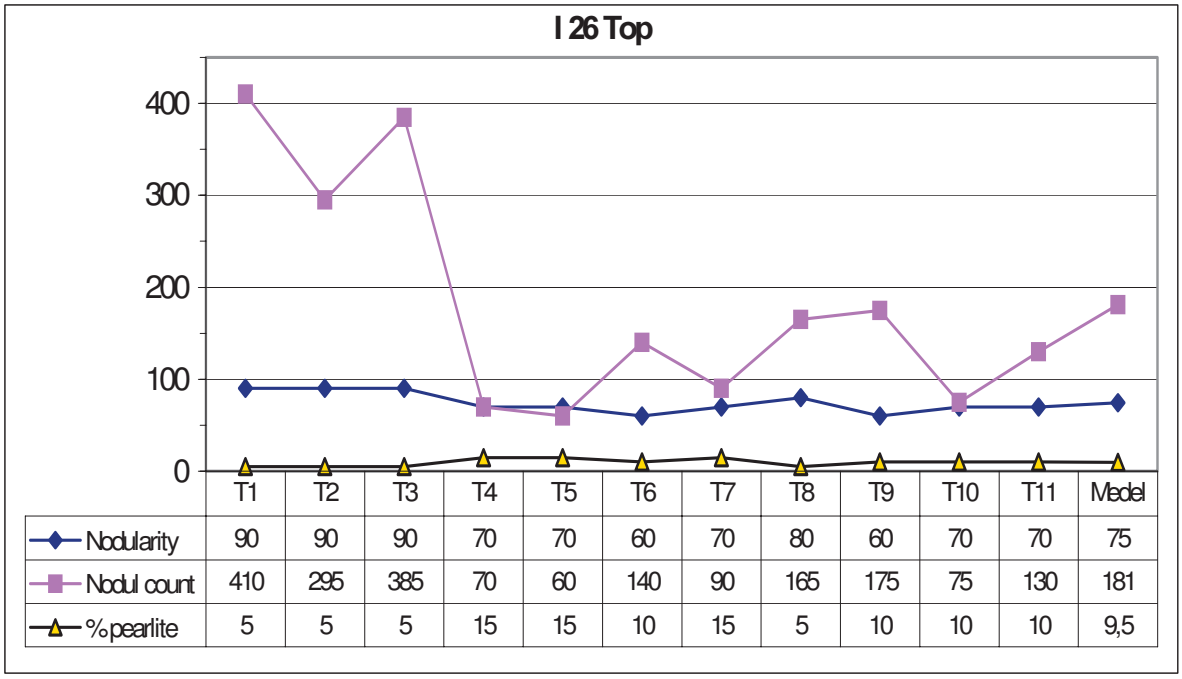

	T1	T2	T3	T4	T5	T6	T7	T8	T9	T10	T11	Medel
Nodularity	90	90	90	70	70	60	70	80	60	70	70	75
Nodul count	410	295	385	70	60	140	90	165	175	75	130	181
%pearlite	5	5	5	15	15	10	15	5	10	10	10	9,5

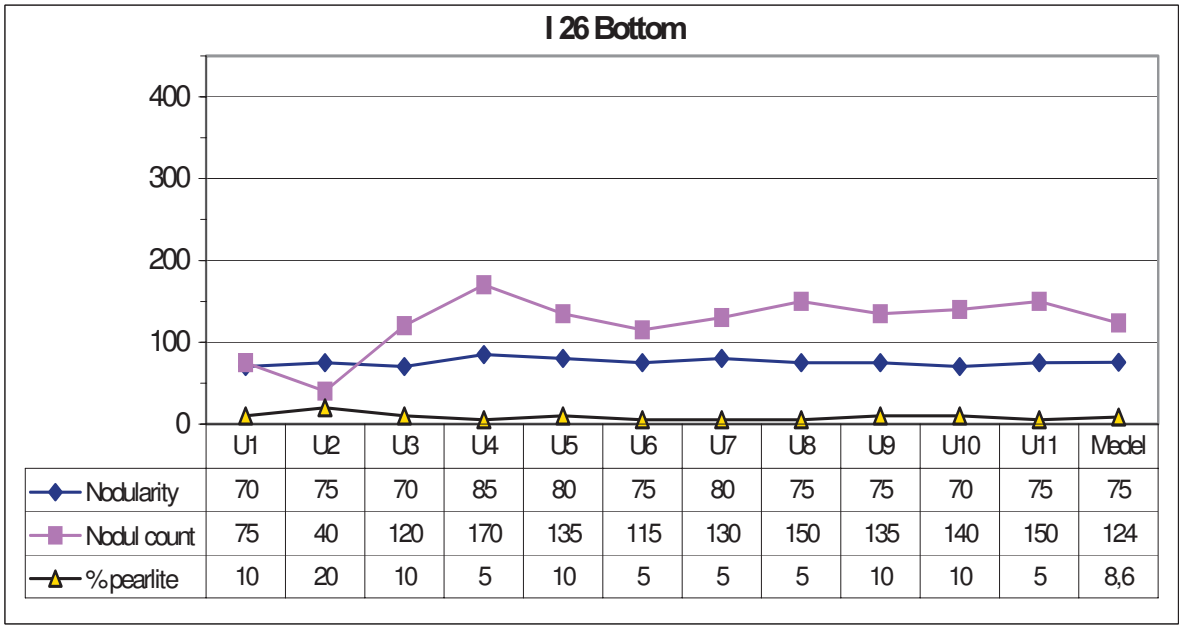

	U1	U2	U3	U4	U5	U6	U7	U8	U9	U10	U11	Medel
Nodularity	70	75	70	85	80	75	80	75	75	70	75	75
Nodul count	75	40	120	170	135	115	130	150	135	140	150	124
%pearlite	10	20	10	5	10	5	5	5	10	10	5	8,6

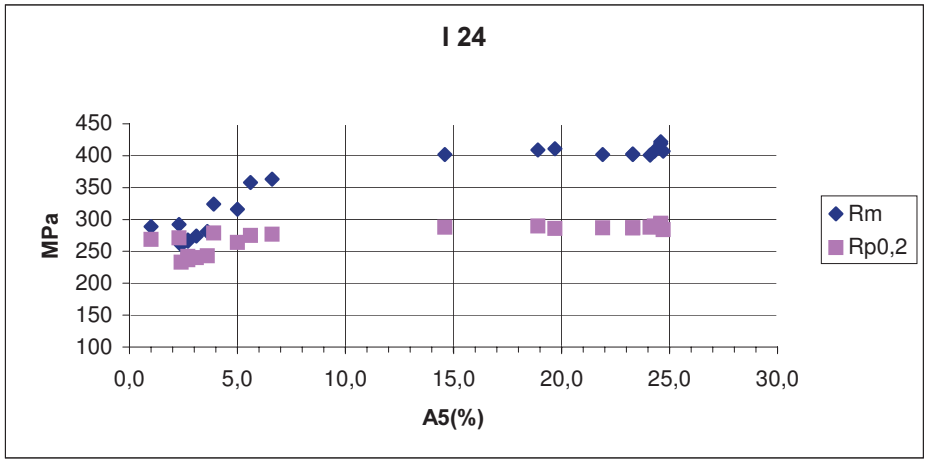
I 24
MPa
450
400
350
300
250
200
150
100
0,0
5,0
10,0
15,0
20,0
25,0
30,0
A5(%)
Rm
Rp0,2

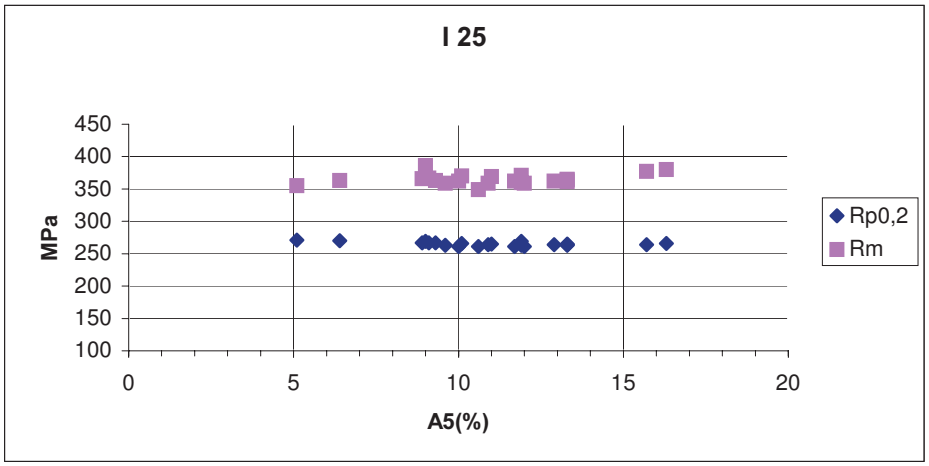
I 25
MPa
450
400
350
300
250
200
150
100
0
5
10
15
20
A5(%)
Rp0,2
Rm

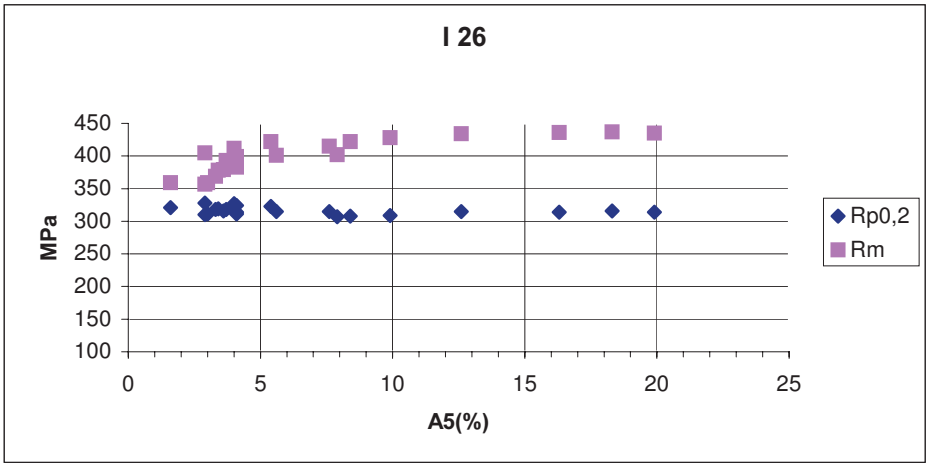
I 26
MPa
450
400
350
300
250
200
150
100
0
5
10
15
20
25
A5(%)
Rp0,2
Rm

Appendix D

Printed 05-08-22
Report SKB0304rep

Stockholm 031021

Fracture toughness testing of nodular cast iron

Fracture mechanics testing of a nodular cast iron has been performed. A first test according to ASTM E 399 / E 1921 showed that non-linear testing according to ASTM E 1820 or similar is required. Pre-tests at 0 °C, +50 °C and + 100°C were performed and after that two more extensive series at 0 °C and +23 °C. The results are given in tables below and on enclosed diagrams.

Test specimens

Blocks of cast iron were delivered by the SKB. The blocks were marked with 3 digit numbers and internal laboratory identifications were added.

The blocks were milled to 15.0 mm x 30.0 mm x (about) 155 mm. Integral edges and straight notches, width 0,3 mm, depth 15 mm, were machined by sparkerosion. Side grooves, 1,5 mm deep, were milled after precracking.

Test equipment

Computer controlled servohydraulic testing machines, MTS 100 kN equipped with digital controllers, INSTRON 8500+, were utilized for precracking. The finals test were run in machine MTS 100 kN, 1.2. The integral transducers for load and piston position were used as well as a clip gage, INSTRON model 2670-120, S/N 4884. All data were stored in a connected pc.

Infrared heaters along the sides of the specimens were used at raised temperatures. To achieve 0 °C the specimens were immersed in isopropanol, cooled with liquified nitrogen. The temperature was in both cases measured with thermocouples welded to the specimens in the vicinity of the crack tip.

Testing and evaluation

The precracking started at ΔK 16 MPam$^{1/2}$ after which the load levels were gradually shedded to about 13,5 MPam$^{1/2}$ at the final depth, 18 mm.

Also the final tests were performed under computer control with unloadings for compliance crack measurements each time the *J*-value was increased 3 kN/m.

The evaluation was made using an in-house computer program, *SENB1820*.

KTH Solid Mechanics, Hans Öberg - Osquars backe 1, SE-100 44 Stockholm, SWEDEN.
Phone: +46 8 790 7547. Fax: +46 8 411 24 18. e-mail: hob@hallf.kth.se

After the final test most of the specimens were heat tinted at about +400 °C during at least 0,5 h, fatigued at ΔK 23 MPam$^{1/2}$ for some mm crack extension and opened.

The fatigue crack front and the final crack front were measured using a microscope provided with a hair cross and attached to a device with digital position read out.

Comments

Tests were performed, to begin with, at different temperatures according to the proposed test program. The very first test, 9719, showed such ductility that non-linear testing was determined.

The final crack front was in many cases very difficult to distinguish. The crack surfaces were at the higher test temperatures very irregular. Fatigue, the standard method for crack front marking, did not work satisfactory why heat tinting was added.

As no obvious variation of the fracture toughness could be found from the first tests some tests were performed at room temperature which normally yields better controlled testing. However, now the average values of the fracture toughness turned out to be higher at +23 °C than at 0 °C why further tests were performed at 0 °C, where the lowest fracture toughness in the actual temperature range was anticipated.

Difficulties to obtain valid values arose mainly due to discrepancies between the start crack length calculated according to ASTM E 1820 and the physical length. This is partly due to that the type of curve that shall be fitted does not correlate well with actual measured data. The errors have however been small, close to acceptable values (with some exception).

Another problem was that the final crack length measured with the compliance method in many cases was to short compared to the optically measured crack front but this may be due to the difficulties to distinguish the final crack front. The crack may grow in an irregular way, with "islands" of broken ligament in front of the crack front an bridges behind. This may also cause the problems with the start crack lengths.

Note that the compliance measurements of the start crack length that are prescribed in ASTM E 1820 were successful, with a scatter that in general was 5 to 10 times lower that required. Any problems with the measuring are thus less plausible.

At 0 °C the problems with crack fronts that are difficult to define and discrepancies between optically measured crack lengths and such measured using the compliance method have been less pronounced in contrast to what normally is observed. Different failure mechanisms at room temperature and at 0 °C may be one explanation.

Results

Test temperature + 0°C.

No	Mark	J_{Ic} / kN/m	Comments
9720	203	28	
9721	402	14	a0q not valid
9722	305	26	
9723	506	16	
9724	411	24	
9725	303	14	a0q not valid, too irregular crack fronts
9726	103	24	
9727	502	20	
9728	301	20	
9802	210	25	
9803	507	15	a0q not valid
9804	105	23	
9805	207	27	
9806	501	17	
9807	101	24	

Test temperature + 23°C.

No.	Mark	J_{Ic} / kN/m	Comments
9801	508	34	
9808	106	32	
9809	202	26	
9810	111	36	not valid, (0,078 mm too much Δa_p error)
9811	401	36	not valid, (0,050 mm too much Δa_p error), too few points in a_{0q}-calc.)
9812	204	33	
9813	112	38	
9814	102	32	
9815	410	36	not valid, (0,175 mm too much Δa_p error)
9816	302	34	
9817	510	31	not valid, (0,055 mm too much Δa_p error)

No.	Mark	J_{Ic} / kN/m	Comments
9818	304	36	
9819	211	29	
9820	505	(8)	not valid, bridges in crack surfaces
9821	201	29	
9822	404	25	not valid, (0,1 mm too much Δa_p error), too few points in a_{0q}-calc.)

Test temperature + 50°C.

No	Mark	J_{Ic} / kN/m	Comments
9729	403	25	not valid
9730	412	36	not valid
9731	509	13	not valid

Test temperature + 100°C.

No	Mark	J_{Ic} / kN/m	Comments
9732	409	36	not valid
9733	108	30	not valid
9734	209	20	not valid

Hans Öberg

Senior research engineer

Appendix E

Printed 05-08-22
Report SKB0401rep

Stockholm 040429

Fracture toughness testing of nodular cast iron, I24 and I25

Fracture mechanics testing of a nodular cast iron from two canisters, I24 and I25 has been performed. at 0 °C and room temperature (RT, +23 °C). The results are given in tables below and on enclosed diagrams.

Test specimens

Blocks of cast iron were delivered by the SKB. The blocks were marked with 3 digit numbers and internal laboratory identifications were added.

The blocks were milled to 15.0 mm x 30.0 mm and sawed to a length of about 140 mm. Integral edges and straight notches, width 0,3 mm, depth 15 mm, were machined by spark erosion. Side grooves, 1,5 mm deep, were milled after precracking.

Test equipment

Computer controlled servohydraulic testing machines, MTS 100 kN equipped with digital controllers, INSTRON 8500+, were utilized for precracking. The finals test were run in machine MTS 100 kN, 1.2. The integral transducers for load and piston position were used as well as a clip gage, INSTRON model 2670-120, S/N 4834. All data were stored in a connected pc.

To achieve 0 °C the specimens were immersed in isopropanol, cooled with liquified nitrogen. The temperature was measured with thermocouples welded to the specimens in the vicinity of the crack tip.

Testing and evaluation

The precracking started at ΔK 16 MPam$^{1/2}$ after which the load levels were gradually shedded to about 13,5 MPam$^{1/2}$ at the final depth, 18 mm.

Also the final tests were performed under computer control with unloadings for compliance crack measurements each time the J-value was increased 3 kN/m.

The evaluation was made using an in-house computer program, *SENB1820*.

KTH Solid Mechanics, Hans Öberg - Osquars backe 1, SE-100 44 Stockholm, SWEDEN.
Phone: +46 8 790 7547. Fax: +46 8 411 24 18. e-mail: hob@hallf.kth.se

After the final test the specimens were heat tinted at about +400 °C during at least 0,5 h, fatigued at ΔK 23 MPam$^{1/2}$ for some mm crack extension and opened.

The fatigue crack front and the final crack front were measured using a microscope provided with a hair cross and attached to a device with digital position read out. In some cases the crack surface was very rough and the crack tip difficult to identify and then a stereo microscope was used to facilitate the measurement of the crack dimensions.

Comments

The final crack front was in many cases very difficult to distinguish and not possible to define without uncertainty. In many of those cases no valid J_{Ic}-values were obtained.

Difficulties to obtain valid values arose mainly from discrepancies between the start crack length calculated according to ASTM E 1820 and the physical length and bad correlation between measured J-Δa-pairs and the best fitted function suggested in the standard (noted as *a0q not valid* in the table below). The errors have however been small, close to acceptable values (with some exception).

Another problem was that the final crack length measured with the compliance method in a few cases was to short compared to the optically measured crack front but this may be due to the difficulties to distinguish the final crack front. The crack may grow in an irregular way, with "islands" of broken ligament in front of the crack front and bridges behind. This may also cause the problems with the start crack lengths.

Note that the compliance measurements of the start crack length that are prescribed in ASTM E 1820 were successful, with a scatter that in general was 5 to 10 times lower that required. Any problems with the measuring are thus less plausible.

At 0 °C the problems with crack fronts that are difficult to define and discrepancies between optically measured crack lengths and such measured using the compliance method have been less pronounced in contrast to what normally is observed. Different failure mechanisms at room temperature and at 0 °C may be one explanation.

Results

I 24. Test temperature + 0°C.

No	Mark	J_{Ic} / kN/m	Comments
10178	101	27	*a0q* not valid
10181	105	28	final crack front too curved, very rough crack surface
10184	205	25	*a0q* not valid
10187	303	34	
10188	404	37	*a0q* not valid
10189	405	25	
10192	502	28	
10193	503	24	

Average 28,5 kN/m. Standard deviation 4.6 kN/m

I 24. Test temperature + 23°C.

No.	Mark	J_{Ic} / kN/m	Comments
10180	104	31	two few unloadings before max load.
10182	108	42	
10183	204	52	
10185	206	48	*a0q* not valid
10186	302	65	
10190	408	50	
10191	501	39	
10194	104	50	crack extension measurement 0.106 mm too high

Average 47.1 kN/m. Standard deviation 10.0 kN/m

Results

I 25. Test temperature + 0°C.

No	Mark	J_{Ic} / kN/m	Comments
10195	202	29	final crack front too curved
10196	204	31	
10197	301	40	
10199	305	34	
10200	401	38	
10203	406	54	
10204	407	38	*a0q* not valid
10206	410	45	

Average 38.6 kN/m. Standard deviation 8.0 kN/m

I 25. Test temperature + 23°C.

No.	Mark	J_{Ic} / kN/m	Comments
10194	104	50	crack extension measurement 0.106 mm too high
10198	304	44	
10201	403	64	
10202	405	74	
10205	409	51	
10207	502	62	crack extension measurement error
10208	504	56	
10209	505	66	

Average 58.5 kN/m. Standard deviation 9.9 kN/m

Hans Öberg

Senior research engineer

Appendix F

Our reference
Bo Erixon
Tel +46-8-6571646
Fax 08-657 37 01
bo.erixon@afconsult.com

Date
2004-12-17

Our reference
bex

ÅF-S REPORT B794 REV. 1

SOLID MECHANICS ANALYSES FOR PROBABILISTIC ANALYSIS OF CANISTER STRUCTURAL STRENGTH

Project nr : 203253

Contents **Page**

1 BACKGROUND 4

2 SUMMARY 5

3 GENERAL 6

3.1 MATERIAL MODEL 6
3.2 MATERIAL NOMENCLATURE 6
3.3 MATERIAL CURVES 6
3.4 BOUNDARY CONDITIONS 2-D 7

4 VERIFICATION 3D – 2D 8

4.1 GEOMETRY 8
4.2 THE MODELS 9
4.3 MATERIAL 11
4.3.1 Material data 11

5 PRESSURE TEST 12

5.1 GEOMETRY 12
5.2 MODELS 14
5.3 MATERIAL 16
5.3.1 Material data cast iron 16
5.3.2 Material data steel cassette 16
5.3.3 Material curve steel cassette 17
5.3.4 Material data steel lid 18
5.3.5 Material curve steel lid 18
5.3.6 Material data copper 19
5.3.7 Material curve copper 19

6 INFLUENCE OF CAST IRON MATERIAL MODEL. 21

6.1 GEOMETRY 21
6.2 MODEL 22
6.3 MATERIAL 23
6.3.1 Material curves 23

ÅF-System AB
Skalholtsgatan 2, Box 35, 164 93 Kista. Telefon 08-657 15 00. Fax 08-657 37 01.
www.afconsult.com. Org. nr 556092-4044. Säte i Stockholm.

7 INFLUENCE OF COPPER CYLINDER 24

7.1 GEOMETRY 24
7.2 MODEL 25
7.3 MATERIAL 26
7.3.1 Material data cast iron 26
7.3.2 Material data steel cassette 26
7.3.3 Material curve steel cassette 27
7.3.4 Material data copper 28
7.3.5 Material curve copper 28

8 INFLUENCE OF ECCENTRICITY FOR THE STEEL CASSETTE 30

8.1 GEOMETRY 30
8.2 MODEL 31
8.3 MATERIAL 32
8.3.1 Material data 32

9 INFLUENCE OF THE CAST IRON INSERT RADIUS AGAINST THE STEEL PIPE CHANNEL 33

9.1 GEOMETRY 33
9.2 MODEL 34
9.3 MATERIAL 35
9.3.1 Material data 35

10 INPUT DATA FOR DNV-PROBABILISTIC ANALYSIS 36

10.1 GEOMETRY 36
10.2 PROBABILISTIC PARAMETERS 37
10.2.1 Analysis ID 37
10.3 MODELS 37
10.4 CRITICAL CROSS-SECTION 38
10.4.1 Result example cross-section– normal case 39
10.4.2 Result example cross-section – extreme case 43

11 REFERENCES 45

APPENDIX

1: 3D-2D, COMPARISON MAXIMUM VALUE
2: 3D-2D, COMPARISON IN CRITICAL SECTIONS
3: PRESSURE TEST, DEFORMATIONS
4: INFLUENCE OF COPPER CYLINDER
5: INFLUENCE OF ECCENTRICITY
6: INFLUENCE OF THE INTERNAL CHANNEL RADIUS
7: INPUT DATA PROBABILISTIC ANALYSIS – NORMAL VALUES
8: INPUT DATA PROBABILISTIC ANALYSIS – EXTREME VALUES
9: COPPER MATERIAL

REPORT HISTORY

Report title: Solid mechanics analysis for probabilistic analysis of canister structural strength.

Date	Activity	Perfo rmed	Inspe cted	Appr oved
2005-03-09 2005-11-11	Report finished Rev.1 Translation from Swedish to English	bex maa	and and	bex maa

1 BACKGROUND

SKB has chosen geographical disposal as the main alternative for storage of spent nuclear fuel. The spent fuel is put in canisters consisting of a cast iron cylinder surrounded by a copper shielding for corrosion protection. These canisters are packaged in bentonite, 500-700 meters down in the rock ground. The requirements say that these canisters shall prevent leakage for a period of 100 000 years. This means that they shall be able to withstand three ice ages. The resulting load on the canister is summarized below.

i. 7MPa hydrostatic pressure at a storage depth of 700m

ii. 7MPa swelling pressure from the surrounding bentonite.

iii. A pressure corresponding to the weight of an inland ice layer of up to 3000 meters. An ice density of 900 kg/m^3 gives an additional pressure of about 30 MPa.

The total outer pressure on a canister will consequently be about 45 MPa. It is difficult to handle these loads with deterministic methods. First of all, there is a considerable spread in the material data, which is the reason for the interest in probabilistic analysis methods.

Fig. 1. Canister for terminal storage of spent nuclear fuel

2 SUMMARY

A number of different analyses have been performed with the purpose to get input data for the probabilistic analysis. The main uncertainty parameter has been the material data, which however became clearer during the working procedure. This is the reason why material data with much larger spread was used in the early analysis compared to the latter.

A 3-D model of the “compression test nr 1 specimen” [9] has been analysed. The agreement between the FEM and the test was good.

A comparison between 2-D and 3-D shows that the 2-D analysis is sufficient when it comes to deliver input data to the probabilistic analysis.

Analysis has also been performed on geometrical deviations. The internal channel corner radius can vary depending on manufacturer, manufacturing method and SKB specification value. The complete steel cassette can be more or less eccentrically oriented relative to the iron insert.

Some test analyses were performed on a material model that can handle different material characteristics in compression and tension. The results show that even if the tensile yield strength and ultimate tensile strength are very low they do not affect the results. Considering this it is enough to use only compression test data in the final analysis as input data for the probabilistic analysis.

Tests including the surrounding copper cylinder were also performed. The results show that only at very high pressures, over 80 MPa, it had a significant influence. Therefore, the copper cylinder is excluded in the final analyses.

The analyses regarding the geometrical deviations, show that different values of the eccentricity for the steel cassette has the largest impact on the results, whereas the radius has less but not a negligible influence.

The parameters that were varied in the final analyses were the corner radius, eccentricity, yield strength and ultimate strength (table in chapter 10.2).

All FEM-analyses are performed using ANSYS version 7.1 and 8.1.

3 GENERAL

3.1 MATERIAL MODEL

The analyses have been performed using an elastic-plastic material model of bilinear type (BISO), except for the copper and the steel, which were defined using a multi linear material model (MISO).

3.2 MATERIAL NOMENCLATURE

Young's modulus = E [N/mm^2]

Tensile strength = $R_{p\,0.2}$ [MPa]

Strain at $R_{p\,0.2}$ = $\varepsilon_{sy} = \dfrac{R_{p\,0.2}}{E}$

Ultimate strength = R_m [MPa]

Tangent modulus = tanmod = $E_T = \dfrac{R_m - R_{p\,0.2}}{\varepsilon_{su} - \varepsilon_{sy}}$

Ultimate strain = ε_{su}

3.3 MATERIAL CURVES

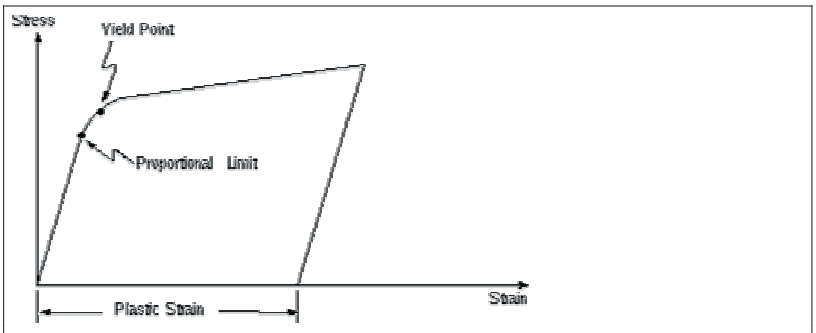

Fig. 2. General stress-strain curve

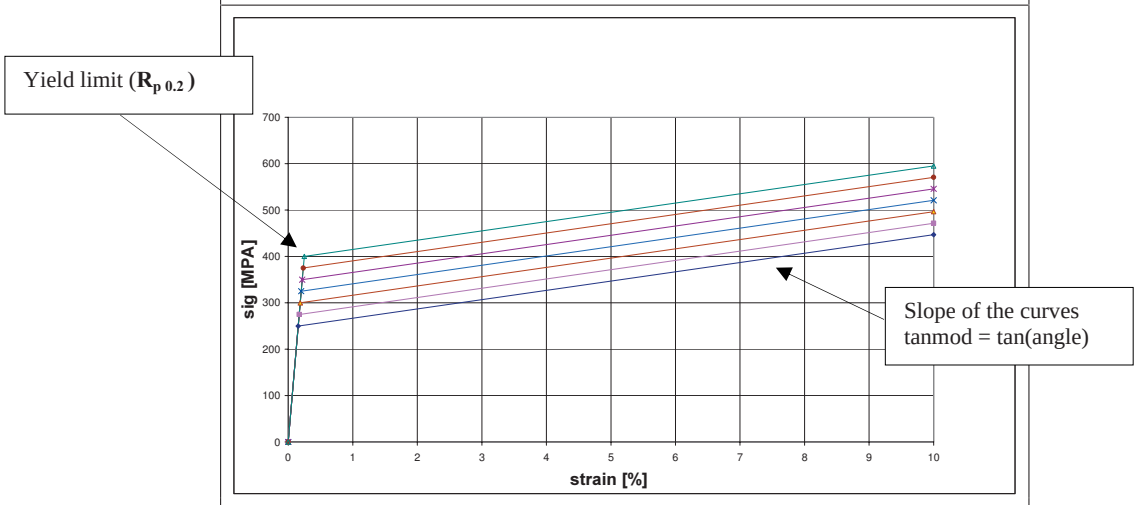

Fig. 3. Used type of curves.

3.4 BOUNDARY CONDITIONS 2-D

The following boundary conditions are true for all 2-D analyses.

- Evenly distributed outer pressure.
- The symmetry sections are constrained in tangential direction.
- The centre node is constrained in the xy-plane.

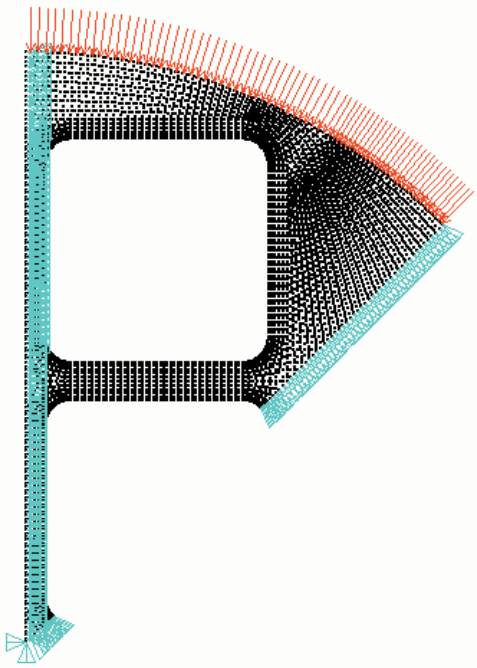

Fig. 4. Boundary conditions 2D

4 VERIFICATION 3D – 2D

The analyses are performed in order to verify that 2-D analyses gives adequate results compared to complete 3-D analyses. The results from the analyses show that the difference between 3-D and 2-D is small enough to exclude 3-D analyses (appendix 1 and 2).

4.1 GEOMETRY

Because of symmetry and the absence of discontinuities in both geometry and loads, only 1/8:th of the geometry has been modelled in 2D and half the length in the 3D-modell. The length of the 3D model is 800 mm. The insert is 750 mm and the bottom is 50 mm.

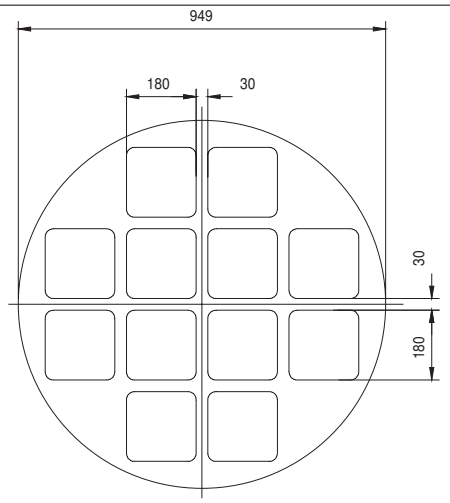

Fig. 5. Complete cross-section

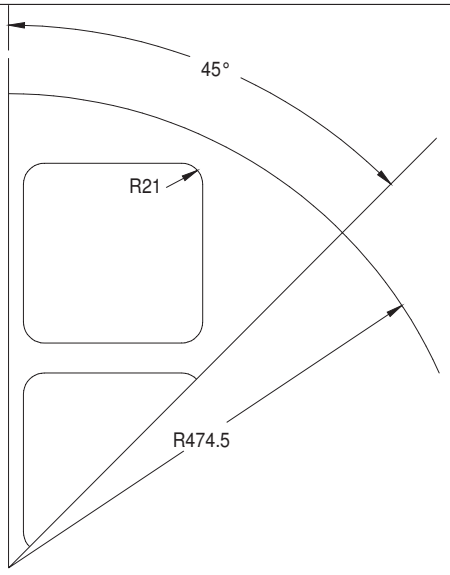

Fig. 6. 1/8 geometry

4.2 THE MODELS

The elements that have been used in the 2D analysis is Ansys element PLANE183 "2-D 8-Node Structural Solid, plain strain" and for 3D SOLID186 ”20-noded structural Solid”.

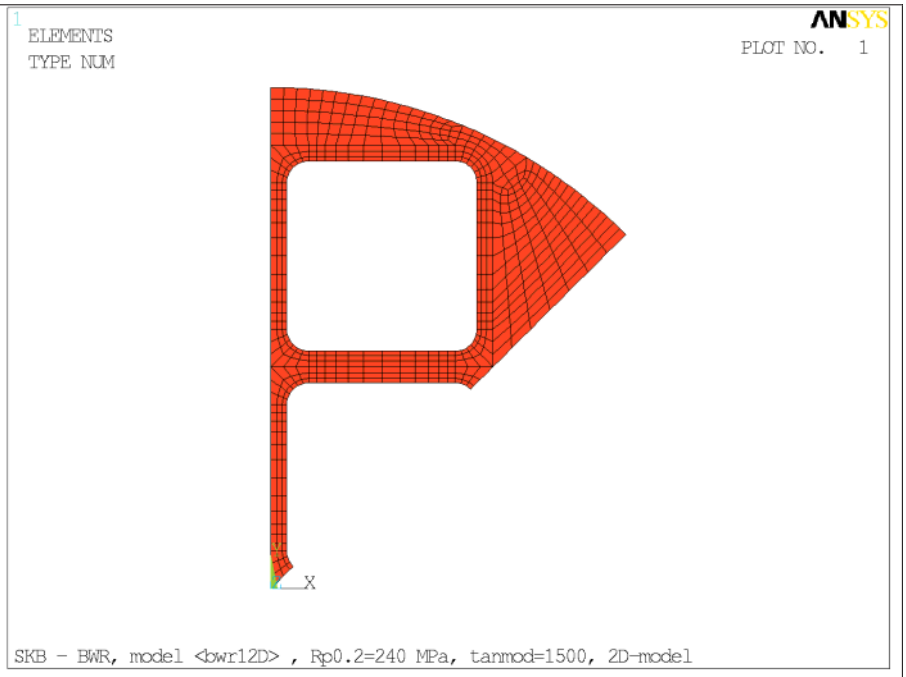

Fig. 7. 2D-model

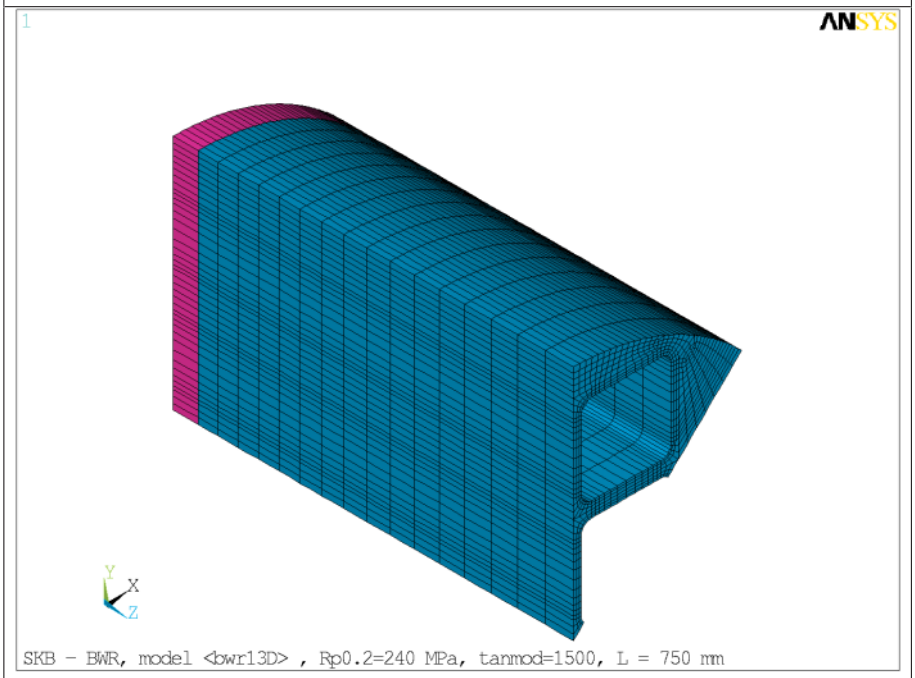

Fig. 8. 3D-model

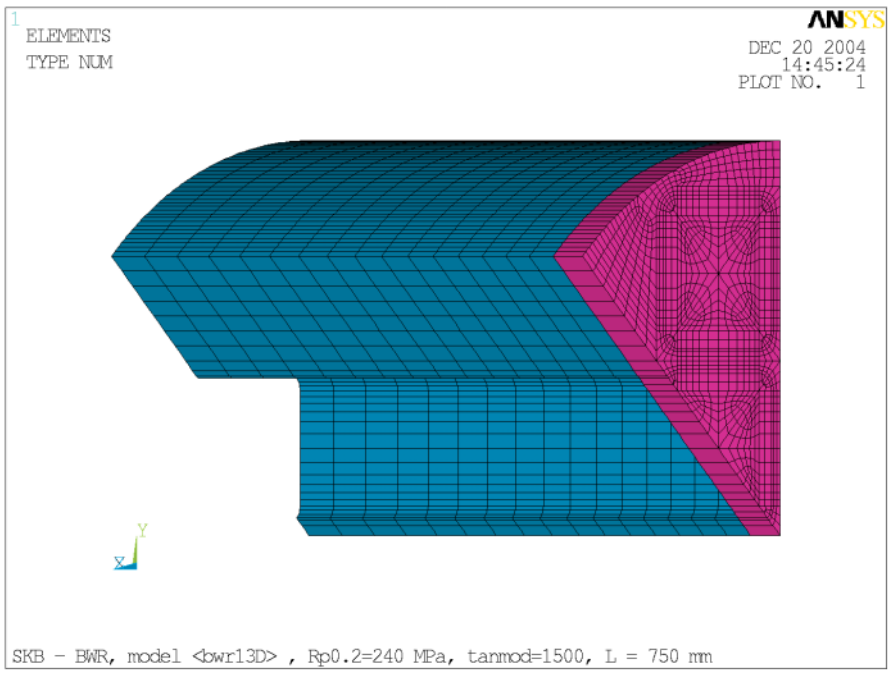

Fig. 9. 3D-model

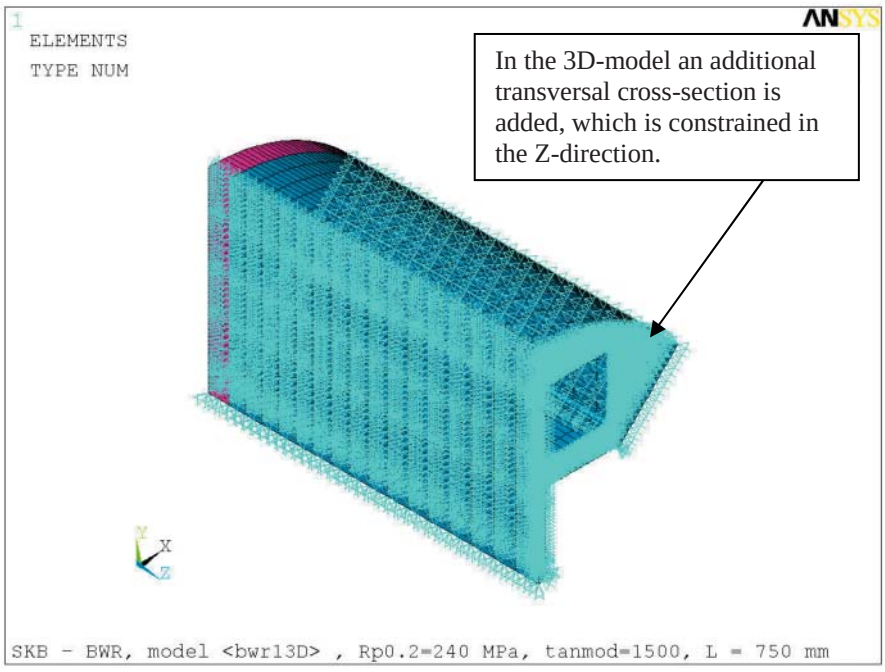

Fig. 10. Boundary conditions 3D

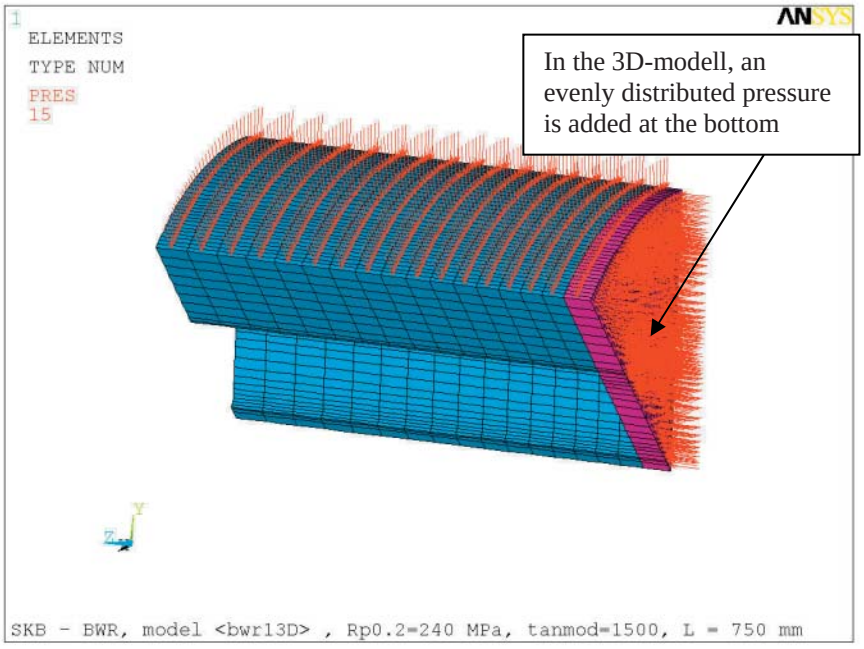

Fig. 11. Loads 3D

4.3 MATERIAL

The models contain only the cast iron.

4.3.1 Material data

Young's modulus = $E = 160000$ N/mm^2

Tensile strength = $R_{p\,0.2} = 240$ MPa

Strain at $R_{p\,0.2}$ = $\varepsilon_{sy} = \frac{R_{p\,0.2}}{E} = 1.5E^{-3}$

Ultimate strength = $R_m = 388$ MPa

Tangent modulus = $\text{tanmod} = E_T = \frac{R_m - R_{p\,0.2}}{\varepsilon_{su} - \varepsilon_{sy}} = 1500$

Ultimate strain = $\varepsilon_{su} = 10\%$

5 PRESSURE TEST

The analyses are performed using a model of the “compression test nr 1 specimen” (Ref. 9). The purpose is to ensure that requisite pressure can be achieved in the test, which was also shown (appendix 3 and ref 9).

5.1 GEOMETRY

The model contains the cast iron part, the steel cassette, the copper cylinder, the copper lid and the steel lid.

Only half the length and ¼:th of the cross-section has been modelled because of symmetry. A few figures showing the geometry are presented below.

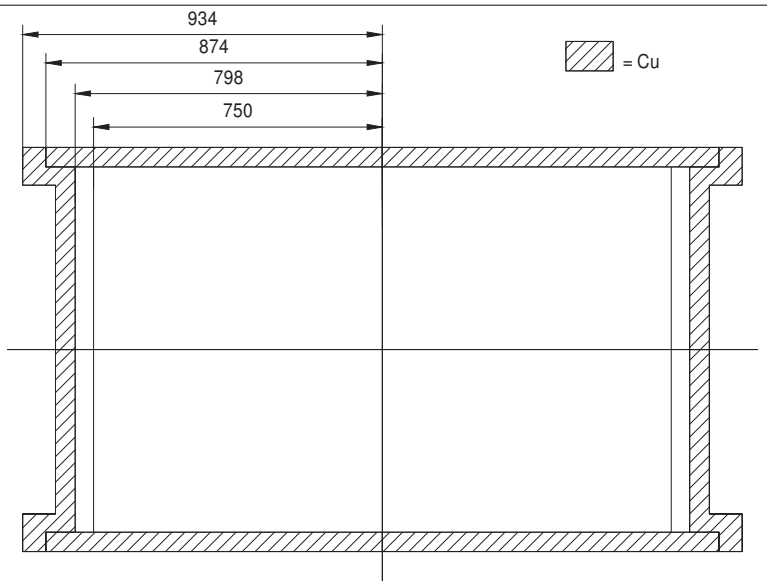

Fig. 12. Complete geometry

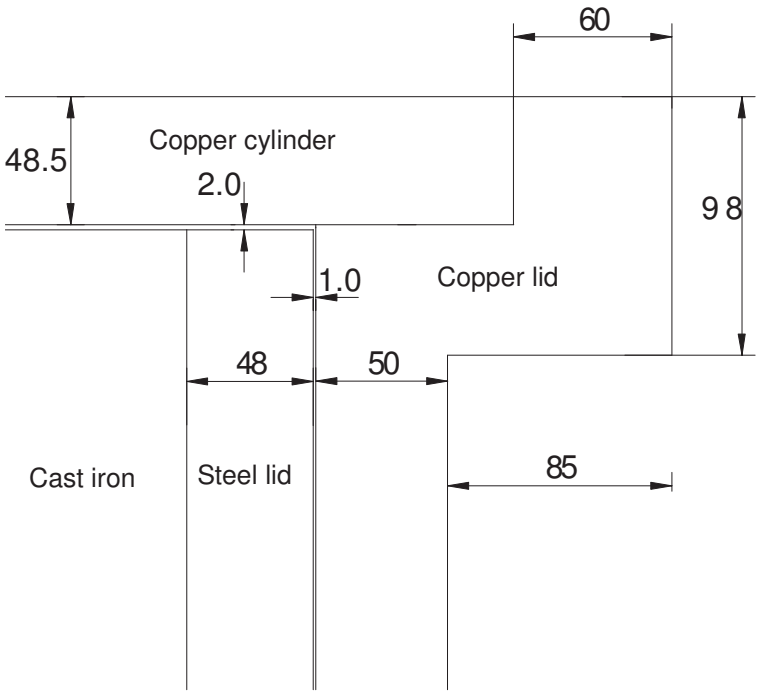

Fig. 13. Detail measures

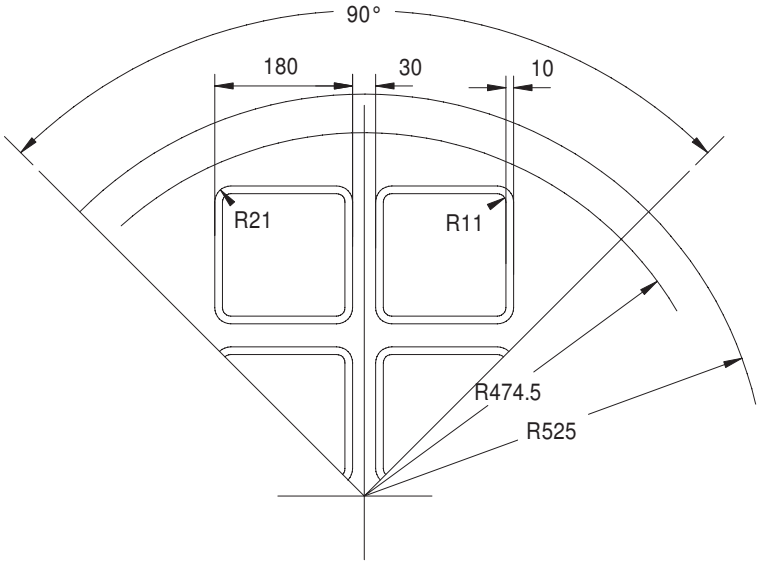

Fig. 14. Cross-section

5.2 MODELS

Ansys element SOLID186 ”20-noded Structural Solid” is used in this model.

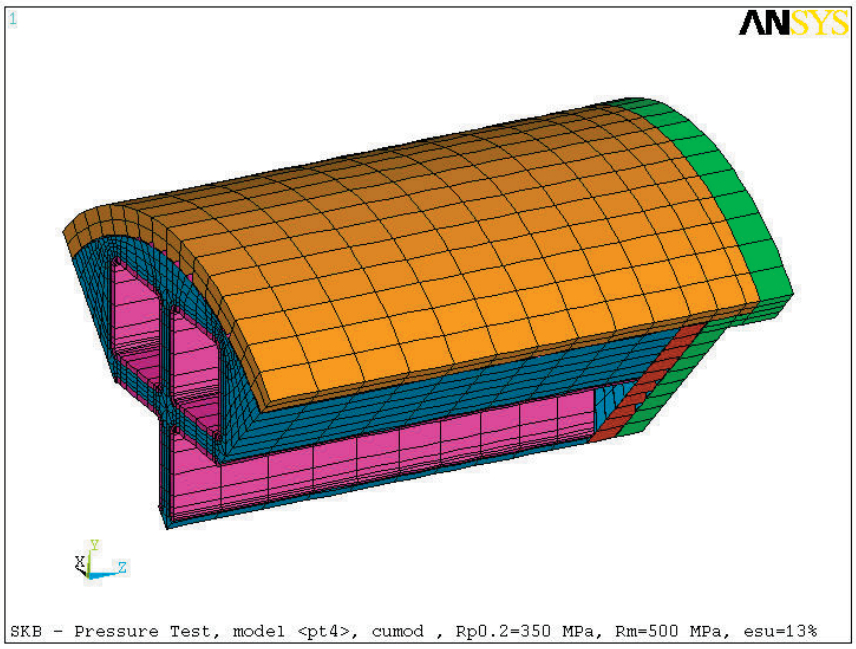

Fig. 15. Model, all parts.

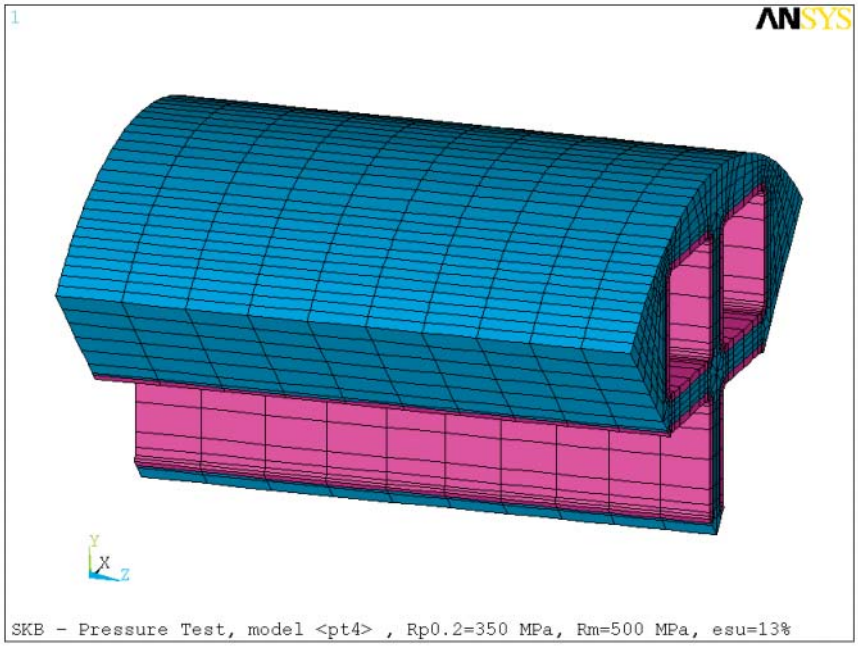

Fig. 16. Model, cast iron and steel cassette

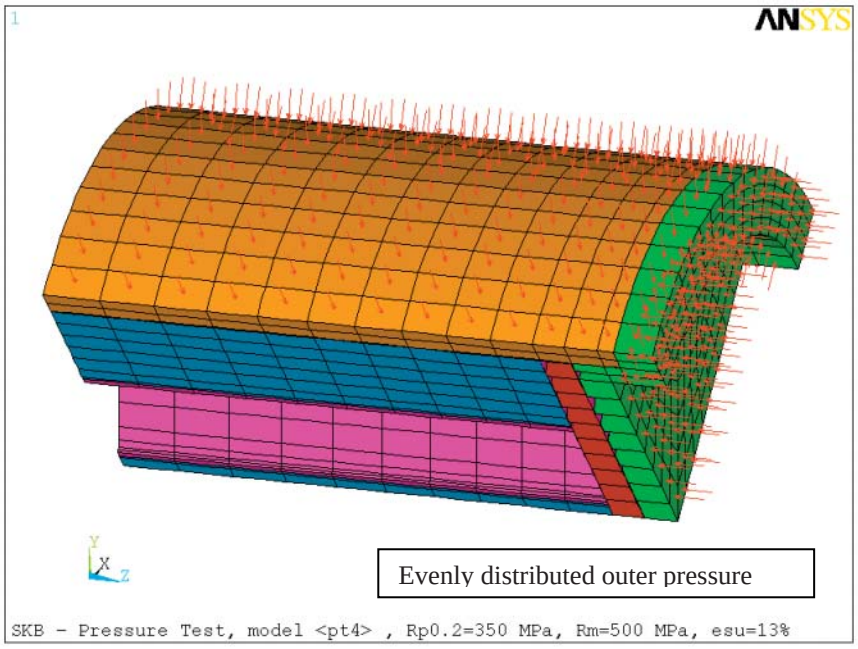

Fig. 17. Loads

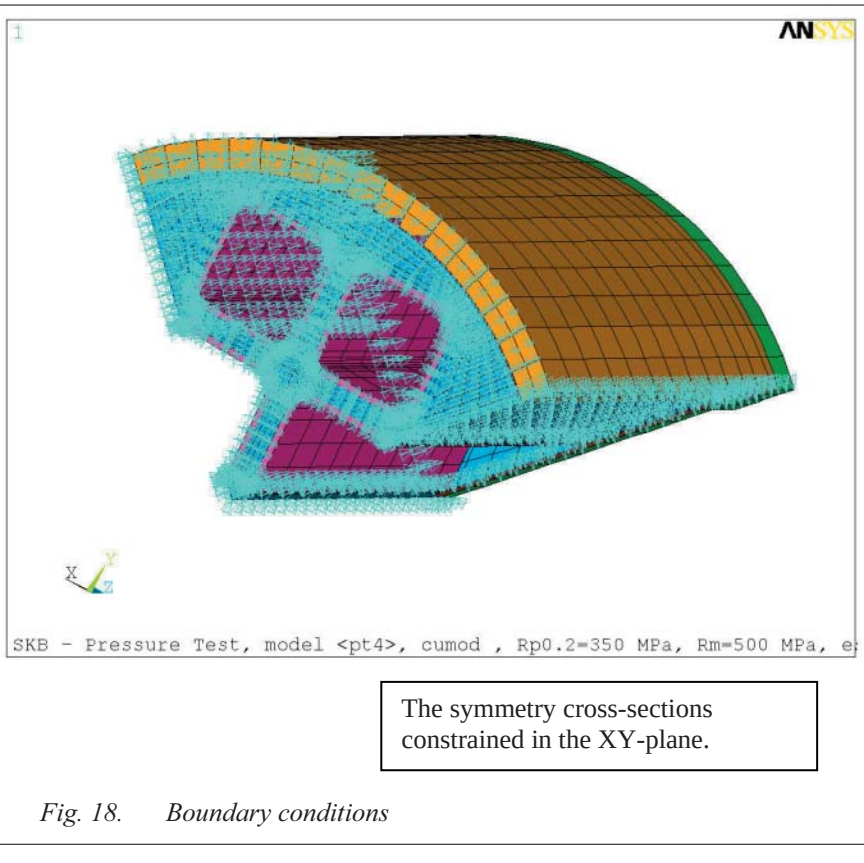

Fig. 18. Boundary conditions

5.3 MATERIAL

Material data with high values on the tensile strength and the ultimate strength have been chosen. This was done to prevent the analyses from showing higher deformations than the test.

5.3.1 Material data cast iron

Material model = BISO

Young's modulus = E = 160000 N/mm^2

Tensile strength = $R_{p\,0.2}$ = 350 MPa

Strain at $R_{p\,0.2}$ = $\varepsilon_{sy} = \frac{R_{p\,0.2}}{E} = 2.2E^{-3}$

Ultimate strength = R_m = 500 MPa

Tangent modulus = tanmod = $E_T = \frac{R_m - R_{p\,0.2}}{\varepsilon_{su} - \varepsilon_{sy}} = 1170$

Ultimate strain = ε_{su} = 13%

5.3.2 Material data steel cassette

Material model = MISO

Name= S355J2H Standard: SS-EN 10 219-1,
Material number 1.0576

Young's modulus = E = 205000 N/mm^2

Tensile strength = $R_{p\,0.2}$ = 355 MPa

Strain at $R_{p\,0.2}$ = $\varepsilon_{sy} = \frac{R_{p\,0.2}}{E} = 1.7E^{-3}$

Ultimate strength = R_m = 560 MPa

Tensile modulus = Not applicable

Ultimate strain = ε_{su} = 20%

5.3.3 Material curve steel cassette

Uniaxial test data. $\sigma_e = \dfrac{Force}{Initial\ area}$ $\varepsilon_e = \dfrac{Length}{Initial\ length}$

Conversion to true stress and strain values.

$\sigma_t = (1+\varepsilon_e)\cdot\sigma_e$

$\varepsilon_t = \log(1+\varepsilon_e)$

Point	σ_e	ε_e	σ_t	ε_t
1	355	1.73E-03	355	1.73E-03
2	355	0.050	373	0.049
3	437	0.100	481	0.095
4	509	0.150	585	0.140
5	560	0.200	672	0.182

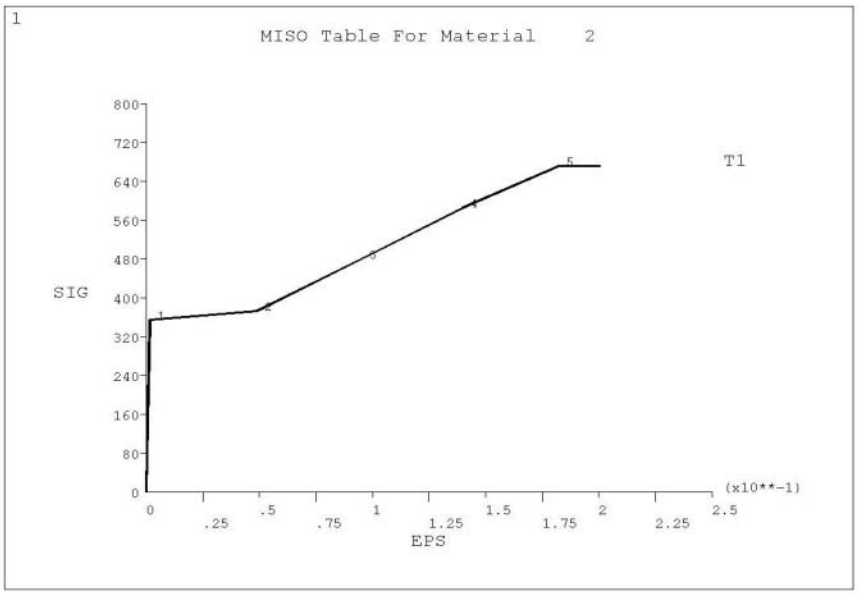

Fig. 19. Stress-strain curve steel cassette

5.3.4 Material data steel lid

Material model = MISO

Name = S355J2G4 Standard: SS-EN 10025, Material number 1.0577

Young's modulus = E = 205000 N/mm^2

Tensile strength = $R_{p\,0.2}$ = 335 MPa

Strain at $R_{p\,0.2}$ = $\varepsilon_{sy} = \frac{R_{p\,0.2}}{E} = 1.6E^{-3}$

Ultimate strength = R_m = 560 MPa

Tensile modulus = Not applicable

Ultimate strain = ε_{su} = 21%

5.3.5 Material curve steel lid

Notation according to 5.3.3

Point	σ_e	ε_e	σ_t	ε_t
1	335	1.63E-03	335	1.63E-03
2	335	0.050	352	0.049
3	425	0.100	468	0.095
4	504	0.150	579	0.140
5	560	0.200	672	0.182

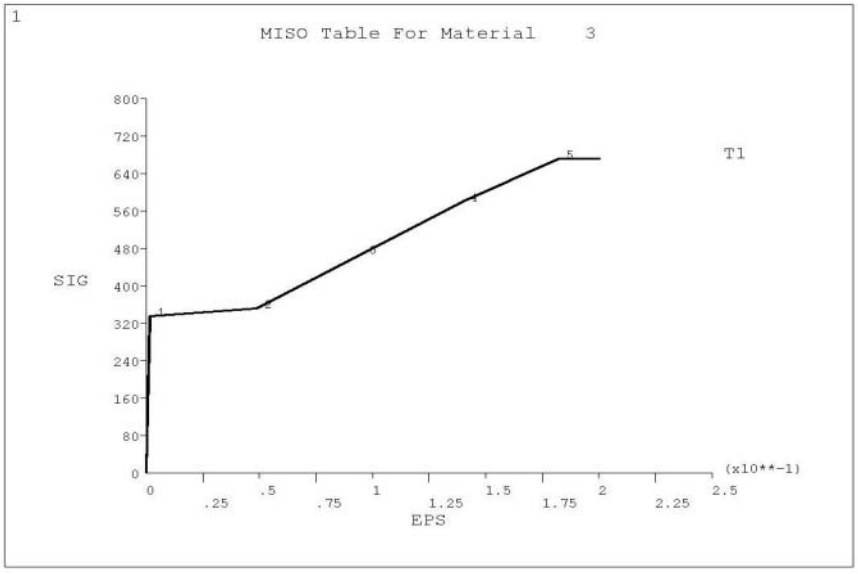

Fig. 20. Stress-strain curve steel lid

5.3.6 Material data copper

Material data is taken from ref. [11].

Material model = MISO

Young's modulus = E = 1.103e5 N/mm^2

Tensile strength = $R_{p\,0.2}$ = 50 MPa

Strain at $R_{p\,0.2}$ = $\varepsilon_{sy} = \frac{R_{p\,0.2}}{E} = 4.5E^{-4}$

Poisson's ratio = ν = 0.33

Shear modulus = $G = \frac{E}{2(1+\upsilon)} = 41470\frac{N}{mm^2}$

5.3.7 Material curve copper

The curve characteristics and the tensile strength is described by the function:

$\sigma_i = K \cdot \delta_i^{\,n} + \sigma_s$

Typical values for copper according to ref. [11].

K = 46000 psi = 317 MPa

n = 0.54

The points describing the curve below are calculated in appendix 9.

Notation according to 5.3.3

Point	σ_t	ε_t
1	50	4.53E-04
2	70	4.08E-03
3	90	1.80E-02
4	110	4.00E-02
5	130	7.00E-02
6	150	0.108
7	170	0.154
8	190	0.207
9	210	0.267
10	230	0.334
11	250	0.408
12	270	0.489
13	290	0.576

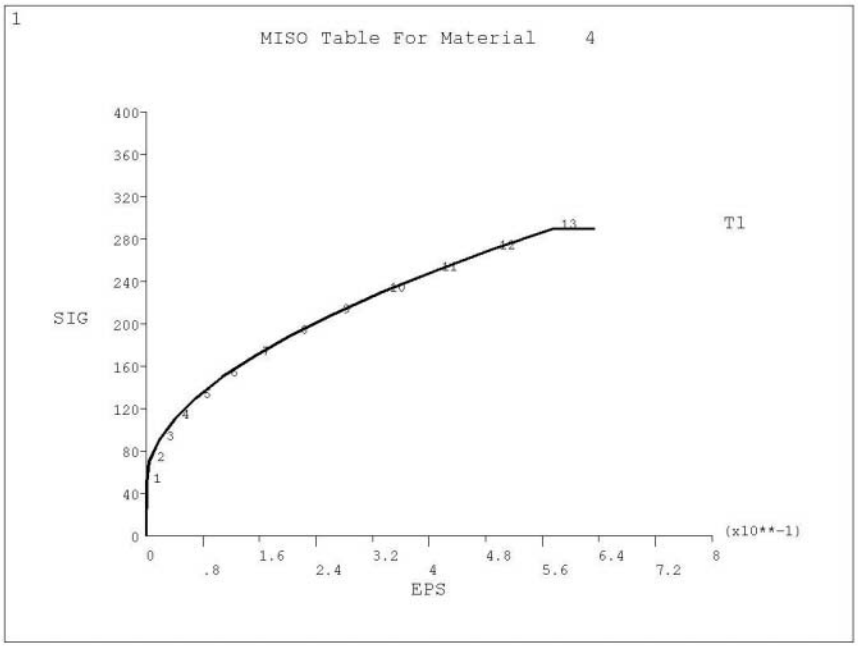

Fig. 21. Stress-strain curve copper

6 INFLUENCE OF CAST IRON MATERIAL MODEL.

The analyses are performed using a material model (Cast Iron) with different values in tension and compression. Quotation from the Ansys manual (ref. 10)

"The **Cast Iron** (CAST, UNIAXIAL) option assumes a modified von Mises yield surface, which consists of the von Mises cylinder in compression and a Rankine cube in tension. It has different yield strengths, flows, and hardenings in tension and compression. Elastic behavior is isotropic, and is the same in tension and compression. The **TB**,CAST command is used to input the plastic Poisson's ration in tension, which can be temperature dependent. Use the **TB**,UNIAXIAL command to enter the yield and hardening in tension and compression."

The results show that even very small values of $R_{p0.2}$ och R_m in tension do not affect the results. Considering this, it is enough to use only compression test data in the probabilistic analysis.

6.1 GEOMETRY

One 1/8:th plane model without steel cassette has been analysed.

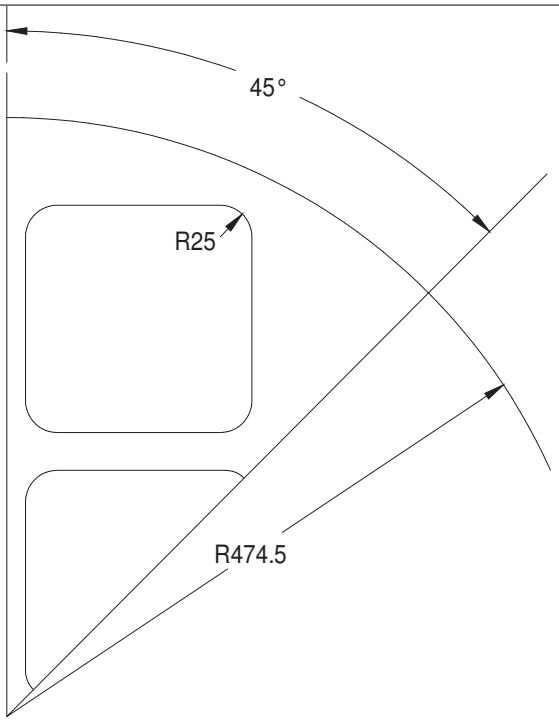

Fig. 22. 1/8 geometry

6.2 MODEL

Ansys element PLANE183 "2-D 8-Node Structural Solid, plain strain" was used in this model.

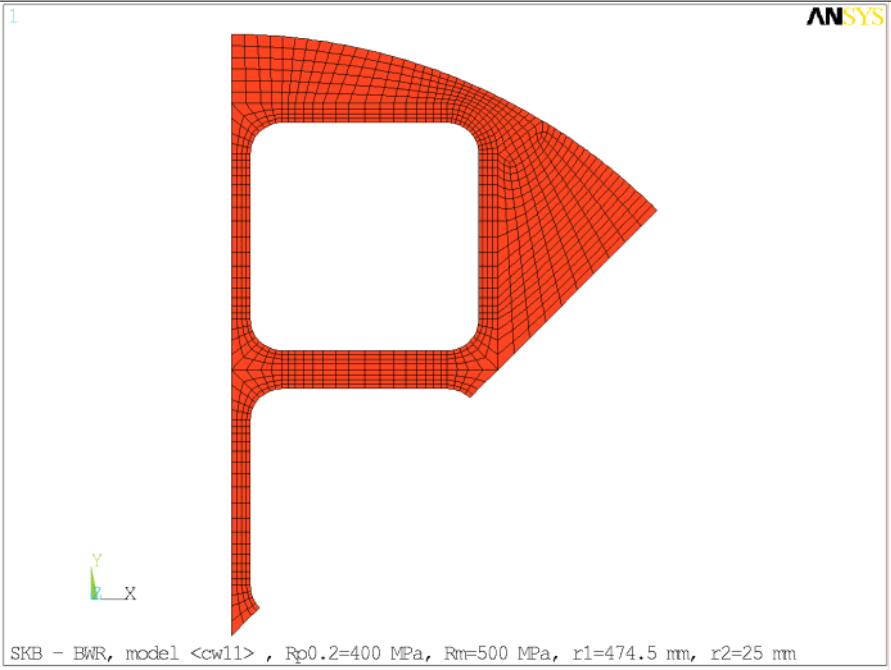

Fig. 23. 1/8 model

6.3 MATERIAL

The analyses have been performed using a bilinear elastic/plastic material model. The material data in tension have gradual been decreased.

		material	tension		compression	
	model	model	$Rp_{0.2}$	Rm	$Rp_{0.2}$	Rm
	cw11	biso	400	500	400	500
	cw21	cast iron	400	500	400	500
	cw22	cast iron	200	250	400	500
	cw23	cast iron	100	125	400	500

6.3.1 Material curves

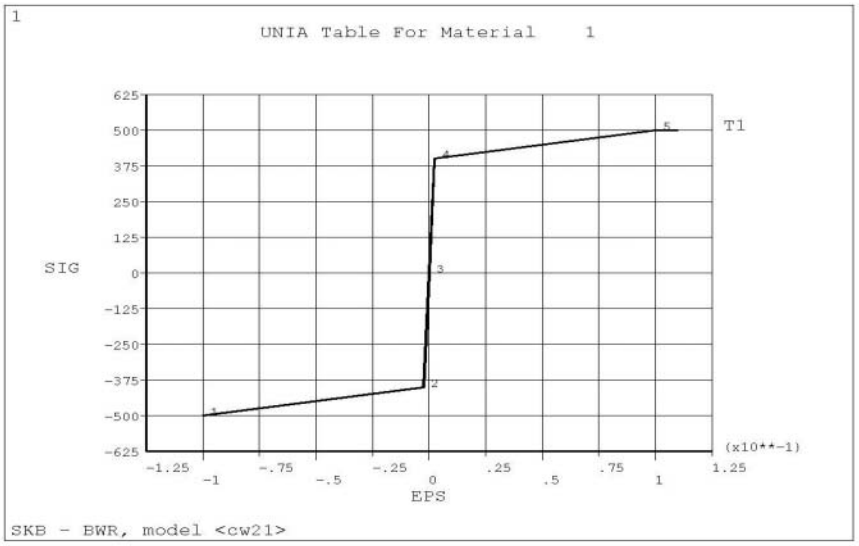

Fig. 24. Stress-strain curve equal in tension and compression

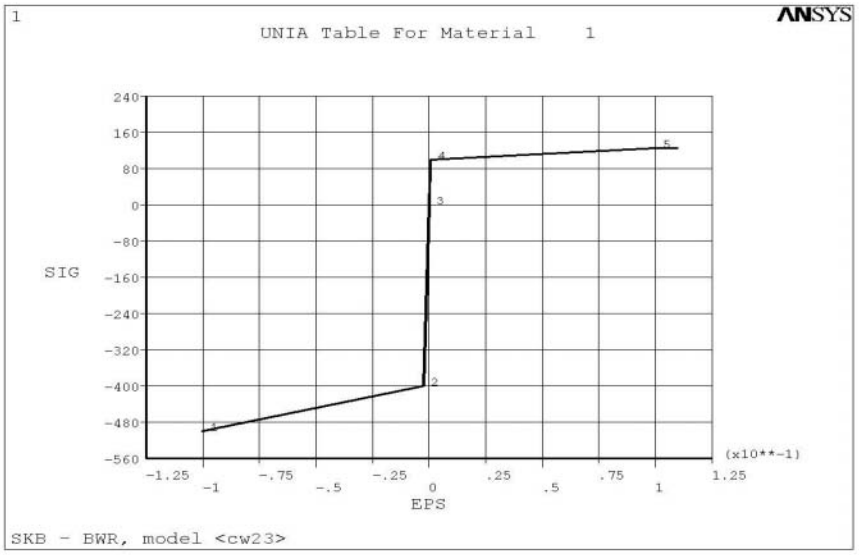

Fig. 25. Stress-stain curve different in tension and compression

7 INFLUENCE OF COPPER CYLINDER

The purpose of theses analysis is to see the influence of the copper cylinder on the stress and strain in the casting.

A plane model with steel cassettes and copper cylinder has been analysed and the results have been compared to the corresponding model without the copper cylinder.

The results show that the copper cylinder has a significant influence on the results only at very high pressures. At a normal pressure of 45 MPa the influence is negligible (appendix 4).

7.1 GEOMETRY

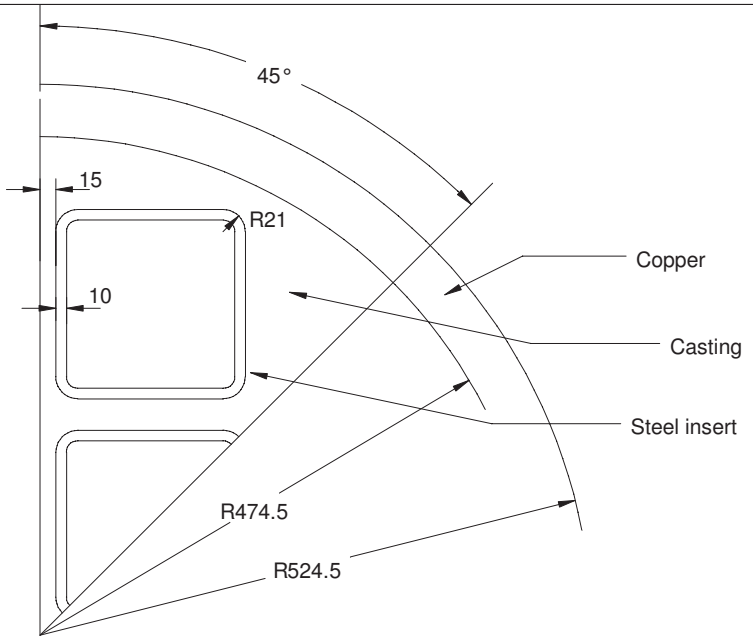

Fig. 26. 1/8 geometry

7.2 MODEL

Ansys element PLANE183 "2-D 8-Node Structural Solid, plain strain", was used in this structure.

There are contact elements in the column between the casting and the copper cylinder. CONTA172 ”2-D 3-Node Surface-to-Surface Contact” and TARGE169 “2-D Target Segment”

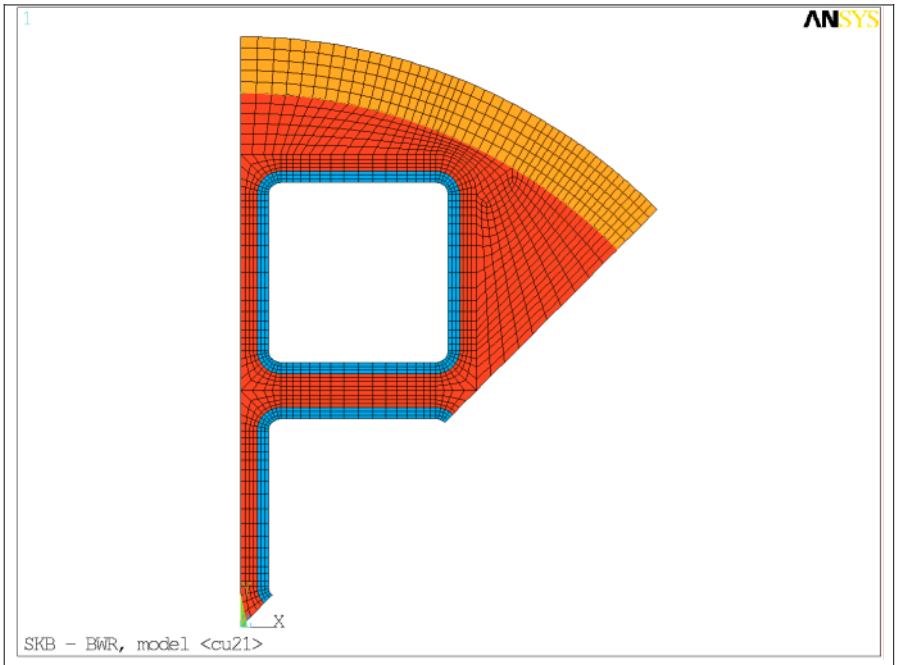

Fig. 27. 1/8 model

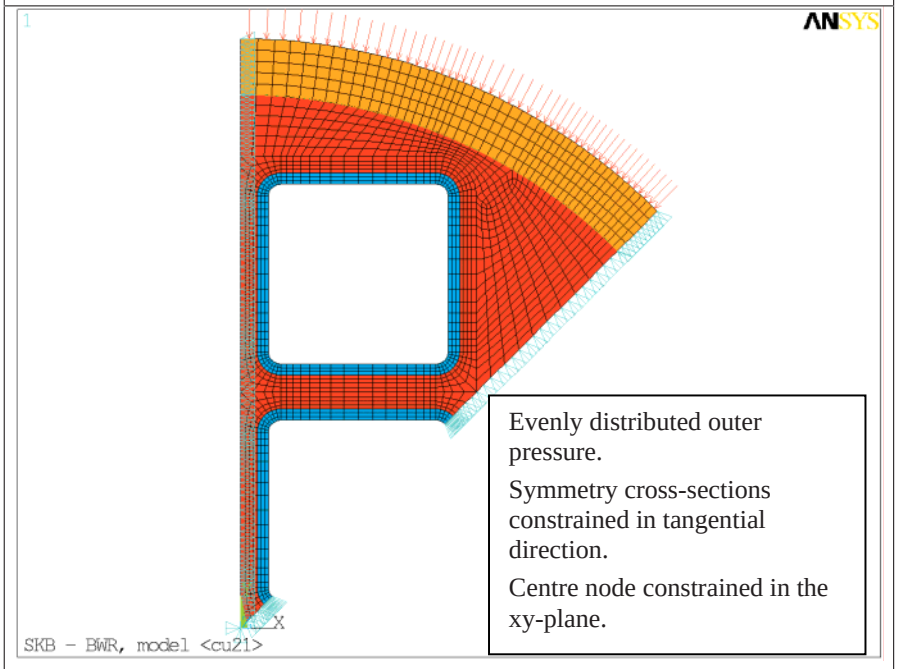

Fig. 28. Boundary conditions and loads

7.3 MATERIAL

7.3.1 Material data cast iron

Material model = BISO

Young's modulus = E = 160000 N/mm^2

Tensile strength = $R_{p\,0.2}$ = 280 MPa

Strain at $R_{p\,0.2}$ = $\varepsilon_{sy} = \frac{R_{p\,0.2}}{E} = 1.75E^{-3}$

Ultimate strength = R_m = 350 MPa

Tensile modulus = tanmod = $E_T = \frac{R_m - R_{p\,0.2}}{\varepsilon_{su} - \varepsilon_{sy}} = 1200$

Ultimate strain = ε_{su} = 6%

7.3.2 Material data steel cassette

Material model = MISO

Name = S355J2H Standard: SS-EN 10 219-1,
Material number 1.0576

Young's modulus = E = 205000 N/mm^2

Tensile strength = $R_{p\,0.2}$ = 355 MPa

Strain at $R_{p\,0.2}$ = $\varepsilon_{sy} = \frac{R_{p\,0.2}}{E} = 1.7E^{-3}$

Ultimate strength = R_m = 560 MPa

Tensile modulus = Not applicable

Ultimate strain = ε_{su} = 20%

7.3.3 Material curve steel cassette

Uniaxial test data. $\sigma_e = \dfrac{Force}{Initial\ area}$ $\varepsilon_e = \dfrac{Length}{Initial\ length}$

Conversion to true stress and strain values.

$\sigma_t = (1+\varepsilon_e)\cdot\sigma_e$

$\varepsilon_t = \log(1+\varepsilon_e)$

Point	σ_e	ε_e	σ_t	ε_t
1	355	1.73E-03	355	1.73E-03
2	355	0.050	373	0.049
3	437	0.100	481	0.095
4	509	0.150	585	0.140
5	560	0.200	672	0.182

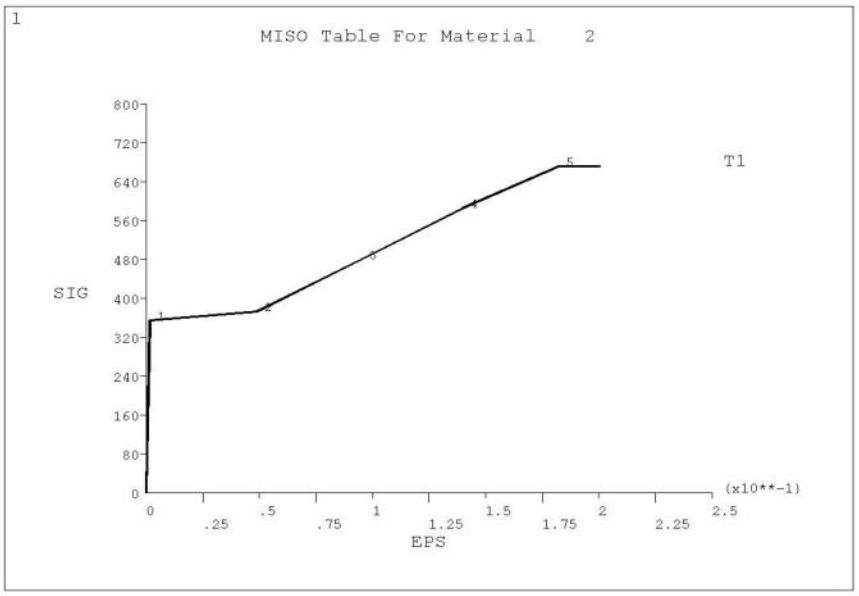

Fig. 29. Stress-strain curve steel cassette

7.3.4 Material data copper

Material data is taken from ref. [11].

Material model = MISO

Young's modulus = E = 1.103e5 N/mm^2

Tensile strength = $R_{p\,0.2}$ = 50 MPa

Strain at $R_{p\,0.2}$ = $\varepsilon_{sy} = \frac{R_{p\,0.2}}{E} = 4.5E^{-4}$

Poisson's ratio = ν = 0.33

Shear modulus = $G = \frac{E}{2(1+\upsilon)} = 41470\frac{N}{mm^2}$

7.3.5 Material curve copper

The characteristics of the curve is described by the function:

$\sigma_i = K \cdot \delta_i^{\,n} + \sigma_s$

Typical values for copper according to ref [11].

K = 46000 psi = 317 MPa

n = 0.54

The points describing the curve below are calculated in appendix 9.

Notation according to 5.3.3

Point	σ_t	ε_t
1	50	4.53E-04
2	70	4.08E-03
3	90	1.80E-02
4	110	4.00E-02
5	130	7.00E-02
6	150	0.108
7	170	0.154
8	190	0.207
9	210	0.267
10	230	0.334
11	250	0.408
12	270	0.489
13	290	0.576

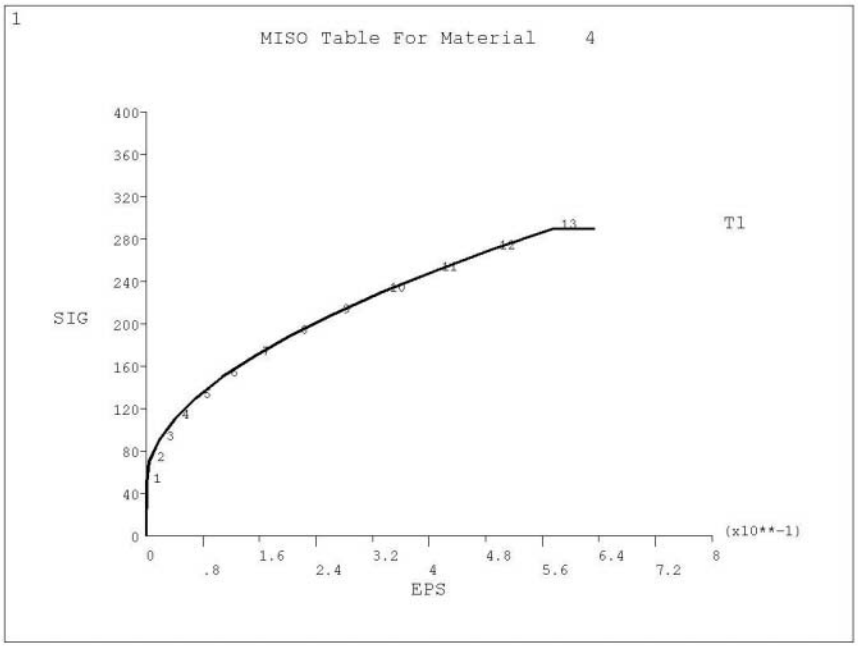

Fig. 30. Stress-strain curve copper

8 INFLUENCE OF ECCENTRICITY FOR THE STEEL CASSETTE

Four analyses were performed with the displacements 0,5 10 and 15 mm. The analyses show that the displacement has a major influence on the failure mechanism plastic collapse (appendix 5).

8.1 GEOMETRY

A plane model without steel cassette has been analysed. The eccentricity has been simulated using different outer radius, which is sufficient since only 1/8:th of the model has been analysed.

Parameters.

Corner radius = R_2 = 20 mm

Outer radius = R_1 = 474.5 mm

R_1 = 469.5 mm

R_1 = 464.5 mm

R_1 = 459.5 mm

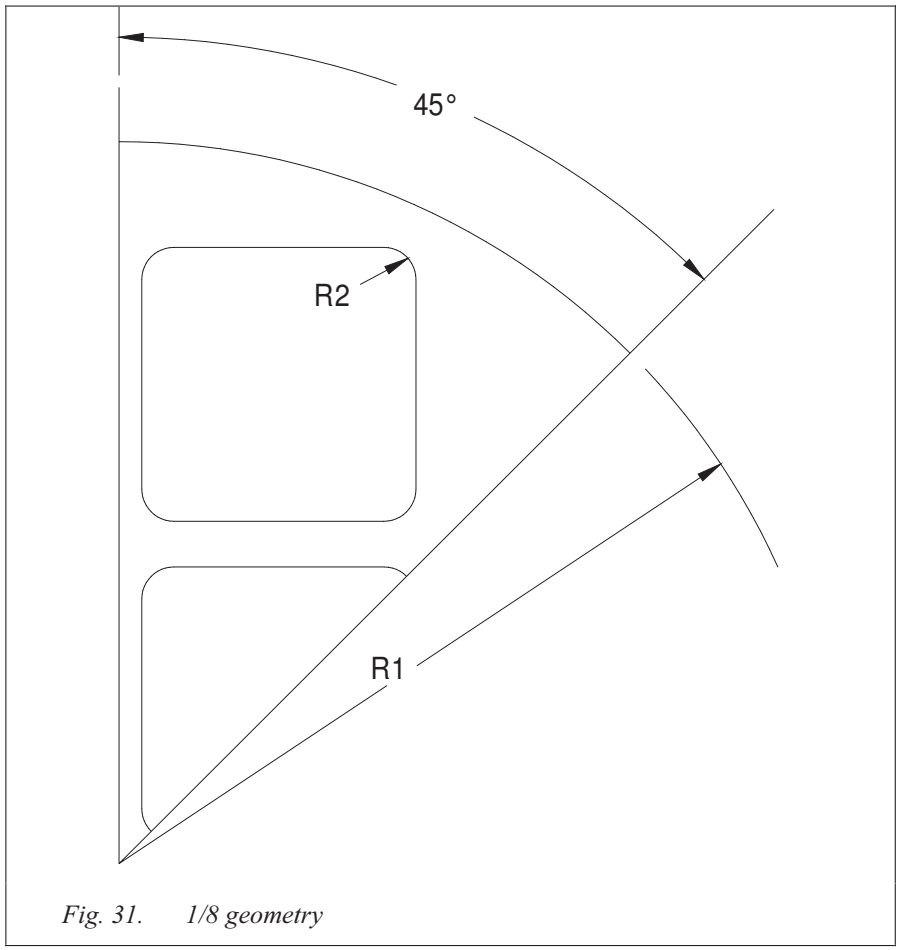

Fig. 31. 1/8 geometry

8.2 MODEL

Ansys element PLANE183 "2-D 8-Node Structural Solid, plain strain" was used in this structure.

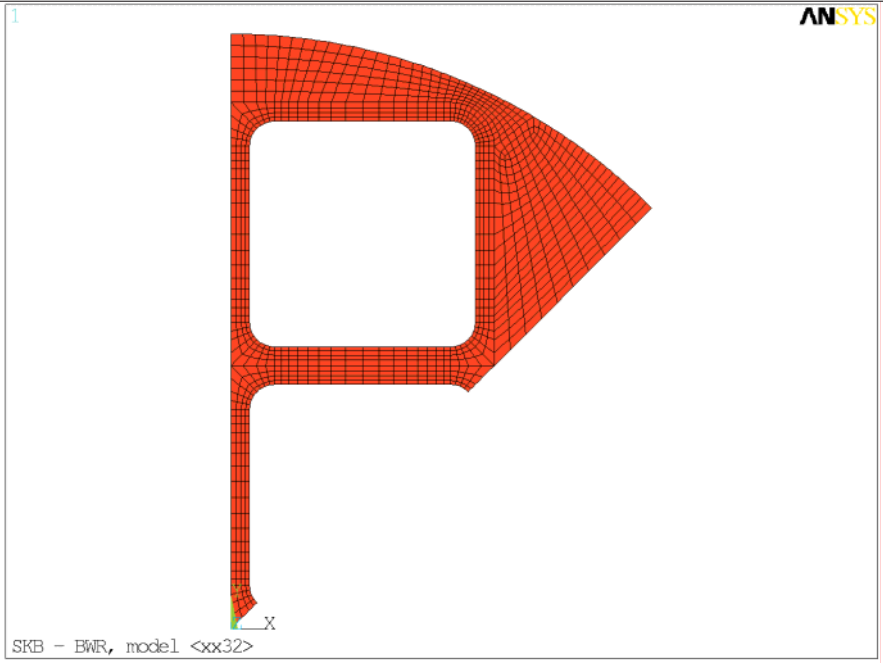

Fig. 32. 1/8 model.R_1 = 474.5 mm. Displacement = 0 mm

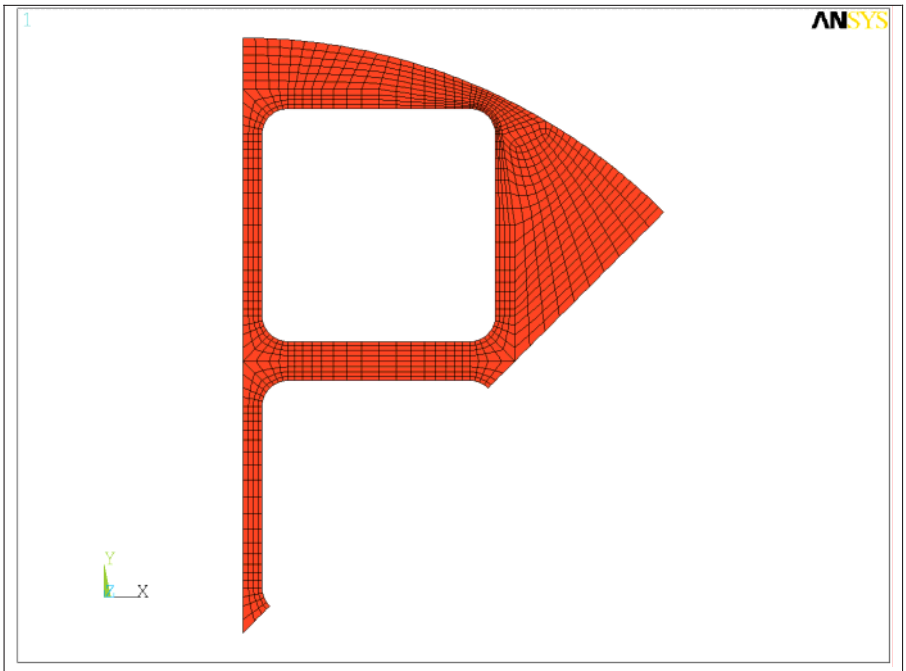

Fig. 33. 1/8 model.R_1 = 459.5 mm. Displacement = 15 mm

8.3 MATERIAL

The models consist of cast iron only.

8.3.1 Material data

Young's modulus = $E = 166000$ N/mm^2

Tensile strength = $R_{p\,0.2} = 270$ MPa

Strain at $R_{p\,0.2}$ = $\varepsilon_{sy} = \frac{R_{p\,0.2}}{E} = 1.6E^{-3}$

Ultimate strength = $R_m = 480$ MPa

Tensile modulus = $\text{tanmod} = E_T = \frac{R_m - R_{p\,0.2}}{\varepsilon_{su} - \varepsilon_{sy}} = 2130$

Ultimate strain = $\varepsilon_{su} = 10\%$

9 INFLUENCE OF THE CAST IRON INSERT RADIUS AGAINST THE STEEL PIPE CHANNEL

Three analysis were performed, using the radius 15, 20 and 25 mm. The analyses show that the radius has a relatively small influence on the failure mechanism plastic collapse (appendix 6).

9.1 GEOMETRY

A plane model without steel cassette has been analysed.

Parameters.

Outer radius = R_1 = 474.5 mm

Corner radius = R_2 = 15 mm

R_2 = 20 mm

R_2 = 25 mm

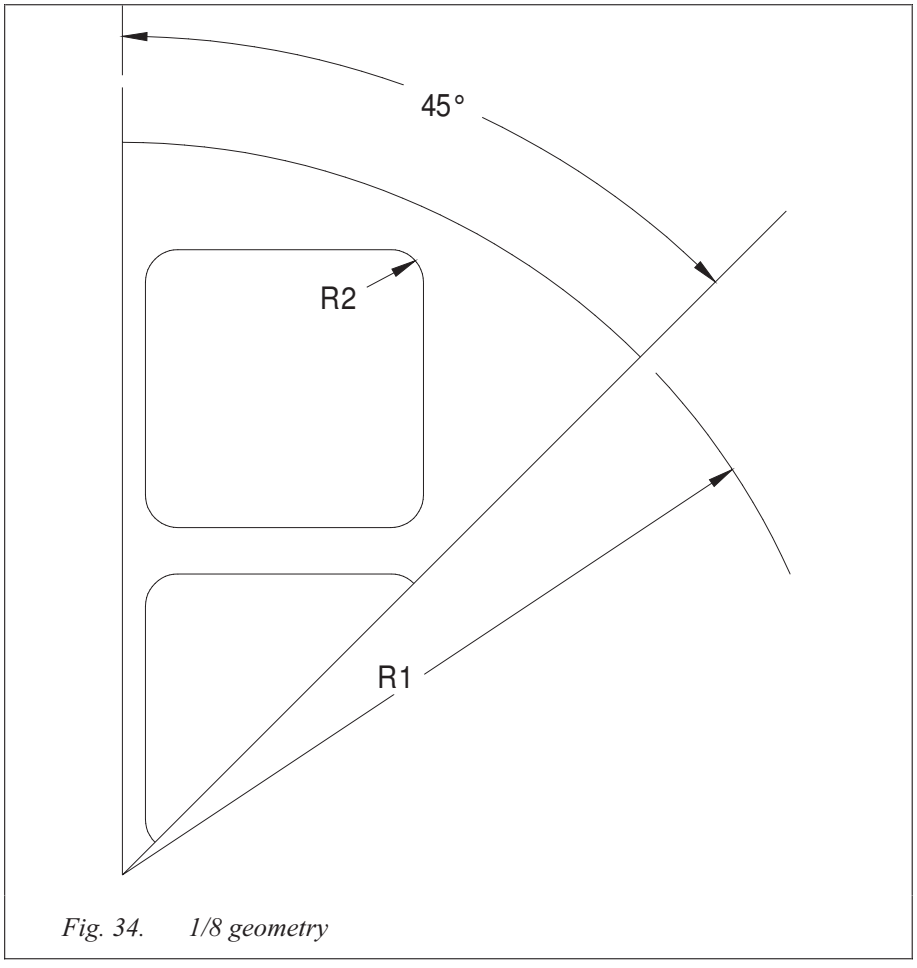

Fig. 34. 1/8 geometry

9.2 MODEL

Ansys element PLANE183 "2-D 8-Node Structural Solid, plain strain" was used in this structure.

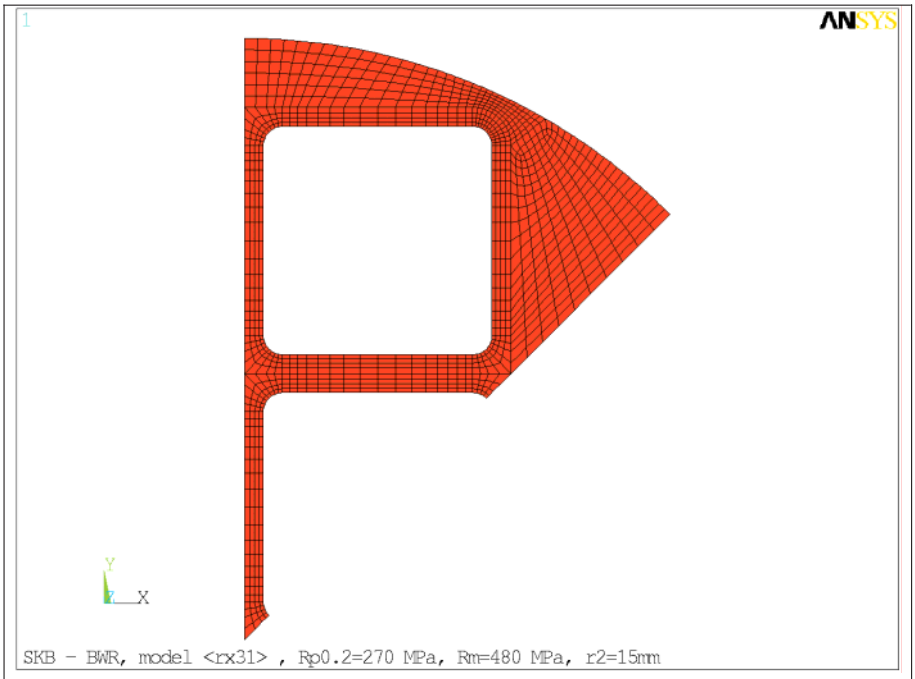

Fig. 35. 1/8 model, r2 = 15 mm

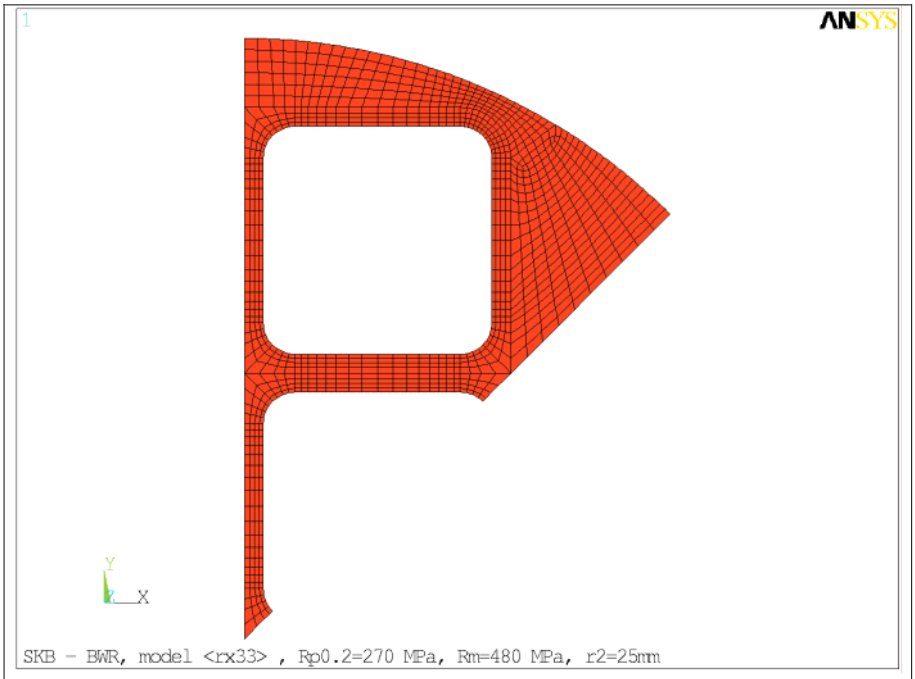

Fig. 36. 1/8 model, r2 = 25 mm

9.3 MATERIAL

The model consist only of cast iron.

9.3.1 Material data

Young's modulus = E = 166000 N/mm^2

Tensile strength = $R_{p\,0.2}$ = 270 MPa

Strain at $R_{p\,0.2}$ = $\varepsilon_{sy} = \frac{R_{p\,0.2}}{E} = 1.6E^{-3}$

Ultimate strength = R_m = 480 MPa

Tensile modulus = tanmod = $E_T = \frac{R_m - R_{p\,0.2}}{\varepsilon_{su} - \varepsilon_{sy}} = 2130$

Ultimate strain = ε_{su} = 10%

10 INPUT DATA FOR DNV-PROBABILISTIC ANALYSIS

The goal with this probabilistic analysis is to determine the probability for the canister to break. Since we know the material data distribution, the defects and the loads, it is possible to determine the probability for fracture or plastic collapse. DNV does here use a deterministic developed model, based on the FEM-analysis shown below, which can describe the relevant failure- and collapse mechanisms included in this study.

Fractures are assumed to be initiated and propagate in Modus I and plastic collapse is assumed to occur when a critical strain level is achieved.

DNV performs such an analysis using in-house developed software.

The stress and strain state in three chosen critical sections are taken from the FEM-analysis. In the subsequent probabilistic analysis, the probability for fracture in a certain given stress state and the probability for collapse in a certain given strain state are calculated.

10.1 GEOMETRY

Plane models without steel cassettes have been analysed.

The material is cast iron. Young's modulus = 166000 N/mm^2. Tensile strength and Ultimate strength according to 10.2

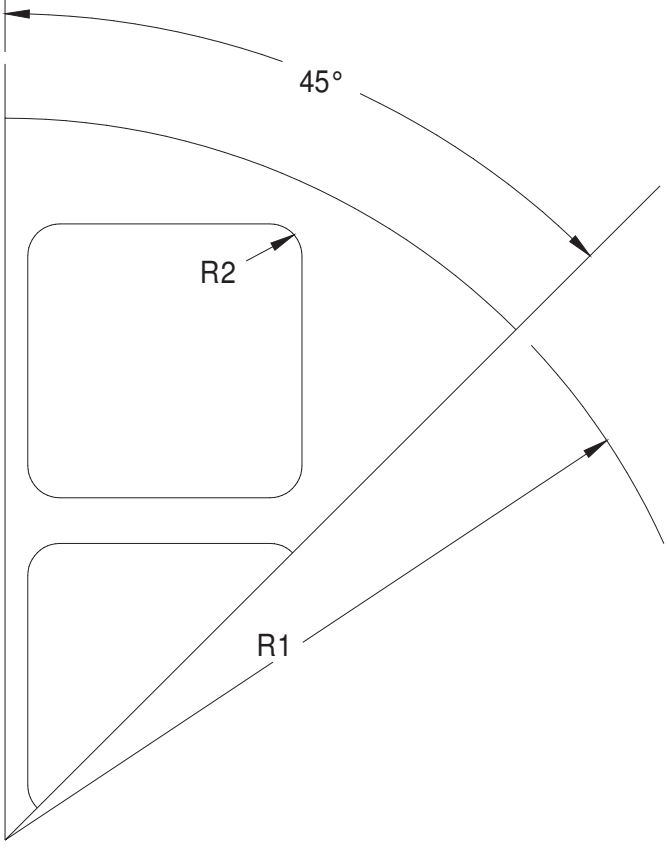

Fig. 37. 1/8 geometry

10.2 PROBABILISTIC PARAMETERS

				Index value					
Parameter	Variable	Index	Quantity	1	2	3	4	5	Unit
Outer radius	r_1	1	4	474.5	469.5	464.5	459.5		mm
Corner radius	r_2	2	3	15	20	25			mm
Tensile strength	$R_{p0.2}$	3	5	200	250	270	290	350	MPa
Ultimate strength	R_m	4	5	400	450	475	500	550	MPa
Number of combinations (analyses)			300						

10.2.1 Analysis ID

The ID of the Analysis (model name) is dnxxxx where xxxx is index 1-4 according to table 10.2

Example dn1222. r_1 = 474.5 mm, r_2 = 20 mm, $R_{p0.2}$ = 250 MPa, R_m = 450 MPa.

10.3 MODELS

Ansys element PLANE183 "2-D 8-Node Structural Solid, plain strain" was used in the plane 2D- models.

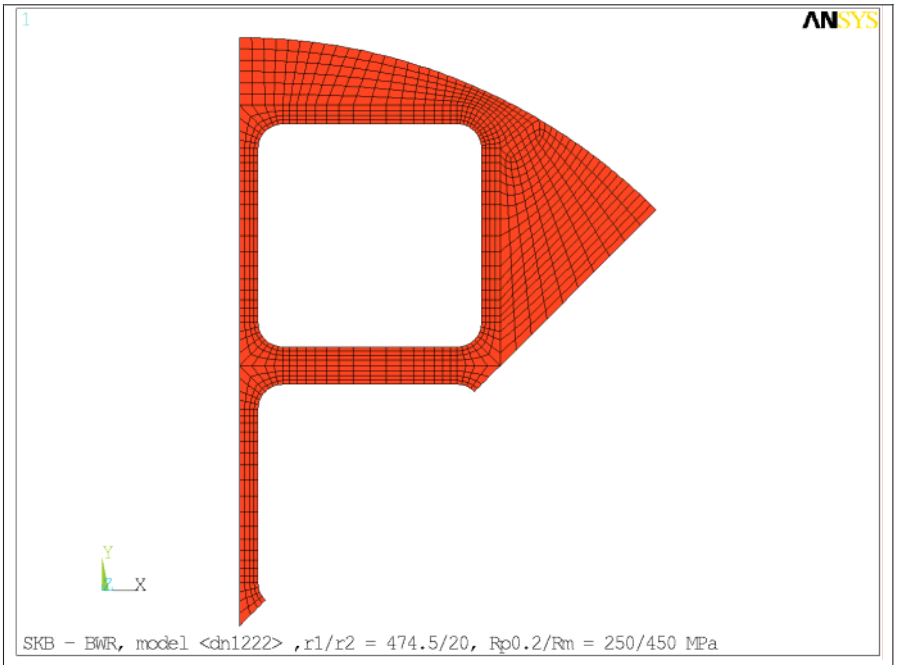

Fig. 38. 1/8 model

10.4 CRITICAL CROSS-SECTION

Stress and strain data is taken from three cross-sections.

Section 1	Thinnest section
Section 2	Most critical section
Section 3	Symmetry section x=0.

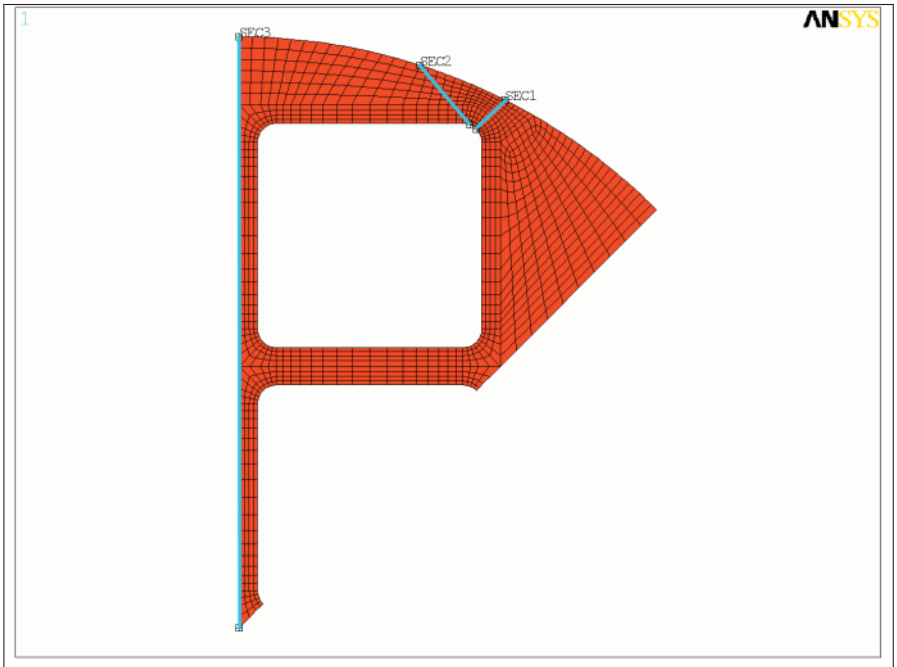

Fig. 39. Critical section 1, 2 and 3.

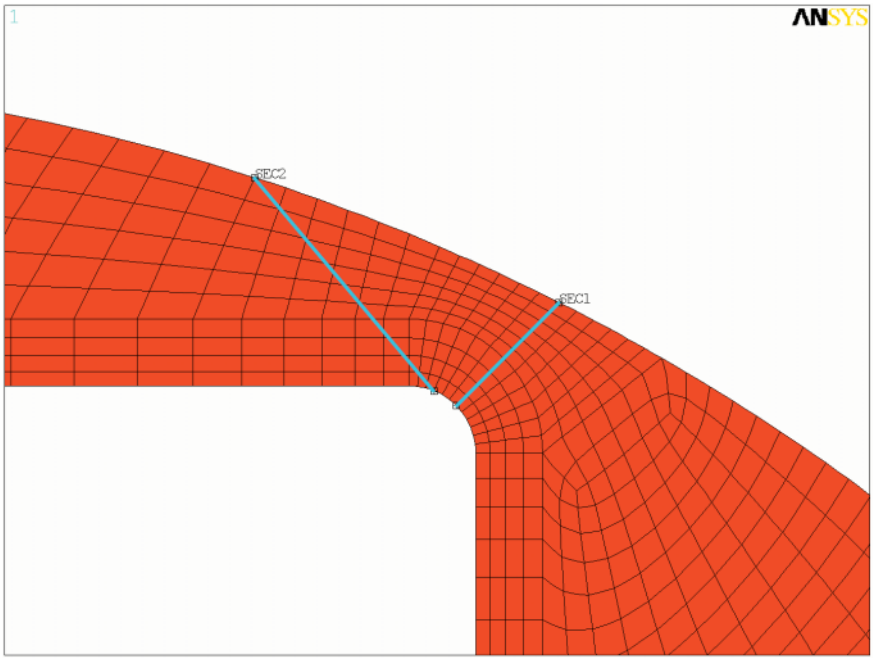

Fig. 40. Critical section 1 and 2.

10.4.1 Result example cross-section– normal case

10.4.1.1 Analysis dn1222.

Parameters according to 10.2.1

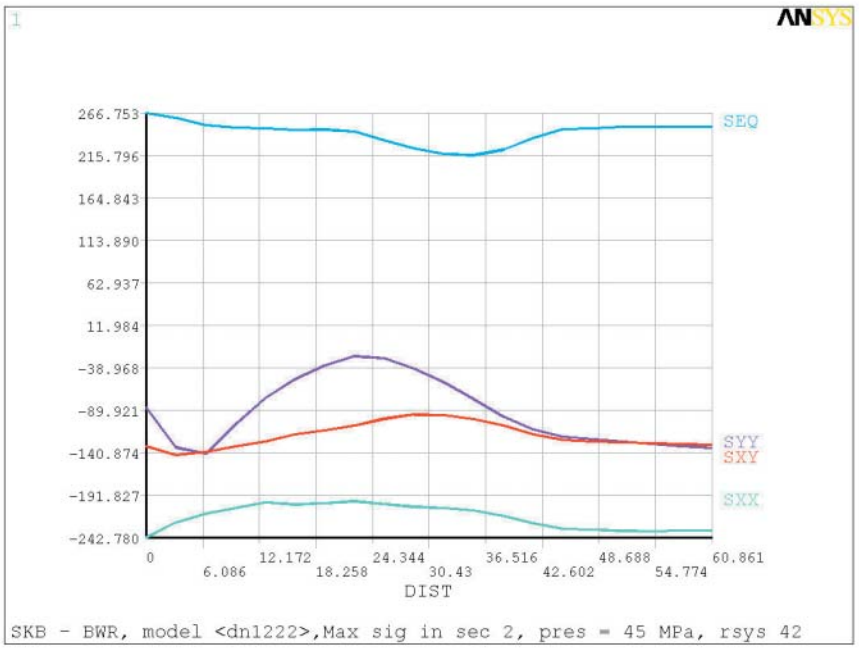

Fig. 41. Section 2, stresses.

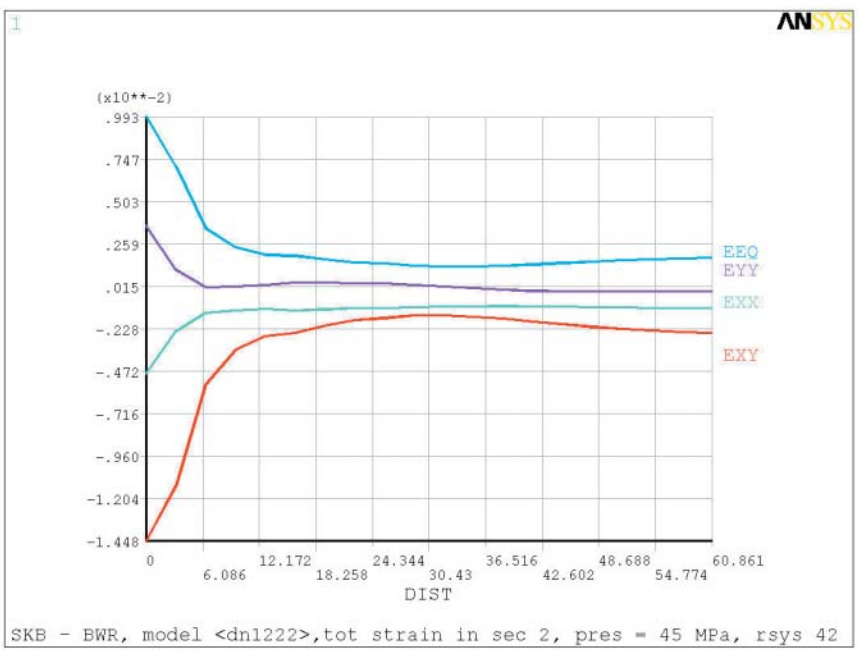

Fig. 42. Section 2 strains.

10.4.1.2 Analysis dn1244.

Parameters according to 10.2.1

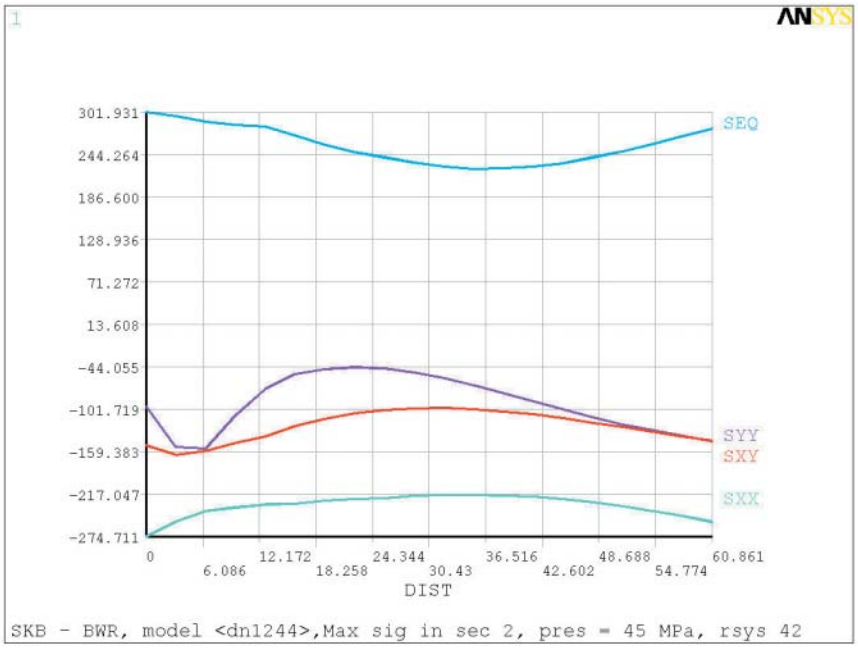

Fig. 43. Section 2, stresses.

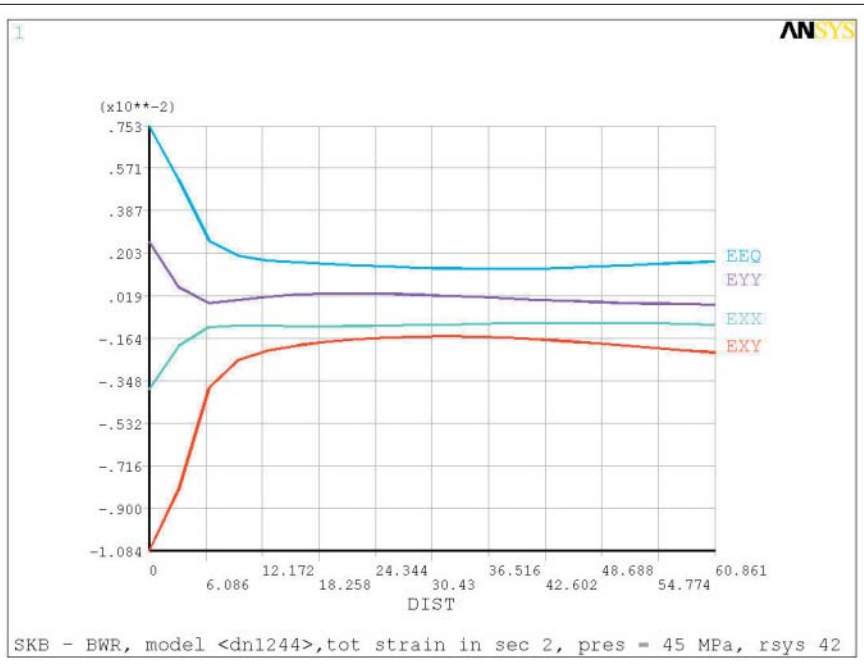

Fig. 44. Section 2, strains.

10.4.1.3 Analysis dn3222.

Parameters according to 10.2.1

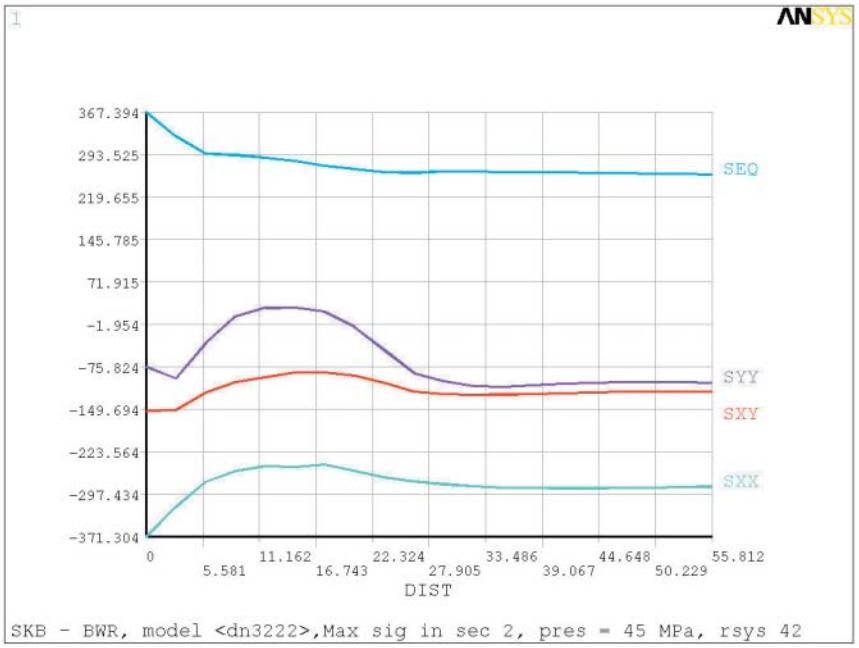

Fig. 45. Section 2, stresses.

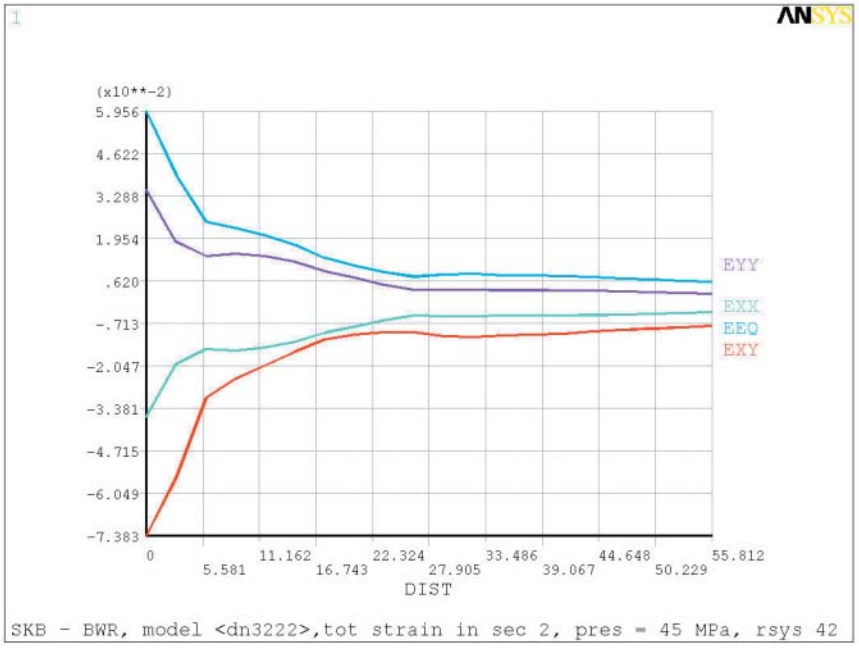

Fig. 46. Section 2, strains.

10.4.1.4 Analysis dn3244.

Parameters according to 10.2.1

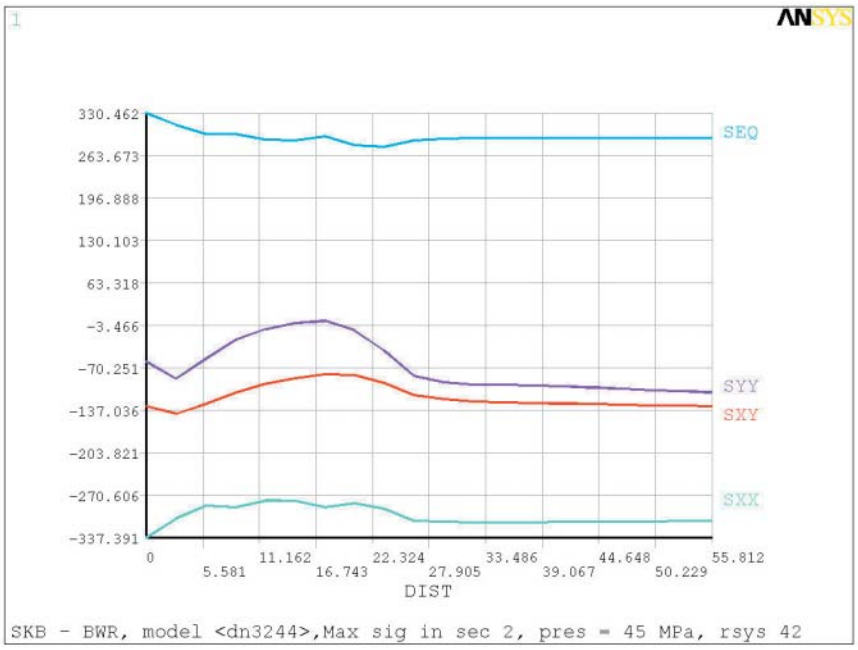

Fig. 47. Section 2, stresses.

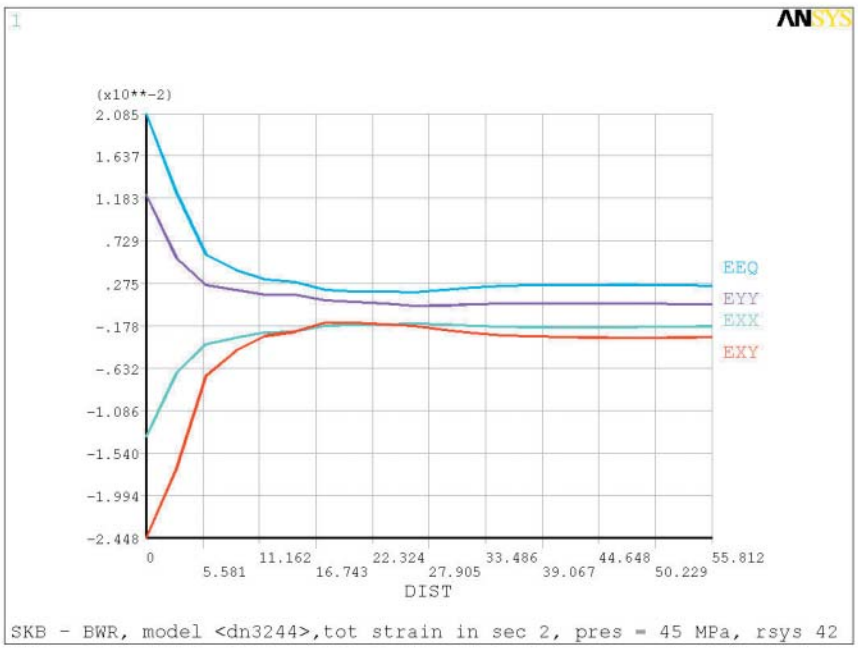

Fig. 48. Section 2, strains.

10.4.2 Result example cross-section – extreme case

10.4.2.1 Analysis dn1355.

Parameters according to 10.2.1

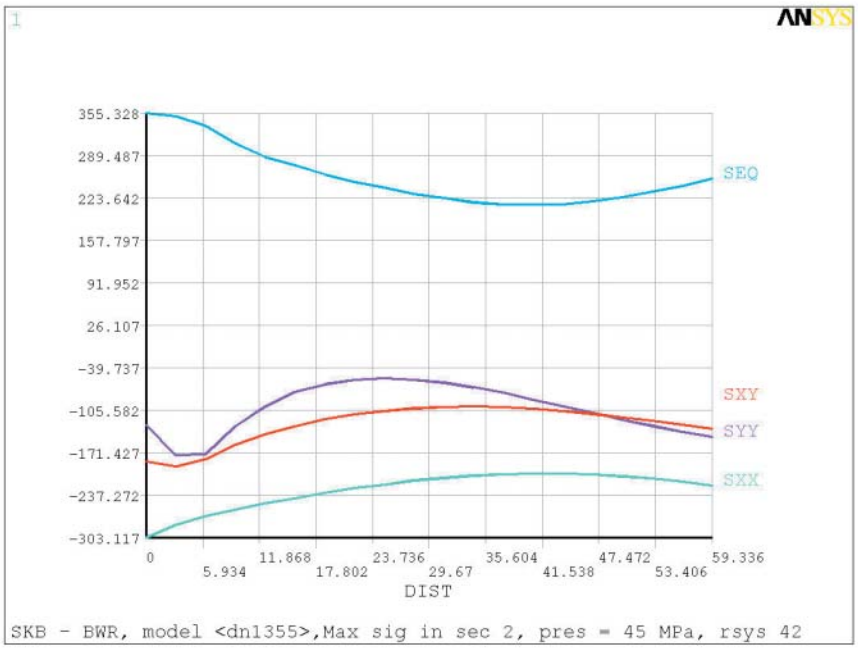

Fig. 49. Section 2, stresses.

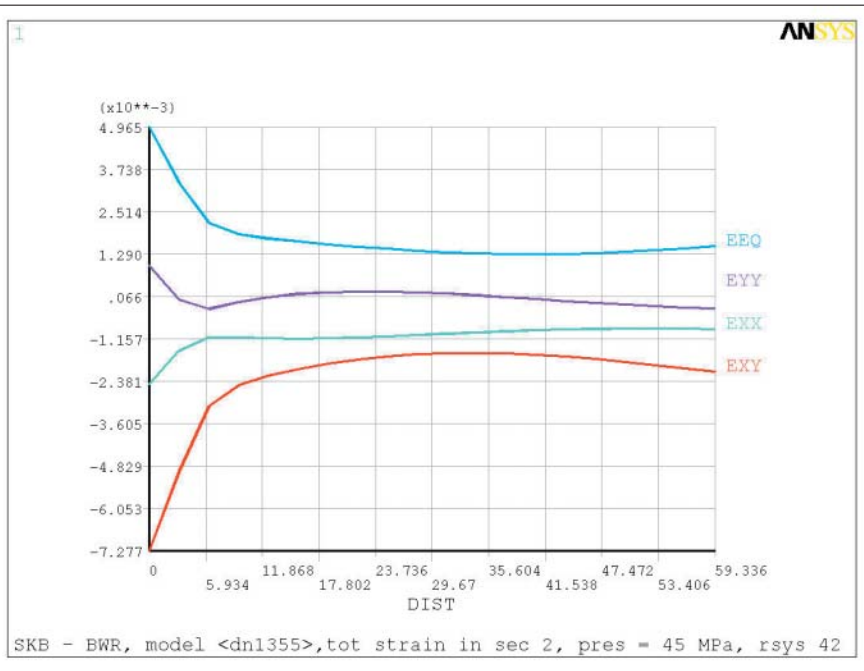

Fig. 50. Section 2, strains.

10.4.2.2 Analysis dn4111.

Parameters according to 10.2.1

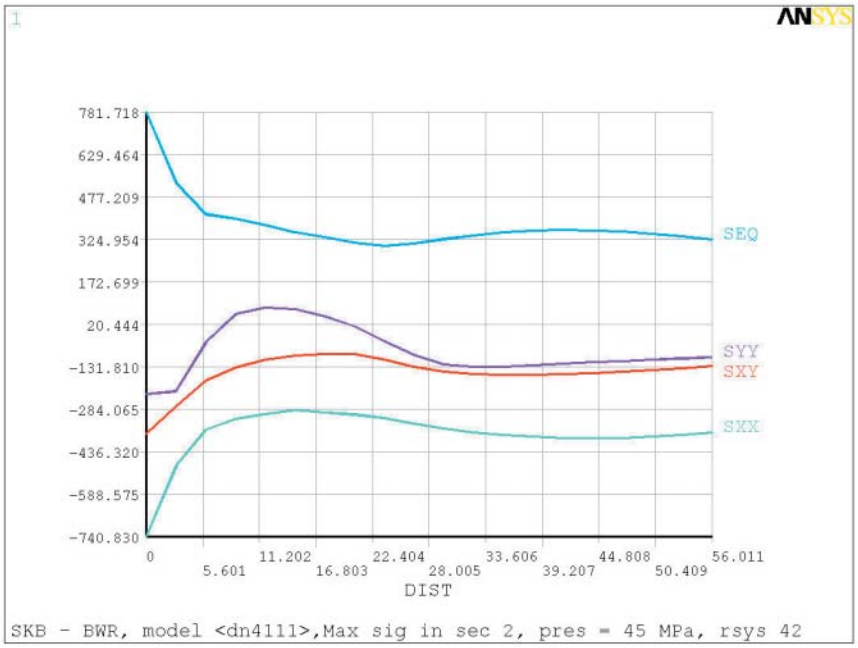

Fig. 51. Section 2, stresses.

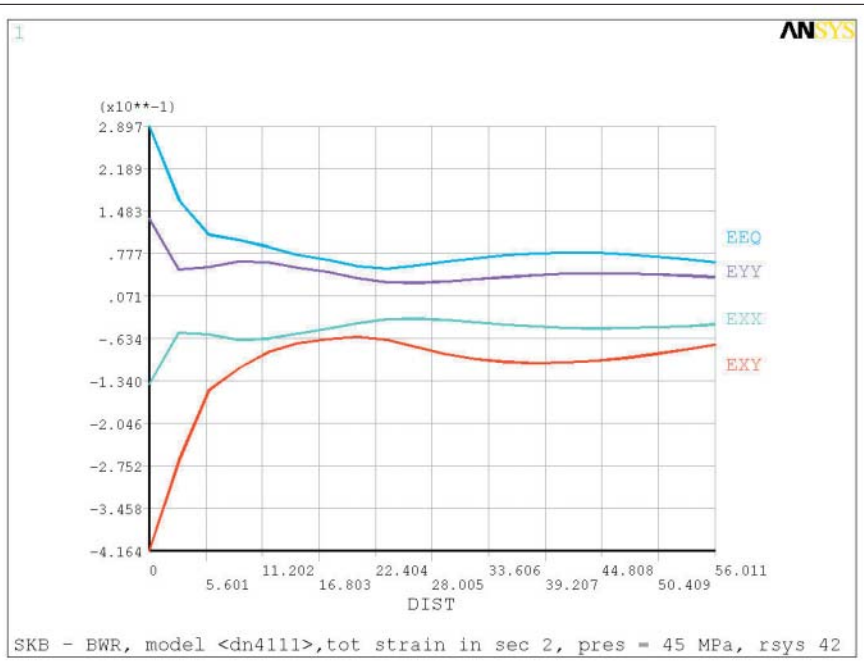

Fig. 52. Section 2, strains.

11 REFERENCES

1) Kollapslast för kapsel, kompletterande analys, ÅF-I Rapport **B413** (1997-10-07),

2) Lagringsbehållare för utbränt kärnbränsle, kollapstryck för gjuten cylinder, ÅF-I Rapport **B274** (1995-06-05)

3) Lagringsbehållare för utbränt kärnbränsle. Skadetålighetsanalys av stålcylindern. ÅF-I Rapport **B238** (1994-09-27).

4) Kollapslast hos kapsel för kärnbränsle – Grunder för sannolikhetsbetraktelser, ÅF-I Rapport **B419** (1998-04-05).

5) Kollapslast för modifierade kapslar inklusive inverkan av fel, ÅF-I Rapport **B593** (2000-03-17).

6) Kollapslast kapslar med modifierade materialdata, ÅF-I Rapport **B633** (2000-12-22).

7) SKB Projekt PM, TI-00-05, juni 2000

8) Kollapskraft kapslar, krav på materialdata. ÅF-I Rapport **B668** (2001-10-29).

9) JRC Report NSU/KN/0401.02 Version 1, Presssure Test of KBS-3 Canister Mock-Up

10) ANSYS Release 8.1 Documentation

11) Elements of Physical Metallurgy, Albert G. Guy, Department of Metallurgical Engineering, University of Florida, 1960.

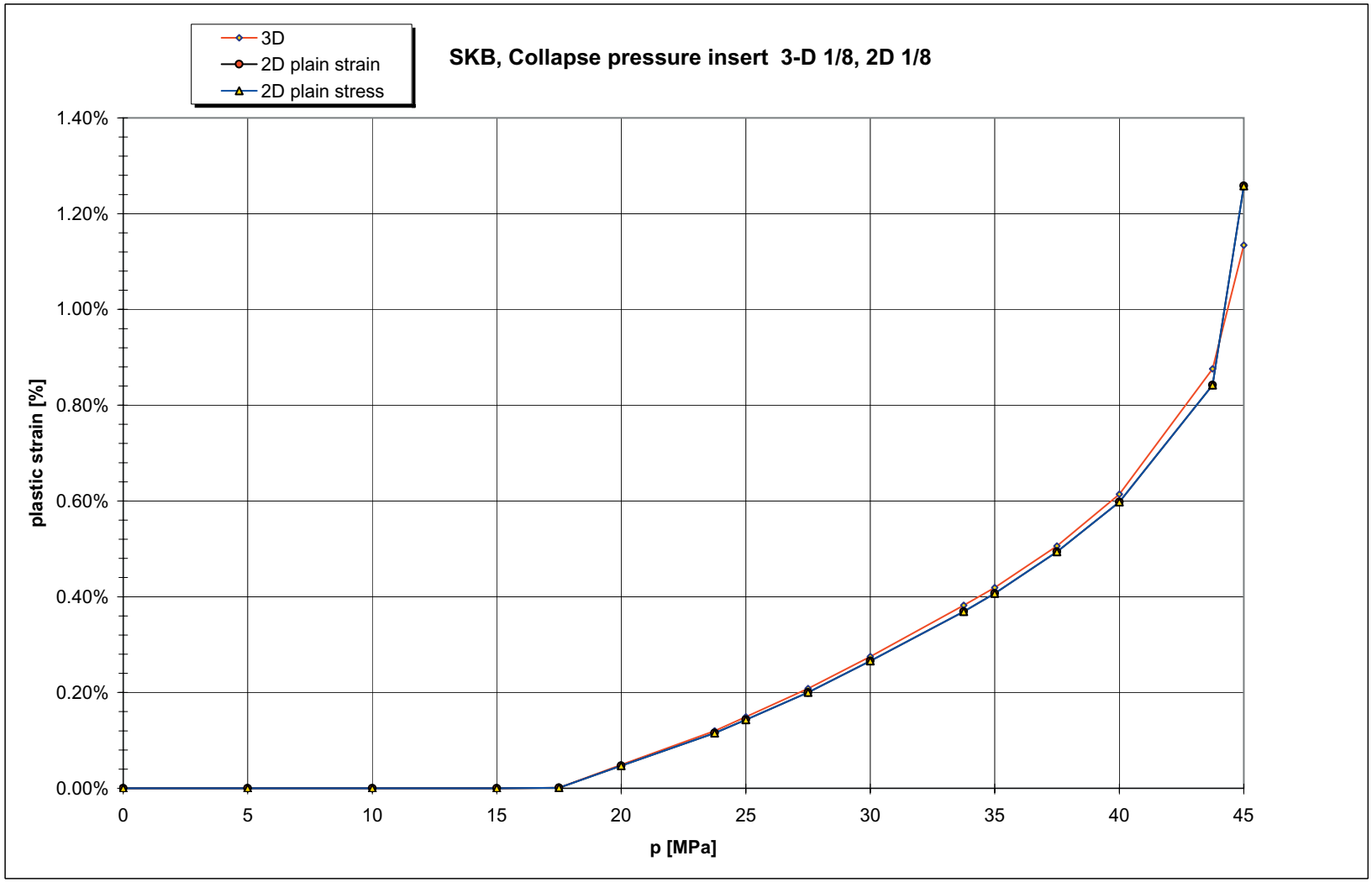
3D
2D plain strain
2D plain stress
SKB, Collapse pressure insert 3-D 1/8, 2D 1/8
plastic strain [%]
1.40%
1.20%
1.00%
0.80%
0.60%
0.40%
0.20%
0.00%
0
5
10
15
20
25
30
35
40
45
p [MPa]

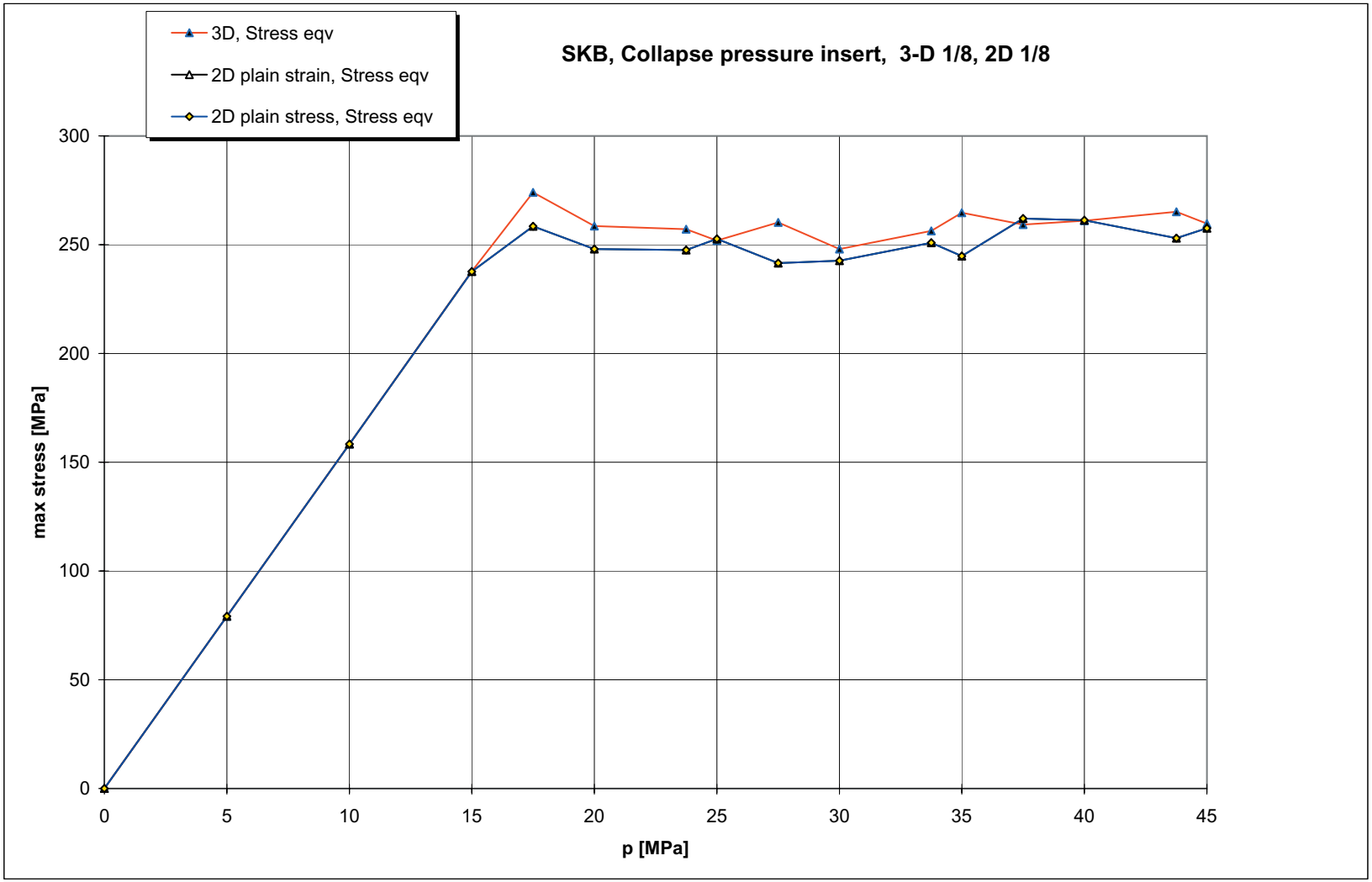
3D, Stress eqv
2D plain strain, Stress eqv
2D plain stress, Stress eqv
SKB, Collapse pressure insert, 3-D 1/8, 2D 1/8
max stress [MPa]
p [MPa]
0
50
100
150
200
250
300
0
5
10
15
20
25
30
35
40
45

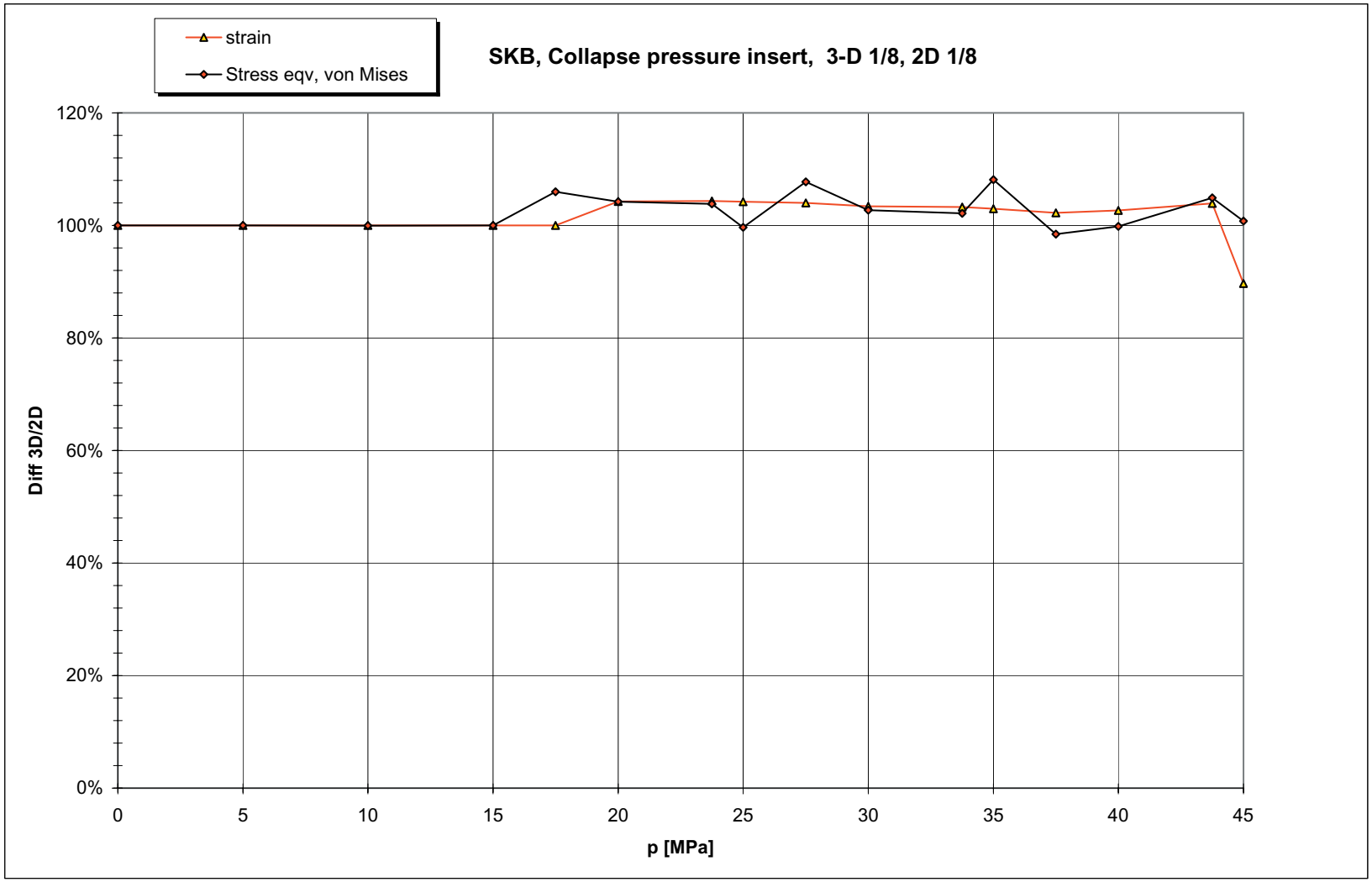
strain
Stress eqv, von Mises
SKB, Collapse pressure insert, 3-D 1/8, 2D 1/8
120%
100%
80%
60%
40%
20%
0%
Diff 3D/2D
0
5
10
15
20
25
30
35
40
45
p [MPa]

SKB, Cast Iron Insert.

assignment : 203253

		3D			2D plain strain			Diff 2D/3D		
	p [MPa]	ε_{max}	σ_{eqvmax}	σ_{intmax}	ε_{max}	σ_{eqvmax}	σ_{intmax}	ε_{max}	σ_{eqvmax}	σ_{intmax}
	0.00	0.00000	0	0.0	0.00000	0	0.0	1.00	1.00	1.00
1	5.00	0.00000	79.20	90.0	0.00000	79.20	89.0	1.00	1.00	1.01
2	10.00	0.00000	158.30	180.1	0.00000	158.40	178.0	1.00	1.00	1.01
3	15.00	0.00000	237.60	270.3	0.00000	237.60	267.1	1.00	1.00	1.01
4	17.50	0.00001	273.90	311.7	0.00001	258.50	290.3	1.00	1.06	1.07
5	20.00	0.00049	258.50	294.5	0.00047	248.00	278.7	1.04	1.04	1.06
6	23.75	0.00120	257.10	294.0	0.00115	247.60	278.4	1.04	1.04	1.06
7	25.00	0.00149	251.80	287.5	0.00143	252.70	284.8	1.04	1.00	1.01
8	27.50	0.00208	260.20	297.5	0.00200	241.50	277.9	1.04	1.08	1.07
9	30.00	0.00275	249.20	283.0	0.00266	242.60	279.7	1.03	1.03	1.01
10	33.75	0.00381	256.30	291.3	0.00369	250.90	281.8	1.03	1.02	1.03
11	35.00	0.00419	264.70	301.2	0.00407	244.80	282.6	1.03	1.08	1.07
12	37.50	0.00505	257.90	295.7	0.00494	262.00	294.9	1.02	0.98	1.00
13	40.00	0.00614	260.80	299.1	0.00598	261.30	294.1	1.03	1.00	1.02
14	43.75	0.00875	265.40	304.5	0.00842	253.00	290.3	1.04	1.05	1.05
15	45.00	0.01128	259.60	297.6	0.01258	257.60	297.5	0.90	1.01	1.00

SKB, Cast Iron Insert. model : bwr13D

assignment : 203253

	p [MPa]	ε_{max}	σ_{eqvmax}	σ_{intmax}	ε_{max} %
	0.00	0.00000	0	0.0	0
1	5.00	0.00000	79.20	90.1	0.00%
2	10.00	0.00000	158.40	180.2	0.00%
3	15.00	0.00000	237.70	270.4	0.00%
4	17.50	0.00001	274.00	311.8	0.00%
5	20.00	0.00049	258.60	294.6	0.05%
6	23.75	0.00120	257.10	294.1	0.12%
7	25.00	0.00149	251.90	287.6	0.15%
8	27.50	0.00208	260.30	297.5	0.21%
9	30.00	0.00275	248.00	282.9	0.28%
10	33.75	0.00382	256.30	291.4	0.38%
11	35.00	0.00419	264.70	301.3	0.42%
12	37.50	0.00506	259.20	297.2	0.51%
13	40.00	0.00614	261.00	299.4	0.61%
14	43.75	0.00876	265.20	304.5	0.88%
15	45.00	0.01134	259.70	297.5	1.13%

SKB, Cast Iron Insert.

assignment : 203253

model : bwr12D
2D plain strain

	p [MPa]	ε_{max}	σ_{eqvmax}	σ_{intmax}	ε_{max} %
	0.00	0.00000	0	0.0	0
1	5.00	0.00000	79.20	89.0	0.00%
2	10.00	0.00000	158.40	178.0	0.00%
3	15.00	0.00000	237.60	267.1	0.00%
4	17.50	0.00001	258.50	290.3	0.00%
5	20.00	0.00047	248.00	278.7	0.05%
6	23.75	0.00115	247.60	278.4	0.12%
7	25.00	0.00143	252.70	284.8	0.14%
8	27.50	0.00200	241.50	277.9	0.20%
9	30.00	0.00266	242.60	279.7	0.27%
10	33.75	0.00369	250.90	281.8	0.37%
11	35.00	0.00407	244.80	282.6	0.41%
12	37.50	0.00494	262.00	294.9	0.49%
13	40.00	0.00598	261.30	294.1	0.60%
14	43.75	0.00842	253.00	290.3	0.84%
15	45.00	0.01258	257.60	297.5	1.26%

SKB, Cast Iron Insert.

assignment : 203253

model : bwr12D
2D plain stress

	p [MPa]	ε_{max}	σ_{eqvmax}	σ_{intmax}	ε_{max} %
	0.00	0.00000	0	0.0	0
1	5.00	0.00000	79.20	89.0	0.00%
2	10.00	0.00000	158.40	178.0	0.00%
3	15.00	0.00000	237.60	267.1	0.00%
4	17.50	0.00001	258.50	290.3	0.00%
5	20.00	0.00047	248.00	278.7	0.05%
6	23.75	0.00115	247.60	278.4	0.12%
7	25.00	0.00143	252.70	284.8	0.14%
8	27.50	0.00200	241.50	277.9	0.20%
9	30.00	0.00266	242.60	279.7	0.27%
10	33.75	0.00369	250.90	281.8	0.37%
11	35.00	0.00407	244.80	282.6	0.41%
12	37.50	0.00494	262.00	294.9	0.49%
13	40.00	0.00598	261.30	294.1	0.60%
14	43.75	0.00842	253.00	290.3	0.84%
15	45.00	0.01258	257.60	297.5	1.26%

SKB, Inserts.

3D -> 2D, Critical section

Assignment : 203253
model : bwr12D
bwr22D
bwr13D

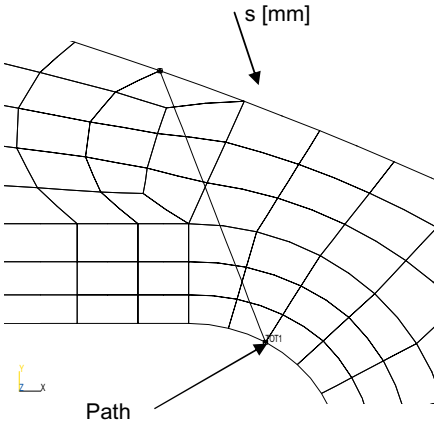

		2D	
	3D	plain strain	plain stress
s [mm]	p = 45 MPa	p = 45 MPa	p = 45 MPa
0.0	0.208%	0.255%	4.230%
2.3	0.134%	0.173%	3.645%
4.6	0.108%	0.146%	3.415%
6.8	0.114%	0.154%	3.296%
9.1	0.107%	0.143%	2.903%
11.4	0.116%	0.152%	2.666%
13.7	0.144%	0.183%	2.663%
15.9	0.189%	0.234%	2.805%
18.2	0.243%	0.293%	3.068%
20.5	0.225%	0.275%	3.153%
22.8	0.219%	0.268%	3.283%
25.1	0.235%	0.283%	3.476%
27.3	0.257%	0.307%	3.610%
29.6	0.296%	0.349%	3.801%
31.9	0.363%	0.421%	4.107%
34.2	0.465%	0.529%	4.640%
36.4	0.569%	0.635%	5.253%
38.7	0.733%	0.808%	6.476%
41.0	0.923%	1.017%	7.963%
43.3	1.134%	1.258%	9.616%

input = psecbwrXXX.lis

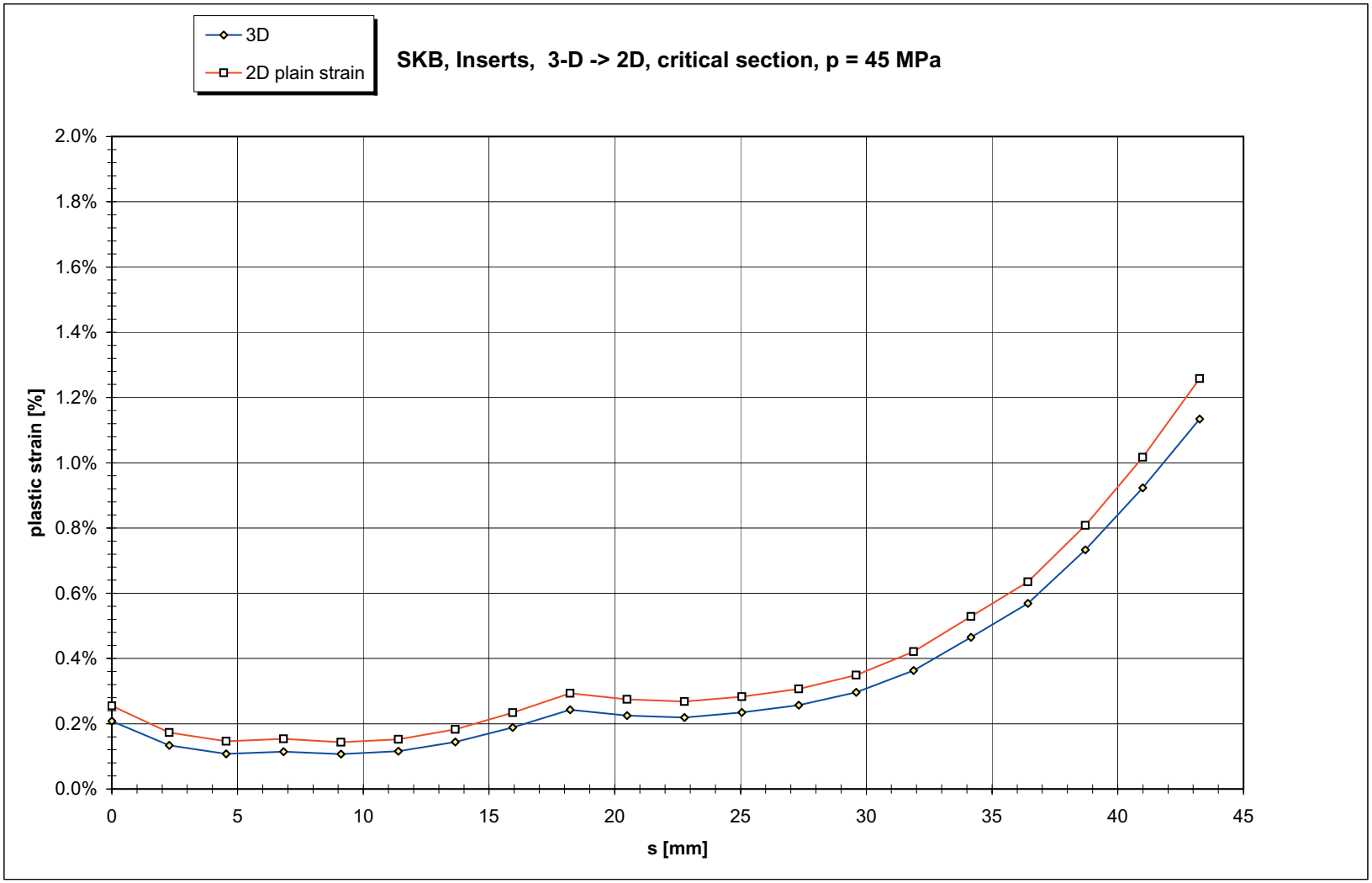
3D
2D plain strain
SKB, Inserts, 3-D -> 2D, critical section, p = 45 MPa
plastic strain [%]
2.0%
1.8%
1.6%
1.4%
1.2%
1.0%
0.8%
0.6%
0.4%
0.2%
0.0%
0
5
10
15
20
25
30
35
40
45
s [mm]

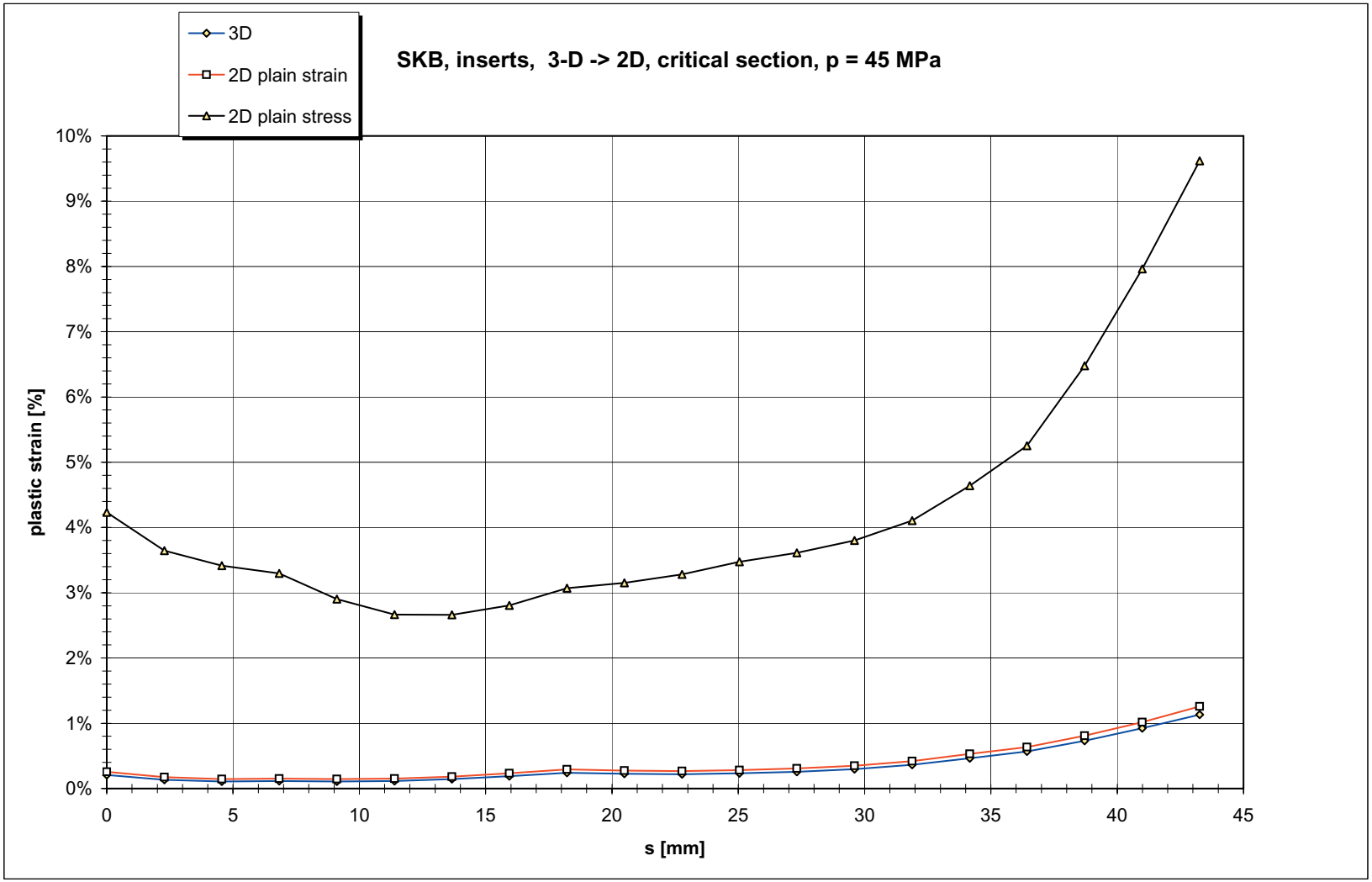
3D
2D plain strain
2D plain stress
SKB, inserts, 3-D -> 2D, critical section, p = 45 MPa
plastic strain [%]
10%
9%
8%
7%
6%
5%
4%
3%
2%
1%
0%
0
5
10
15
20
25
30
35
40
45
s [mm]

SKB, inserts.

3D -> 2D, sym section, x=0, stress xyz

assignment 203253
model : bwr12D-13D

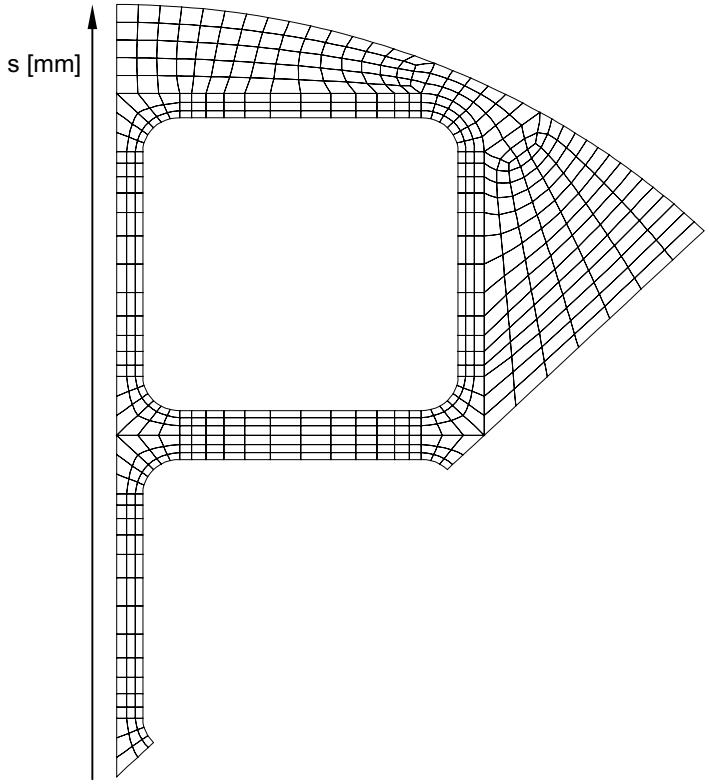

p = 45 MPa

		3D			2D plain strain			2D plain stress		
	s [mm]	sigx	sigy	sigz	sigx	sigy	sigz	sigx	sigy	sigz
1	0.0	-158.6	-149.9	-115.0	-157.3	-148.7	-91.8	-155.8	-147.9	0.0
2	8.0	-143.9	-163.6	-114.7	-142.7	-162.3	-91.5	-141.7	-161.9	0.0
3	16.1	-121.3	-187.2	-115.0	-120.3	-185.8	-91.8	-118.0	-188.9	0.0
4	24.1	-90.9	-220.4	-115.8	-90.5	-218.8	-92.8	-85.2	-228.1	0.0
5	32.2	-57.7	-248.1	-114.1	-57.0	-246.0	-90.9	-56.9	-254.0	0.0
6	40.2	-21.6	-268.6	-109.5	-21.2	-266.6	-86.4	-23.0	-268.8	0.0
7	48.3	-3.4	-274.8	-107.4	-4.2	-273.4	-89.2	-0.1	-266.4	0.0
8	56.3	0.0	-275.2	-107.5	-0.5	-273.3	-92.0	3.3	-263.4	0.0
9	64.3	0.4	-274.7	-106.9	0.6	-272.3	-91.5	0.8	-262.8	0.0
10	72.4	0.1	-274.7	-105.8	0.2	-272.3	-89.9	-0.5	-263.5	0.0
11	80.4	0.0	-274.8	-105.8	0.0	-272.3	-89.8	-0.3	-263.6	0.0
12	88.5	-0.1	-274.9	-106.0	-0.1	-272.4	-89.8	0.1	-263.5	0.0
13	96.5	0.0	-274.9	-106.3	0.0	-272.4	-90.0	0.0	-263.5	0.0
14	104.6	0.0	-274.9	-106.5	0.0	-272.5	-90.2	0.0	-263.5	0.0
15	112.6	0.0	-274.9	-106.5	0.0	-272.4	-90.0	0.0	-263.5	0.0
16	120.6	-0.1	-274.9	-106.5	-0.1	-272.4	-89.8	0.1	-263.5	0.0
17	128.7	0.0	-274.9	-106.6	0.0	-272.4	-89.8	-0.2	-263.6	0.0
18	136.7	0.1	-274.8	-106.8	0.1	-272.3	-89.8	-0.6	-263.6	0.0
19	144.8	0.4	-274.9	-108.3	0.6	-272.3	-91.3	0.7	-262.9	0.0
20	152.8	0.1	-275.3	-109.2	-0.3	-273.2	-92.0	2.9	-263.2	0.0
21	160.9	-2.7	-275.2	-109.7	-3.7	-273.6	-89.9	1.5	-265.8	0.0
22	168.9	-17.7	-270.2	-111.6	-17.3	-267.9	-85.6	-18.6	-269.3	0.0
23	176.9	-51.8	-251.1	-116.5	-50.8	-248.9	-89.9	-53.4	-256.9	0.0
24	185.0	-79.7	-224.8	-117.2	-78.2	-223.2	-90.4	-80.6	-231.0	0.0
25	193.0	-103.6	-194.7	-115.7	-101.6	-193.5	-88.6	-107.5	-194.3	0.0
26	201.1	-122.2	-171.8	-114.7	-120.4	-170.8	-87.4	-127.1	-166.6	0.0
27	209.1	-133.0	-161.7	-115.3	-132.4	-160.3	-87.8	-134.9	-156.3	0.0
28	217.1	-127.9	-168.6	-116.1	-128.2	-167.0	-88.6	-127.3	-163.8	0.0
29	225.2	-114.2	-186.6	-117.7	-115.2	-184.8	-90.0	-111.2	-185.7	0.0
30	233.2	-90.4	-218.3	-120.4	-91.7	-216.5	-92.5	-85.3	-226.1	0.0
31	241.3	-60.5	-245.8	-120.0	-58.8	-245.3	-91.2	-56.2	-248.9	0.0
32	249.3	-26.2	-267.8	-116.6	-24.7	-266.7	-88.4	-25.8	-263.7	0.0

		3D			2D plain strain			2D plain stress		
	s [mm]	sigx	sigy	sigz	sigx	sigy	sigz	sigx	sigy	sigz
33	257.4	-4.7	-276.3	-115.5	-5.7	-274.7	-94.1	-2.6	-263.0	0.0
34	265.4	-0.6	-277.3	-117.7	-1.0	-276.0	-100.9	3.7	-259.5	0.0
35	273.4	0.4	-276.5	-118.1	0.9	-274.3	-100.3	0.9	-258.7	0.0
36	281.5	0.1	-276.6	-117.6	0.3	-274.3	-98.1	-0.4	-259.4	0.0
37	289.5	0.0	-276.6	-117.8	0.1	-274.3	-97.6	-0.3	-259.5	0.0
38	297.6	0.0	-276.6	-118.2	-0.1	-274.5	-97.6	0.1	-259.5	0.0
39	305.6	0.0	-276.7	-118.8	0.0	-274.5	-97.9	0.0	-259.5	0.0
40	313.7	0.0	-276.7	-119.5	0.0	-274.5	-98.3	0.0	-259.5	0.0
41	321.7	0.0	-276.7	-119.9	0.0	-274.5	-98.1	0.0	-259.5	0.0
42	329.7	0.0	-276.7	-120.4	-0.1	-274.5	-97.7	0.1	-259.5	0.0
43	337.8	0.0	-276.7	-120.9	0.0	-274.4	-97.6	-0.2	-259.5	0.0
44	345.8	0.0	-276.7	-121.4	0.2	-274.2	-97.6	-0.6	-259.6	0.0
45	353.9	0.2	-276.6	-122.5	0.7	-274.3	-99.6	0.5	-258.9	0.0
46	361.9	0.2	-276.8	-123.5	0.0	-275.2	-100.9	2.6	-259.0	0.0
47	370.0	-1.6	-277.0	-124.4	-3.5	-276.4	-98.9	3.0	-261.1	0.0
48	378.0	-13.4	-273.1	-126.3	-13.9	-270.5	-87.2	-15.3	-265.7	0.0
49	386.0	-56.7	-253.1	-134.1	-52.5	-252.8	-91.6	-48.4	-255.8	0.0
50	394.1	-95.0	-219.4	-136.3	-92.5	-218.7	-93.4	-80.3	-232.8	0.0
51	402.1	-117.3	-183.3	-132.9	-113.4	-183.2	-89.0	-92.0	-194.3	0.0
52	410.2	-129.4	-150.0	-127.3	-123.9	-150.6	-82.4	-96.3	-156.1	0.0
53	418.2	-127.8	-126.5	-120.5	-122.9	-127.1	-75.0	-97.7	-132.5	0.0
54	426.3	-124.8	-106.7	-114.4	-121.3	-107.0	-68.5	-104.6	-110.3	0.0
55	434.3	-120.8	-89.4	-108.8	-118.9	-89.5	-62.5	-112.8	-90.6	0.0
56	442.3	-115.6	-74.2	-103.4	-115.5	-74.2	-56.9	-120.6	-74.3	0.0
57	450.4	-108.4	-62.3	-98.5	-110.0	-62.3	-51.7	-126.4	-61.8	0.0
58	458.4	-97.2	-53.3	-93.1	-100.6	-53.2	-46.1	-128.0	-52.5	0.0
59	466.5	-81.2	-47.2	-87.3	-86.3	-47.1	-40.0	-124.4	-46.6	0.0
60	474.5	-59.3	-44.4	-80.6	-66.1	-44.4	-33.1	-114.2	-44.3	0.0

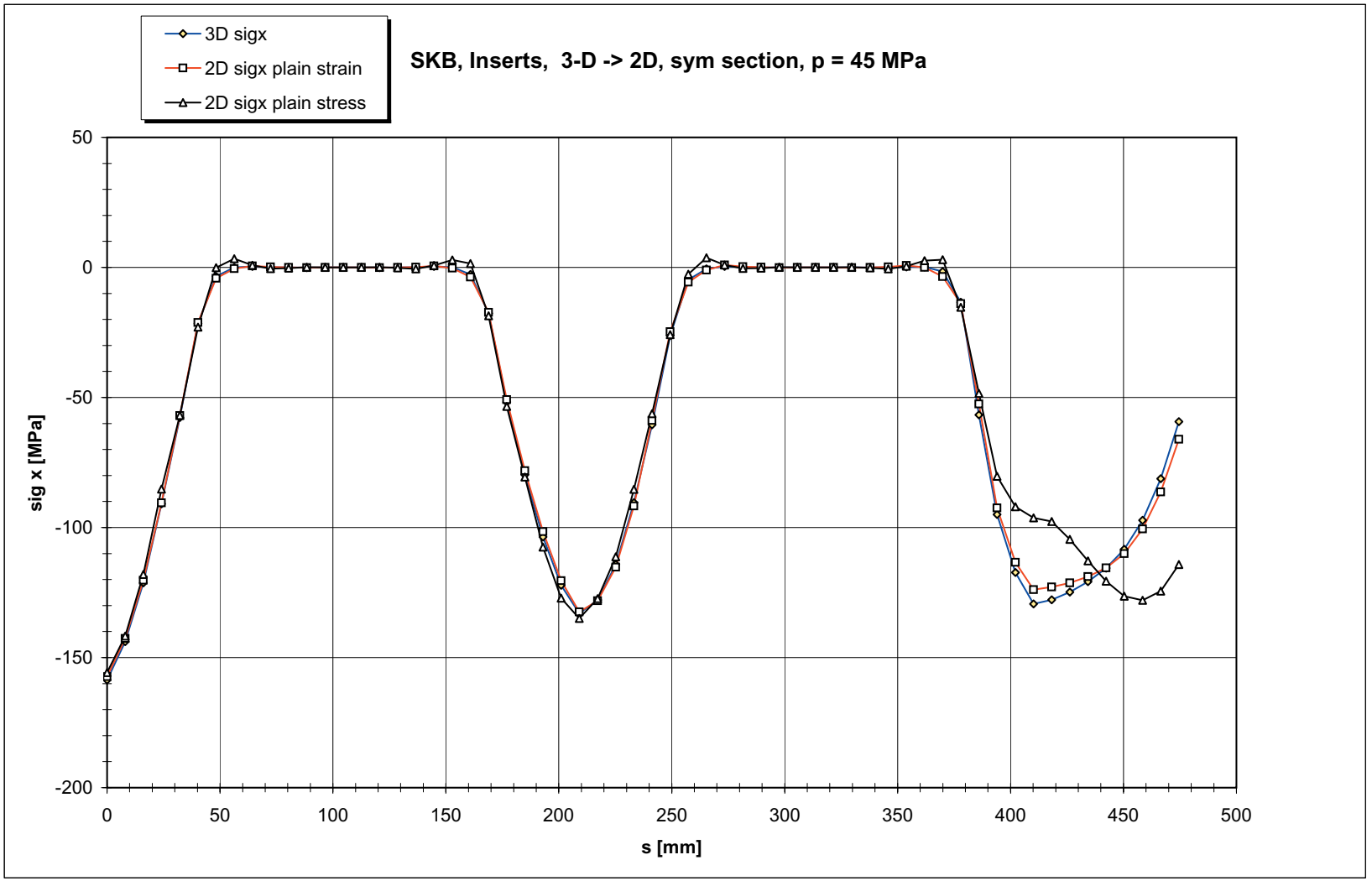
3D sigx
2D sigx plain strain
2D sigx plain stress
SKB, Inserts, 3-D -> 2D, sym section, p = 45 MPa
sig x [MPa]
s [mm]
50
0
-50
-100
-150
-200
0
50
100
150
200
250
300
350
400
450
500

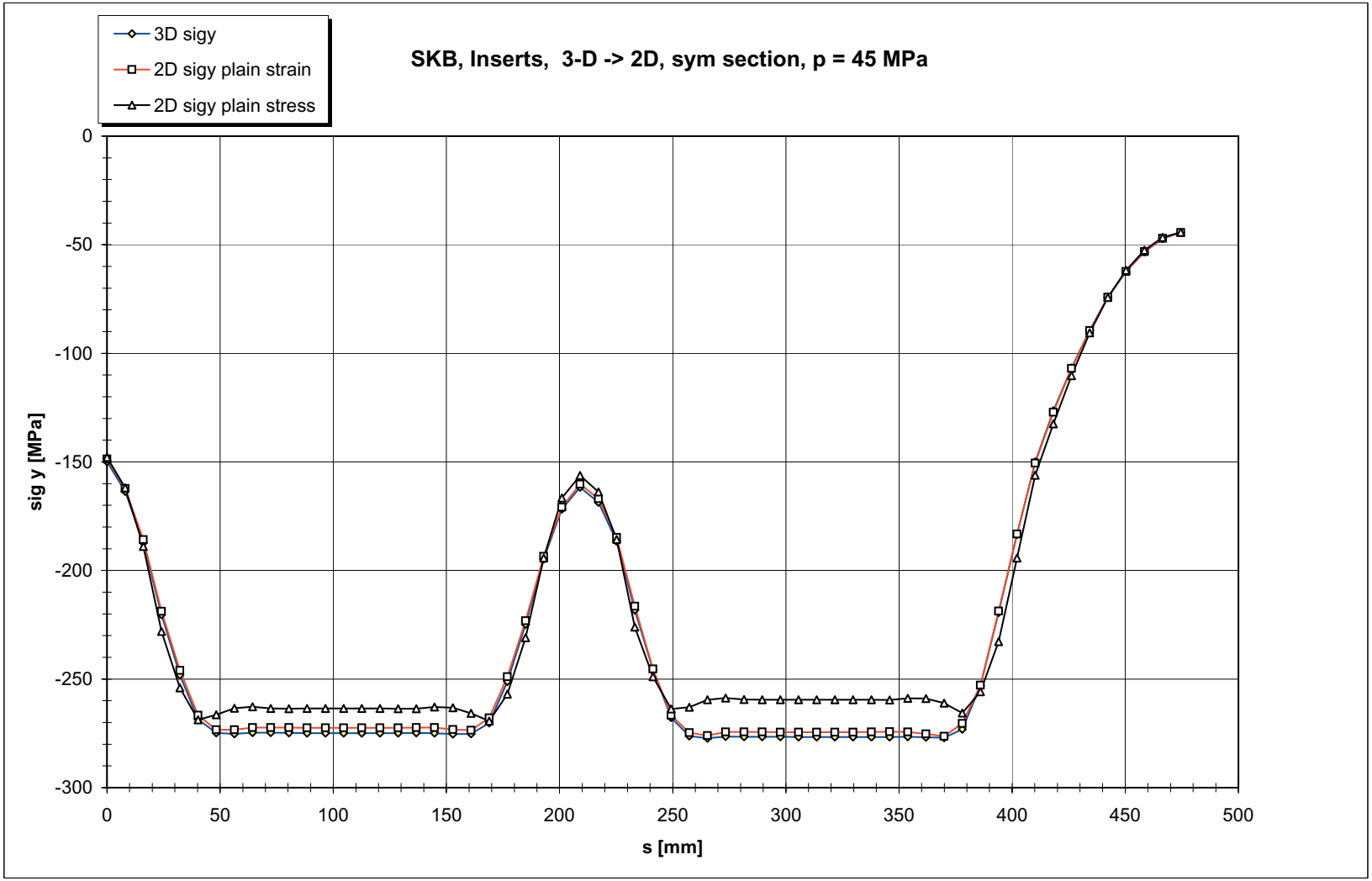
3D sigy
2D sigy plain strain
2D sigy plain stress
SKB, Inserts, 3-D -> 2D, sym section, p = 45 MPa
sig y [MPa]
0
-50
-100
-150
-200
-250
-300
0
50
100
150
200
250
300
350
400
450
500
s [mm]

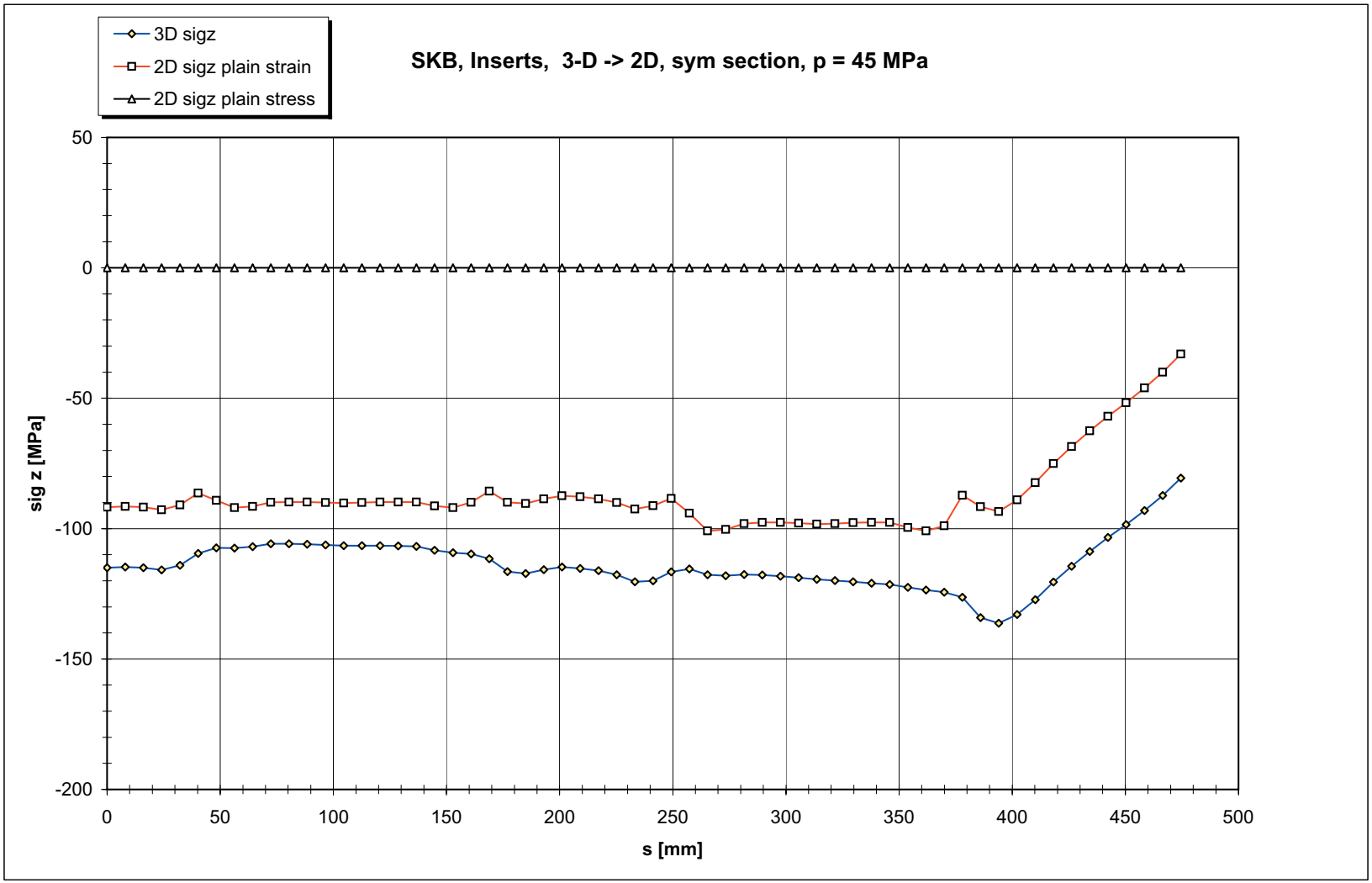
3D sigz
2D sigz plain strain
2D sigz plain stress
SKB, Inserts, 3-D -> 2D, sym section, p = 45 MPa
sig z [MPa]
50
0
-50
-100
-150
-200
0
50
100
150
200
250
300
350
400
450
500
s [mm]

SKB, Pressure Test

model : **pt4**

assignment : 203253

		copper		casting	
	p [MPa]	90 deg	45 deg	90 deg	45 deg
	0.00	0.00	0.00	0.00	0.00
1	5.00	0.21	0.21	0.01	0.01
2	5.50	0.33	0.33	0.01	0.01
3	6.44	0.99	0.99	0.01	0.01
4	8.55	1.86	1.86	0.00	0.00
5	10.00	1.87	1.87	0.01	0.01
6	13.33	1.89	1.89	0.03	0.02
7	15.00	1.90	1.90	0.04	0.03
8	18.33	1.92	1.92	0.06	0.05
9	20.00	1.93	1.93	0.07	0.06
10	23.33	1.95	1.95	0.09	0.07
11	25.00	1.96	1.96	0.10	0.08
12	28.33	1.98	1.98	0.12	0.10
13	30.00	2.00	1.99	0.13	0.10
14	33.33	2.02	2.01	0.15	0.12
15	35.00	2.03	2.02	0.15	0.13
16	38.33	2.05	2.04	0.17	0.14
17	40.00	2.06	2.06	0.18	0.15
18	43.33	2.08	2.08	0.20	0.17
19	45.00	2.09	2.09	0.21	0.18
20	48.33	2.11	2.11	0.23	0.19
21	50.00	2.12	2.12	0.24	0.20
22	53.33	2.15	2.14	0.26	0.22
23	55.00	2.16	2.15	0.27	0.22
24	58.33	2.18	2.17	0.29	0.24
25	60.00	2.19	2.18	0.30	0.25
26	63.33	2.22	2.20	0.33	0.27
27	65.00	2.23	2.21	0.34	0.27
28	68.33	2.25	2.23	0.36	0.29
29	70.00	2.26	2.24	0.37	0.30
30	73.33	2.29	2.26	0.39	0.32

Radial deflection [mm]

All points in the symmetry section. Z = 0

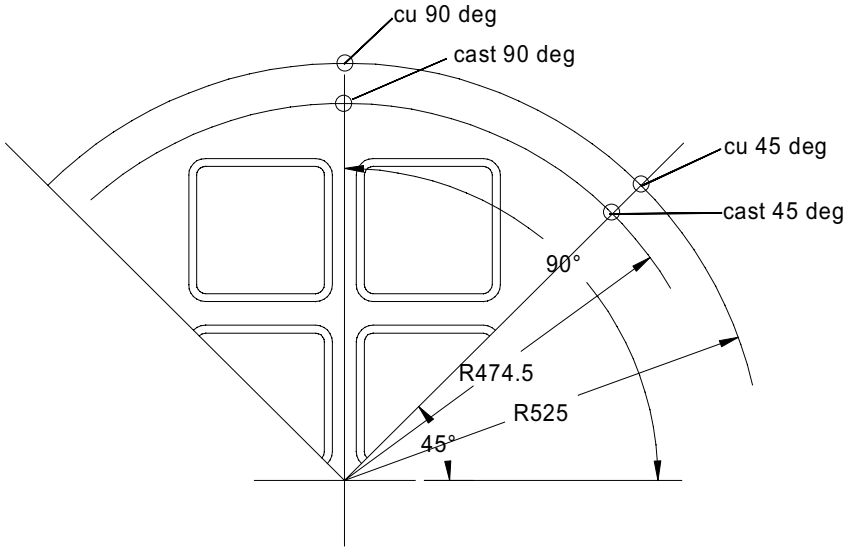

		copper		casting	
	p [MPa]	90 deg	45 deg	90 deg	45 deg
31	75.00	2.30	2.27	0.40	0.33
32	78.33	2.32	2.30	0.42	0.34
33	80.00	2.33	2.31	0.43	0.35
34	83.33	2.36	2.33	0.46	0.37
35	85.00	2.37	2.34	0.47	0.38
36	88.33	2.40	2.36	0.49	0.40
37	90.00	2.41	2.37	0.50	0.40
38	93.33	2.44	2.40	0.53	0.42
39	95.00	2.45	2.41	0.54	0.43
40	97.50	2.47	2.42	0.56	0.45
41	98.50	2.48	2.43	0.57	0.45
42	99.50	2.49	2.44	0.57	0.46
43	100.00	2.49	2.44	0.58	0.46
44	101.00	2.50	2.45	0.59	0.47
45	102.00	2.51	2.46	0.60	0.47
46	103.00	2.52	2.46	0.60	0.48
47	104.00	2.53	2.47	0.62	0.48
48	105.00	2.54	2.48	0.63	0.49
49	106.00	2.55	2.49	0.64	0.50
50	107.00	2.57	2.49	0.65	0.50
51	108.00	2.58	2.50	0.66	0.51
52	109.00	2.59	2.51	0.68	0.52
53	110.00	2.61	2.52	0.69	0.53
54	115.00	2.95	2.59	1.03	0.59
55	120.00	3.84	2.83	1.92	0.81
56	125.00	5.18	3.29	3.27	1.27
57	127.50	5.95	3.56	4.07	1.55
58	128.00	6.12	3.62	4.24	1.61
59	128.50	6.29	3.68	4.41	1.67
60	129.00	6.46	3.74	4.58	1.73
61	129.69	6.69	3.82	4.83	1.81
62	130.00	6.80	3.86	4.94	1.85
63	130.63	7.02	3.94	5.16	1.93
64	131.80	7.44	4.08	5.60	2.09

Radial deflection [mm]

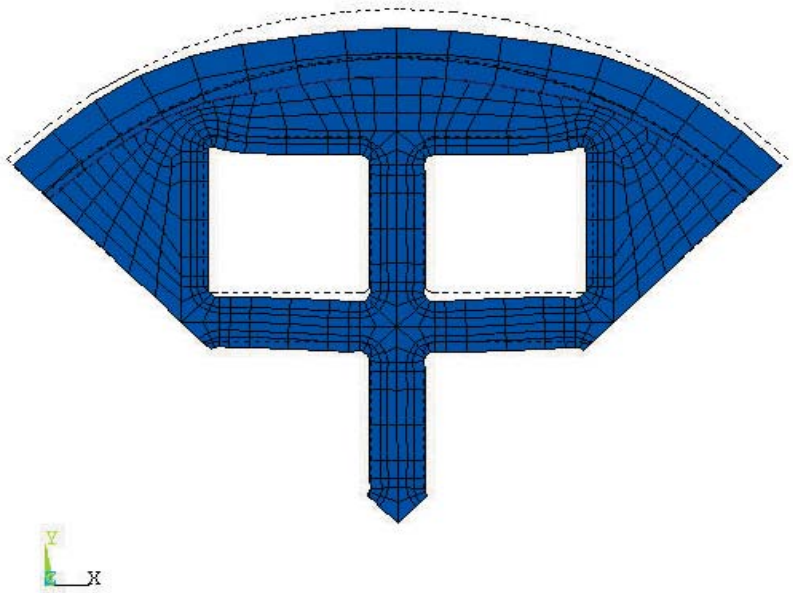

		copper		casting	
	p [MPa]	90 deg	45 deg	90 deg	45 deg
65	134.43	8.44	4.42	6.63	2.45
66	135.00	8.66	4.49	6.86	2.53
67	136.13	9.11	4.64	7.33	2.69
68	138.26	10.00	4.93	8.25	3.01
69	140.00	10.77	5.18	9.04	3.28
70	143.49	12.41	5.71	10.71	3.87
71	145.00	13.13	5.96	11.45	4.14
72	148.03	14.61	6.49	12.95	4.71
73	150.00	15.57	6.86	13.94	5.10
74	153.95	17.49	7.68	15.89	5.96
75	155.00	17.99	7.89	16.41	6.18
76	157.11	18.99	8.33	17.42	6.64
77	160.00	20.33	8.98	18.79	7.31

Radial deflection [mm]

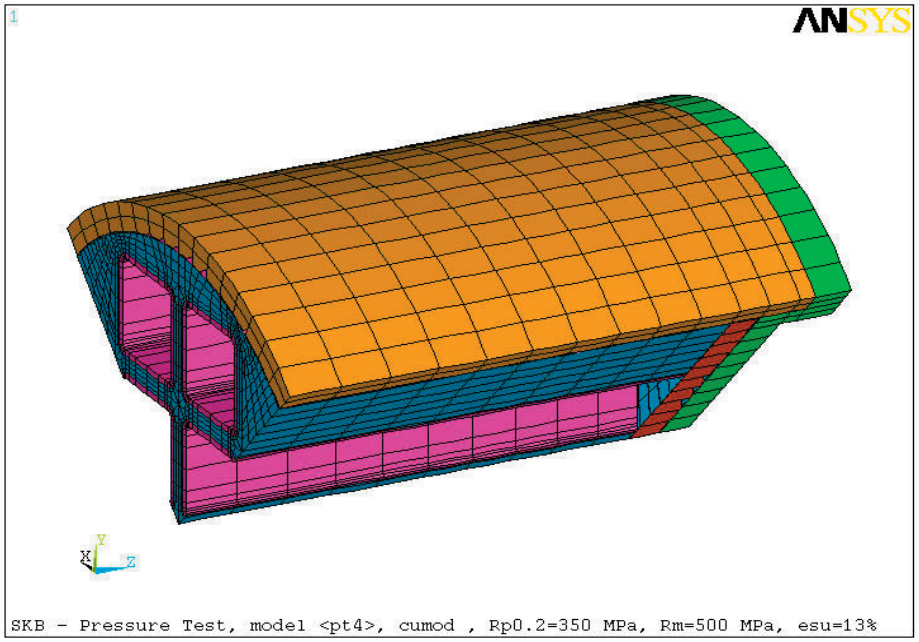

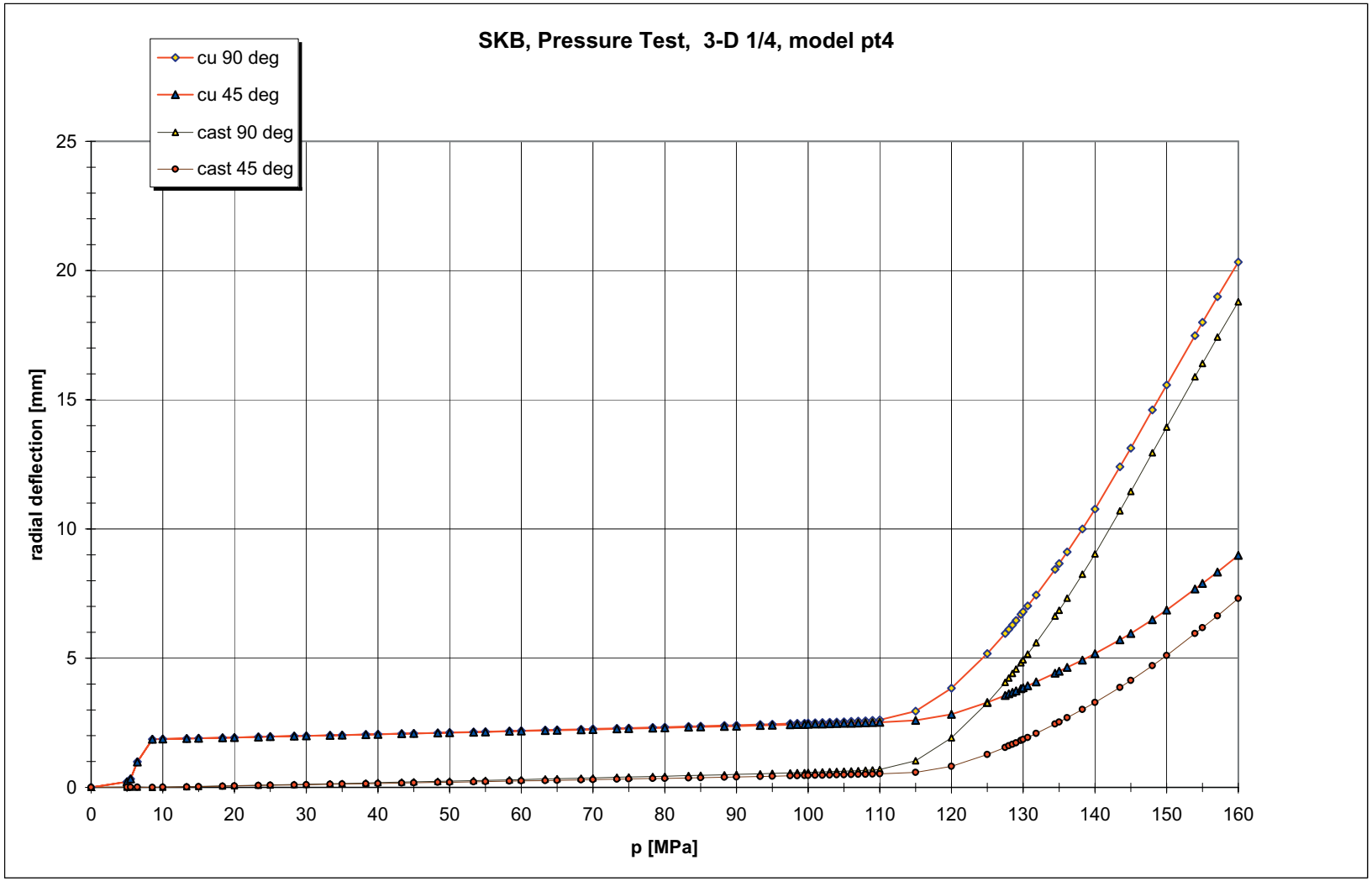
SKB, Pressure Test, 3-D 1/4, model pt4
cu 90 deg
cu 45 deg
cast 90 deg
cast 45 deg
radial deflection [mm]
p [MPa]
0
5
10
15
20
25
0
10
20
30
40
50
60
70
80
90
100
110
120
130
140
150
160

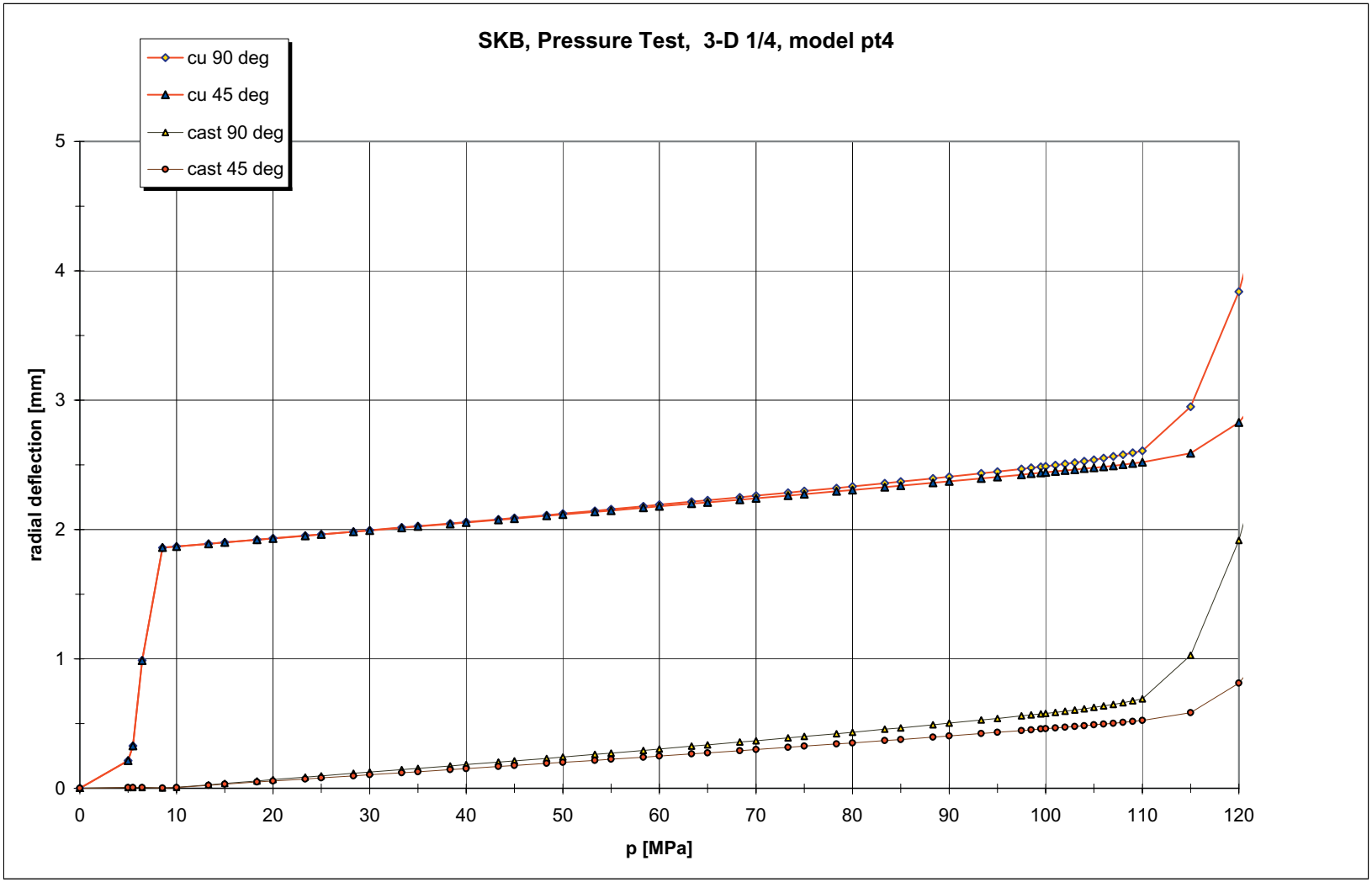
SKB, Pressure Test, 3-D 1/4, model pt4
cu 90 deg
cu 45 deg
cast 90 deg
cast 45 deg
radial deflection [mm]
p [MPa]
0
1
2
3
4
5
0
10
20
30
40
50
60
70
80
90
100
110
120

SKB, Collapse pressure insert.
verification

assignment : 203253
model : r12 r15 r21 r27

Influence of copper cylinder.

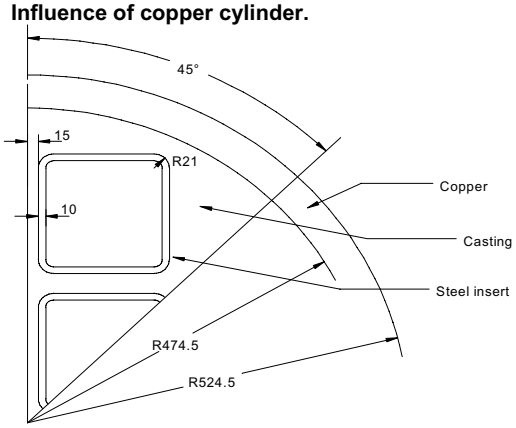

	r = 21 mm with copper cylinder						
	plastic strain			σ_{eqv}			max
p [MPa]	steel	casting	copper	steel	casting	copper	cont pres
0.000	0.00%	0.00%	0.00%	0.00	0.00	0.00	0.00
5.000	0.00%	0.00%	0.00%	68.20	22.20	8.80	9.70
10.000	0.00%	0.00%	0.00%	136.50	44.30	17.50	19.40
15.000	0.00%	0.00%	0.00%	204.70	66.50	26.30	29.00
17.500	0.00%	0.00%	0.00%	238.80	77.60	30.60	33.90
20.000	0.00%	0.00%	0.00%	273.00	88.60	35.00	38.70
23.750	0.00%	0.00%	0.00%	324.20	105.30	41.60	46.00
25.000	0.00%	0.00%	0.00%	341.30	110.80	43.80	48.40
27.500	0.00%	0.00%	0.00%	375.40	121.90	48.10	53.30
30.000	0.00%	0.00%	0.00%	384.10	133.00	50.70	58.10
33.750	0.05%	0.01%	0.01%	374.10	150.20	51.00	65.30
35.000	0.07%	0.02%	0.02%	379.70	156.30	50.60	67.50
37.500	0.10%	0.03%	0.03%	362.20	168.40	51.30	71.80
40.000	0.13%	0.05%	0.05%	372.10	181.00	54.60	75.80
43.750	0.19%	0.08%	0.08%	375.20	200.00	54.20	81.90
45.000	0.21%	0.10%	0.10%	365.10	206.60	54.90	84.00
47.500	0.26%	0.12%	0.12%	363.70	219.70	56.40	88.60
50.000	0.30%	0.15%	0.15%	383.70	232.50	58.10	93.20
53.750	0.38%	0.20%	0.20%	381.40	252.20	60.60	100.20
56.875	0.44%	0.21%	0.21%	386.50	267.10	61.50	103.90
60.000	0.50%	0.22%	0.22%	401.00	280.60	61.90	106.50
62.500	0.55%	0.23%	0.23%	391.80	284.60	62.20	108.70
65.000	0.61%	0.23%	0.23%	377.60	280.30	62.50	110.90
68.750	0.73%	0.24%	0.24%	373.50	284.70	62.90	114.40
74.375	0.94%	0.25%	0.25%	375.90	283.90	63.40	119.70
80.000	1.19%	0.25%	0.25%	358.30	283.60	63.80	125.10
82.500	1.32%	0.26%	0.26%	360.00	283.40	64.10	127.60
85.000	1.47%	0.30%	0.26%	363.50	286.00	64.30	130.20
88.750	1.76%	0.42%	0.27%	369.20	285.40	64.50	134.30
94.375	2.62%	0.90%	0.30%	371.00	290.30	65.60	141.50
100.000	5.97%	2.66%	0.56%	401.90	321.30	73.10	147.10

SKB, Collapse pressure insert.

verification

assignment : 203253

model : r12 r15 r21 r27

Influence of copper cylinder

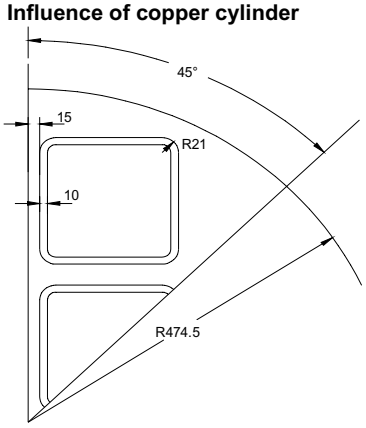

	r = 21 mm					
	plastic strain		σ_{eqv}		σ_{int}	
p [MPa]	steel	casting	steel	casting	steel	casting
0.000	0.00%	0.00%	0.00	0.00	0.00	0.00
5.000	0.00%	0.00%	74.20	23.30	83.30	26.00
10.000	0.00%	0.00%	148.40	46.60	166.70	51.90
15.000	0.00%	0.00%	222.70	70.00	250.10	77.90
17.500	0.00%	0.00%	259.80	81.60	291.80	90.90
20.000	0.00%	0.00%	297.00	93.30	333.50	103.90
23.750	0.00%	0.00%	352.70	110.80	396.10	123.40
25.000	0.00%	0.00%	371.30	116.60	416.90	129.90
27.500	0.00%	0.00%	381.80	128.30	428.00	142.90
30.000	0.04%	0.00%	376.20	140.30	422.20	156.30
33.750	0.09%	0.00%	360.00	158.90	403.30	177.10
35.000	0.10%	0.00%	366.10	165.20	410.60	184.20
37.500	0.13%	0.00%	376.60	177.90	424.00	198.50
40.000	0.18%	0.00%	354.60	190.50	407.00	212.60
43.750	0.24%	0.00%	374.30	209.80	420.50	234.30
45.000	0.26%	0.00%	385.30	216.00	432.80	241.30
47.500	0.31%	0.00%	377.10	228.30	422.60	255.20
50.000	0.36%	0.00%	368.30	241.00	413.70	269.60
53.750	0.44%	0.00%	395.90	259.90	444.80	290.90
56.875	0.50%	0.00%	394.70	274.80	443.40	307.70
60.000	0.58%	0.00%	384.10	285.20	431.30	319.30
62.500	0.64%	0.02%	375.70	279.90	423.00	315.30
65.000	0.72%	0.05%	376.10	281.60	423.10	317.40
68.750	0.86%	0.09%	374.80	285.90	425.70	323.30
74.375	1.10%	0.17%	357.90	284.90	413.30	322.50
80.000	1.44%	0.31%	363.90	283.70	414.80	326.10
82.500	1.72%	0.47%	374.50	285.30	416.10	329.00
85.000	2.08%	0.69%	364.50	288.60	417.90	332.20
88.750	3.46%	1.41%	372.70	296.50	423.90	342.40
92.500	6.90%	3.40%	423.70	320.60	489.20	370.20
98.125	12.29%	6.96%	549.90	363.80	635.00	420.10
100.000	14.18%	8.13%	593.00	377.90	684.80	436.40

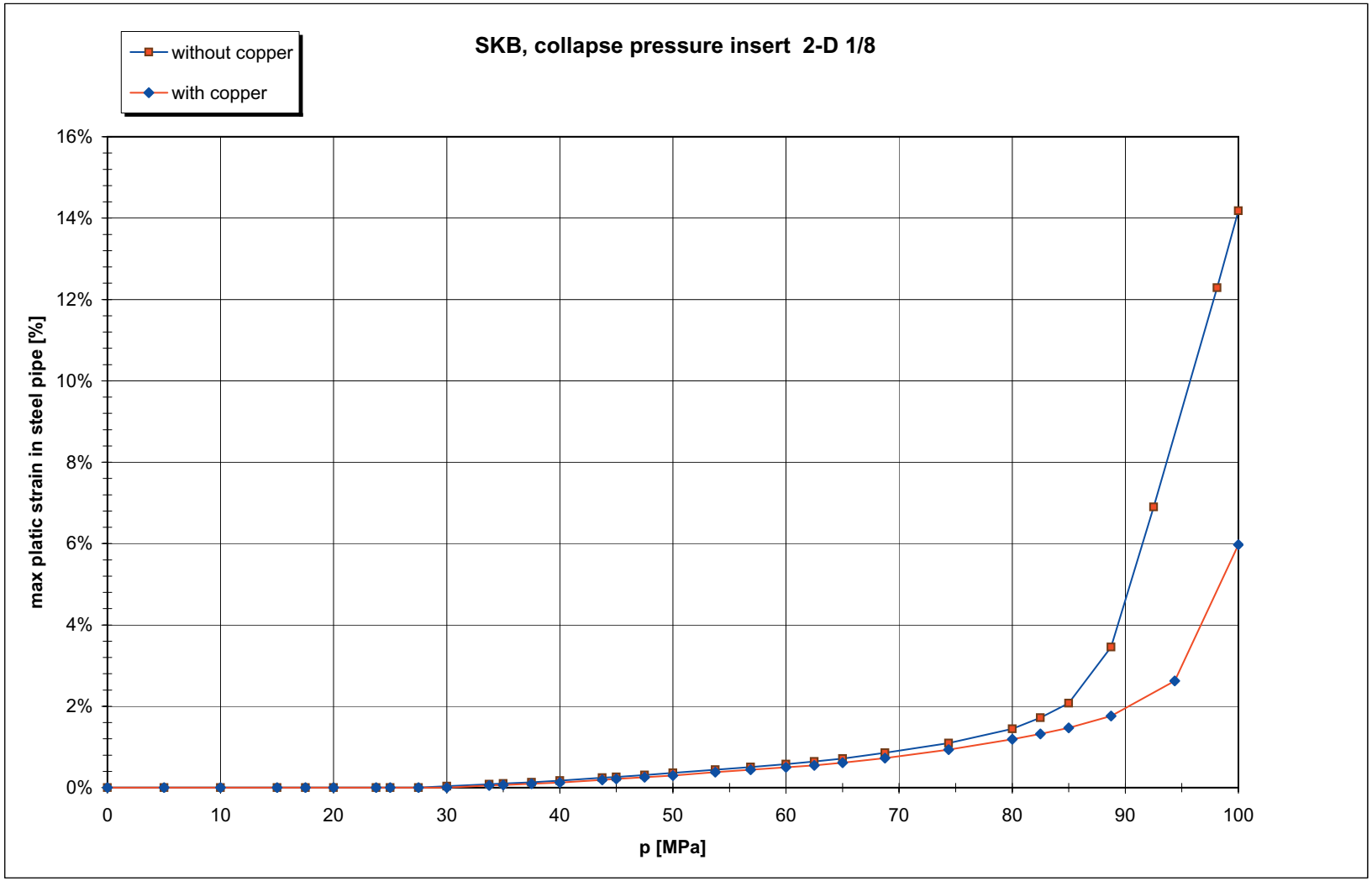
SKB, collapse pressure insert 2-D 1/8
without copper
with copper
max platic strain in steel pipe [%]
16%
14%
12%
10%
8%
6%
4%
2%
0%
0
10
20
30
40
50
60
70
80
90
100
p [MPa]

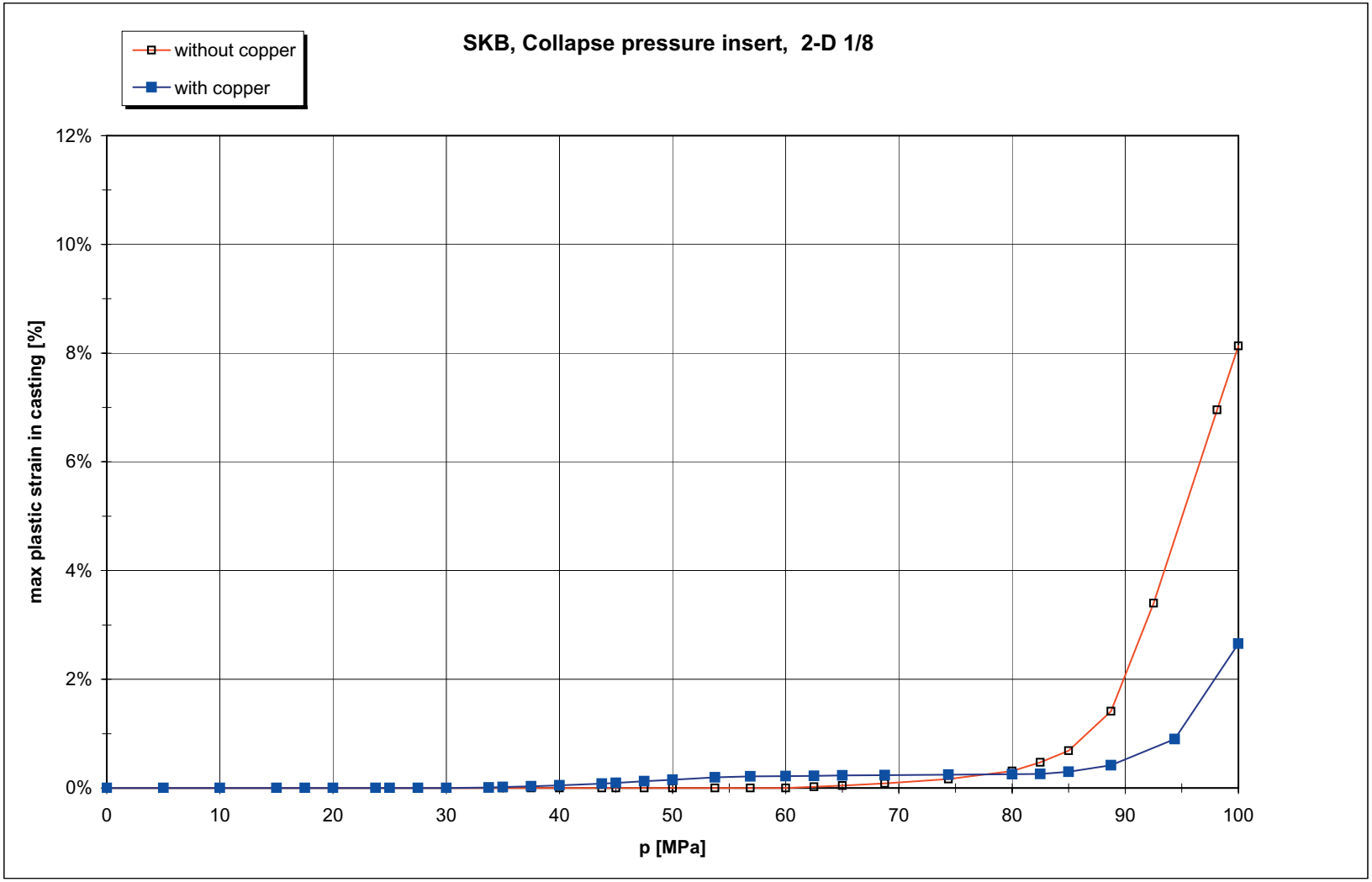
SKB, Collapse pressure insert, 2-D 1/8
without copper
with copper
max plastic strain in casting [%]
12%
10%
8%
6%
4%
2%
0%
0
10
20
30
40
50
60
70
80
90
100
p [MPa]

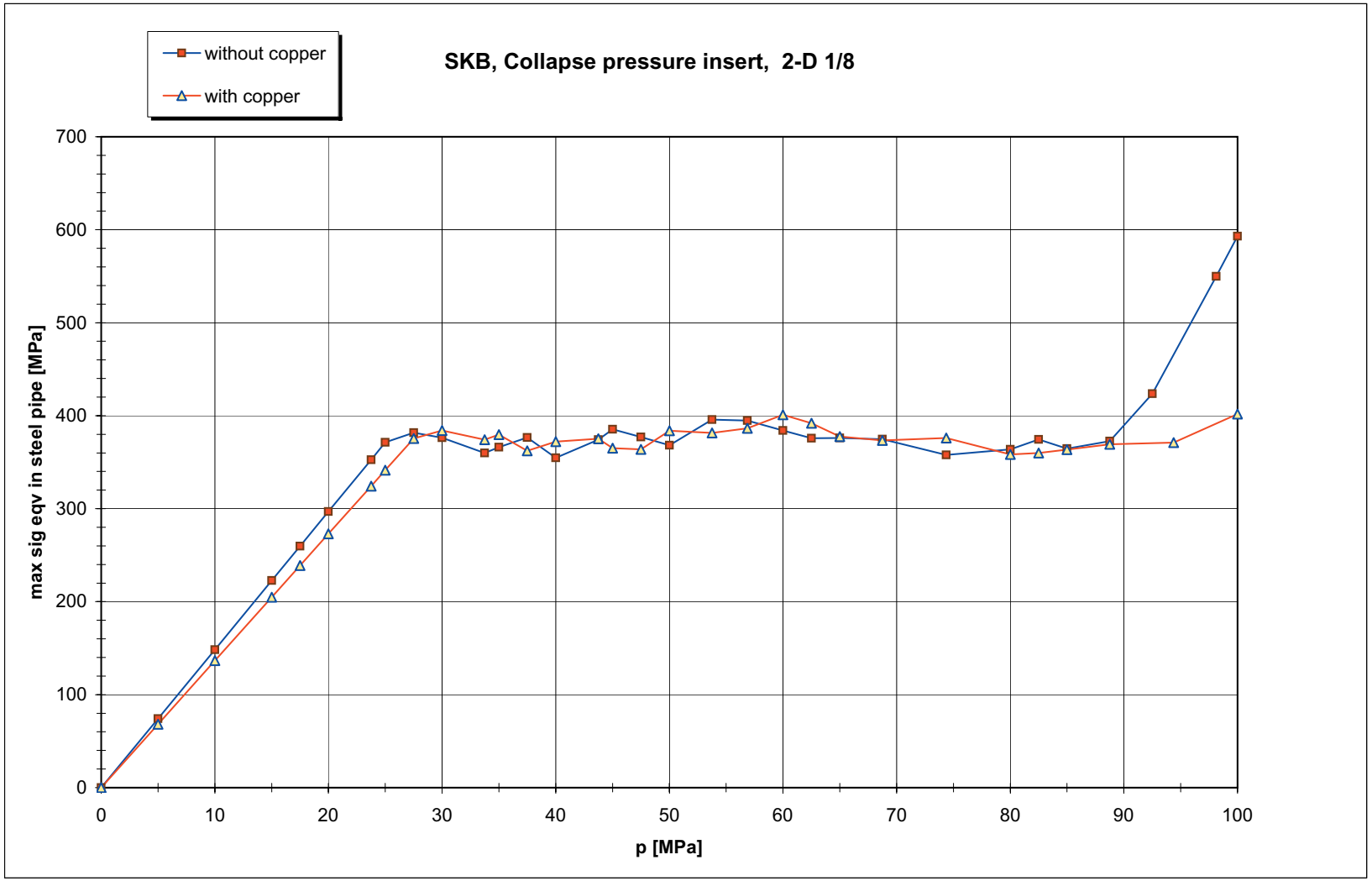
without copper
with copper
SKB, Collapse pressure insert, 2-D 1/8
max sig eqv in steel pipe [MPa]
p [MPa]
0
100
200
300
400
500
600
700
0
10
20
30
40
50
60
70
80
90
100

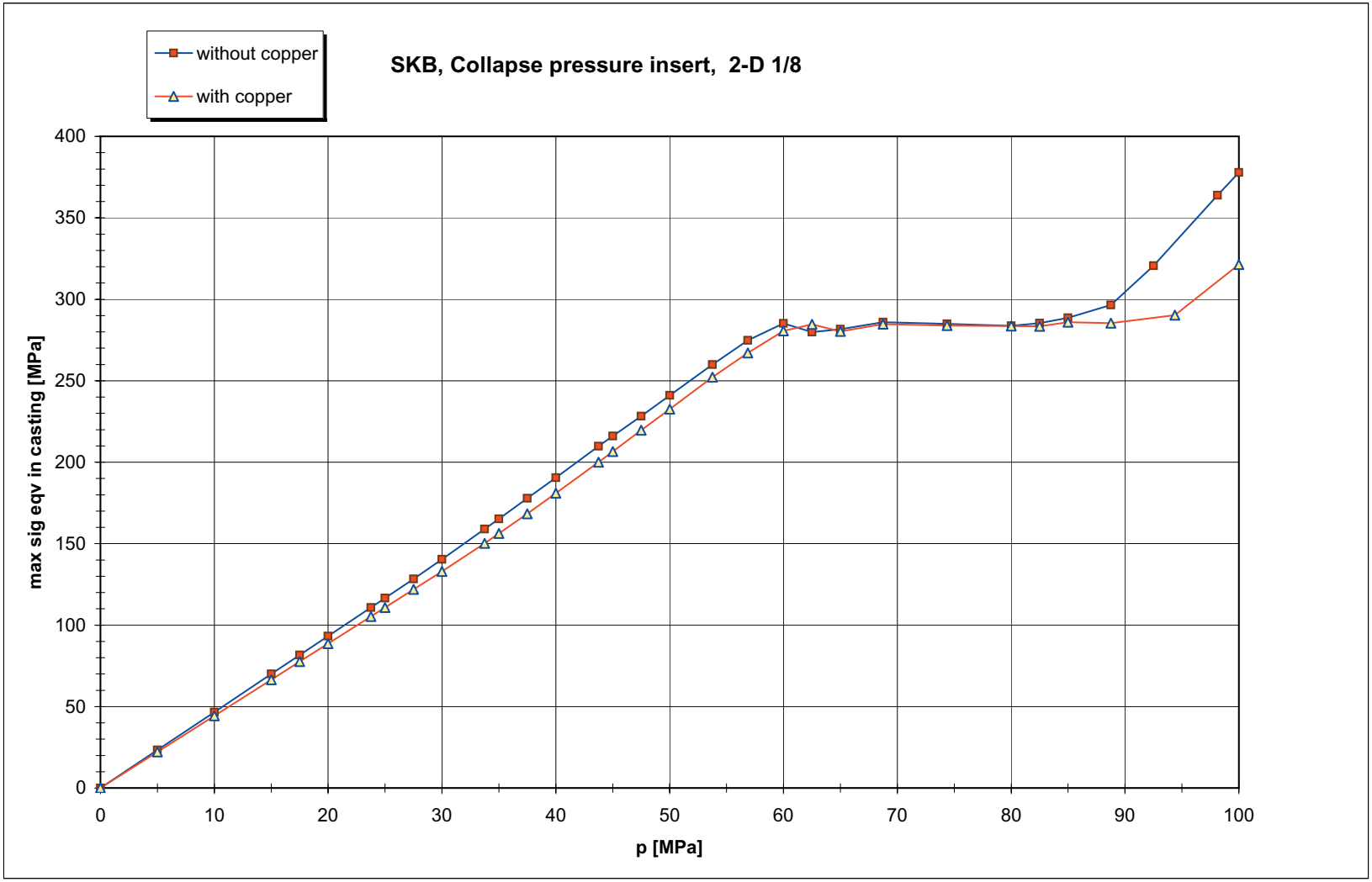
without copper
with copper
SKB, Collapse pressure insert, 2-D 1/8
max sig eqv in casting [MPa]
p [MPa]
0
50
100
150
200
250
300
350
400
0
10
20
30
40
50
60
70
80
90
100

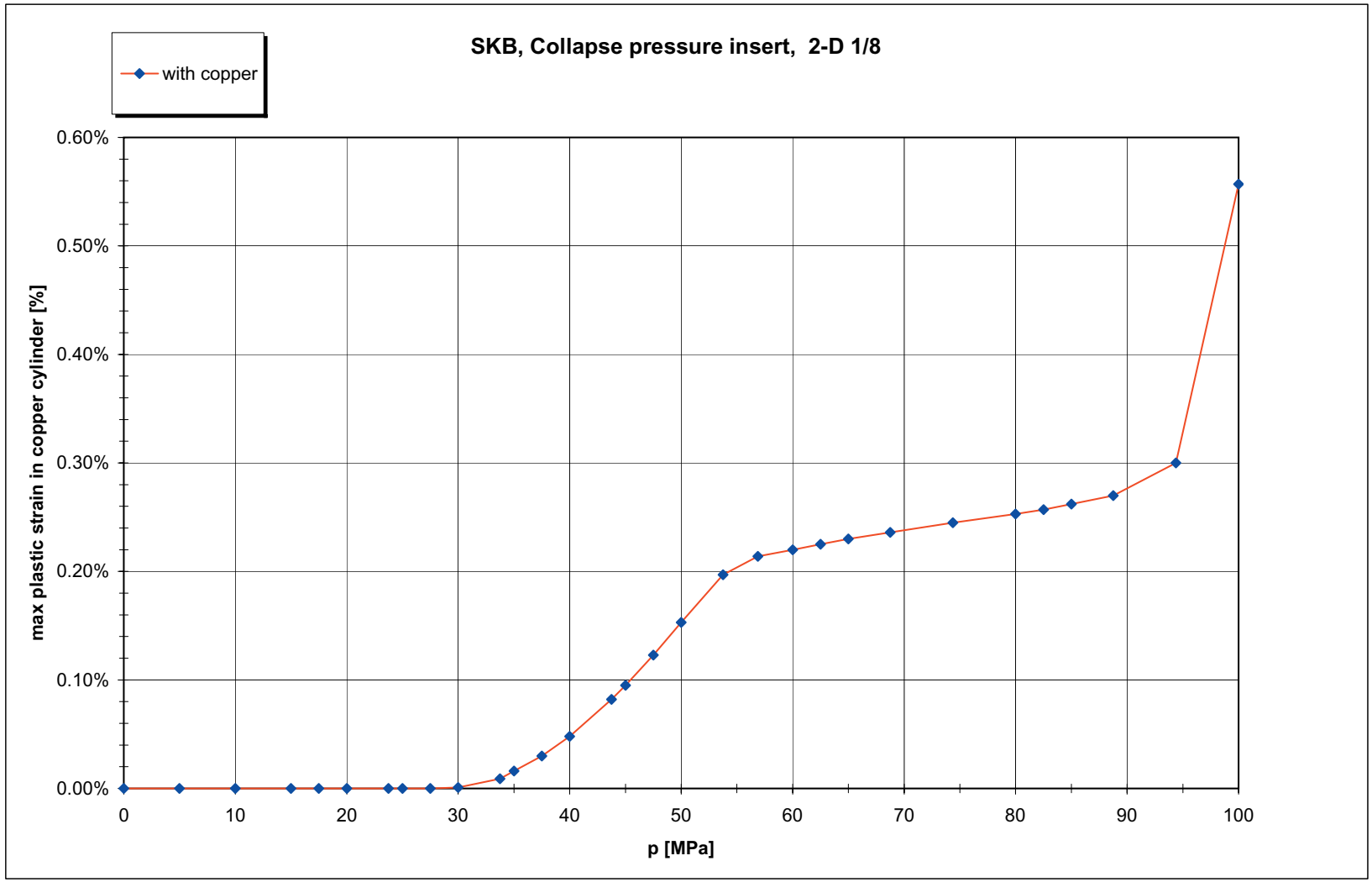
SKB, Collapse pressure insert, 2-D 1/8
with copper
max plastic strain in copper cylinder [%]
0.60%
0.50%
0.40%
0.30%
0.20%
0.10%
0.00%
0
10
20
30
40
50
60
70
80
90
100
p [MPa]

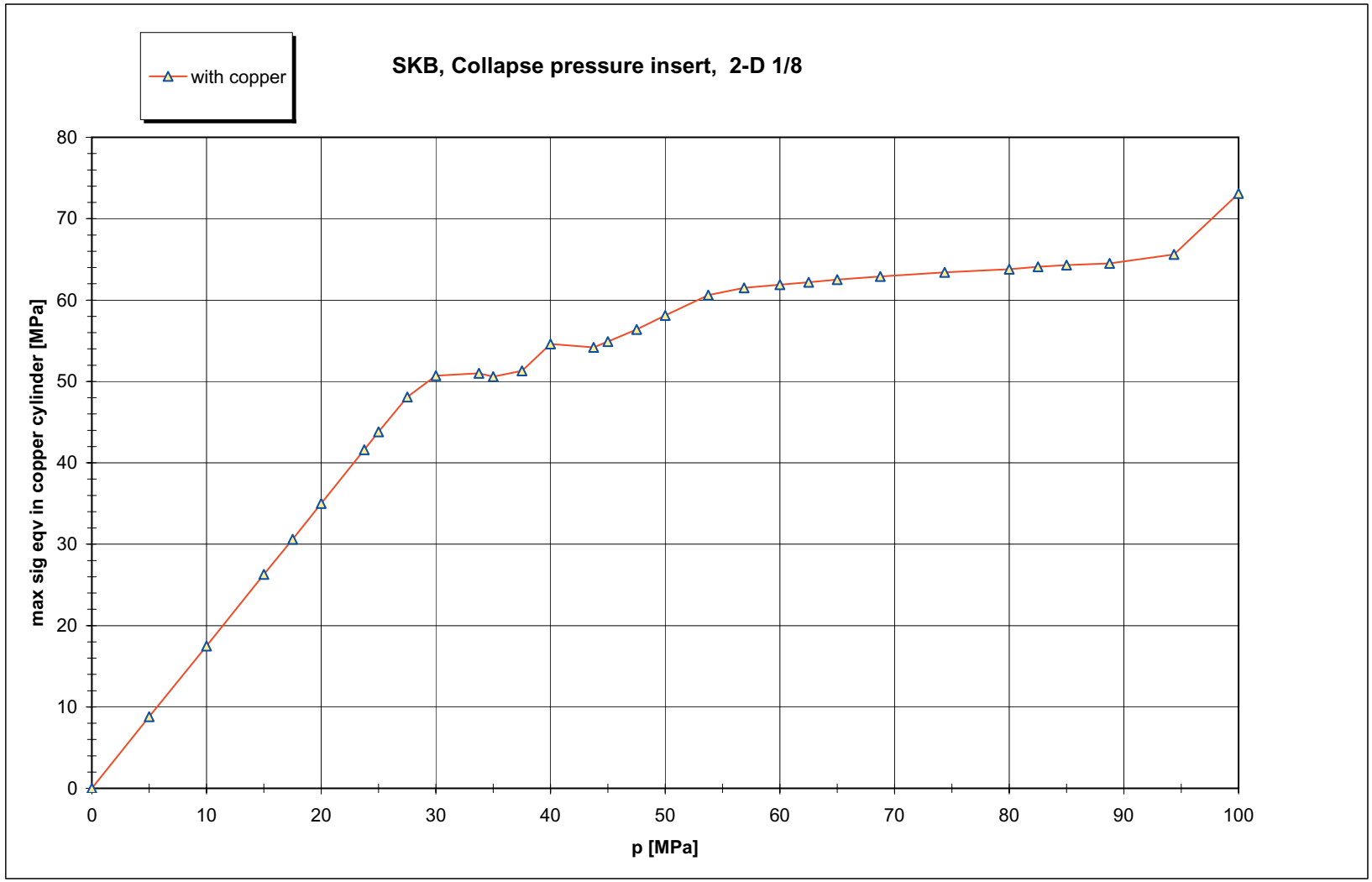
with copper
SKB, Collapse pressure insert, 2-D 1/8
max sig eqv in copper cylinder [MPa]
p [MPa]
0
10
20
30
40
50
60
70
80
90
100

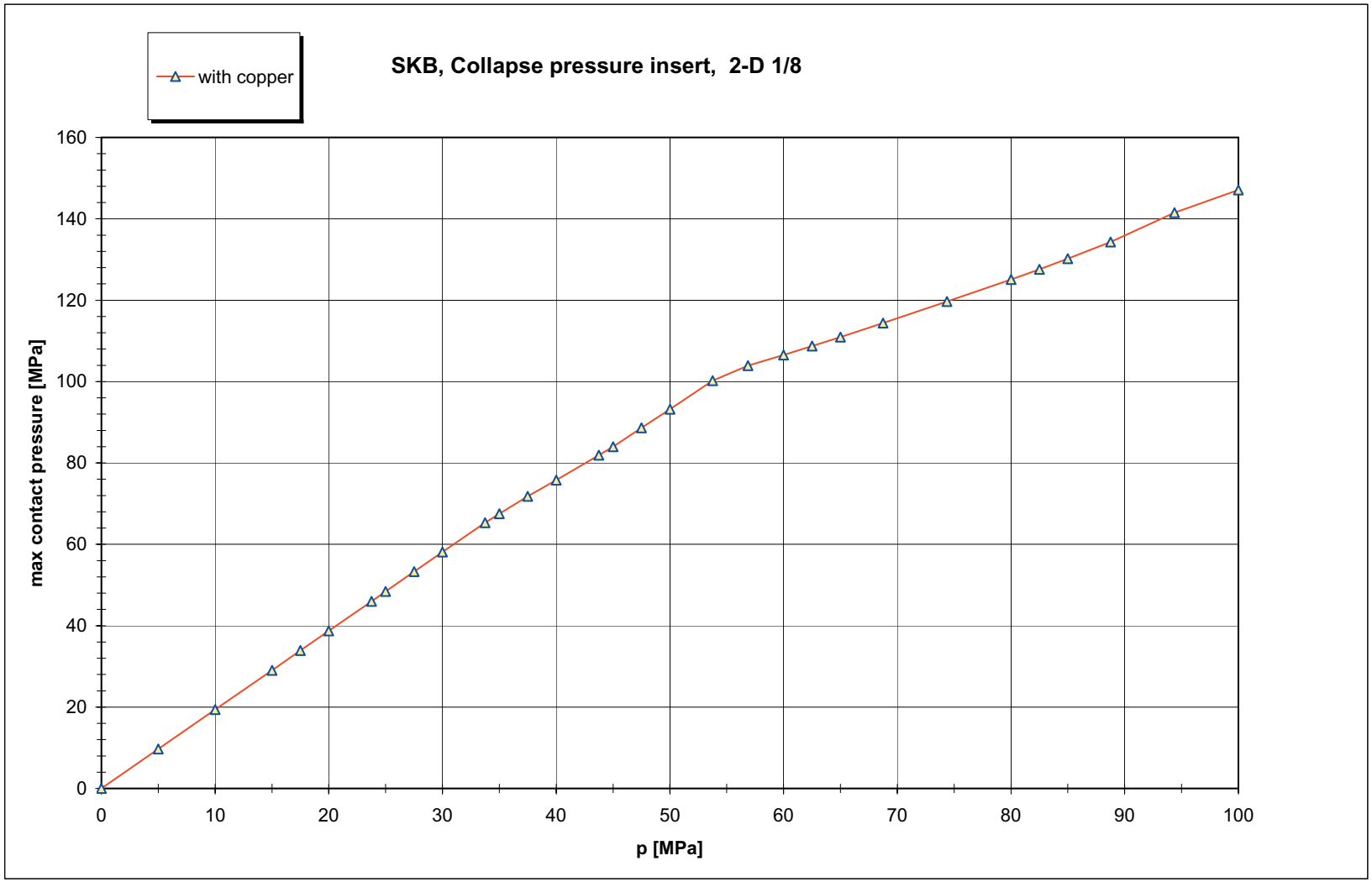
with copper
SKB, Collapse pressure insert, 2-D 1/8
max contact pressure [MPa]
p [MPa]
0
20
40
60
80
100
120
140
160
0
10
20
30
40
50
60
70
80
90
100

SKB, Collapse pressure inserts.

verification

assignment : 203253
model : r21 cu21

Influence of copper cylinder, critical section

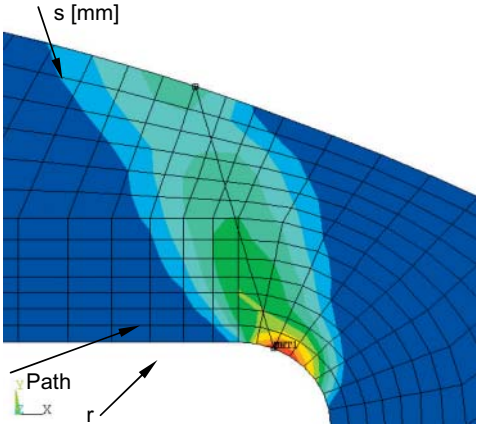

	plastic strain, p = 100 MPa, r = 21 mm			
s [mm]	without coppe	with copper		
0.0	4.73%	1.36%		
3.0	4.41%	1.28%		
5.9	4.10%	1.23%		
8.9	3.72%	1.12%		
11.9	3.53%	0.99%		
14.8	4.02%	0.98%		
17.8	4.62%	1.13%		
20.8	5.11%	1.34%		
23.8	5.26%	1.36%		
26.7	5.52%	1.49%		
29.7	5.86%	1.68%		
32.7	6.00%	1.70%		
35.6	6.21%	1.76%		
38.6	6.54%	1.90%		
41.6	7.08%	2.17%		
44.5	7.46%	2.49%		
47.5	7.34%	2.47%		
50.5	7.39%	2.65%		
53.4	9.27%	3.64%		
56.4	13.93%	5.97%		

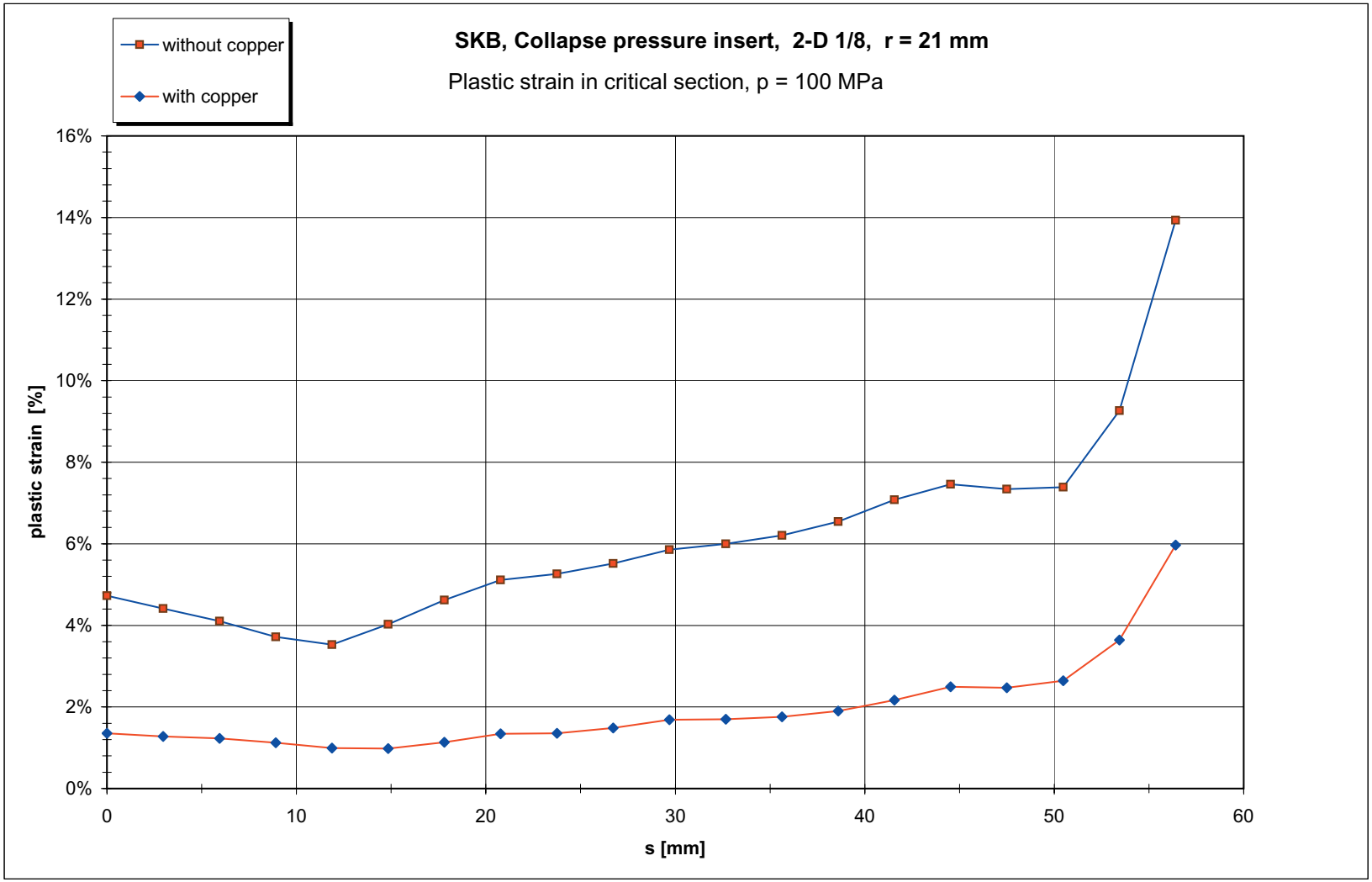
SKB, Collapse pressure insert, 2-D 1/8, r = 21 mm
Plastic strain in critical section, p = 100 MPa
without copper
with copper
plastic strain [%]
16%
14%
12%
10%
8%
6%
4%
2%
0%
0
10
20
30
40
50
60
s [mm]

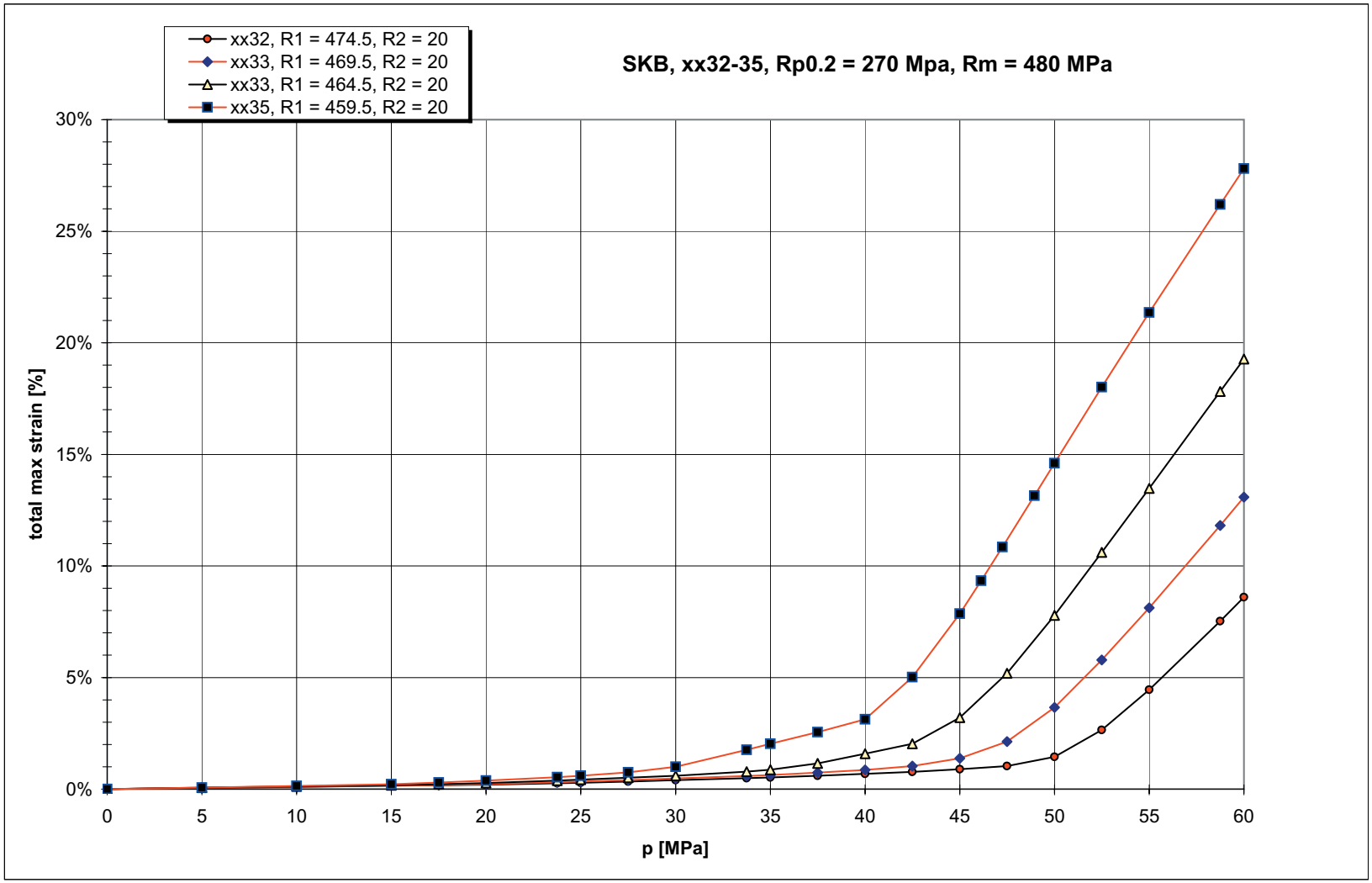
xx32, R1 = 474.5, R2 = 20
xx33, R1 = 469.5, R2 = 20
xx33, R1 = 464.5, R2 = 20
xx35, R1 = 459.5, R2 = 20
SKB, xx32-35, Rp0.2 = 270 Mpa, Rm = 480 MPa
total max strain [%]
30%
25%
20%
15%
10%
5%
0%
0
5
10
15
20
25
30
35
40
45
50
55
60
p [MPa]

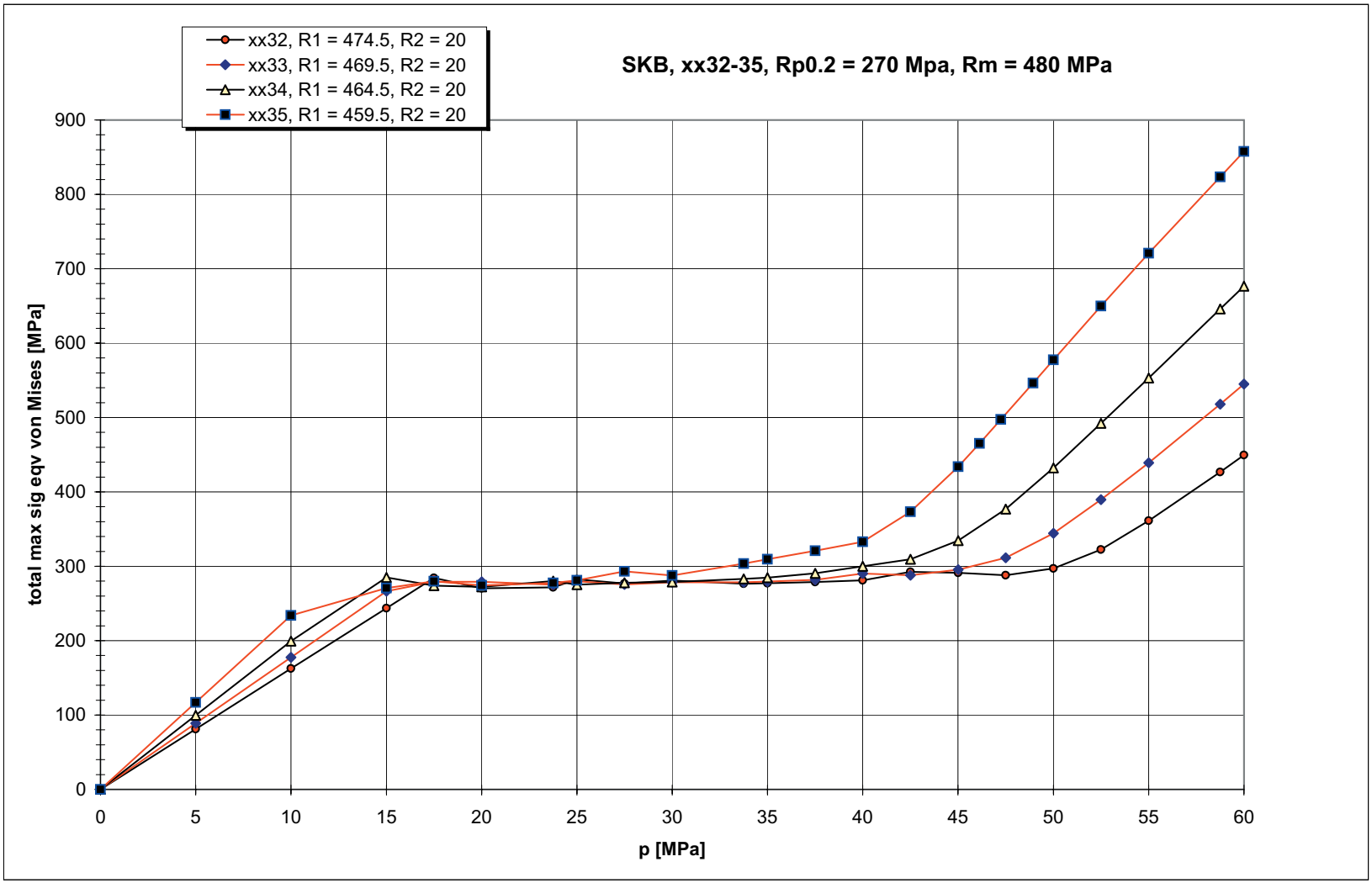
xx32, R1 = 474.5, R2 = 20
xx33, R1 = 469.5, R2 = 20
xx34, R1 = 464.5, R2 = 20
xx35, R1 = 459.5, R2 = 20
SKB, xx32-35, Rp0.2 = 270 Mpa, Rm = 480 MPa
total max sig eqv von Mises [MPa]
0
100
200
300
400
500
600
700
800
900
0
5
10
15
20
25
30
35
40
45
50
55
60
p [MPa]

SKB, Cast iron insert.

assignment : 203253

model : xx32 r2 = 20

2D plain strain r1 = 474.5

	p [MPa]	ε_{max}	σ_{eqvmax}	σ_{intmax}	ε_{max} %
	0.00	0.00000	0	0.0	0.00%
1	5.00	0.00049	81.20	91.3	0.05%
2	10.00	0.00098	162.50	182.6	0.10%
3	15.00	0.00147	243.80	274.0	0.15%
4	17.50	0.00171	284.40	319.8	0.17%
5	20.00	0.00194	270.20	305.4	0.19%
6	23.75	0.00258	271.60	310.1	0.26%
7	25.00	0.00283	282.40	315.3	0.28%
8	27.50	0.00337	276.90	314.1	0.34%
9	30.00	0.00398	280.90	317.0	0.40%
10	33.75	0.00490	276.60	319.0	0.49%
11	35.00	0.00524	277.30	319.9	0.52%
12	37.50	0.00598	278.90	321.9	0.60%
13	40.00	0.00680	281.00	324.0	0.68%
14	42.50	0.00775	292.50	329.1	0.78%
15	45.00	0.00887	291.20	329.1	0.89%
16	47.50	0.01030	288.10	332.7	1.03%
17	50.00	0.01446	297.00	342.9	1.45%
18	52.50	0.02644	322.50	372.4	2.64%
19	55.00	0.04450	361.10	416.9	4.45%
20	58.75	0.07529	426.70	492.7	7.53%
21	60.00	0.08602	449.60	519.1	8.60%

SKB, Cast iron insert.
assignment : 203253

model : xx33
2D plain strain

r2 = 20
r1 = 469.5

	p [MPa]	ε_{max}	σ_{eqvmax}	σ_{intmax}	ε_{max} %
	0.00	0.00000	0	0.0	0.00%
1	5.00	0.00053	88.80	99.8	0.05%
2	10.00	0.00107	177.60	199.7	0.11%
3	15.00	0.00161	266.50	299.6	0.16%
4	17.50	0.00178	279.10	313.3	0.18%
5	20.00	0.00222	279.10	313.8	0.22%
6	23.75	0.00304	275.30	312.5	0.30%
7	25.00	0.00335	279.90	315.1	0.34%
8	27.50	0.00403	275.50	316.4	0.40%
9	30.00	0.00473	278.40	318.5	0.47%
10	33.75	0.00587	278.60	321.6	0.59%
11	35.00	0.00632	279.60	322.8	0.63%
12	37.50	0.00734	281.80	325.3	0.73%
13	40.00	0.00856	290.20	328.4	0.86%
14	42.50	0.01032	288.10	332.7	1.03%
15	45.00	0.01376	295.50	341.2	1.38%
16	47.50	0.02123	311.40	359.6	2.12%
17	50.00	0.03658	344.20	397.4	3.66%
18	52.50	0.05782	389.50	449.7	5.78%
19	55.00	0.08118	439.20	507.2	8.12%
20	58.75	0.11808	517.80	598.0	11.81%
21	60.00	0.13084	545.00	629.3	13.08%

SKB, Cast iron insert.

assignment : 203253

model : xx34 r2 = 20

2D plain strain r1 = 464.5

	p [MPa]	ε_{max}	σ_{eqvmax}	σ_{intmax}	ε_{max} %
	0.00	0.00000	0	0.0	0.00%
1	5.00	0.00060	99.70	112.0	0.06%
2	10.00	0.00120	199.40	224.2	0.12%
3	15.00	0.00173	284.90	320.1	0.17%
4	17.50	0.00217	273.90	307.4	0.22%
5	20.00	0.00275	272.40	311.1	0.28%
6	23.75	0.00383	280.20	315.6	0.38%
7	25.00	0.00423	275.20	317.0	0.42%
8	27.50	0.00507	277.80	319.4	0.51%
9	30.00	0.00599	278.90	321.9	0.60%
10	33.75	0.00784	282.90	326.6	0.78%
11	35.00	0.00865	284.60	328.6	0.87%
12	37.50	0.01147	290.60	335.5	1.15%
13	40.00	0.01581	299.90	346.3	1.58%
14	42.50	0.02031	309.50	357.4	2.03%
15	45.00	0.03198	334.40	386.1	3.20%
16	47.50	0.05188	376.80	435.1	5.19%
17	50.00	0.07786	432.20	499.1	7.79%
18	52.50	0.10604	492.20	568.3	10.60%
19	55.00	0.13470	553.20	638.8	13.47%
20	58.75	0.17822	645.80	745.7	17.82%
21	60.00	0.19277	676.70	781.4	19.28%

SKB, Cast iron insert.
assignment : 203253

model : xx35
2D plain strain

r2 = 20
r1 = 459.5

	p [MPa]	ε_{max}	σ_{eqvmax}	σ_{intmax}	ε_{max} %
	0.00	0.00000	0	0.0	0.00%
1	5.00	0.00070	116.90	131.4	0.07%
2	10.00	0.00141	233.90	262.9	0.14%
3	15.00	0.00219	270.70	307.4	0.22%
4	17.50	0.00290	279.90	315.2	0.29%
5	20.00	0.00378	274.20	315.5	0.38%
6	23.75	0.00535	277.50	320.2	0.54%
7	25.00	0.00593	281.20	321.7	0.59%
8	27.50	0.00744	293.20	329.7	0.74%
9	30.00	0.01002	287.50	332.0	1.00%
10	33.75	0.01761	303.70	350.7	1.76%
11	35.00	0.02030	309.50	357.4	2.03%
12	37.50	0.02555	320.70	370.3	2.56%
13	40.00	0.03132	333.00	384.5	3.13%
14	42.50	0.05016	373.20	430.9	5.02%
15	45.00	0.07858	433.80	500.9	7.86%
16	46.13	0.09337	465.30	537.2	9.34%
17	47.25	0.10848	497.40	574.4	10.85%
18	48.94	0.13146	546.30	630.8	13.15%
19	50.00	0.14605	577.40	666.7	14.61%
20	52.50	0.18016	649.90	750.4	18.02%
21	55.00	0.21359	720.90	832.4	21.36%
22	58.75	0.26200	823.60	951.0	26.20%
23	60.00	0.27810	857.70	990.3	27.81%

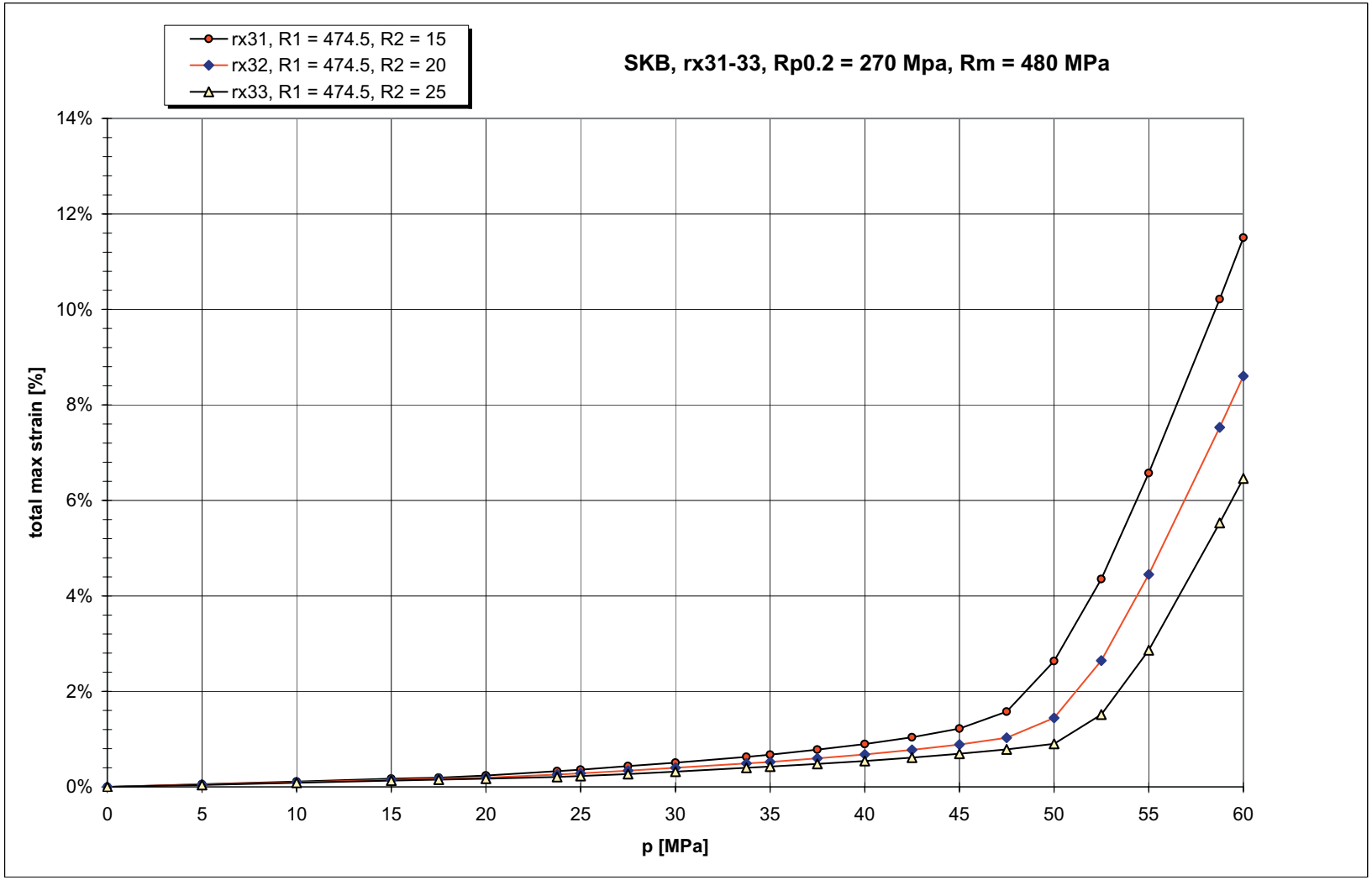
rx31, R1 = 474.5, R2 = 15
rx32, R1 = 474.5, R2 = 20
rx33, R1 = 474.5, R2 = 25
SKB, rx31-33, Rp0.2 = 270 Mpa, Rm = 480 MPa
total max strain [%]
14%
12%
10%
8%
6%
4%
2%
0%
0
5
10
15
20
25
30
35
40
45
50
55
60
p [MPa]

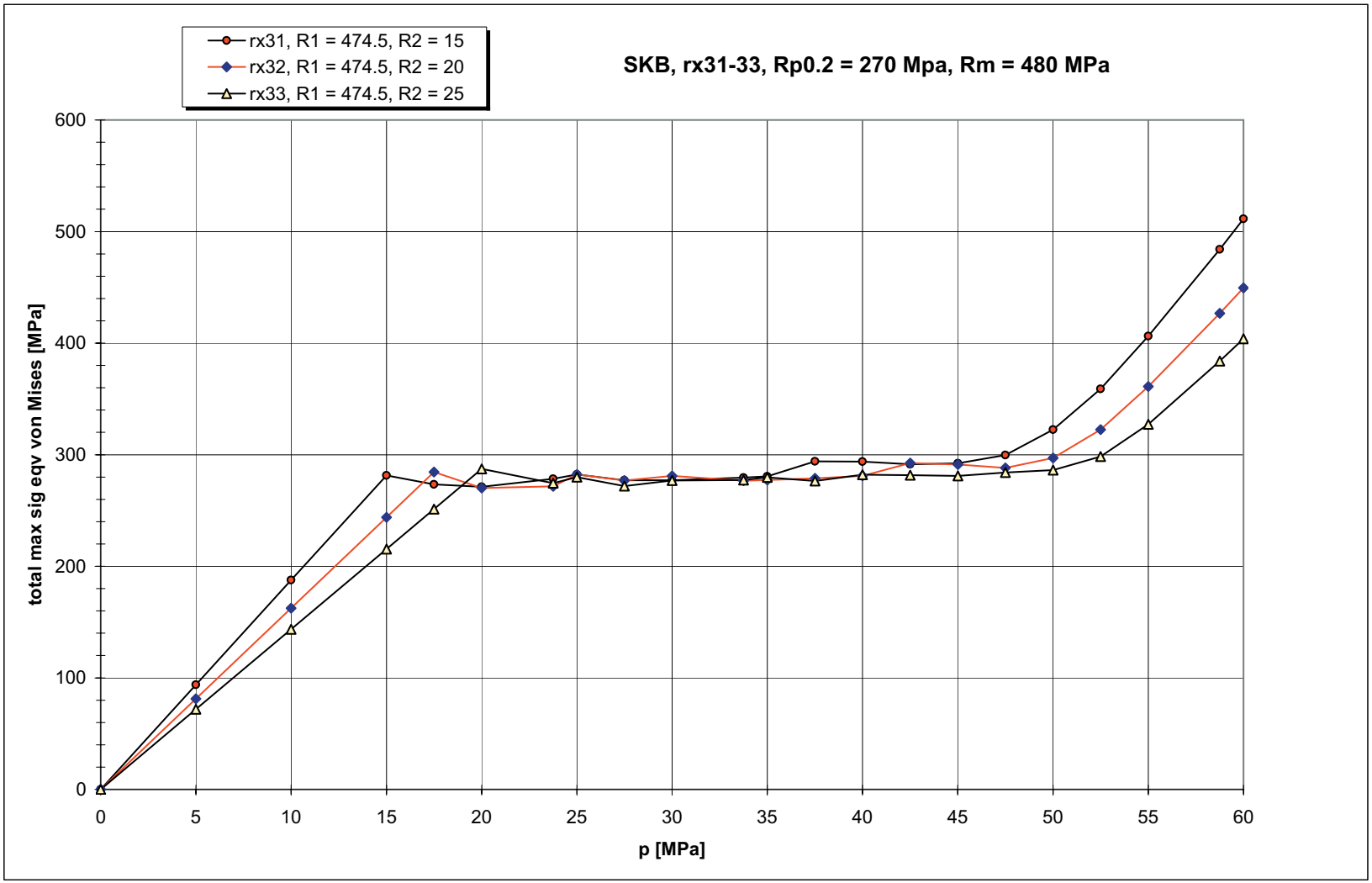
rx31, R1 = 474.5, R2 = 15
rx32, R1 = 474.5, R2 = 20
rx33, R1 = 474.5, R2 = 25
SKB, rx31-33, Rp0.2 = 270 Mpa, Rm = 480 MPa
total max sig eqv von Mises [MPa]
p [MPa]
0
100
200
300
400
500
600
0
5
10
15
20
25
30
35
40
45
50
55
60

SKB, Cast iron insert. model : rx31 r2 = 15

assignment : 203253 2D plain strain

	p [MPa]	ε_{max}	σ_{eqvmax}	σ_{intmax}	ε_{max} %
	0.00	0.00000	0	0.0	0.00%
1	5.00	0.00056	93.80	105.4	0.06%
2	10.00	0.00113	187.60	210.8	0.11%
3	15.00	0.00170	281.50	316.3	0.17%
4	17.50	0.00194	273.40	306.7	0.19%
5	20.00	0.00239	271.20	308.9	0.24%
6	23.75	0.00330	278.50	313.6	0.33%
7	25.00	0.00361	282.20	318.2	0.36%
8	27.50	0.00435	277.10	317.4	0.44%
9	30.00	0.00508	277.00	319.5	0.51%
10	33.75	0.00629	279.50	322.6	0.63%
11	35.00	0.00673	280.50	323.8	0.67%
12	37.50	0.00778	294.10	330.8	0.78%
13	40.00	0.00896	293.80	330.4	0.90%
14	42.50	0.01038	291.40	332.9	1.04%
15	45.00	0.01223	292.20	337.4	1.22%
16	47.50	0.01574	299.70	346.1	1.57%
17	50.00	0.02633	322.40	372.2	2.63%
18	52.50	0.04351	359.00	414.6	4.35%
19	55.00	0.06574	406.40	469.3	6.57%
20	58.75	0.10217	484.00	558.9	10.22%
21	60.00	0.11501	511.30	590.4	11.50%

SKB, Cast iron insert. model : rx32 r2 = 20

assignment : 203253 2D plain strain

	p [MPa]	ε_{max}	σ_{eqvmax}	σ_{intmax}	ε_{max} %
	0.00	0.00000	0	0.0	0.00%
1	5.00	0.00049	81.20	91.3	0.05%
2	10.00	0.00098	162.50	182.6	0.10%
3	15.00	0.00147	243.80	274.0	0.15%
4	17.50	0.00171	284.40	319.8	0.17%
5	20.00	0.00194	270.20	305.4	0.19%
6	23.75	0.00258	271.60	310.1	0.26%
7	25.00	0.00283	282.40	315.3	0.28%
8	27.50	0.00337	276.90	314.1	0.34%
9	30.00	0.00398	280.90	317.0	0.40%
10	33.75	0.00490	276.60	319.0	0.49%
11	35.00	0.00524	277.30	319.9	0.52%
12	37.50	0.00598	278.90	321.9	0.60%
13	40.00	0.00680	281.00	324.0	0.68%
14	42.50	0.00775	292.50	329.1	0.78%
15	45.00	0.00887	291.20	329.1	0.89%
16	47.50	0.01030	288.10	332.7	1.03%
17	50.00	0.01446	297.00	342.9	1.45%
18	52.50	0.02644	322.50	372.4	2.64%
19	55.00	0.04450	361.10	416.9	4.45%
20	58.75	0.07529	426.70	492.7	7.53%
21	60.00	0.08602	449.60	519.1	8.60%

SKB, Cast iron insert. model : rx33 r2 = 25

assignment : 203253 2D plain strain

	p [MPa]	ε_{max}	σ_{eqvmax}	σ_{intmax}	ε_{max} %
	0.00	0.00000	0	0.0	0.00%
1	5.00	0.00043	71.80	80.7	0.04%
2	10.00	0.00086	143.60	161.4	0.09%
3	15.00	0.00130	215.40	242.2	0.13%
4	17.50	0.00151	251.30	282.6	0.15%
5	20.00	0.00173	287.30	323.1	0.17%
6	23.75	0.00209	274.40	308.2	0.21%
7	25.00	0.00229	279.90	315.1	0.23%
8	27.50	0.00271	271.90	311.1	0.27%
9	30.00	0.00321	276.80	313.5	0.32%
10	33.75	0.00398	277.20	316.3	0.40%
11	35.00	0.00426	279.70	317.1	0.43%
12	37.50	0.00482	276.40	318.8	0.48%
13	40.00	0.00544	282.00	320.5	0.54%
14	42.50	0.00614	281.70	322.3	0.61%
15	45.00	0.00693	280.90	324.3	0.69%
16	47.50	0.00785	284.00	326.6	0.79%
17	50.00	0.00901	286.30	329.5	0.90%
18	52.50	0.01515	298.40	344.6	1.52%
19	55.00	0.02865	327.30	377.9	2.87%
20	58.75	0.05527	384.00	443.4	5.53%
21	60.00	0.06461	403.90	466.4	6.46%

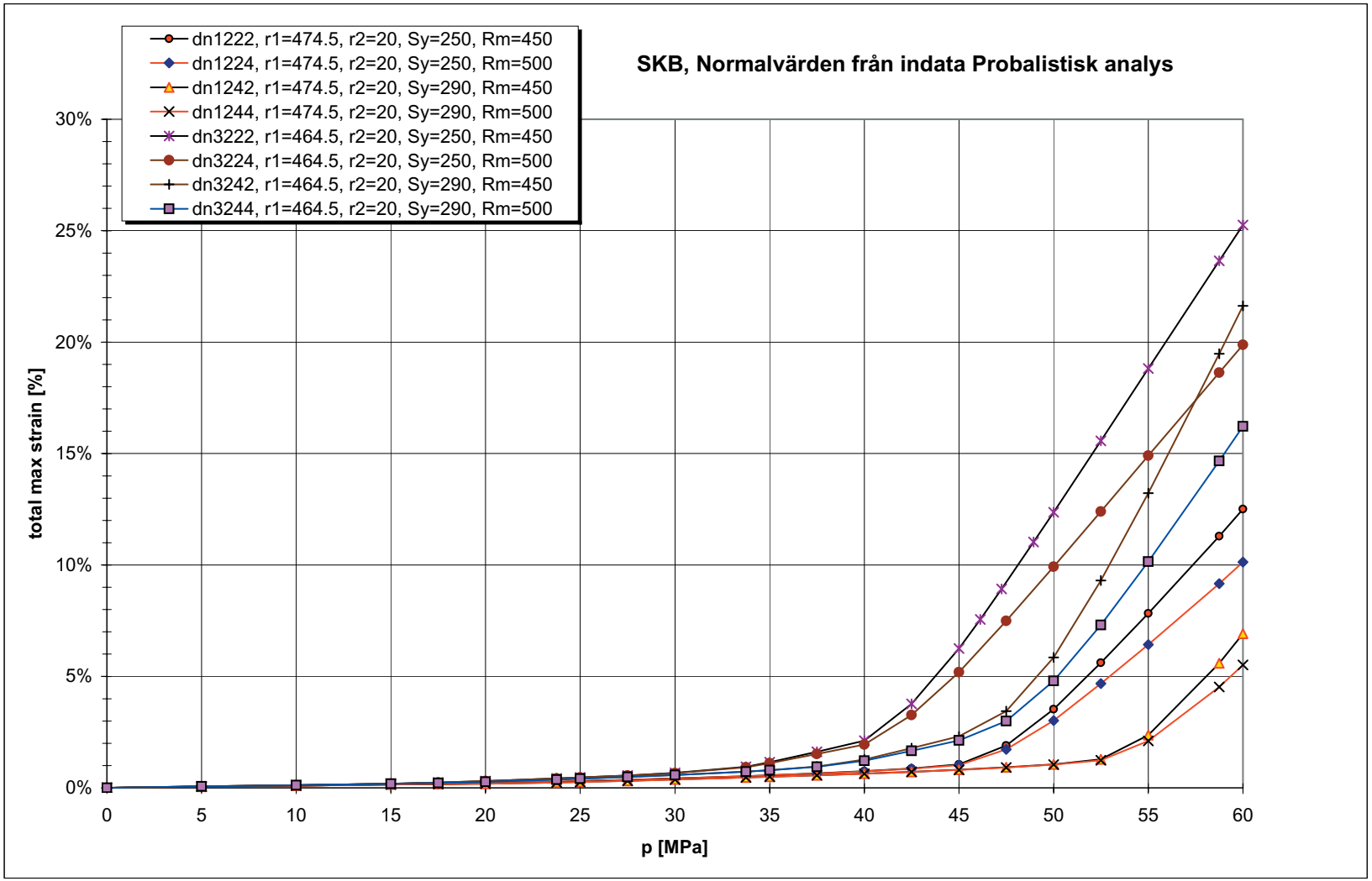
SKB, Normalvärden från indata Probalistisk analys
dn1222, r1=474.5, r2=20, Sy=250, Rm=450
dn1224, r1=474.5, r2=20, Sy=250, Rm=500
dn1242, r1=474.5, r2=20, Sy=290, Rm=450
dn1244, r1=474.5, r2=20, Sy=290, Rm=500
dn3222, r1=464.5, r2=20, Sy=250, Rm=450
dn3224, r1=464.5, r2=20, Sy=250, Rm=500
dn3242, r1=464.5, r2=20, Sy=290, Rm=450
dn3244, r1=464.5, r2=20, Sy=290, Rm=500
total max strain [%]
30%
25%
20%
15%
10%
5%
0%
0
5
10
15
20
25
30
35
40
45
50
55
60
p [MPa]

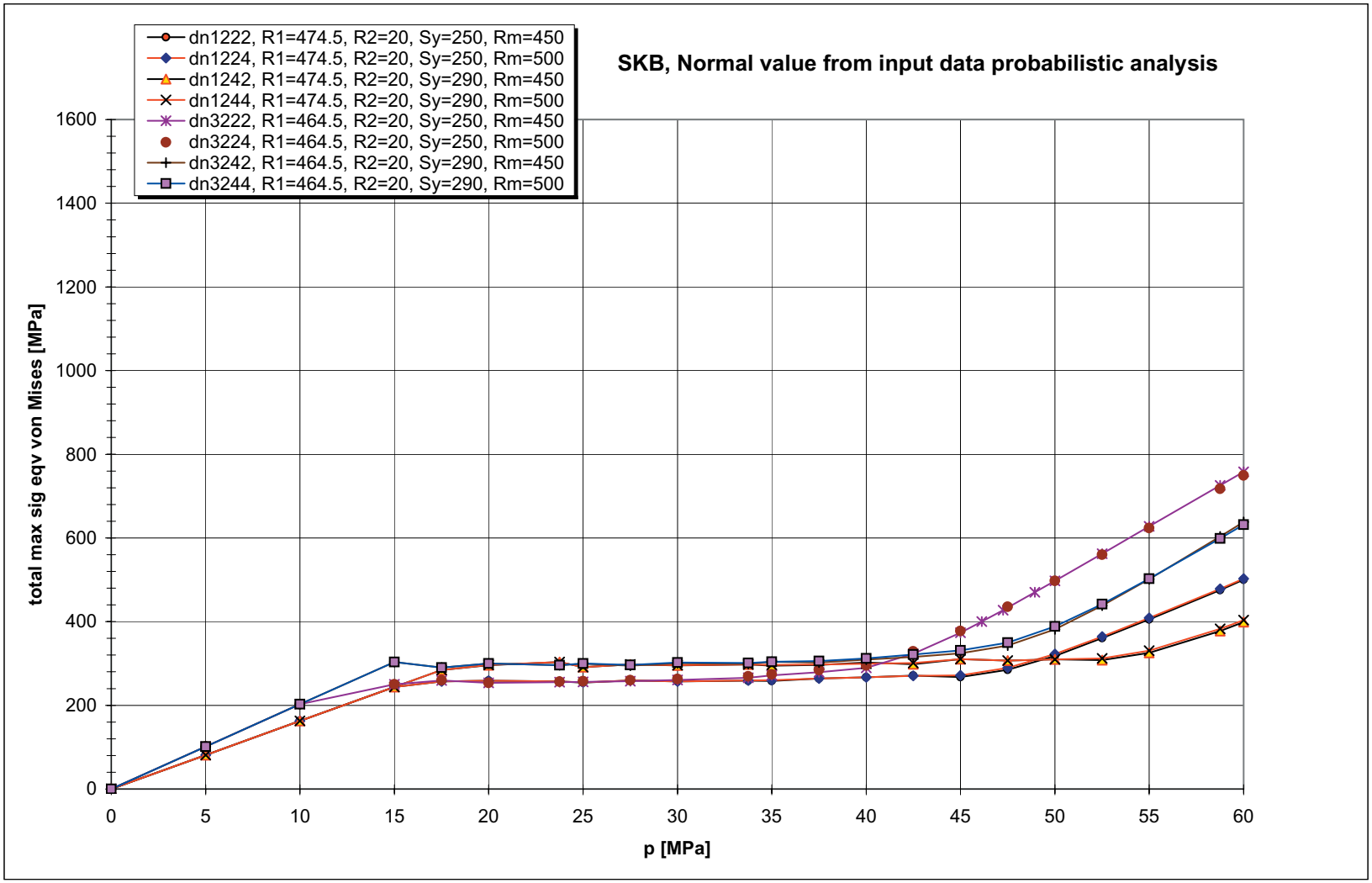
SKB, Normal value from input data probabilistic analysis
dn1222, R1=474.5, R2=20, Sy=250, Rm=450
dn1224, R1=474.5, R2=20, Sy=250, Rm=500
dn1242, R1=474.5, R2=20, Sy=290, Rm=450
dn1244, R1=474.5, R2=20, Sy=290, Rm=500
dn3222, R1=464.5, R2=20, Sy=250, Rm=450
dn3224, R1=464.5, R2=20, Sy=250, Rm=500
dn3242, R1=464.5, R2=20, Sy=290, Rm=450
dn3244, R1=464.5, R2=20, Sy=290, Rm=500
total max sig eqv von Mises [MPa]
0
200
400
600
800
1000
1200
1400
1600
p [MPa]
0
5
10
15
20
25
30
35
40
45
50
55
60

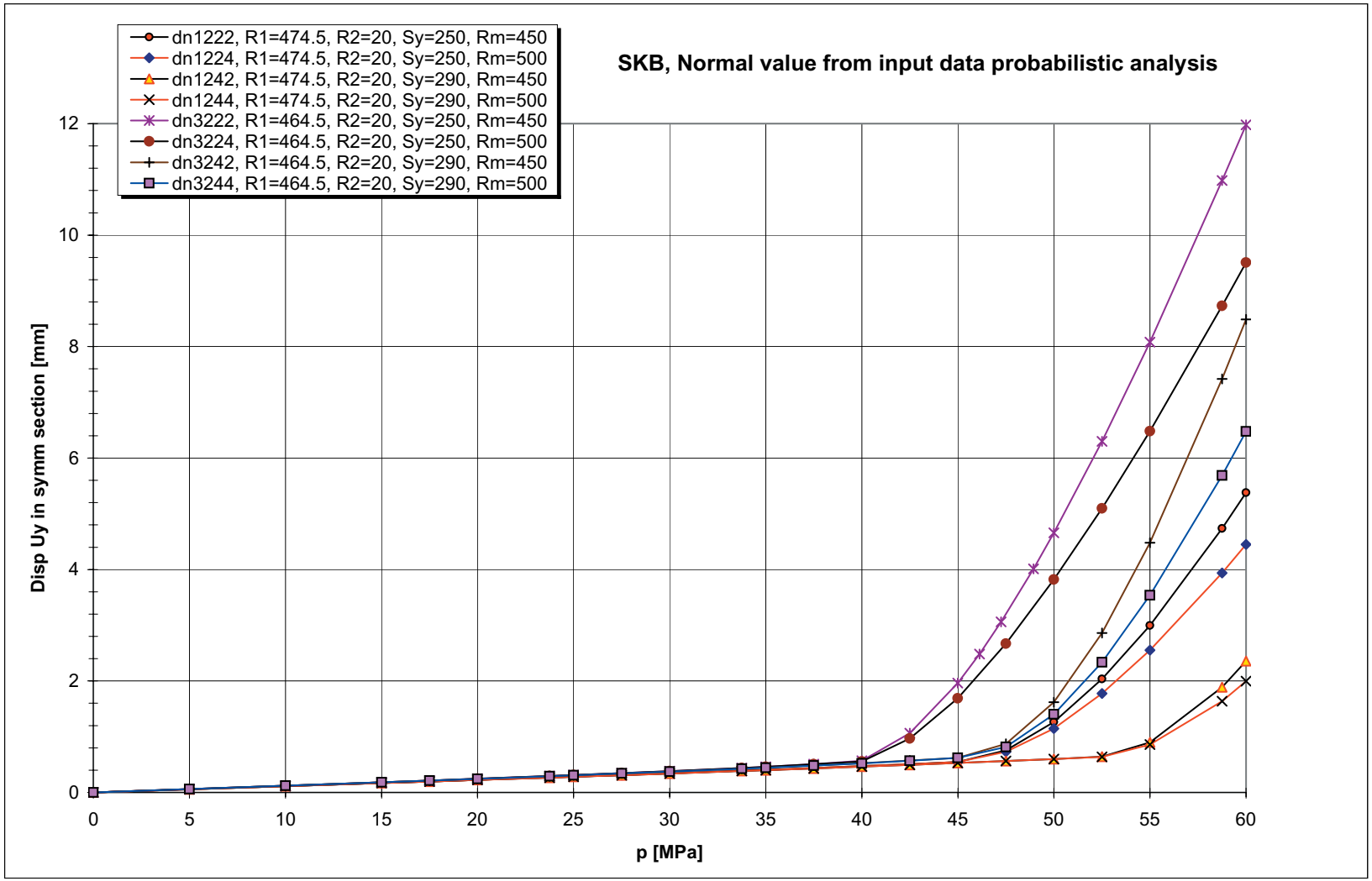
SKB, Normal value from input data probabilistic analysis
dn1222, R1=474.5, R2=20, Sy=250, Rm=450
dn1224, R1=474.5, R2=20, Sy=250, Rm=500
dn1242, R1=474.5, R2=20, Sy=290, Rm=450
dn1244, R1=474.5, R2=20, Sy=290, Rm=500
dn3222, R1=464.5, R2=20, Sy=250, Rm=450
dn3224, R1=464.5, R2=20, Sy=250, Rm=500
dn3242, R1=464.5, R2=20, Sy=290, Rm=450
dn3244, R1=464.5, R2=20, Sy=290, Rm=500
Disp Uy in symm section [mm]
0
2
4
6
8
10
12
0
5
10
15
20
25
30
35
40
45
50
55
60
p [MPa]

SKB, Cast iron inserts.

assignment : 203253

model : dn1222
2D plain strain

r2 = 20
r1 = 474.5
Sy = 250
Rm = 450

	p [MPa]	ε_{max}	σ_{eqvmax}	σ_{intmax}	u_y	ε_{max} %
	0.00	0.00000	0	0.0	0	0.00%
1	5.00	0.00049	81.20	91.3	0.06	0.05%
2	10.00	0.00098	162.50	182.6	0.11	0.10%
3	15.00	0.00147	243.80	274.0	0.17	0.15%
4	17.50	0.00162	257.00	288.5	0.20	0.16%
5	20.00	0.00201	258.90	291.1	0.22	0.20%
6	23.75	0.00274	256.90	288.9	0.27	0.27%
7	25.00	0.00302	254.50	290.2	0.28	0.30%
8	27.50	0.00362	259.30	292.4	0.31	0.36%
9	30.00	0.00424	257.40	294.2	0.34	0.42%
10	33.75	0.00525	258.90	296.8	0.39	0.53%
11	35.00	0.00563	258.00	297.8	0.41	0.56%
12	37.50	0.00647	263.90	299.8	0.44	0.65%
13	40.00	0.00746	267.10	302.2	0.47	0.75%
14	42.50	0.00866	270.80	305.0	0.51	0.87%
15	45.00	0.01048	267.80	309.3	0.55	1.05%
16	47.50	0.01898	285.10	329.2	0.76	1.90%
17	50.00	0.03528	318.20	367.4	1.26	3.53%
18	52.50	0.05618	360.60	416.4	2.04	5.62%
19	55.00	0.07824	405.30	468.0	2.99	7.82%
20	58.75	0.11291	475.50	549.1	4.74	11.29%
21	60.00	0.12512	500.30	577.6	5.38	12.51%

SKB, Cast iron inserts.

assignment : 203253

model : dn1224
2D plain strain

r2 = 20
r1 = 474.5
Sy = 250
Rm = 500

	p [MPa]	ε_{max}	σ_{eqvmax}	σ_{intmax}	u_y	ε_{max} %
	0.00	0.00000	0	0.0	0	0.00%
1	5.00	0.00049	81.20	91.3	0.06	0.05%
2	10.00	0.00098	162.50	182.6	0.11	0.10%
3	15.00	0.00147	243.80	274.0	0.17	0.15%
4	17.50	0.00162	257.10	288.6	0.20	0.16%
5	20.00	0.00201	259.00	291.2	0.22	0.20%
6	23.75	0.00274	257.00	289.6	0.27	0.27%
7	25.00	0.00301	254.70	291.0	0.28	0.30%
8	27.50	0.00361	259.70	293.5	0.31	0.36%
9	30.00	0.00422	257.20	295.7	0.34	0.42%
10	33.75	0.00522	259.60	298.9	0.39	0.52%
11	35.00	0.00560	260.00	300.1	0.41	0.56%
12	37.50	0.00642	263.80	302.6	0.44	0.64%
13	40.00	0.00739	267.00	305.5	0.47	0.74%
14	42.50	0.00856	270.70	308.9	0.51	0.86%
15	45.00	0.01023	271.80	313.8	0.55	1.02%
16	47.50	0.01723	289.50	334.3	0.73	1.72%
17	50.00	0.03014	322.30	372.1	1.15	3.01%
18	52.50	0.04676	364.40	420.8	1.78	4.68%
19	55.00	0.06432	408.90	472.2	2.55	6.43%
20	58.75	0.09163	478.10	552.0	3.94	9.16%
21	60.00	0.10126	502.50	580.2	4.45	10.13%

SKB, Cast iron inserts.

assignment : 203253

model : dn1242
2D plain strain

r2 = 20
r1 = 474.5
Sy = 290
Rm = 450

	p [MPa]	ε_{max}	σ_{eqvmax}	σ_{intmax}	u_y	ε_{max} %
	0.00	0.00000	0	0.0	0	0.00%
1	5.00	0.00049	81.20	91.3	0.06	0.05%
2	10.00	0.00098	162.50	182.6	0.11	0.10%
3	15.00	0.00147	243.80	274.0	0.17	0.15%
4	17.50	0.00171	284.40	319.8	0.20	0.17%
5	20.00	0.00183	296.10	332.5	0.22	0.18%
6	23.75	0.00241	303.20	341.4	0.27	0.24%
7	25.00	0.00267	291.00	332.0	0.28	0.27%
8	27.50	0.00318	297.80	334.9	0.31	0.32%
9	30.00	0.00375	295.40	336.7	0.34	0.38%
10	33.75	0.00467	297.90	339.2	0.39	0.47%
11	35.00	0.00499	294.80	340.0	0.40	0.50%
12	37.50	0.00563	296.60	341.4	0.43	0.56%
13	40.00	0.00637	302.00	342.9	0.46	0.64%
14	42.50	0.00720	298.40	344.5	0.50	0.72%
15	45.00	0.00814	310.40	349.2	0.53	0.81%
16	47.50	0.00923	306.90	348.4	0.56	0.92%
17	50.00	0.01057	309.80	350.9	0.60	1.06%
18	52.50	0.01280	308.00	355.1	0.64	1.28%
19	55.00	0.02372	325.30	375.7	0.90	2.37%
20	58.75	0.05588	377.70	436.1	1.89	5.59%
21	60.00	0.06911	399.20	460.9	2.36	6.91%

SKB, Cast iron inserts.

assignment : 203253

model : dn1244 2D plain strain

r2 = 20
r1 = 474.5
Sy = 290
Rm = 500

	p [MPa]	ε_{max}	σ_{eqvmax}	σ_{intmax}	u_y	ε_{max} %
	0.00	0.00000	0	0.0	0	0.00%
1	5.00	0.00049	81.20	91.3	0.06	0.05%
2	10.00	0.00098	162.50	182.6	0.11	0.10%
3	15.00	0.00147	243.80	274.0	0.17	0.15%
4	17.50	0.00171	284.40	319.8	0.20	0.17%
5	20.00	0.00183	296.20	332.5	0.22	0.18%
6	23.75	0.00241	303.40	341.5	0.27	0.24%
7	25.00	0.00266	291.50	332.5	0.28	0.27%
8	27.50	0.00317	297.90	335.4	0.31	0.32%
9	30.00	0.00374	295.70	337.8	0.34	0.37%
10	33.75	0.00465	297.60	340.8	0.38	0.47%
11	35.00	0.00497	296.40	341.8	0.40	0.50%
12	37.50	0.00560	297.80	343.6	0.43	0.56%
13	40.00	0.00633	299.40	345.5	0.46	0.63%
14	42.50	0.00715	301.10	347.6	0.50	0.72%
15	45.00	0.00807	310.20	349.9	0.53	0.81%
16	47.50	0.00913	306.70	352.5	0.56	0.91%
17	50.00	0.01042	309.70	355.8	0.60	1.04%
18	52.50	0.01241	312.40	360.7	0.64	1.24%
19	55.00	0.02107	330.90	382.0	0.86	2.11%
20	58.75	0.04525	382.50	441.7	1.64	4.53%
21	60.00	0.05520	403.70	466.2	2.00	5.52%

SKB, Cast iron inserts.

assignment : 203253

model : dn3222 2D plain strain

r2 = 20
r1 = 464.5
Sy = 250
Rm = 450

	p [MPa]	ε_{max}	σ_{eqvmax}	σ_{intmax}	u_y	ε_{max} %
	0.00	0.00000	0	0.0	0	0.00%
1	5.00	0.00061	101.10	113.8	0.06	0.06%
2	10.00	0.00122	202.40	227.6	0.12	0.12%
3	15.00	0.00183	250.30	283.4	0.18	0.18%
4	17.50	0.00238	259.60	292.5	0.21	0.24%
5	20.00	0.00306	253.80	290.4	0.25	0.31%
6	23.75	0.00422	255.10	294.1	0.29	0.42%
7	25.00	0.00464	256.00	295.2	0.31	0.46%
8	27.50	0.00558	257.90	297.6	0.35	0.56%
9	30.00	0.00672	260.30	300.4	0.38	0.67%
10	33.75	0.00947	265.80	306.9	0.44	0.95%
11	35.00	0.01147	271.60	311.6	0.46	1.15%
12	37.50	0.01615	279.30	322.6	0.51	1.62%
13	40.00	0.02119	289.60	334.4	0.57	2.12%
14	42.50	0.03770	323.10	373.0	1.06	3.77%
15	45.00	0.06252	373.40	431.2	1.96	6.25%
16	46.13	0.07558	399.90	461.7	2.48	7.56%
17	47.25	0.08922	427.50	493.7	3.06	8.92%
18	48.94	0.11030	470.20	542.9	4.01	11.03%
19	50.00	0.12370	497.30	574.3	4.66	12.37%
20	52.50	0.15573	562.10	649.1	6.30	15.57%
21	55.00	0.18818	627.70	724.9	8.08	18.82%
22	58.75	0.23645	725.30	837.5	10.98	23.65%
23	60.00	0.25255	757.80	875.0	11.98	25.26%

SKB, Cast iron inserts.

assignment : 203253

model : dn3224
2D plain strain

r2 = 20
r1 = 464.5
Sy = 250
Rm = 500

	p [MPa]	ε_{max}	σ_{eqvmax}	σ_{intmax}	u_y	ε_{max} %
	0.00	0.00000	0	0.0	0	0.00%
1	5.00	0.00061	101.10	113.8	0.06	0.06%
2	10.00	0.00122	202.40	227.6	0.12	0.12%
3	15.00	0.00183	250.40	283.5	0.18	0.18%
4	17.50	0.00238	259.80	292.7	0.21	0.24%
5	20.00	0.00305	253.90	291.2	0.25	0.31%
6	23.75	0.00420	256.50	295.6	0.29	0.42%
7	25.00	0.00462	257.50	297.0	0.31	0.46%
8	27.50	0.00554	259.90	299.9	0.35	0.55%
9	30.00	0.00667	262.70	303.3	0.38	0.67%
10	33.75	0.00927	269.30	311.0	0.44	0.93%
11	35.00	0.01103	273.80	316.1	0.46	1.10%
12	37.50	0.01517	284.30	328.3	0.51	1.52%
13	40.00	0.01947	295.20	340.8	0.56	1.95%
14	42.50	0.03269	328.70	379.6	0.97	3.27%
15	45.00	0.05185	377.30	435.7	1.69	5.19%
16	47.50	0.07489	435.70	503.1	2.67	7.49%
17	50.00	0.09919	497.20	574.1	3.82	9.92%
18	52.50	0.12400	560.00	646.6	5.10	12.40%
19	55.00	0.14910	623.50	719.9	6.48	14.91%
20	58.75	0.18631	717.50	828.5	8.73	18.63%
21	60.00	0.19878	749.10	865.0	9.51	19.88%

SKB, Cast iron inserts.

assignment : 203253

model : dn3242
2D plain strain

r2 = 20
r1 = 464.5
Sy = 290
Rm = 450

	p [MPa]	ε_{max}	σ_{eqvmax}	σ_{intmax}	u_y	ε_{max} %
	0.00	0.00000	0	0.0	0	0.00%
1	5.00	0.00061	101.10	113.8	0.06	0.06%
2	10.00	0.00122	202.40	227.6	0.12	0.12%
3	15.00	0.00183	303.70	341.6	0.18	0.18%
4	17.50	0.00214	290.20	328.6	0.21	0.21%
5	20.00	0.00269	299.80	337.6	0.24	0.27%
6	23.75	0.00371	295.90	336.5	0.29	0.37%
7	25.00	0.00410	299.60	337.7	0.31	0.41%
8	27.50	0.00489	294.70	339.7	0.34	0.49%
9	30.00	0.00577	300.80	341.7	0.38	0.58%
10	33.75	0.00730	298.60	344.7	0.43	0.73%
11	35.00	0.00795	304.20	346.0	0.44	0.80%
12	37.50	0.00955	302.30	349.0	0.48	0.96%
13	40.00	0.01265	309.30	354.8	0.52	1.27%
14	42.50	0.01781	315.70	364.6	0.57	1.78%
15	45.00	0.02313	324.40	374.6	0.62	2.31%
16	47.50	0.03445	342.80	395.8	0.87	3.45%
17	50.00	0.05850	381.90	441.0	1.62	5.85%
18	52.50	0.09306	438.10	505.9	2.86	9.31%
19	55.00	0.13225	501.70	579.4	4.48	13.23%
20	58.75	0.19478	603.20	696.5	7.42	19.48%
21	60.00	0.21628	638.00	736.7	8.49	21.63%

SKB, Cast iron inserts.

assignment : 203253

model : dn3244 2D plain strain

r2 = 20
r1 = 464.5
Sy = 290
Rm = 500

	p [MPa]	ε_{max}	σ_{eqvmax}	σ_{intmax}	u_y	ε_{max} %
	0.00	0.00000	0	0.0	0	0.00%
1	5.00	0.00061	101.10	113.8	0.06	0.06%
2	10.00	0.00122	202.40	227.6	0.12	0.12%
3	15.00	0.00183	303.70	341.6	0.18	0.18%
4	17.50	0.00214	290.40	328.8	0.21	0.21%
5	20.00	0.00269	299.90	337.8	0.24	0.27%
6	23.75	0.00371	296.00	337.6	0.29	0.37%
7	25.00	0.00408	299.90	339.0	0.31	0.41%
8	27.50	0.00487	296.20	341.5	0.34	0.49%
9	30.00	0.00574	302.10	343.9	0.37	0.57%
10	33.75	0.00725	301.30	347.8	0.43	0.73%
11	35.00	0.00789	304.00	349.4	0.44	0.79%
12	37.50	0.00943	306.00	353.3	0.48	0.94%
13	40.00	0.01219	311.90	360.1	0.52	1.22%
14	42.50	0.01665	321.40	371.1	0.57	1.67%
15	45.00	0.02128	331.30	382.5	0.62	2.13%
16	47.50	0.02996	349.80	403.9	0.82	3.00%
17	50.00	0.04803	388.40	448.5	1.40	4.80%
18	52.50	0.07305	441.80	510.2	2.34	7.31%
19	55.00	0.10157	502.60	580.4	3.54	10.16%
20	58.75	0.14670	598.80	691.4	5.69	14.67%
21	60.00	0.16222	631.80	729.6	6.48	16.22%

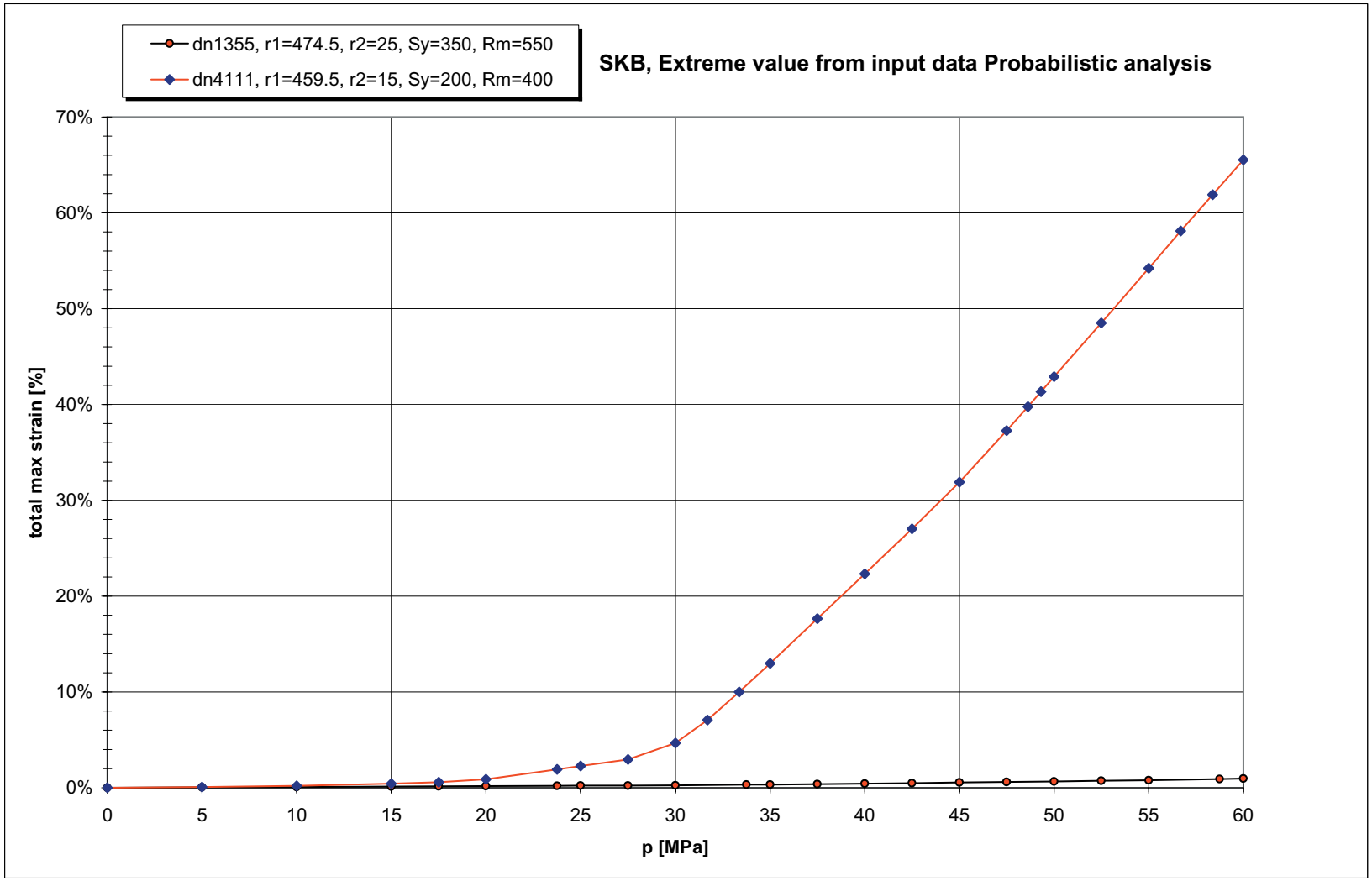
dn1355, r1=474.5, r2=25, Sy=350, Rm=550
dn4111, r1=459.5, r2=15, Sy=200, Rm=400
SKB, Extreme value from input data Probabilistic analysis
total max strain [%]
70%
60%
50%
40%
30%
20%
10%
0%
0
5
10
15
20
25
30
35
40
45
50
55
60
p [MPa]

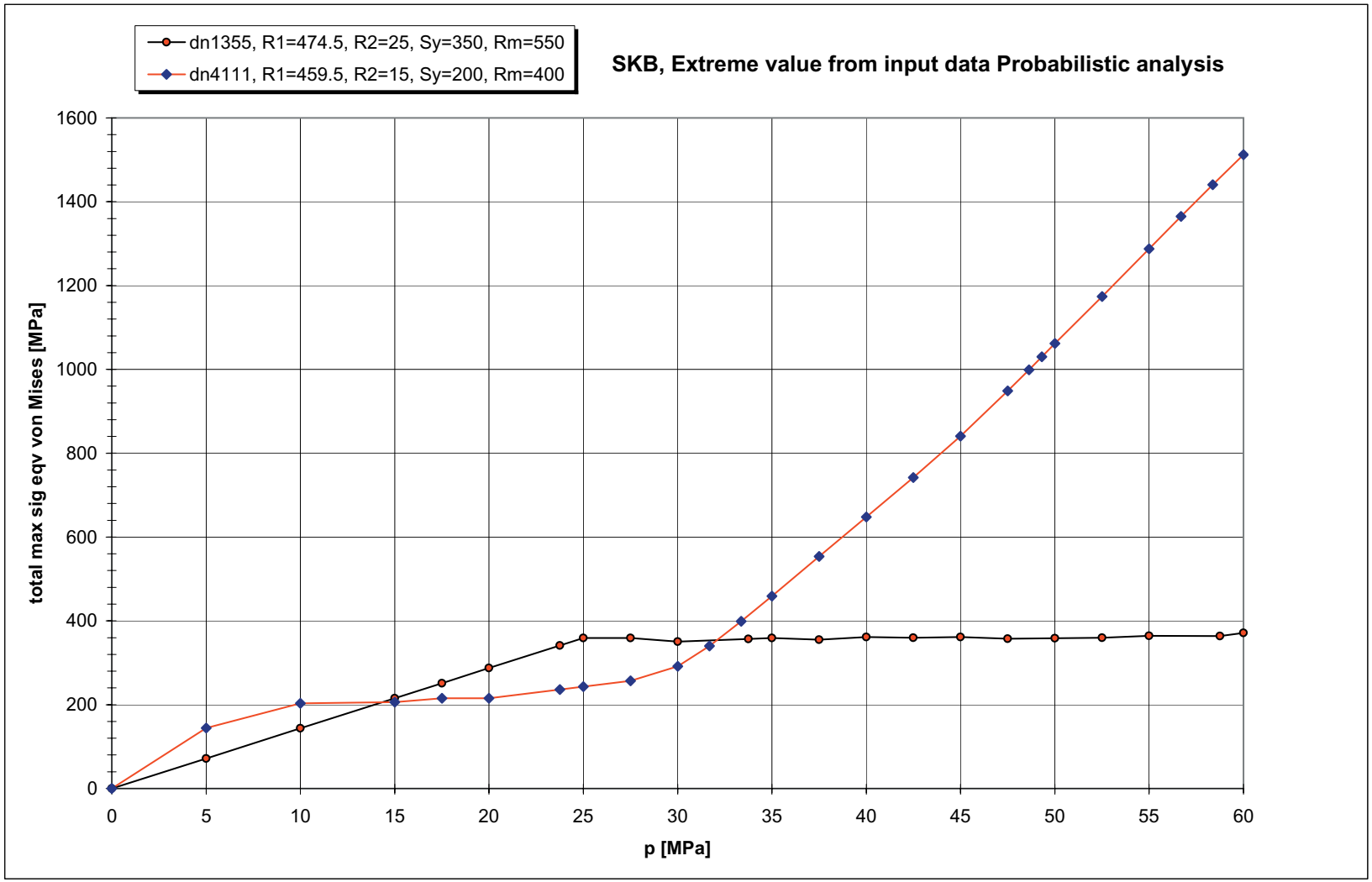
dn1355, R1=474.5, R2=25, Sy=350, Rm=550
dn4111, R1=459.5, R2=15, Sy=200, Rm=400
SKB, Extreme value from input data Probabilistic analysis
total max sig eqv von Mises [MPa]
p [MPa]
0
200
400
600
800
1000
1200
1400
1600
0
5
10
15
20
25
30
35
40
45
50
55
60

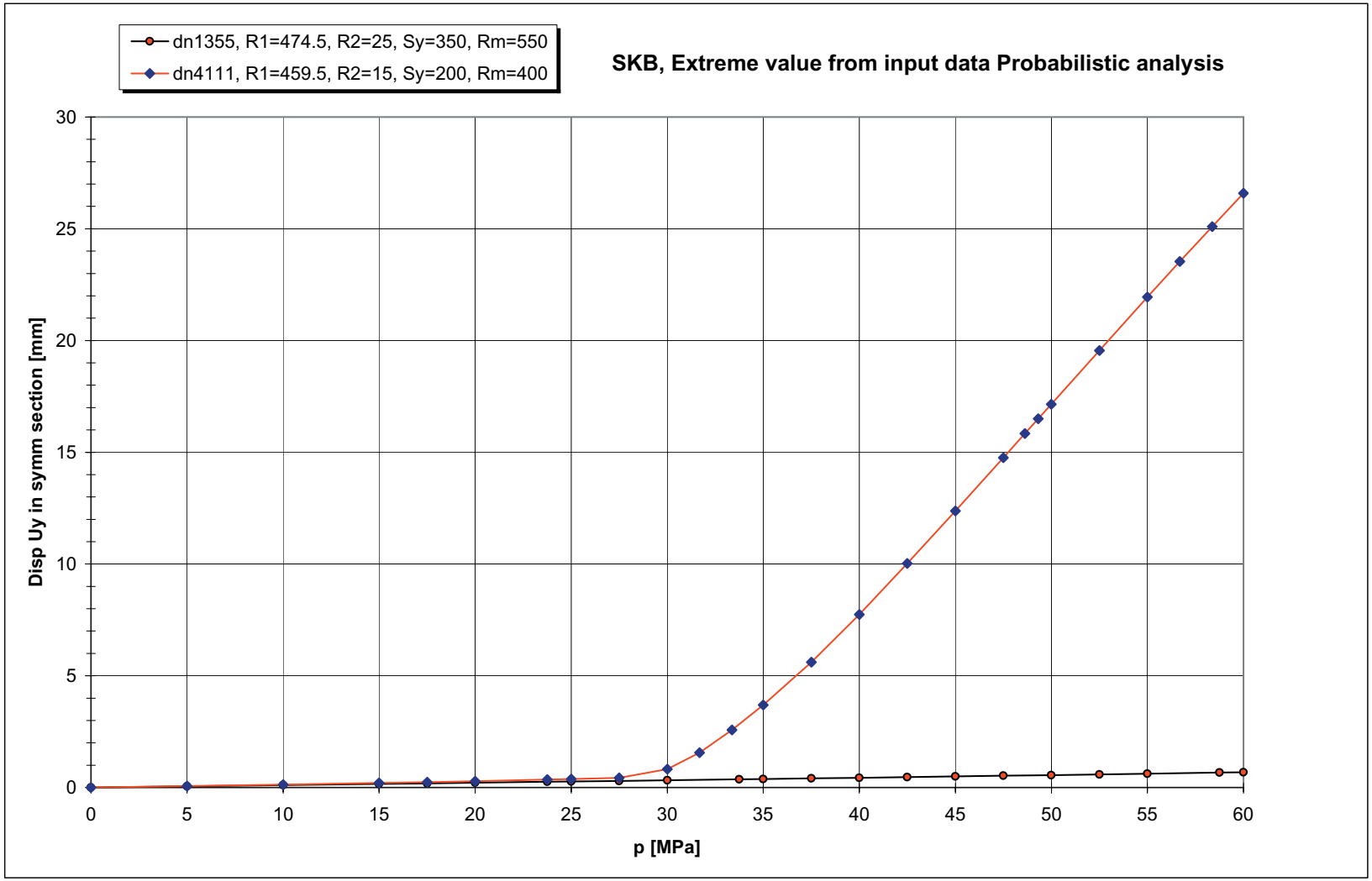
dn1355, R1=474.5, R2=25, Sy=350, Rm=550
dn4111, R1=459.5, R2=15, Sy=200, Rm=400
SKB, Extreme value from input data Probabilistic analysis
Disp Uy in symm section [mm]
p [MPa]
0
5
10
15
20
25
30
35
40
45
50
55
60

SKB, cast iron inserts.

assignment : 203253

model : dn1355
2D plain strain

r2 = 25
r1 = 474.5
Sy = 350
Rm = 550

	p [MPa]	ε_{max}	σ_{eqvmax}	σ_{intmax}	u_y	ε_{max} %
	0.00	0.00000	0	0.0	0	0.00%
1	5.00	0.00043	71.80	80.7	0.05	0.04%
2	10.00	0.00086	143.60	161.4	0.11	0.09%
3	15.00	0.00130	215.40	242.2	0.16	0.13%
4	17.50	0.00151	251.30	282.6	0.19	0.15%
5	20.00	0.00173	287.30	323.1	0.22	0.17%
6	23.75	0.00206	341.20	383.7	0.26	0.21%
7	25.00	0.00216	359.20	403.9	0.27	0.22%
8	27.50	0.00228	359.10	403.3	0.30	0.23%
9	30.00	0.00261	350.60	397.1	0.32	0.26%
10	33.75	0.00319	357.00	401.4	0.37	0.32%
11	35.00	0.00340	359.30	402.6	0.38	0.34%
12	37.50	0.00388	355.20	405.1	0.41	0.39%
13	40.00	0.00439	361.50	407.1	0.44	0.44%
14	42.50	0.00490	359.70	408.9	0.47	0.49%
15	45.00	0.00544	361.70	410.6	0.50	0.54%
16	47.50	0.00599	357.40	412.2	0.53	0.60%
17	50.00	0.00660	358.60	413.8	0.56	0.66%
18	52.50	0.00724	359.90	415.4	0.59	0.72%
19	55.00	0.00793	364.60	417.1	0.62	0.79%
20	58.75	0.00914	363.80	420.1	0.67	0.91%
21	60.00	0.00959	371.40	421.1	0.68	0.96%

SKB, Cast iron inserts.

assignment : 203253

model : dn4111 2D plain strain

r2 = 15
r1 = 459.5
Sy = 200
Rm = 400

	p [MPa]	ε_{max}	σ_{eqvmax}	σ_{intmax}	u_y	ε_{max} %
	0.00	0.00000	0	0.0	0	0.00%
1	5.00	0.00087	144.40	162.4	0.07	0.09%
2	10.00	0.00200	203.20	230.1	0.13	0.20%
3	15.00	0.00425	206.20	237.4	0.20	0.43%
4	17.50	0.00581	215.10	241.8	0.24	0.58%
5	20.00	0.00888	215.20	248.5	0.28	0.89%
6	23.75	0.01916	236.00	272.5	0.36	1.92%
7	25.00	0.02265	243.10	280.7	0.38	2.27%
8	27.50	0.02955	257.00	296.8	0.43	2.96%
9	30.00	0.04672	291.70	336.8	0.83	4.67%
10	31.69	0.07072	340.20	392.8	1.56	7.07%
11	33.38	0.09995	399.20	461.0	2.57	10.00%
12	35.00	0.12968	459.30	530.3	3.69	12.97%
13	37.50	0.17661	553.90	639.6	5.61	17.66%
14	40.00	0.22312	647.60	747.8	7.75	22.31%
15	42.50	0.27011	742.10	856.9	10.02	27.01%
16	45.00	0.31906	840.60	970.6	12.37	31.91%
17	47.50	0.37266	948.60	1095.3	14.76	37.27%
18	48.63	0.39773	998.90	1153.4	15.84	39.77%
19	49.31	0.41337	1030.30	1189.7	16.50	41.34%
20	50.00	0.42906	1061.70	1226.0	17.15	42.91%
21	52.50	0.48512	1173.90	1355.5	19.55	48.51%
22	55.00	0.54220	1287.80	1487.0	21.94	54.22%
23	56.69	0.58106	1365.20	1576.4	23.54	58.11%
24	58.38	0.61896	1440.50	1663.4	25.10	61.90%
25	60.00	0.65524	1512.50	1746.5	26.59	65.52%

Stress-strain curve Copper:
acc. to "Elements of Physical Metallurgy", Albert G. Guy, University of Florida

$i := .00, .001 .. .54$

$\delta(i) := i$

$E := 16 \cdot 10^6 \cdot psi$ $E = 1.103 \times 10^5\ MPa$

$S_0 := 8000 \cdot psi$ $S_0 = 55.158\ MPa$

$n := .54$

$K := 46000 \cdot psi$ $K = 317.159\ MPa$

$\sigma_1(i) := K \cdot \delta(i)^n + S_0$

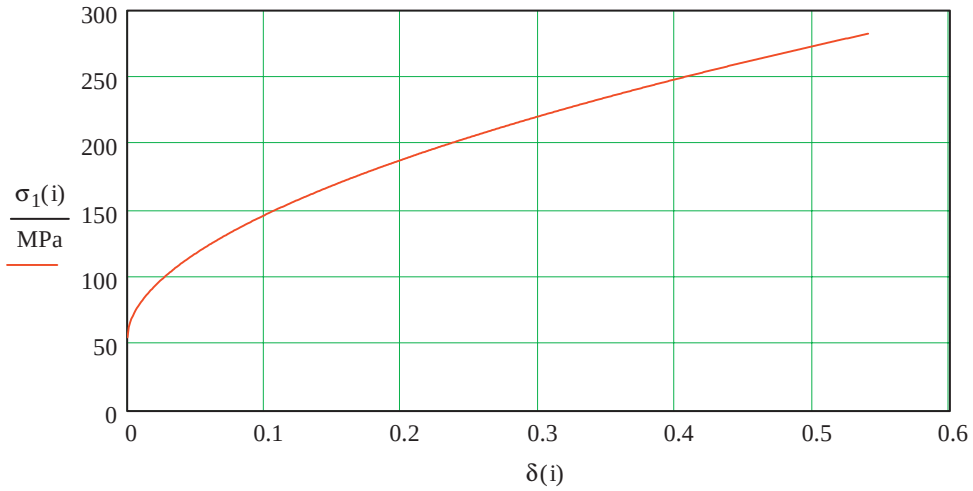

Stress-strain curve Copper:
acc. to "Elements of Physical Metallurgy", Albert G. Guy, University of Florida

$$\varepsilon_t(\sigma) := \frac{\sigma}{E}$$

$$\delta_t(\sigma) := \frac{(\sigma - S_0)^{\frac{1}{n}}}{K^{\frac{1}{n}}} \qquad \delta_{tot}(\sigma) := \frac{\sigma}{E} + \left[\frac{\Phi(\sigma - S_0)\cdot(\sigma - S_0)}{K}\right]^{\frac{1}{n}}$$

$\sigma := 50\cdot MPa, 70\cdot MPa .. 290\cdot MPa$

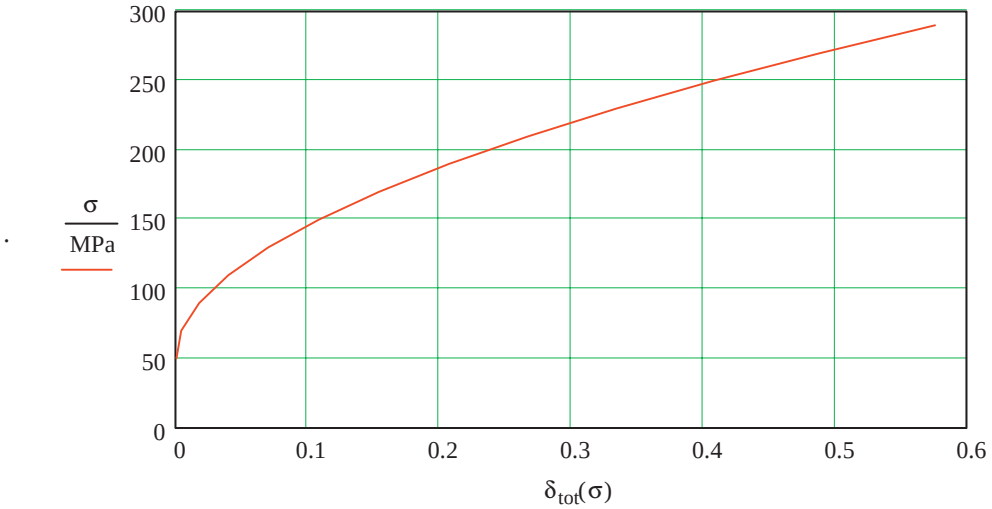

σ / MPa	$\delta_{tot}(\sigma)$ =
50	$4.532\cdot10^{-4}$
70	$4.081\cdot10^{-3}$
90	0.018
110	0.04
130	0.07
150	0.108
170	0.154
190	0.207
210	0.267
230	0.334
250	0.408
270	0.489
290	0.576

ISSN 1404-0344
CM Digitaltryck AB, Bromma, 2005